CRANFIELD UNIVERSITY

SCHOOL OF INDUSTRIAL AND MANUFACTURING SCIENCE

PhD. THESIS

ACADEMIC YEAR 1995 - 1996

NEAL C. JACKSON

FACTORS AFFECTING THE EXFOLIATION CORROSION OF ALUMINIUM ALLOYS

SUPERVISOR : Dr. M. J. ROBINSON

DECEMBER 1996

ABSTRACT

Aluminium alloys suffer from localised attack termed exfoliation corrosion which is intergranular in nature where the attack proceeds around the elongated grains present in the microstructure. The formation of a more voluminous corrosion product than the original material results in the lifting of grains giving the characteristic of exfoliation corrosion - lamellar attack. This results in surface degredation in the form of pitting, flaking or blistering. The precipitates present within the microstructure and the grain shape can alter how susceptible the material is to exfoliation corrosion. The distribution of precipitates present can be altered by heat treatment which affects the exfoliation corrosion susceptibility. A study on the effects of heat treatment and grain shape on exfoliation corrosion has been completed for two AlCuMg alloys (2014 and 2024) and two aluminium - lithium alloys (8090 and 2091). A MASTMAASIS salt - spray cabinet was used to determine the exfoliation corrosion susceptibility of all the alloys. A four - point bend test was developed to determine the depth of penetration and compared to depths measured metallographically.

The results for the 2XXX series alloys suggest that as the grain aspect ratio increases the exfoliation susceptibility increases. Although the aspect ratio did not differ greatly between each alloy, the different phases present in the two alloys seem to contribute more markedly to the susceptibility. Heat treatment in the 2024 alloy suggested that the peak - aged condition gave a higher susceptibility to corrosion than the under - aged and over - aged conditions. Results indicated that the heat treatment has a greater effect on exfoliation corrosion than the grain aspect ratio, showing that the grain boundary microstructure is an important factor in the exfoliation process. The four - point bend test tended to underestimate the depth of attack by virtue of measuring the whole area of the specimen whereas metallographic measurements only took into account the attacked areas. End grain testing suggested that the attack can not only proceed longitudinally but also "short - circuit" down the transverse path of the elongated grains in the 2XXX series alloys. For the aluminium - lithium alloys the over - aged condition showed more resistance to attack than the under - aged and peak - aged conditions but the under - aged was more resistant to attack for the 2091 alloy. Stress corrosion cracking showed trends similar to exfoliation corrosion.

CONTENTS

FIGURES

Page No.

Figure

Page No.

Page No.

TABLES

Page No.

CHAPTER ONE

1.0. Introduction

High strength, wrought aluminium alloys such as the 2XXX (AlCuMg) and 7XXX (AlZnMgCu) series have been used for many years in a number of parts of commercial and military aircraft. Components usually take the form of rolled, extruded and forged products. One major drawback in the use of these alloys is the fact that they possess a relatively low resistance to exfoliation corrosion and stress corrosion cracking. Exfoliation occurs because the wrought alloy products have an elongated grain structure. This type of corrosion is very damaging to any component on the aircraft as the attack is insidious in nature. If corrosion continues undetected then disaster may strike in that the corroded paths can act as sites for initiation of cracks which can lead to failure by fatigue. Recent developments include the introduction of aluminium - lithium alloys such as 8090 and 2091. These offer an improvement upon the density and stiffness over the conventional aerospace alloys but are still susceptible to exfoliation.

Exfoliation is a localised form of corrosion that takes place on wrought aluminium alloys with an elongated microstructure. The corrosion results in several forms of surface degradation ranging from pitting, powdering or flaking to the formation of blisters several millimetres in diameter. In general the corrosion follows an intergranular path around the elongated grains due to galvanic differences between the age - hardened precipitates and the solute denuded matrix. The formation of corrosion products which have a volume of approximately three times that of the aluminium alloy introduce large wedging stresses lifting the surface grains of the material and promoting further attack on material underneath. This reduces the thickness of the material where the remaining thickness reduces the load bearing capacity of any component on the aircraft. The heat treatment condition and grain shape of the alloy both play an important role in exfoliation corrosion. Heat treatment results in microstructural changes mainly affecting the precipitate distribution at the grain boundaries and, in turn the exfoliation susceptibility of an alloy. The over - aged condition usually shows superior resistance to attack than the under - aged and peak - aged conditions. Grain shape of aluminium alloys can be expressed as

the aspect ratio (ratio of the length of the grain over the width) where, the higher the ratio the more susceptible the material is to attack by providing a more favourable route for attack. Components are normally in plate form where there is a different grain structure through the cross section - longer, "pancake - shaped" grains occur at the mid section of the plate due to rolling during processing.

A specific requirement for exfoliation corrosion to occur is the environment. Although the presence of water is a basic requirement, halide ions such as chlorides provides a more aggressive environment which accelerates the corrosion. Some factors which can increase susceptibility are a lowering of the pH of the solution, increasing the halide ion concentration, increasing the temperature and an increase in the humidity of the environment. Exfoliation does not only occur on the external surfaces of aircraft but internally as well where liquid spillages such as coffee can cause corrosion in galley locations.

The main emphasis of this research was to study the metallurgical factors that control the depth of exfoliation damage as an aid to assessing the remaining life of structural components. Alloys 2014, 2024, 8090 and 2091 were used in the programme. Effects of heat treatment and grain aspect ratio on the exfoliation susceptibility in these alloys were studied. A four - point bend test was used to determine the effective remaining thickness of specimens after periods of corrosion in an acidified salt fog test environment. Metallography was used to confirm these bend test results. The results were compared with those from specimens which were exposed to a coastal marine atmosphere to represent more closely the conditions experienced on aircraft. End grain measurements were carried out to determine the direction of attack around the elongated grains in the 2XXX series alloys to gain a further insight to the corrosion mechanism for the different alloys. In addition, stress corrosion tests were carried out on 2014, 2024 and 2091 and the results compared to those from the exfoliation tests.

CHAPTER TWO

2.0. LITERATURE SURVEY

2.1. History and Development of Aluminium Alloys

There has been a considerable development in the use of aluminium alloys over the last few decades and this is reflected in the fact that this metal is now widely used in most major sectors of activity such as aerospace, land and sea transport, the building industry, packaging, and engineering. This very favourable, dominant position achieved by aluminium and its alloys is due to major research and development programmes that, over the years, have resulted in:

1. A continuous improvement in the properties of alloys and existing products.
2. The continual development of new grades of alloys offering improved performances or more specifically adapted to new requirements.

As with most aerospace systems, designers are primarily concerned with strength - to - weight ratio, durability which includes corrosion resistance, damage tolerance and the stability of properties in the operating environment. Another concern for the designer is that of economic considerations which includes material costs and maintainability. Recent research in the field of composite materials has produced exciting developments, but aluminium has remained the focal point due to its extensive use in aircraft structures and the availability of aluminium manufacturing facilities (1).

2.1.1. Development of Aluminium Alloys

Aluminium alloys have been used to save weight and provide high durability in many airframe structures since the advent of powered flight, from the early Schwarz and Zeppelin airships to the modern Concorde and Tupelov TU144 aircraft. Today these materials are used in aerospace applications which range from space suits and coatings to structural parts and launch vehicles. They are also used successfully in the rail industry, the automobile industry and shipping. Over the years certain heat treatments and

changes in compositions have improved properties in these alloys such as corrosion resistance, hardness, high strength and fracture toughness.

The Wright brothers used cast aluminium in engine components for its low weight but the strength of the material was low. AlCuMg alloys were developed by Wilm (2) and have been used for many decades. The Duralumin (AlCu) alloy was first used in the 1914 Zeppelin airships (3) as structural components but the strengthening mechanism was not understood. The discovery of precipitation hardening at Alcoa led to the development of a heat treatable Duralumin alloy (2017) which was used in airplane propellers until the higher strength 2025 alloy was discovered (4). The first all aluminium plane was the Junkers - F13 (5) introduced in Europe in 1920, but the proportion of aluminium on most planes was small until the 1930s. These alloys had a good strength - to - weight ratio but the corrosion resistance was low which was improved by the development of the alclad process in which the alloy is protected by a thin cladding of unalloyed aluminium. Further developments led to Super Duralumin (2024 - T3) (6), an AlCuMgMn type alloy which was stronger than Duralumin. This material was used in the DC - 3 as alclad 2024 - T3 and saved a considerable amount of weight in the airframe and is still being used as the material for the fuselage on today's commercial aircraft. By the 1930s it was discovered that alloys containing zinc had higher strengths than that of the AlCuMg type alloys but were brittle and susceptible to stress corrosion cracking. This led to the development of a chromium - containing AlZnMgCu type alloy in the 1940s (4) known as 7075 - T6 and was used in the Mitsubishi Zero aircraft during the second World War. 7075 - T6 was also used in the Enola Gay (5) which strengthened the aircraft enough to be able to carry the first atomic bomb. This was the first 7XXX series alloy which was resistant to stress corrosion cracking in the short transverse direction whereas the 2024 - T3 alloy was resistant to fatigue.

Over the years planes grew larger and the structural components became thicker to carry the increased loads. This led to research into stress corrosion and corrosion - resistant tempers and new materials. The Germans developed an alloy 7079-T6 (5) which showed higher fracture toughness than 7075 in laboratory testing but in environmental

conditions of service the alloy was very susceptible to stress corrosion. Alcoa developed a stress corrosion resistant temper T73 (7) for 7075. This temper consists of artificially ageing at a low temperature to produce a fine precipitate distribution, followed by a higher temperature ageing at about 160^0C. Double ageing results in a better combination of strength and corrosion resistance. The 7075 - T73 was used as the forgings that support the tail engine and wings on the Douglas DC - 10. The use of 7075 - T6 on the Lockhead L - 1011 Tristar brought about the problem of exfoliation corrosion which was controlled by the development of the T76 temper (6) but with a slight reduction in strength. Research into alloys containing higher levels of copper than 7075 led to the development of 7050 (8) which met target property goals and was used for much of the internal structure of the F - 18 Hornet in the T74 temper. In this alloy both the copper and zinc contents were increased and the chromium completely replaced by zirconium. In the 1970s an AlZnMgCu alloy was developed (7) with impurity elements of iron and silicon which provided higher fracture toughness which was known as 7475. Other alloys which improved the fracture toughness were those of 2048, 2124 and 2419 (9).

Most aircraft that are in use today were designed in the 1960s and 1970s and are still using the materials that were developed in those years. The commercial aircraft builders continued to use 7075 - T6 and 2024 - T3 for the thinner sections and 7075 - T73 for the thicker plate. With the oil embargo during the 1970s the need for lighter and stronger materials arose to save weight for a decrease in fuel consumption. Modifications of 2024 and 7075 such as 2234 - T3511 extrusions, 2324 - T39 plate and 7150 - T6 plate were developed (6) in the 1980s to provide this higher strength and lower weight. These materials are used for the wing and other structural parts of the Boeing 757 and 767 aircraft.

2.1.2. Development of Aluminium - Lithium Alloys

Although 2XXX and 7XXX series alloys have been the dominant aluminium alloys used in aircraft for many years now (10), the development of aluminium base alloys containing lithium spans several decades (11). Since lithium is the lightest metallic

element, alloying it with aluminium significantly reduces the density of aluminium alloys, and early work at Alcoa (12) showed that lithium also increases aluminium's elastic modulus. Lithium also provides the basis for solution and precipitation hardening. The density of aluminium alloys decreases by 3% and the elastic modulus is increased by 6% for every 1% of lithium added (13). A 15% reduction in the weight of airframes (14) can be achieved using the improvements of density and stiffness achieved by these lithium additions. Figure 2.1 shows that reducing the density has been shown to be the most efficient way to achieve minimum weight and improve the overall performance (15). Analysis of the different parts of an airframe show that weight can be saved by decreasing density, increasing elastic modulus, and incresing the durability and damage tolerance (DADT) as well as by decreasing strength. A major disadvantage with lithium is that it contributes to low fracture toughness in these alloys and is a consequence of the metastable, coherent δ' phase (Al_3Li) (16).

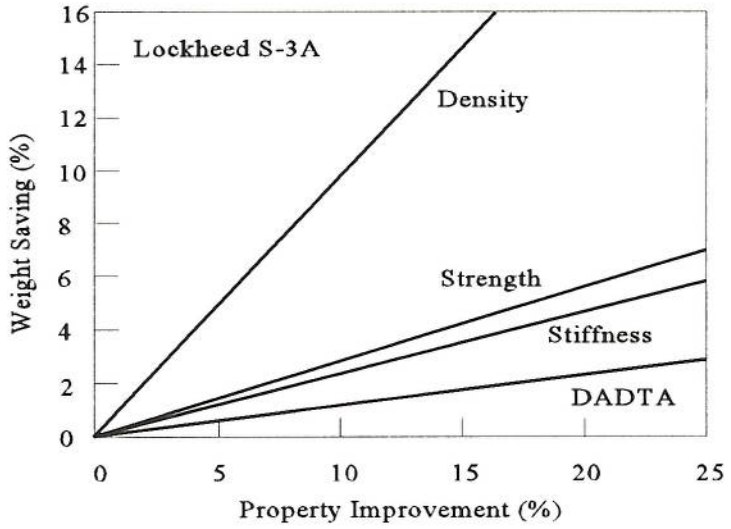

Figure 2.1. : The influence of various properties on structural weight savings of the S-3A aircraft (15).

The earliest use of lithium as a solute was recorded in 1921 (17). A thorough historical review on the development of AlLi alloys was presented at the first aluminium - lithium conference by Balmuth and Schmidt (11). An alloy called Scleron with small

additions of lithium was developed in 1924 by the Germans which was the first commercial aluminium - lithium alloy and this was compared with Duralumin (a heat treatable AlCuMg alloy) which had a lower yield strength. Scleron was an aluminium - zinc alloy with only 0.1% lithium and had the composition Al-12Zn-3Cu-0.6Mn-0.1Li. This alloy was selected for certain automotive applications. Although the Scleron alloy was not successful, interest in the aluminium - lithium alloys remained, especially when it was discovered that high strengths could be achieved with these types of alloys. The potential for high strength in AlCuLi type alloys was not discovered until 1942 when I. M. LeBaron (18) applied for a patent on Al - Cu - Li - X alloys which was granted in 1945. The continued research into lithium additions led to the development of X - 2020 in 1957 at Alcoa which was optimised to provide maximum compressive strength and stiffness. This alloy was used in the experimental North American Navy reconnaissance plane RA5C Vigilante (19) as wing skins. Alcoa terminated the production of X - 2020 in 1969 due to its poor fracture toughness. The research into aluminium - lithium was also proceeding in Russia with the development of 01420, with a chemical composition of Al-5Mg-2Li-0.5Mn (20). This alloy had excellent corrosion resistance similar to that found in the 5XXX series alloys with an increase in strength due to precipitation hardening.

During the seventies the Ministry of Defence supported research and development with Fulmer Research Institute and High Duty Alloys Ltd on aluminium - lithium alloys based on the 01420 type alloy. The Royal Aircraft Establishment became involved in 1978 trying to reduce the density even further without any detriment to the mechanical properties (21). The alloys investigated were based on several different systems comprising AlMgLi, AlLiCu, AlLiCuMg, AlLiMgSi and AlLiZnMg. With variations in composition and heat treatments the toughness and strength of these alloys could be balanced. The alloy type AlLiCuMg demonstrated the best balance between strength and fracture toughness which was later patented as 8090 (21). A high strength variation of this alloy was developed by the British Aluminium Company and was known as 8091. Three strength variants of the 8090 alloy are known as Lital A, Lital B and Lital C (22). These are medium strength, high strength and damage tolerant aluminium - lithium alloys which

have been produced to replace 2014 - T6, 7075 - T6 and 2024 - T3 respectively.

The development of aluminium - lithium alloys proceeded rapidly during the eighties in a series of AlLi conferences focusing on binary and ternary alloys, properties and microstructural characteristics and production of low density aluminium alloys. Table 2.1 shows designations and compositions of the new aluminium - lithium alloys (14). The properties of most of the new alloys appear sensitive to small variations in composition and processing.

Early efforts indicated that fracture toughness would be the most difficult target to meet. In 1981 research into ALITHALITE alloys was carried out by Alcoa (23) for low - density replacements for 2024 - T3X and 7075 products. One alloy with composition Al-2.7Cu-2.2Li-0.12Zr had subsequently been developed in 1984 by Alcoa which was designated as 2090. This alloy exhibited good fracture toughness and corrosion behaviour. Further work prevailed on this alloy (24) and in 1987 it was available in a product form and a variety of tempers. These tempers were developed for each product form to allow some tradeoffs in mechanical properties available for specific airframe applications. 2090 was chosen by McDonnell Douglas for use as floor beams in its MD - 11 jet liners. Another alloy of this type was developed in 1985 by Pechiney (5) with similar properties to the 2090 but with lower levels of copper and lithium.

This reduction in density and increased stiffness resulting in weight savings has led British Aerospace Military Aircraft Ltd (BAe MAL) to consider aluminium - lithium alloys for use on the European Fighter Aircraft (25). All sheet components for the front fuselage of the EFA were designed in 8090 sheet. This alloy was used in the T62 temper and showed good fatigue properties and corrosion resistance, but the fracture toughness required improvement which could be improved using a lamellar recrystallised grain structure. Other recent uses for aluminium - lithium alloys have been in the construction of the Westland - Agusta EH101 helicopter (26). 8090 and Al - 905XL are extensively used on the fuselage of the EH101 giving weight reductions in excess of 200Kg. Weldalite 049, a precipitation strengthened alloy which was patented in the U.S.

Table 2.1. : Current Aluminium - Lithium Alloys and Compositions (14).

Element	Alloy						
	2090 Alcoa 8/6/84	2091 C. Pechiney 4/8/95	8090 Alcan May 1985	8090A Alcoa Late 1985	8091 Alcan 29/3/85	X8092 Alcoa May 1985	X8192 Alcoa August 1985
Si	0.10	0.20	0.20	0.10	0.30	0.10	0.10
Fe	0.12	0.30	0.30	0.15	0.50	0.15	0.15
Cu	2.4-3.0	1.5-2.5	1.0-1.6	1.1-1.6	1.5-2.2	0.5-0.8	0.4-0.7
Mn	0.05	0.10	0.10	0.05	0.10	0.05	0.05
Mg	0.25	1.1-1.9	0.6-1.3	0.8-1.4	0.5-1.2	0.9-1.4	0.9-1.4
Cr	0.05	0.10	0.10	0.05	0.10	0.05	0.05
Ni	-	-	-	-	-	-	-
Zn	0.10	0.25	0.25	0.10	0.25	0.10	0.10
Ti	0.15	0.10	0.10	0.15	0.10	0.15	0.15
Li	1.9-2.6	1.7-2.3	2.2-2.7	2.1-2.7	2.4-2.8	2.1-2.7	2.3-2.9
Zr	0.08-0.15	0.04-0.16	0.04-0.16	0.08-0.15	0.08-0.16	0.05-0.15	0.08-0.15

in 1991 (27) has been considered (28) for use in cryogenic propellant tanks to reduce cost and weight for the USA National Launch Systems, reducing the weight of the launch vehicle by 30%. This alloy has the composition Al-4.75Cu-1.3Li-0.4Ag-0.4Mg-0.14Zr with the silver and magnesium refining and making the precipitates small.

2.2. The Microstructure of Aluminium Alloys

2.2.1. The Microstructure of 2XXX Series Alloys

The 2XXX series group of alloys are based on the AlCu binary alloy with varying additions of elements such as magnesium, manganese, silicon and iron together with smaller additions of titanium, zirconium or chromium. These form various precipitates within the structure and control microstructural properties that can affect tensile and fracture behaviour, strength and corrosion resistance. Alloys from this group can undergo natural ageing where age hardening and precipitation occur over long periods of time. This hardening is related to the formation of Guinier - Preston zones through dispersion hardening and internal strain hardening.

Heat treatment involves a solution treatment to dissolve all the solute elements, followed by a rapid quench which produces a supersaturated solid solution. Artificial ageing can then be applied to the material producing varying tempers such as under - aged, peak - aged and over - aged conditions. This heat treatment affects the type of precipitate and their distribution within the structure and speeds up the precipitation process which increases the yield strength. Particles which form on ageing act as pins on slip planes and prevent plastic deformation, improving the mechanical properties of the material. The growth of precipitates during artificial ageing increase the effect of pinning the slip planes. Figure 2.2 (29) shows the variation of microhardness with time at different ageing temperatures. These curves show the classic age - hardening behaviour in that they show a peak hardness which shifts at higher temperatures. The AlCuMg alloys are the most commonly used age hardenable aluminium alloy. The two main alloys which belong to the 2XXX series are 2014 and 2024.

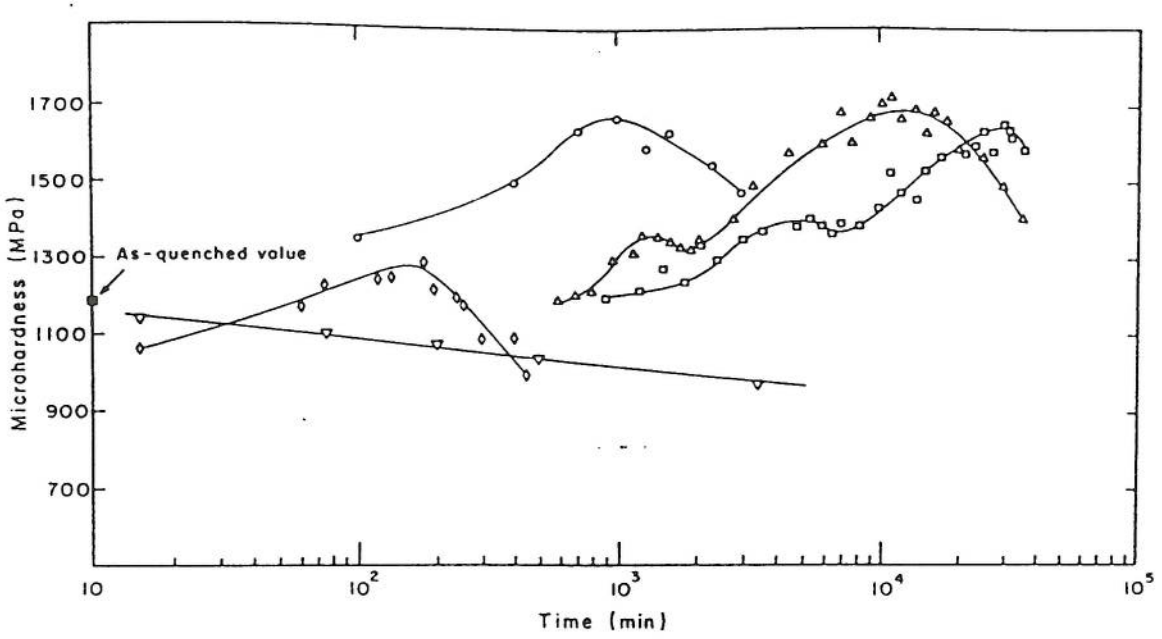

Figure 2.2. : Ageing curves at different temperatures for a rapidly quenched 2014 alloy: □ - 75°C, Δ - 100°C, ○ - 125°C, ◇ - 160°C and▽ - 190°C (29).

2.2.1.1. The Aluminium - Copper Binary Phase Diagram

Figure 2.3 shows the binary phase diagram for aluminium - copper (30). In aluminium rich aluminium - copper binary alloys, aluminium forms a eutectic with the constituent designated θ. This constituent melts at 591°C and the homogeneity range is from 46.4% to 47.8% copper. The ideal composition of $CuAl_2$ (θ) is 46.1% copper (31), just outside the homogeneity range. On casting a 4% copper alloy, a solid solution is obtained in which the copper is not distributed randomly. After heating the alloy at a temperature just below the solidus (540°C), rapid quenching preserves the solid solution and freezes the copper and lattice vacancies (formed during the solution treatment). This temperature must not exceed the solidus as melting produces a non ductile eutectic which decreases strength and ductility increasing the susceptibility to quench cracking. The use of a rapid quench prevents the diffusion of solute vacancy pairs to locations .such as grain boundaries, other vacancies and impurity atoms. This diffusion causes particles of transition phases to be formed at grain boundaries before the formation of Guinier -

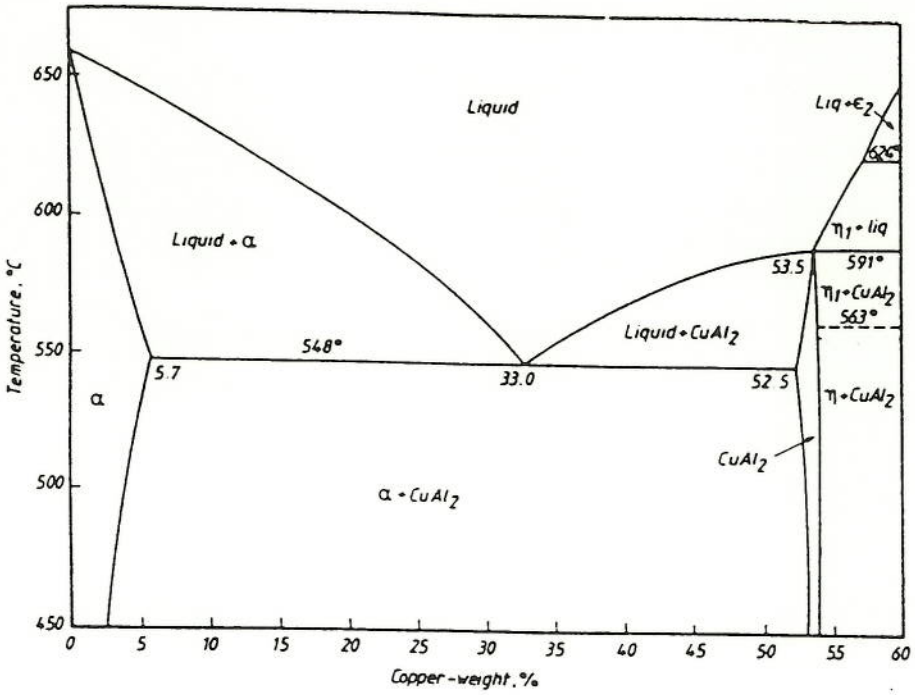

Figure 2.3. : Phase diagram for aluminium - copper binary system (29).

Preston zones in the grains lowering the strength and decreasing the susceptibility to intergranular corrosion. The solid solution decomposes on tempering to form another solid solution with excess copper as clusters which form the nuclei for the formation of type I Guinier - Preston zones (32). These give rise to Guinier - Preston compounds which are θ" and have a tetragonal lattice. At a tempering temperature of 200°C, tetragonal θ' is formed which develops into θ, the equilibrium phase and has a body centered tetragonal structure. This phase softens the alloy, decreasing the susceptibility to stress corrosion cracking by eliminating any internal residual stresses which are caused by rapid quenching. AlCuMg alloys are quench sensitive allowing some solute elements to form as coarse precipitates. The full precipitation sequence in an AlCu binary alloy is (33):

supersaturated solid solution → GPZ (I) → GPZ (II) → θ' ($CuAl_2$) → θ ($CuAl_2$)

The microstructure of an AlCuMg alloy can be seen in figure 2.4 (33) which illustrates the grain structure and constituent particle distribution in the three orientations of an extruded plate. The grains are flattened and elongated parallel to the longitudinal

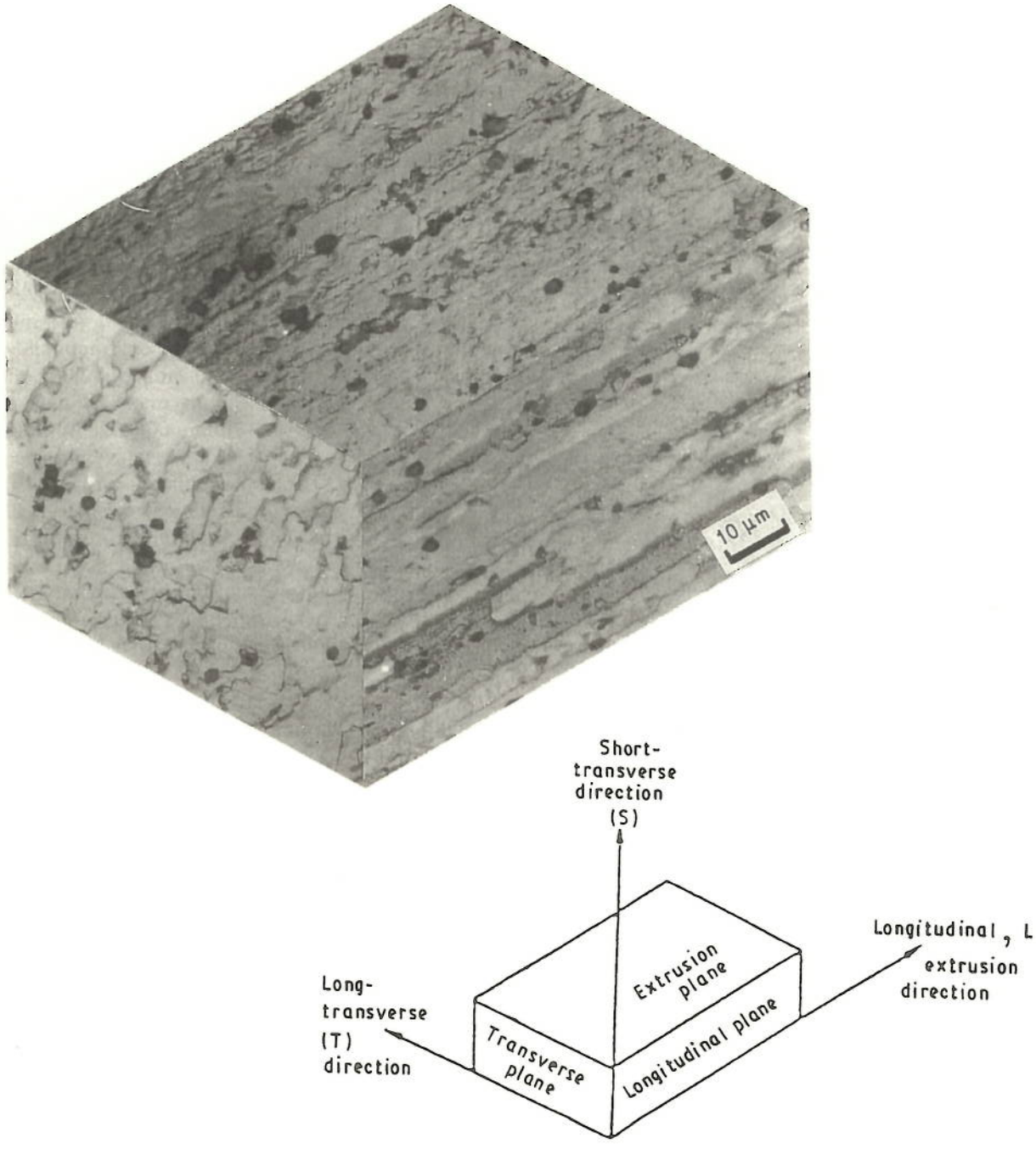

Figure 2.4. : Micrograph showing particle density and distribution along the three orientations of an extruded plate (33).

direction. There are large second phase particles present which are potential nucleation sites for void formation. The larger, irregular shaped particles are Al_7Cu_2Fe and $Al_{20}Cu_2(FeMn)_3$ (34) and the smaller particles are the manganese containing dispersoids $Al_{20}Cu_2Mn_3$ (35). Normal, wrought 2024 contains these precipitates where the latter causes grains formed during solution heat treatment to be elongated and flattened. 2014 differs from 2024 in that the magnesium content is lower and the silicon content is higher. There are other coarse particles present in these alloys which take the shape of rods ($MnAl_6$) and spheres ($CrAl_7$) (36).

2.2.1.2. Precipitation in AlCuMg Alloys

Figures 2.5 and 2.6 (37) represent the phase diagram at 460^0C and at room temperature showing that the equilibrium phases are θ ($CuAl_2$) and S ($CuMgAl_2$). The precipitation sequence in AlCuMg alloys is (38):
supersaturated solid solution → GPB zones → S" ($CuMgAl_2$) → S' ($CuMgAl_2$) → S ($CuMgAl_2$)

The S' phase which is partially coherent with the matrix is the intermediate phase or metastable phase of the equilibrium S phase. Many investigators have studied this predominant S phase (39, 40, 41, 42). Radmilovic et al (39) observed that there is a continuous nucleation of S' during ageing for 72 hours at 190^0C. The S' phase precipitates generally nucleate on dislocations but have been reported to occur at unidentifiable sites in the matrix (43). It has been suggested that the clustering of Cu and Mg produce sites for the nucleation of S' (41). Gupta et al (41) found that the S' precipitates are a strained version of the S phase and they grow as laths on {210} matrix planes along <100> matrix directions. Jin Yan et al (40) showed that the crystal structure of S is orthorhombic with lattice parameters a = 0.4nm, b = 0.461nm and c = 0.718nm. Further studies of the AlCuMg alloy identified a new phase present within the structure (44). This phase is called X appears as bulk - like precipitates with different size. This X phase has a C - face centered orthorhombic crystal structure with lattice parameters of a = 0.492nm, b = 0.852nm and c = 0.701nm. The X phase precipitates as rod shaped particles and, through prolonged ageing they exist as cuboid shape.

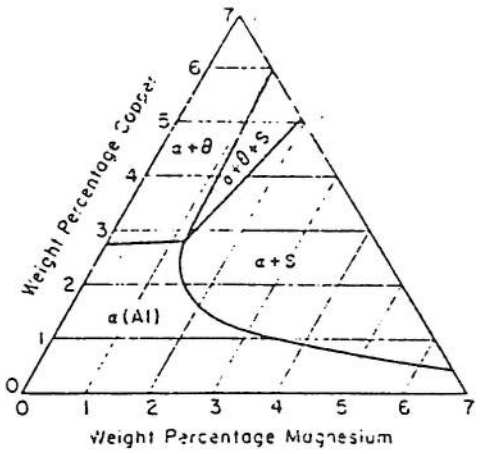

Figure 2.5. : Diagram showing the aluminium corner of the AlCuMg phase diagram at 460^{0}C (37).

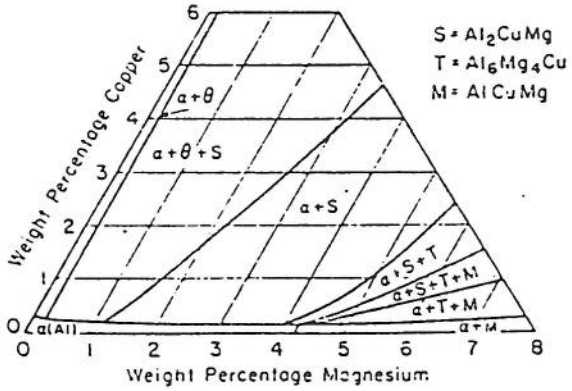

Figure 2.6. : Diagram showing the aluminium corner of the AlCuMg phase diagram at room temperature (37).

2.2.1.3. Thermomechanical Ageing

Another type of heat treatment available is that of thermomechanical ageing (TMA) to improve properties in 2XXX series alloys such as ductility, toughness and stress corrosion resistance. Singh et al (45) studied the effect of thermomechanical ageing (TMA) on a 2014 alloy. This involved TMA treatments which included partial peak - ageing, warm rolling and further ageing to peak hardness level at 160^0C. These treatments led to precipitate - dislocation networks of different densities and caused a marked improvement in the tensile properties. This dislocation substructure controls the coarsening of second phase precipitate particles which are responsible for improving the overall properties in aluminium alloys. Singh concluded that dispersoids such as $Al_4CuMg_5Si_4$ and $Al_{12}(Fe,Mn)_3Si$ can contribute to the strengthening of the alloy but the $CuAl_2$ or $CuMgAl_2$ precipitates and dislocation substructure are the major contributors to the strength.

2.2.1.4. Alloying Additions to the AlCu Binary System

Commercial aluminium - copper alloys contain iron and silicon as the principal impurities. Iron can occur as $FeAl_3$ or as one of the ternary precipitates α (FeSi), β (FeSi) or β (FeCu). Silicon can occur in the elemental form, α (FeSi) or β (FeSi). Binary aluminium copper alloys are used as master alloys for the making of more complex alloys with several additions on the binary alloy.

2.2.1.4.1. Magnesium Additions

The addition of magnesium to binary aluminium - copper alloys enhances both the rate and magnitude of natural ageing (33). The copper magnesium ratio is important in determining which precipitates are present within the alloy - whether they are the θ or S type precipitates. In alloys with high magnesium content the $CuMgAl_2$ phase predominates whereas in alloys with low magnesium contents the $CuAl_2$ phase predominates (46). Wyss et al (47) studied two aluminium alloys - one without (2419)

and the other with 0.18% magnesium (2519) and concluded that the addition of magnesium improved the yield strength. The mechanism for this improvement in strength is the formation of magnesium - vacancy clusters which increase nucleation of Guinier - Preston zones. Magnesium can increase work hardening by a reduction in dislocation mobility or an increase of the dislocation density. Figure 2.7 (37) shows the effect of magnesium on the yield strength of aluminium - copper binary alloys.

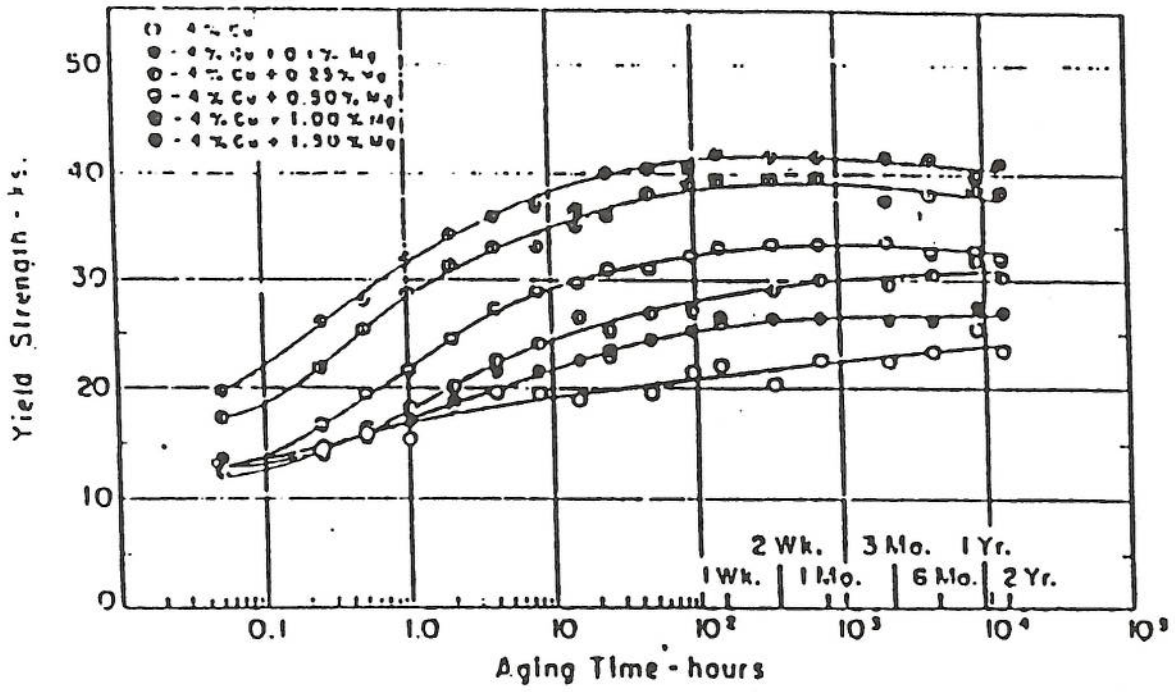

Figure 2.7. : Diagram showing the effects of magnesium on the yield strength of aluminium alloys (37)

2.2.1.4.2. Silicon Additions

The addition of silicon to AlCuMg alloys modifies their precipitation behaviour and results in improved mechanical properties. Wilson (48) suggested that silicon increases the effective binding energy between the solute atoms, vacancies and Guinier - Preston zones, so enhancing the stability of the zones and raising the temperature at which the S' precipitate can form. According to Chaturvedi et al (49) silicon reduces the activation

energy and the frequency factor for the formation of Guinier - Preston zones. This produces a finer dispersion of the S' phase.

2.2.2. The Microstructure of Aluminium - Lithium Alloys

Aluminium - lithium alloys which are available today are based on the AlLi binary system with major alloying additions of copper, magnesium and zirconium. These elements form precipitates within the structure which can improve the mechanical properties of the alloys. Other elements present such as iron and silicon form complex, coarse precipitates which also affect the properties within the material. The main microstructural features of AlLi type alloys are grain structure, matrix and grain boundary precipitation. All of these features can be controlled by heat treatment and the use of alloying additions. For example, transition element additions can produce grain structures which vary between an equiaxed, recrystallised structure and an unrecrystallised pancake structure, containing extensive subgrains.

2.2.2.1. Precipitation of the δ Phase

Figure 2.8 shows the binary aluminium - lithium phase diagram (50) which is a typical eutectic system with maximum solid solubility of lithium in aluminium of around 4wt%. When AlLi type alloys are quenched from the solid solution (α matrix which is a fcc structure) and aged below the solvus temperature, homogeneous precipitation of the metastable, dominant δ' (Al_3Li) phase occurs. In addition to δ', the matrix contains lath - like precipitates of the δ (AlLi) phase which has a bcc structure and an associated precipitate free zone develops in the grain boundaries. It is well known that strengthening in aluminium - lithium alloys is due to the δ' phase (13, 51, 52). This is due to the fact that δ' precipitates, which are ordered and coherent with the α matrix, impede the motion of dislocations. Also, an increase in the volume fraction of δ' increases the peak strength. However, a high degree of planar slip is associated with this phase during plastic deformation of aluminium - lithium alloys which can reduce the ductility (13). These particles have an fcc $L1_2$ structure with a low lattice misfit relative to α - Al.

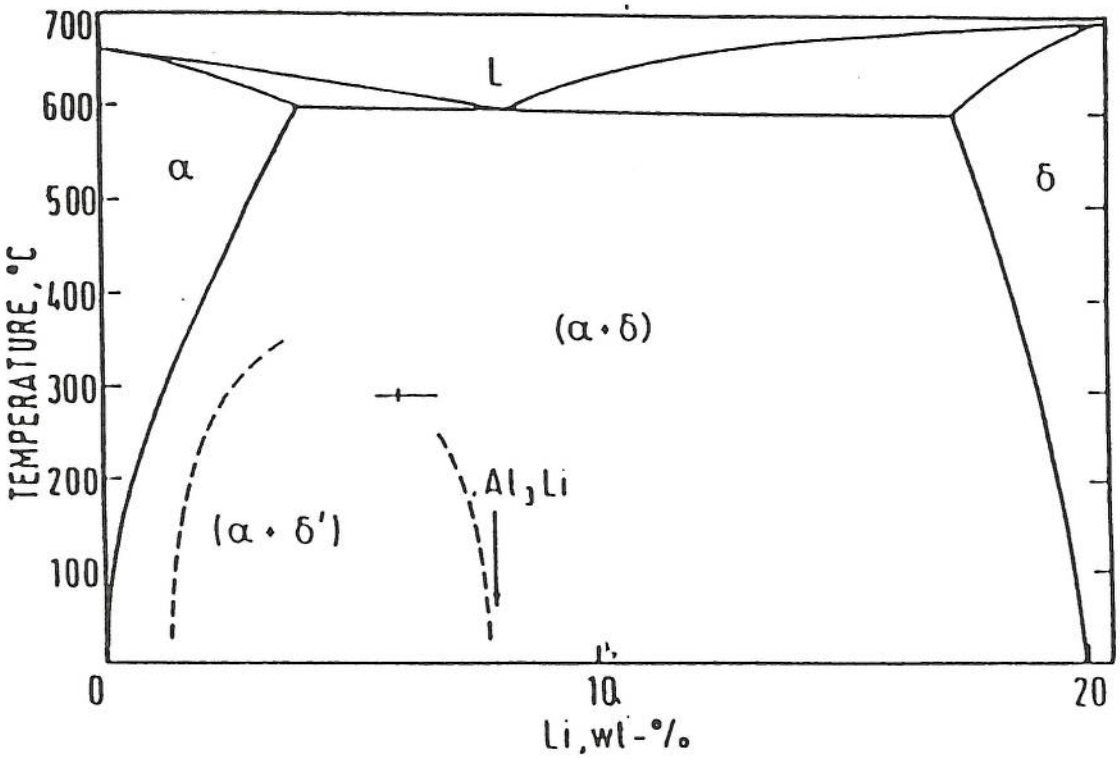

Figure 2.8. : Diagram showing the binary aluminium - lithium equilibrium phase system (50).

The precipitation sequence is generally accepted to occur (51, 53) as follows:

$$\alpha \text{ solid solution} \rightarrow \alpha_1 + \delta' \rightarrow \alpha_0 + \delta$$

As can be seen from the precipitation sequence, prolonged ageing results in the formation of the δ phase which is stable and semi - coherent with the aluminium matrix surrounded by misfit dislocations. It has a plate morphology with a {111} plane, a cubic structure and has a large lattice mismatch. The mechanism of δ formation is poorly understood. Niskanen et al (54) suggested that the formation of δ on grain boundaries occurs by the preferential coarsening of the δ' particles. Williams et al (55) noted that the δ precipitates are surrounded by "misfit" dislocations. He concluded that δ nucleates heterogeneously on dislocations and grain boundaries independently of the δ' phase and can be present in the matrix only in over - aged microstructures. However, work carried out by Kaufman et al (51) proved that these dislocations are not related to the formation of the δ phase. They are associated with the considerable volume

change that occurs when the δ transforms to α and δ'. The formation of this phase during heat treatment should be avoided since it has a deleterious effect on the material's properties. The δ phase is extremely anodic compared to the matrix such that localised corrosion occurs at boundaries or in the matrix where this phase is located. Rapid solidification can be used to suppress the formation of δ by increasing the solid solubility of lithium. During ageing the δ' precipitates coarsen according to Lifschitz - Wagner kinetics (56) showing an increase in the average radius, r with $(time)^{1/3}$. This phenomenon is termed Ostwald ripening where larger particles grow at the expense of smaller ones. Preferential coarsening of δ' occurs at structural defects such as dislocations or grain boundaries. Development and growth of precipitate free zones as a result of this preferential coarsening of δ' in the grain boundaries by enhanced diffusion has been reported (57) depleting the grain boundaries of solute. The growth of these precipitate free zones approximates to $(time)^{1/3}$.

The coherency of the δ' precipitate induces a strong tendency toward strain localisation (58) due to precipitate shearing. This phenomenon reduces the ductility and fracture toughness in aluminium - lithium alloys. Strain localisation results in bands of deformation which act as stress concentrators at grain boundary triple joints from which cracks can nucleate and propagate. Numerous modifications (52, 59, 60) can be made to minimise the strain localisation in aluminium - lithium alloys. These can be controlling grain morphology, reducing the width of the precipitate free zone or the introduction of co - precipitating phases which reduce the slip band length. A reduction in grain size decreases the slip length and reduces the stress concentration at grain boundaries and grain boundary triple joints. Small grains enhance multiple slip at low strains producing homogeneous deformation which increases the ductility. The presence of alloying additions to the aluminium - lithium binary alloy reduces strain localisation by promoting homogeneous deformation (59) and alters each of the above characteristics.

The commercial AlLiCuX alloys have a complex precipitate structure and a number of phases precipitating during ageing which can be seen in figure 2.9 (14). These alloying additions can affect properties such as fracture toughness, stress corrosion and corrosion susceptibility and other engineering properties. The types of alloy seen in figure 2.9 cover

the major precipitates present in alloys such as 8090, 2091 and 2090. Precipitates present are T_1 (Al_2CuLi), T_2 (Al_6CuLi_3), θ' (Al_2Cu), S' (Al_2CuMg) and β' (Al_3Zr). In alloys where a secondary precipitate is present (apart from the δ' matrix precipitate) heterogeneous nucleation of θ', S' and T_1 occurs on low angle grain boundaries.

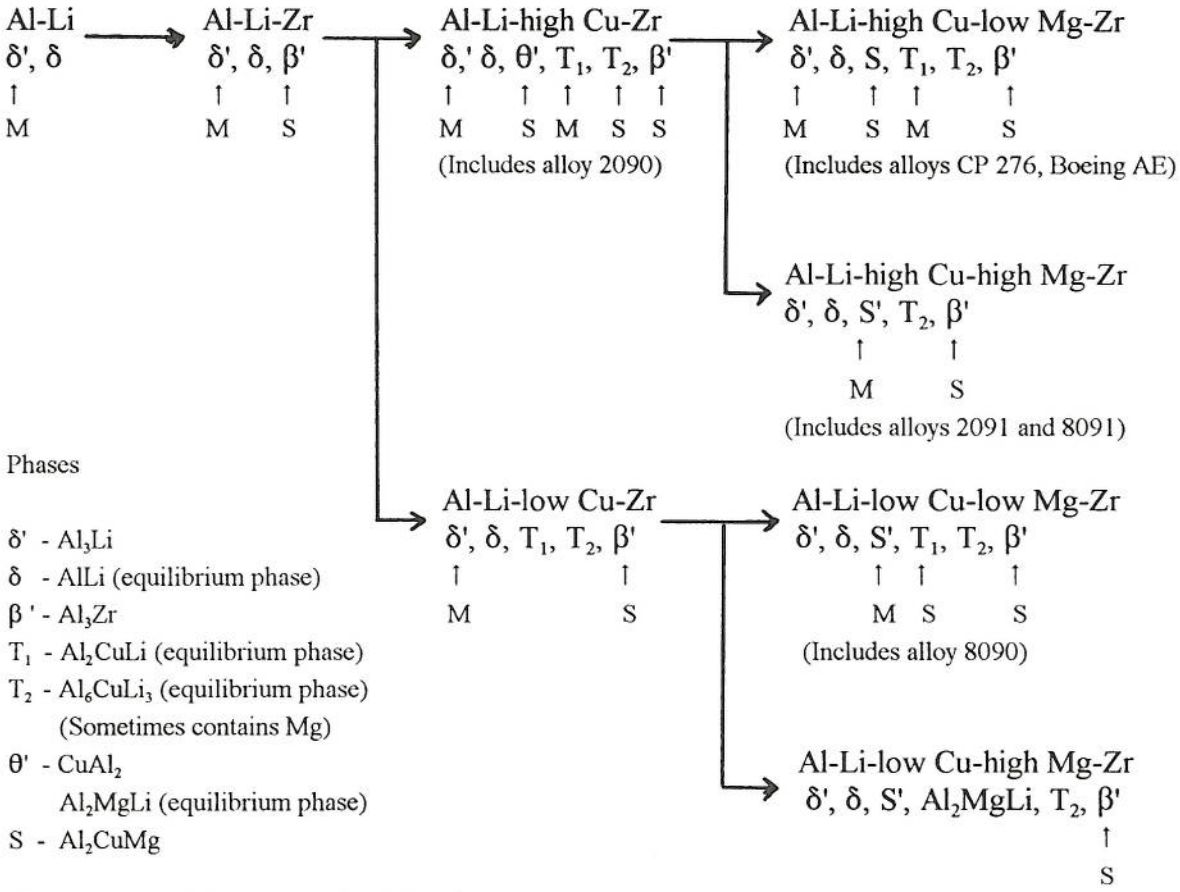

Figure 2.9. : A schematic illustration of the precipitate phases that form in AlLiX alloys (14).

2.2.2.2. Alloying Additions to the Aluminium - Lithium Binary System

Major additions which are made to the aluminium - lithium binary alloy are copper, magnesium and zirconium. These additions alter the properties of the alloy by the precipitation of extra phases within the microstructure.

2.2.2.2.1. Magnesium Additions

The microstructure of an AlLiMg alloy in the early stages of ageing is similar to the AlLi binary alloy with one notable effect of a reduction in the solubility of lithium. It has been suggested that magnesium alters the kinetics of the δ' precipitation by either partially substituting for lithium in the δ' (61), or by reducing the solubility of lithium which increases the volume fraction of δ'. Thus magnesium can act as a solid solution strengthener. It has been reported that for every 1% magnesium added to AlLi the tensile strength increases by 50MPa (62). The precipitation sequence for magnesium containing Al - Li alloy is:

$$\alpha \text{ (supersaturated solid solution)} \rightarrow \delta' \rightarrow AlLi$$

However it is known (60) that increasing the magnesium : lithium ratio the ternary phase T (Al_2MgLi) forms. This phase is present as coarse rods or laths on grain boundaries and dislocations. In the later stages of precipitation, magnesium enters into the precipitation sequence and the sequence is as follows (21, 57, 60):

$$\alpha \text{ (supersaturated solid solution)} \rightarrow \delta' \rightarrow Al_2MgLi$$

Combinations of magnesium and lithium greater than 5% can have an adverse effect on the ductility by the formation of the ternary phase on the grain boundaries. Al_2MgLi is usually found in alloys containing more than 4% magnesium or in the over - aged condition. It was reported by Wilkes et al (63) that the precipitation of δ' and Al_2MgLi increases the hardness during the early stages of precipitation. Further ageing increases the volume fraction of Al_2MgLi while δ' coarsens and dissolves but with no increase in the hardness. This phase also reduces the strain localisation associated with δ' so improving the fracture toughness.

2.2.2.2.2. Copper Additions

The addition of copper in the early stages of ageing is similar to that of magnesium in that the maximum solid solubility of lithium in aluminium decreases at all temperatures. Copper also provides additional, beneficial precipitation reactions that occur independently of δ' formation. The strength associated with these alloys is the co - precipitation of the copper rich phases (53). The precipitation sequence in AlLiCu type alloys depends on the copper and lithium contents. For alloys containing high copper and low lithium levels the precipitation sequence is (57, 64):

$$\alpha_{ss} \rightarrow \begin{cases} \delta' \rightarrow \delta \\ \text{GP Z's} \rightarrow \theta'' \rightarrow \theta' \rightarrow \theta\ (Al_2Cu) \end{cases}$$

However, for alloys containing high lithium and low copper levels the precipitation sequence is as follows:

$$\alpha_{ss} \rightarrow \begin{cases} \delta' \rightarrow \delta \\ T_1\ (Al_2CuLi) \end{cases}$$

The strengthening phases at various copper : lithium ratios can be seen in figure 2.10 (65). The Al_2Cu phase is primarily responsible for strengthening the material and precipitates as platelets with a tetragonal structure on {100} matrix planes.

Strengthening is also affected by the Al_2CuLi phase which precipitates as platelets with a hexagonal structure on {111} matrix planes (14). In commercial AlLiCu alloys such as 2090, the predominant strengthening phase after ageing to the peak - aged condition is T_1. Both the θ' and T_1 phases nucleate heterogeneously on grain boundaries and dislocations reducing the volume fraction and the distribution of δ'. This improves the ductility and toughness by reducing the degree of strain localisation associated with δ'. Another copper containing phase present in AlLiCu type alloys is that of T_2 (Al_6CuLi_3)

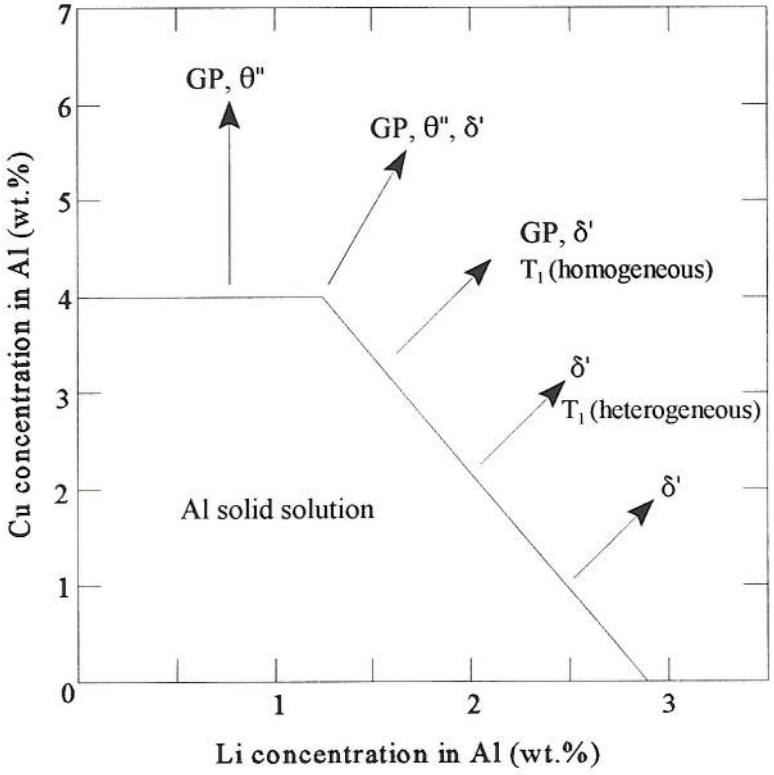

Figure 2.10. : The solvus line at 500°C at the aluminium - rich end of the AlLiCu system showing the strengthening phases at various copper and lithium contents (65).

which nucleates predominantly on high angle grain boundaries (14, 53, 60). However, the formation of these T_2 phases leads to the development of precipitate free zones along the grain boundaries and a reduction in ductility and fracture toughness. The relative concentration of these phases is dependent on ageing time (66) - δ' nucleates during quenching and reaches a maximum volume fraction before the peak - aged condition. Both the T_1 and the grain boundary T_2 phases grow throughout the ageing process at the expense of δ'. This is typical for the alloy 2090 (Al-2Li-3Cu) where all the above phases are present within the structure. A schematic illustration of the microstructure of 2090 after peak ageing can be seen in figure 2.11 (67). However, the continuous, coarse T_2 particles at the grain boundaries in the peak - aged condition results

in a non homogenous microstructure and an increase in the susceptibility to exfoliation corrosion.

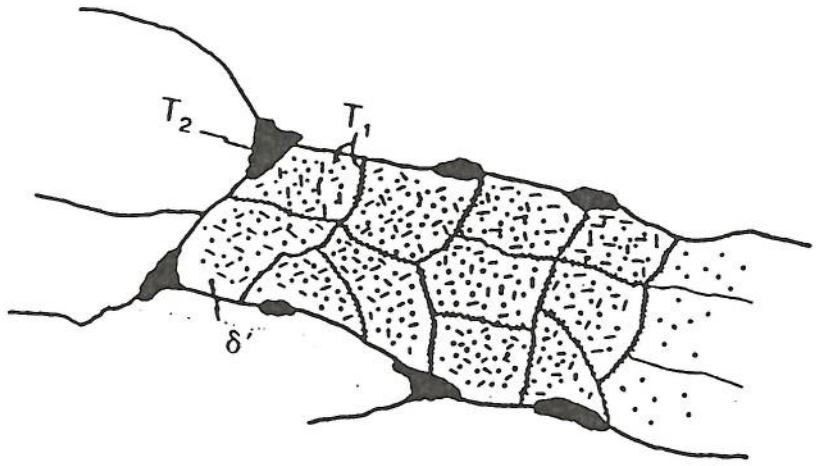

Figure 2.11. : Microstructure of 2090 after ageing to the peak - aged condition (67).

2.2.2.2.3. Zirconium Additions

This element acts as a grain refiner and recrystallisation inhibitor (23, 50). It is a dispersoid forming element which controls the final grain structure and is present as a fine dispersion of metastable and coherent, cubic β' (Al_3Zr) particles. This β' phase also acts as a preferential nucleation site for δ' (it has the same $L1_2$ type structure), is highly resistant to dislocation shear, the volume fraction of β' through small additions of zirconium is high enough to improve the mechanical properties (68) and AlLiZr alloys tend to age more rapidly than similar alloys (69). With the fact that β' acts as nucleation sites for δ', the major microstructural feature in AlLiZr alloys is the presence of composite particles where δ' grows on a β' core. These composite particles continue to grow at the expense of the smaller δ'.

In alloys containing both copper and magnesium such as 8090 and 2091 (AlLiCuMg) other phases precipitate of which the S' (Al_2CuMg) phase, which is finer and more uniform than θ' and T_1, seems to have had the most attention (39, 50, 52, 60, 64, 68).

The addition of small amounts of magnesium to a high copper alloy such as 2090 suppresses the formation of θ' and introduces the S' phase. This phase has an orthorhombic crystal structure and appears as rods or needles along the {100} matrix plane. There are two ways in which the S' phase can nucleate (39) - firstly, excess copper and magnesium concentrations induced by the growth of δ' together with vacancies act as favourable nucleation sites and, secondly, nucleation occurs on matrix or subgrain boundary dislocations. In alloys with fairly high levels of magnesium such as 8090 only the S' is present (52). However, at lower levels of magnesium both the T_1 and S' phases are present in the microstructure. Thus the copper magnesium ratio within these alloys affects the S' precipitation providing improved combinations of properties for these materials.

2.3. Stress Corrosion Cracking

2.3.1. Introduction

Intergranular corrosion, exfoliation corrosion and, above all, stress corrosion cracking (SCC) can cause failures within structural components, reducing the service life of an aircraft. The initiation and propagation of stress corrosion cracks leading to these service failures can be caused by metallurgical, environmental or mechanical factors. In aluminium alloys with highly directional grain structures, SCC generally occurs along grain boundaries providing the alloy is susceptible, there is a specific environment (water vapour or aqueous halide solutions) and there is a sufficient tensile stress. SCC is associated with high strength, wrought aluminium alloys such as the 2XXX, 5XXX and 7XXX series alloys whereas 3XXX and 6XXX series are considered immune to SCC. In general, the stress is applied perpendicular to the grain boundaries where cracks can initiate and propagate with ease along these boundaries. The occurrence of internal, residual stresses present in thick sections of plate caused by heat treatment and the fabrication process can lead to stresses high enough to cause SCC. There are a large number of sites from which these cracks can initiate (70). These include stress raisers, corrosion pits, fatigue cracks and areas of intergranular corrosion.

2.3.2. Proposed Mechanisms for Stress Corrosion Cracking in High Strength Aluminium Alloys

There has been a large number of researchers who have proposed several mechanisms for the SCC of aluminium alloys. These mechanisms fall into three main categories which are anodic dissolution (cracking due to preferential corrosion along grain boundaries), hydrogen embrittlement (weakening of the grain boundaries due to the absorption of hydrogen) and passive film (rupturing of the passive film along grain boundaries leads to cracking). There are several sub - models within the three main mechanisms mentioned above.

Stress has always played a major role in the SCC of aluminium alloys. Logan (71) measured electrochemical solution potentials of stressed, notched specimens. The greatest change in potential was recorded in the plastic deformation region of the stress - strain curve which was attributed to a repair mechanism of the oxide film. It was concluded that the mechanism of SCC was that of film - rupture. Higher stresses lead to an increase in the crack growth rates.

2.3.2.1. Anodic Dissolution

In the anodic dissolution model there is a potential difference between the grain boundaries and the matrix due to the formation of precipitates along the boundaries. In a corrosive environment these precipitates become anodic relative to the matrix and become sites of corrosion attack. Early work at Alcoa (72) demonstrated the relationship between microstructure and corrosion attack in alloy 2024. It was concluded that the intergranular attack was due to the anodic dissolution of the depleted zone present along the grain boundaries. In a review of many authors work, Gruhl (73) stated that AlCuMg alloys are regarded as SCC susceptible. The main factor responsible is that of intergranular corrosion which occurs without stress but is accelerated under stress (74).

Work carried out by Sugimoto et al (75) and Urushino et al (76) looked at the

stress corrosion lives of Al-4%Cu and AlCuMg alloys in relation to pitting potentials in a 1M NaCl solution. In the aged conditions alloys susceptible to intergranular corrosion and SCC have two pitting potentials - one for the grains and one for the grain boundaries. The pitting potential for the grain boundaries is lower than that for the grains and selective attack of these boundaries by Cl^- ions in solution occurs at potentials above that for the grain boundaries. This type of attack promotes intergranular SCC at these potentials if a tensile stress is applied where mechanical tearing enhances the dissolution reaction. Sugimoto (75) showed that the SCC is related to the pitting dissolution in the grains or grain boundaries - in the over - aged condition pitting within the matrix affects SCC whereas in the initial stage of ageing, pitting along the grain boundaries leads to SCC. Precipitates along the grain boundary act as cathodic sites and SCC results from the selective attack of copper denuded zones along the grain boundaries. Preferential dissolution along grain boundaries is caused by the copper depletion in the precipitate free zone (74). Changes between the two pitting potentials of the grains, E_{pit} (matrix), and grain boundaries, E_{pit} (G.B.) during ageing affects the susceptibility to SCC. This change in potential can be seen in figure 2.12 (76). The maximum difference between the two potentials relates to the maximum SCC susceptibility ie when the grain boundaries are attacked. Potential differences also affect the failure mode - transgranular attack occurs at low differences and intergranular attack prevails when the difference increases. Urushino (76) concluded that SCC in 2024 is a direct result of pitting dissolution of the solute - denuded zones along the grain boundaries. Figure 2.13 shows schematic models put forward by Sugimoto (75) and Urushino (76).

Anodic dissolution also occurs in many aluminium - lithium alloys. Rinker et al (77) studied the SCC resistance of 2020 and showed that preferential corrosion of the T_1 phase results in SCC. The electrochemical potential difference between the T_1 precipitates and the interior of the grains provides the driving force for the preferential dissolution of these precipitates. The resistance to SCC of 2020 was higher than that for 2024 because of a reduced tendency for the formation of copper depleted zones at the grain boundary. Buis (78) evaluated the SCC of 2090 in artificial seawater under constant immersion. Cracks initiated from corrosion pits and some stress corrosion failures occurred

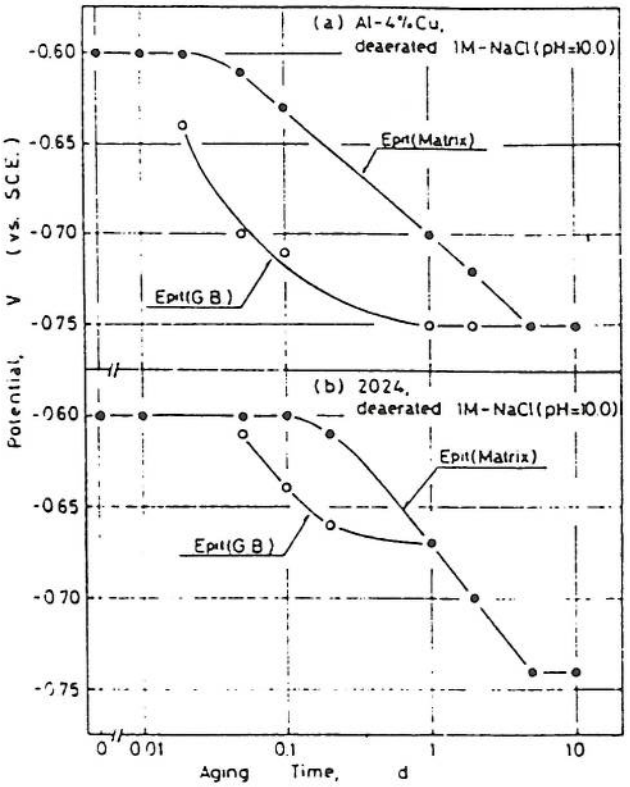

Figure 2.12. : Difference in pitting potentials between the grains and grain boundaries for Al-4Cu and 2024 in 1M NaCl (76).

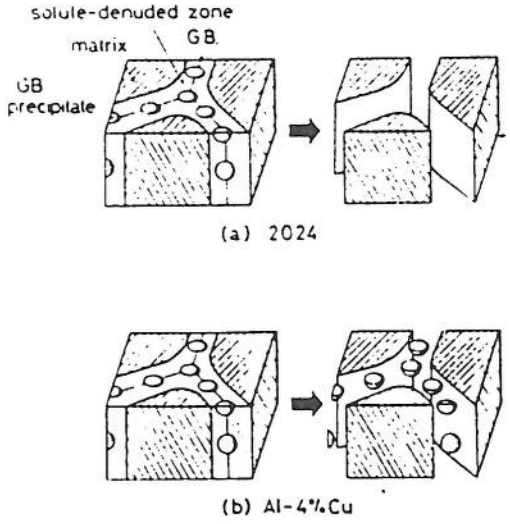

Figure 2.13. : Models for intergranular SCC in 2024 and Al-4Cu alloys (76).

at loads lower than the yield strength. In NaCl solutions the corrosion can be extensive enough to lower the stress corrosion susceptibility by producing large, blunted cracks, reducing the possibility of crack nucleation. In artificial seawater the corrosion susceptibility is lower which inhibits the formation of blunt cracks and stress cracks can initiate rapidly. In the initiation stage of the electrochemical corrosion reaction the protective oxide layer is weakened and ruptured. During propagation, metallic ions build up at the crack tip which hydrolise resulting in a local acidic solution. This led to the possibility of both hydrogen and local anodic dissolution causing SCC of 2090 in artificial seawater. However, it was concluded that anodic dissolution by the preferential dissolution of the T_1 phase was the mechanism of SCC under these conditions.

2.3.2.2. Hydrogen Embrittlement

Lumsden and Allen (79) evaluated the SCC of 8090 by using the slow strain rate method in 0.5M NaCl solution. For the three ageing conditions - under - aged, peak - aged and over - aged, samples failed by SCC at a potential of -700mV but did not fail by SCC at lower potentials. An increase in the susceptibility to SCC as the strain rate decreased led to the idea of a film rupture - anodic dissolution model. Crack growth results from dissolution following the strain - induced rupture of the passive film at the crack tip. Another possibility of the failure mode was that of hydrogen induced cracking where the susceptibility of SCC increases as the testing time increases. It proved difficult to identify the failure mechanism - whether by hydrogen induced cracking or film rupture - anodic dissolution. However, Disson et al (80) put forward that the mechanism of SCC for 2091 was a combination of anodic dissolution and hydrogen embrittlement. Specimens were subjected to permanent and alternate immersion tests in 3.5% NaCl solution together with additions of hydrogen peroxide where the time to failure and the fracture surfaces were examined. During anodic polarisation the SCC was accelerated whereas, under cathodic polarisation there seemed to be no SCC which confirmed an electrochemical mechanism. A loss in ductility was observed during mechanical overload at the end of testing showing an intergranular zone of propagation on the fracture surface which was attributed to hydrogen embrittlement. The occurrence of hydrogen embrittlement in high

strength aluminium alloys suggests that SCC may be controlled by the direct action of hydrogen in these materials rather than anodic dissolution.

The contribution of hydrogen induced cracking to SCC is mainly attributed to the 7XXX series alloys and an extensive report by Burleigh (81) has showed this to be the case. Hydrogen is suspected in SCC for the following reasons - discontinuous cracking process, small influence of corrosion, existence of an SCC threshold stress, pickled aluminium specimens are more susceptible and higher hydrogen concentration at the grain boundaries. The detrimental effect of internal hydrogen on the ductility of high strength AlZnMg alloys was first investigated by Gest and Troiano (82). They looked at the effect of hydrogen permeation of SCC under anodic and cathodic conditions. SCC failures occurred by hydrogen permeation at the cathodic, anodic and rest potentials by a form of discontinuous cracking. A literature review by Gruhl (73) on AlZnMg(Cu) alloys proposed that corrosion produces hydrogen which diffuses into the grain boundaries and embrittles them. The separation strength of the grain boundaries is reduced when hydrogen is present. Tensile stresses effectively open up the lattice allowing more hydrogen to diffuse inward. Yan Yin (83) speculated that hydrogen not only weakens the bonding of the grain boundaries but also weakens the bonding between the constitute phases and the grain boundary. A higher volume of hydrogen produces more weakened zones increasing the susceptibility to SCC. The Mg - H complex plays an important role - it accelerates the transport of hydrogen to the grain boundaries. Only grain boundaries which form a favourable path relative to the stress direction suffer from embrittlement and when the stress exceeds the remaining strength failure occurs. Figure 2.14 shows a schematic representation of different orientations of grain boundaries perpendicular to the applied stress.

Koch (84) exposed specimens of 7075 alloy in hydrogen gas and several cracks were observed on the specimen surface. When these specimens were pulled in tension failure initiated at these cracks and the fracture surfaces showed intergranular cracking which was perpendicular to the applied load. It was suggested that hydrogen diffuses along the grain boundaries ahead of the crack tip and plastic deformation of the precipitate free

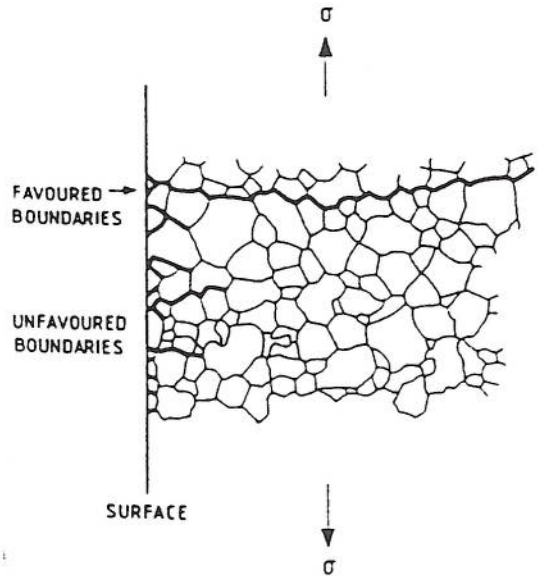

Figure 2.14. : Development of brittle grain boundaries under applied stress (73).

zone increases the mobility of hydrogen. Wu - Yang Chu et al (85) studied the nucleation and propagation of hydrogen induced cracking and SCC in 3.5% NaCl and pure water. Charging the specimens produced a plastic zone ahead of the crack where hydrogen had diffused which increased with time. The growth of cracks in specimens exposed to aqueous solutions was the same as for the charged specimens which suggested a hydrogen induced delayed cracking mechanism. Baumgartner (86) stressed specimens of $AlZnMg_3$ and the crack growth was not a continuous process but found to be a discontinuous process of jumps and stops carried forward by hydrogen embrittlement. Regions of high stress intensity are the favourable sites for hydrogen absorption. It was concluded that the presence of precipitate free zones diminishes the stress and slows the crack growth. Kim et al (87) studied the effect of hydrogen recombination poisons on SCC initiation and propagation in aluminium alloys. It was concluded that the anodic dissolution rate and the hydrogen reduction rate decreased due to the inhibition of hydrogen recombination. The initiation and propagation of SCC decreased in the presence of the poisons due to enhanced hydrogen permeation to the crack tip and the time to failure decreases as the concentration of the poison increases.

The formation of hydrides in aluminium alloys also affects the SCC of these materials (84, 88, 89). Hydrides formed from solid solutions lead to large volume changes and are present in the microstructure under high stresses. This volume change applies a tensile stress to the surrounding matrix. Koch (84) observed flakes of AlH_3 on the fracture surfaces of 7075 and speculated that the embrittlement of this alloy could be due to hydride formation. Chene et al (88) found that, after charging, some of the hydride AlH_3 is present in the microstructure. It was also shown that decohesion of the Al_2CuMg type precipitates which was due to the preferential interaction of hydrogen with this phase leads to embrittlement. The magnesium present segregated to the grain boundaries during ageing and interacted with hydrogen to produce Mg or Mg - Al hydrides. The hydrides which form in aluminium - lithium alloys are of the form $LiAlH_4$ (89) and the formation of these hydrides is sufficient for environmental embrittlement. The ease of crack initiation at the grain boundaries can be explained by the failure of brittle hydrides at these boundaries.

The role of hydrogen embrittlement has also been studied in a 2024 alloy in the longitudinal direction on the reduction of fracture area in tensile specimens by Zeides and Roman (90). It was suggested that hydrogen embrittlement is caused by hydrogen induced enhancement of plastic deformation localisation. A ductile mode of fracture resulted from the formation, growth and linking of voids within the specimen. A film fracture morphology was evident on the fracture surfaces where the film appeared cracked which was attributed to a "mud - crack" pattern. This was believed to be the result of mechanical damage due to hydrogen induced plastic shear localisation accompanying fracture development.

A film - induced cleavage model has been observed by Pugh (91) which contributed to transgranular stress corrosion cracking (TGSCC). This was different from the fracture related to the anodic dissolution at the crack tip for intergranular SCC. TGSCC failures occurred by cleavage - discontinuous brittle fracture through the grain boundaries.

2.3.3. Testing Methods for Stress Corrosion Cracking

In a recent review of testing environmental assisted cracking (92) which is a time dependent process, standard test methods can be divided into the following groups:

1) Constant total strain.
2) Constant load.
3) Dynamic straining.

The laboratory testing is accelerated to make a comparison with service lifetimes. This can be done by applying severe mechanical stressing, more severe environments, raising the temperature and anodic or cathodic polarisation. The laboratory testing is sometimes carried out on unstressed specimens to evaluate the effect of residual stress or hydrogen charging on crack formation and propagation. In constant total strain, testing can be carried out on sheet or plate material. A typical example is the bend test which can be of the form of two, three or four - point loading. The four - point bend test is the most popular test of the three due to a larger area of uniform stress. Other tests utilising total strain make use of different specimens examples of which are the C ring and tuning fork specimens. In constant load testing, as the test time increases, there is an increasing stress due to the reduction in cross sectional area of the specimen by corrosion in a corrosive environment. For assessing the susceptibility to SCC the time to failure is measured and can be evaluated over a range of applied stresses. The simplest method of applying a constant load is the use of a dead weight suspended on one end of a specimen. Dynamic straining makes use of the slow strain rate test which consists of subjecting a specimen to an increasing strain in a specific environment. The environment normally consists of an aqueous 3.5% NaCl solution to which varying additions can be added to increase the corrosivity of the solution. The test can be used in tension or bending on plain, notched or precracked specimens. An advantage of this test is that the susceptibility to SCC can be assessed at an early stage. The common parameters which are used to assess the susceptibility are - time to failure, ductility, maximum load achieved and the percentage of SCC on the fracture surface. The average

SCC velocity may be estimated from the length of the longest crack on the fracture surface divided by the time of testing to failure. Crack initiation differs for different materials as the cracks initiate from pits within the structure when subjected to a corrosive environment.

2.3.3.1. Directional Effects on Stress Corrosion Cracking

The highly directional grain structure in aluminium alloys influences the mechanical properties and resistance to SCC. For these materials, testing can be carried out in a number of directions. The two main orientations for testing is where the load can be applied parallel (longitudinally) and in the short transverse direction (perpendicularly) to the principal grain axis. Work carried out by Ugiansky et al (93) looked at the directional effects in the SCC of tensile specimens in a 7075 aluminium alloy. The stress corrosion times to failure changed considerably in different orientations. Although the same applied load was used, cracks initiated at almost the same time for the longitudinal and transverse specimens but crack propagation was more difficult in the longitudinal specimen as the crack path lay along grain boundaries parallel to the stress direction. This can be illustrated in figure 2.15 where the straighter path for longitudinal grains gave the higher SCC susceptibility due to an easier pathway for crack propagation coupled with a higher resolved stress normal to the grain boundaries. In the longitudinal direction the crack must deviate greatly from a plane normal to the applied stress. As several specimens were machined from different parts of the plate material, it was shown that the susceptibility to SCC in the orientations tested increased toward the centre of the plate.

Figure 2.16 shows the orientation effects on the resistance to SCC as reported by Sprowls and Brown (94). The lowest resistance to SCC occurs when stressing perpendicular to the principal grain axis in the short transverse direction for an elongated microstructure.

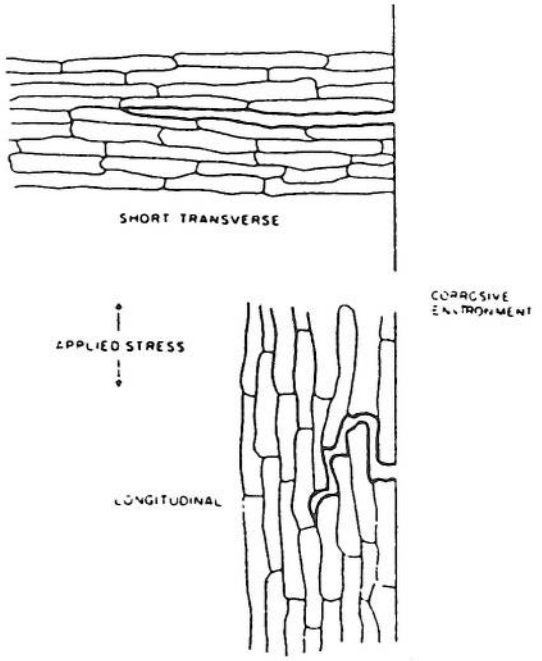

Figure 2.15. : Diagram showing the stress corrosion propagation through an elongated grain structure when stressed in the short transverse and longitudinal directions (93).

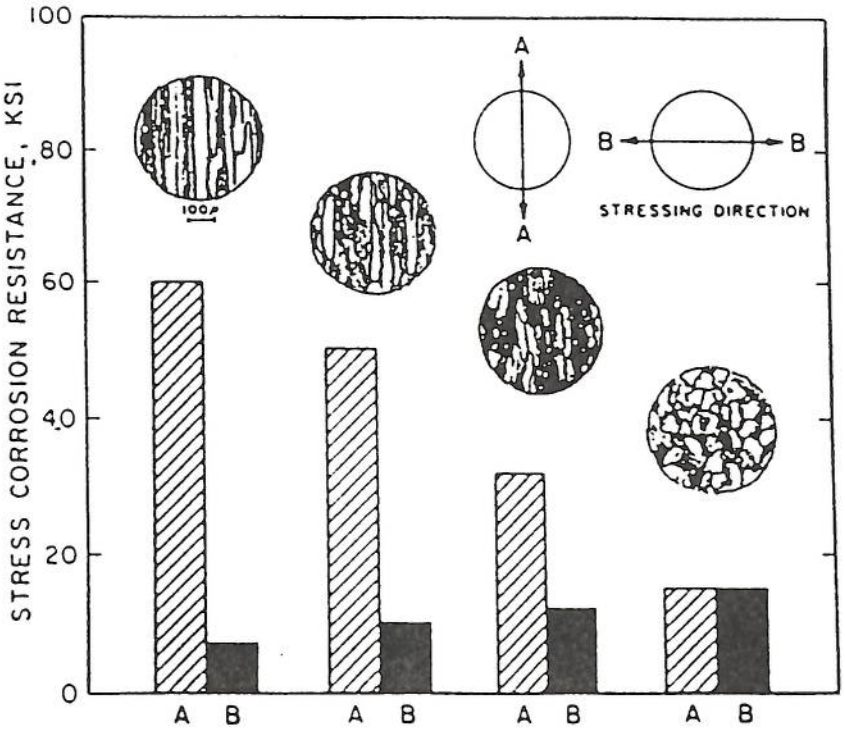

Figure 2.16. : Graph showing the effect of grain geometry and stressing direction on stress corrosion resistance of 7075-T6 with, A parallel and, B perpendicular to the principal grain axis (94).

2.3.3.2. The V-K Diagram

In the use of smooth specimens for stress corrosion testing the failure is influenced by the fracture toughness of the material. However, by using precracked specimens for stress corrosion testing a better comparison can be made with structures in service as they may contain notches or flaws which intensify the stress. This testing involves subjecting a specimen, in which a crack has been developed from a machined notch, either to a constant load at the loading points or to an increasing load during exposure to an aggressive environment. Precracked specimens make use of fracture mechanics to establish a stress intensity factor, K, and the crack propagation velocity (time taken for a certain crack length). The resistance to SCC under stress and in the presence of a flaw can be measured by using its crack velocity verses stress intensity curve. This plot is called the V - K diagram and can be seen in figure 2.17 (95).

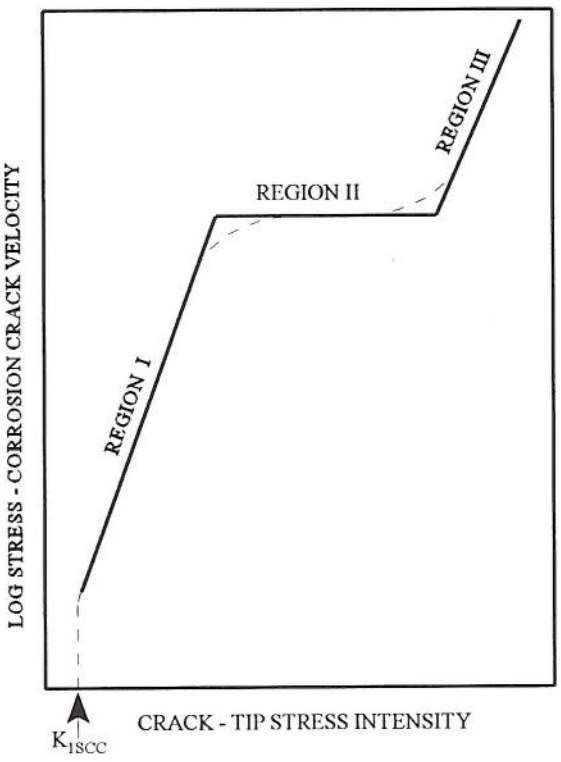

Figure 2.17. : Diagram showing the effect of stress intensity on the growth rate of stress corrosion cracks (95).

There are three parts to the V - K plot:

1) Region I which is at low stress intensities where the crack velocity is stress dependent.
2) Region II which is at intermediate stress intensities where the crack velocity is stress independent.
3) Region III at high stress intensities and the crack velocity may be stress dependent.

Experimentally produced V - K plots for commercial alloys normally show regions I and II but not region III. In region I there is a linear relationship and region II exhibits a plateau velocity. Stage I behaviour produces the threshold stress intensity, K_{ISCC}, below which no crack growth occurs. For aluminium alloys, K_{ISCC} values occur at stress intensities where crack growth rates are extremely low. The K_{ISCC} value is normally recorded when the crack velocity falls to $10^{-10}ms^{-1}$. The type of specimen mainly attributed to work associated with the V - K plot is that of the double cantilever beam (DCB). This type of specimen is very convenient to use and it can be tested in different orientations from the wrought product, usually in plate form. The stress intensity factor can be calculated from the knowledge of the crack length, displacement, modulus of the material and half width of the specimen.

Blain et al (96) used constant loading of specimens (increasing K values) and constant displacement (decreasing K) to determine the accuracy of K values calculated for the crack tip on specimens of 2024. DCB specimens were tested in the short transverse and short longitudinal directions. It was concluded that the short transverse direction provided a more direct path for stress corrosion to propagate along due to the more elongated grains. The results for the stress intensities were plotted on a V - K diagram and the true stress intensity differed from the measured value due to the formation of corrosion product or residual stresses at the crack tip. Dorward et al (97) tested 7XXX and 2XXX series alloys in a marine atmosphere and concluded that corrosion product wedging which leads to self - loading conditions affects the crack growth resistance of aluminium alloys. It was found that an increase in the copper content and a greater susceptibility to exfoliation corrosion increased self - loading

conditions. In the under - aged condition alloys such as 2014 and 2024 were prone to self loading but ageing to an over - aged condition rendered the material resistant to wedging. Lee and Pyun (98) studied the corrosion potential, corrosion rate and critical plane strain stress intensity for SCC K_{ISCC} of 2024 DCB specimens in a $NaCl + H_2O_2$ test solution. Region II of the V - K diagram was shortened as the ageing time increased to an over - aged condition increasing the failure time. The susceptibility of SCC can also be determined by K_{IC} which is the initial stress intensity. The greater the difference between K_{IC} and K_{ISCC} the greater the susceptibility to SCC. This ratio decreased as the ageing increased.

2.3.3.3. The Slow Strain Rate Test

The use of the slow strain rate test in determining the susceptibility has been investigated. Lumsden and Allen (79) strain tested 8090 under deaerated conditions in a 0.5 M NaCl solution and looked at the ageing condition and strain rate effects on the susceptibility to stress corrosion. The alloy was susceptible to SCC in all the under - , peak - and over - aged conditions during strain rate testing but the maximum susceptibility occurred in the under - aged condition. As the strain rate decreased the susceptibility to SCC increased. A relationship between the strain rate and failure is important in that at high rates, specimens break mechanically and SCC does not have time to occur, whereas at slow rates, repassivation of a protective film takes place. Maitra (99) tested tensile specimens from a 2124 alloy using the slow strain rate technique and alternate immersion. Tests showed that in the over - aged state no failure occurred under alternate immersion. It was concluded that there was a good correlation between the two testing methods with the slow strain rate being more reproducible, quicker and cheaper than the conventional alternate testing.

2.3.3.4. Alternate and Permanent Immersion Tests

The more conventional testing methods are those of alternate and permanent immersion. Alternate immersion normally involves subjecting a specimen to a wetting and

drying cycle in a 3.5% NaCl solution. It has been shown that aluminium alloys which fail in alternate immersion tests can be immune to environmentally assisted cracking or do not exhibit sufficient crack growth when they are permanently immersed in 3.5% NaCl solution (70, 100, 101). Holroyd et al (100) showed that for immersed DCB specimens of 8090 (loaded to stress intensity factors approaching short transverse K_{IC} values) in a 3.5% NaCl solution, no crack propagation was observed up to three months of testing. Braun (101, 102, 103) showed that, in alternate immersion tests the SCC susceptibilities of a 2014 (101) in the short transverse direction, 8090 (102) and 2091 (103) in the longitudinal direction were very low and no failures were observed in constant immersion in 3.5% NaCl solution. However, if the test solution changes with additions such as 0.5% Na_2CrO_4 with a reduction in the pH to acidified conditions (pH = 3) failures do occur under constant immersion conditions (101). Braun (103) made a comparison between laboratory testing and outdoor exposure. For 2091 short transverse specimens SCC occurred after one year of outdoor exposure testing and the same SCC resistance was found in the alternate immersion test. This seemed to show that the alternate immersion test is a more reliable way of predicting the SCC life of aluminium - lithium alloys in natural environments. Kelly and Robinson (104) used EXCO solution to test unrecrystallised 8090 sheet material in constant immersion conditions under an applied load. The sheet material was attached to two mandrils to which a constant load was applied. The peak - aged material showed the least resistance to SCC.

2.3.4. The Effect of Microstructure and Heat Treatment on Stress Corrosion Cracking

Changes in the composition, grain structure and precipitate phases through additional elements and certain heat treatments affect the resistance to SCC in aluminium alloys. Alloying elements form solid solutions which alter the electrochemical nature within the structure. Minor alloying additions such as Cr, Mn, Zr, Ti, V and Ni can reduce the SCC susceptibility of aluminium alloys in the short and longitudinal directions. Major alloying additions such as copper and magnesium affect the susceptibility to SCC. It was shown (76) that an increase in the magnesium content of AlCuMg type alloys decreases the susceptibility. Maitra (105) studied the SCC in a 2124 alloy with differing copper

and magnesium contents. With a high magnesium content the $CuMgAl_2$ precipitate is dominant whereas, with low magnesium contents the $CuAl_2$ precipitate is dominant. Specimens containing $CuAl_2$ precipitates failed at shorter times than those containing the $CuMgAl_2$ phase. The difference between the susceptibility to SCC was attributed to the electrochemical nature of the precipitates.

In copper - rich aluminium alloys the stress corrosion susceptibility is reduced. The addition of copper has been found to improve the yield strength and stress corrosion resistance (70). Hardwick et al (106) studied the influence of copper additions in Al-6Zn-2Mg alloys and concluded that an addition of 2% copper, in combination with ageing to the peak - aged and over - aged conditions removed the susceptibility of hydrogen embrittlement. In comparison the original alloy containing 0.1% Cu showed hydrogen embrittlement for all ageing treatments. However, Holroyd et al (100) showed that the addition of copper to the AlLi binary alloy increases the susceptibility to stress corrosion. Meletis and Huang (107) showed that the increase in susceptibility was attributed to the formation of T_1 (Al_2CuLi) and that this phase was responsible for hydrogen entry into the structure. The T_1 precipitates at the grain boundaries are more reactive than those within the grains and reactivity increases when a stress is applied. Hongbin and Reshun (108) showed that the T_2 precipitates are responsible for the stress corrosion resistance in a 2091 alloy. It was shown that annealing prior to ageing reduces the volume fraction of T_2 at the grain boundaries which increases the resistance to SCC. Moore et al (109) studied the copper content in AlCuLi weldalite alloys which are high copper alloys (4.3 - 6.3% Cu) and, reducing the copper content increases the tensile ductility. Longer time to failure in tensile specimens was recorded with a decrease in the copper content. An increase in the copper content of an alloy makes the alloy more electropositive. Sarkar et al (110) showed that increasing the copper content decreased the crack velocity which was attributed to the electrochemical activity of the precipitates as a function of the copper content. A reduction in the rate of dissolution of the grain boundary precipitates and the reduced rate of hydrogen reduction and absorption at the crack tip at the more noble potential reduces the SCC. Over - ageing reduces the stress concentrations at the grain boundaries and increases the volume fraction of the precipitates. This increase in

the volume fraction produces a lower anodic current density, reducing the crack velocity.

Maitra (105) has shown the relationship between the grain morphology and SCC susceptibility in a 2124 alloy. The grain morphology was defined as the total grain boundary surface area per unit volume of the material (S_V) - S_V is a summation of the grain size and shape. An increase in the value of S_V results in a decrease in the failure under the alternate immersion test. However, it was concluded that it is a combination of the composition and S_V that affects the resistance to SCC.

There have been many studies on the influence of ageing on the stress corrosion resistance in aluminium alloys. Generally, the under - aged alloy shows the most susceptibility with resistance increasing as the ageing continues to the over - aged condition. Figure 2.18 (70) shows the relationship between strength, stress corrosion susceptibility and heat treatment in aluminium alloys.

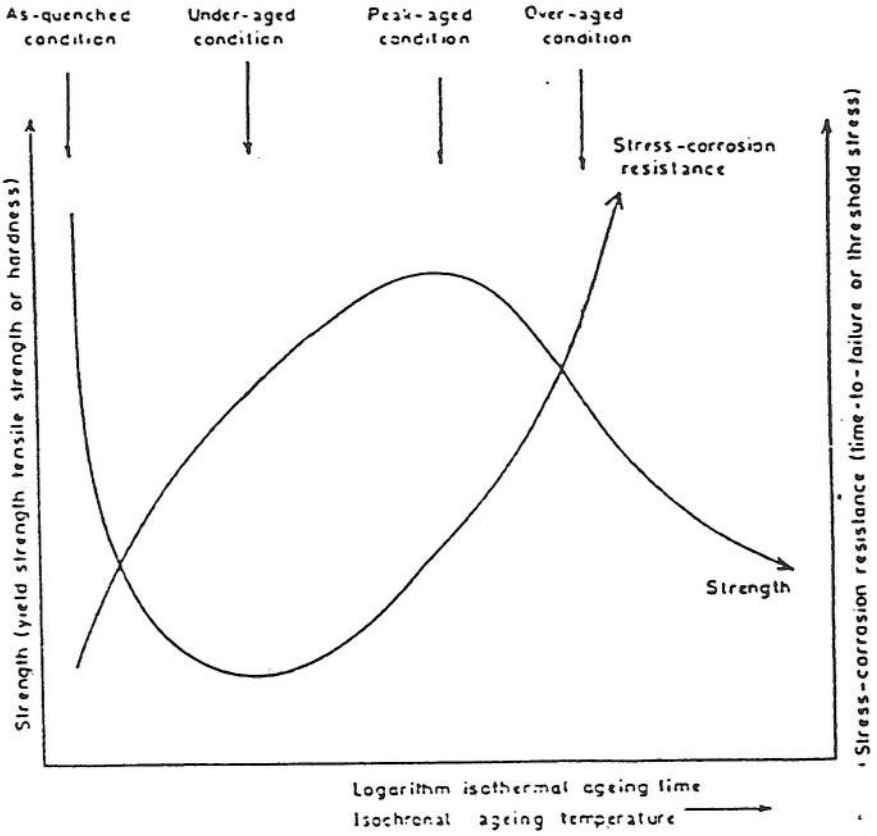

Figure 2.18. : Diagram showing the effect of heat treatment on the stress corrosion cracking susceptibility of aluminium alloys (70).

Studies on the heat treatment effects in Al-4Cu (75) and AlCuMg alloys (76) have shown that, as ageing increases the susceptibility decreases. The least resistance was found during the early stages of ageing for both the binary alloy and the more complex alloy. Plots of ageing time against stress corrosion life can be seen in figures 2.19 and 2.20. In the Al-4Cu alloy, a lower ageing temperature of 130^{0}C increased the time to reach maximum susceptibility as compared to ageing at 170^{0}C where the maximum occurred after a few hours of ageing (near to the over - aged condition). Lee and Pyun (98) heat treated a 2024 - T6 specimen at 170^{0}C, 190^{0}C and 220^{0}C for five hours to the under - , peak - and over - aged conditions. In the initial stage of ageing up to the peak - aged condition precipitation takes place at the grain boundaries resulting in a more anodic corrosion potential and precipitation is negligible during over - ageing. This results in a differing SCC behaviour - interparticle spacing in the under - aged condition and dislocation movement through the precipitates in the grains in the over - aged condition causes a stress concentration at the grain boundaries. Zailiang et al (111) subjected an AlCuMgSi alloy to two - step ageing which made the SCC sensitivity decrease dramatically and the crack growth rate decreased by two orders of magnitude. It was concluded that an ageing treatment of 160^{0}C at eight hours followed by 190^{0}C at two hours produced the best SCC resistance and high strength. GP zones and θ" form under the initial ageing treatment and large precipitates of the θ phase form by the second ageing treatment on the grain boundaries which increased the resistance to SCC. It was concluded that the GP zones and the θ" phase are the most sensitive and the θ phase does not have any sensitivity to SCC.

Dorward and Hasse (112) showed that the 2090 alloy was susceptible to SCC in the under - aged condition for both the short transverse and the more tortuous pathway in the longitudinal direction. The resistance improved in the peak - aged condition where SCC was virtually immune in the longitudinal direction. This was attributed to the grain boundary regions being anodic in the under - aged condition where the lithium containing T_1 phase is present. This phase dissolves preferentially leading to stress corrosion susceptibility. Gray (113) showed that the increase in susceptibility in the under - aged condition is attributed to the preferential dissolution of the grain boundary precipitates as

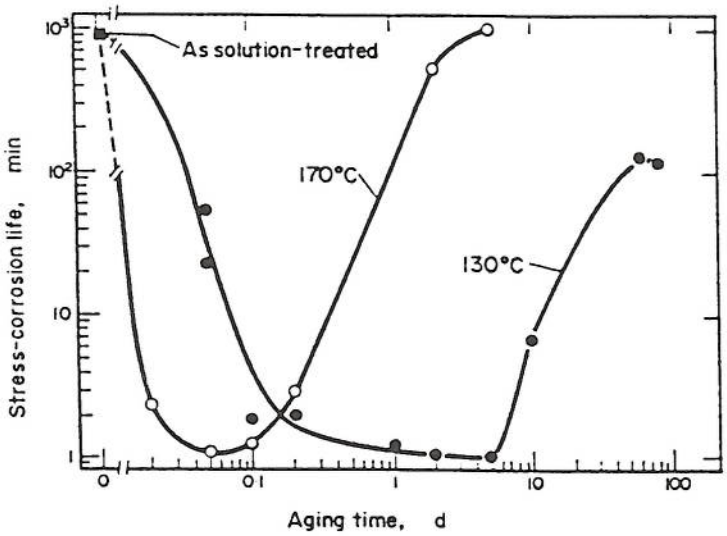

Figure 2.19. : Graph showing the effect of ageing time at 130^{0}C and 170^{0}C on stress corrosion life of Al-4Cu (75).

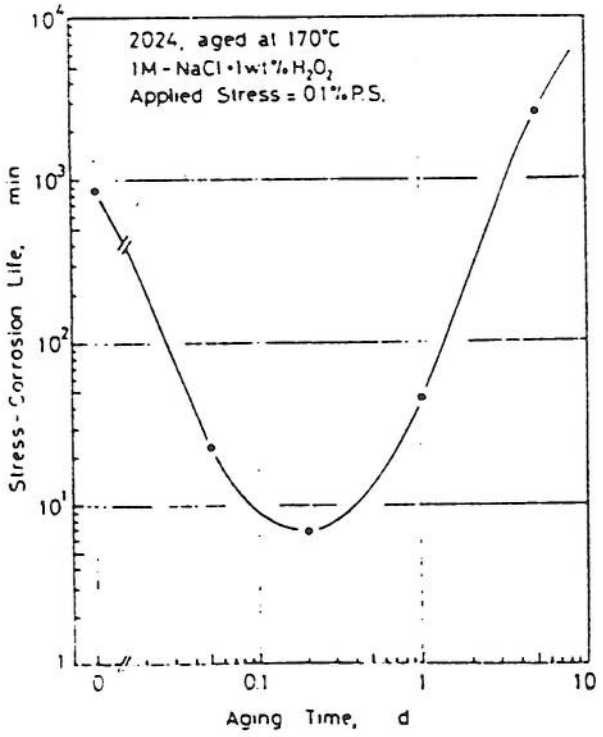

Figure 2.20. : Graph showing the effect of ageing time at 170^{0}C on stress corrosion life of 2024 (76).

a result of the potential difference between the anodic grain boundary and the matrix. Two - step over - ageing results in a reduction in the potential difference which reduces the driving force for SCC. However, it has also been shown that the under - aged condition shows the best SCC resistance. Zhengfu et al (114) tested the influence of applied potentials and heat treatment on an AlLiCuMg alloy and found that the peak-aged condition gave the worst SCC resistance. It was concluded that the presence of the T_2 phase present along the grain boundaries in the peak - aged condition was anodic relative to the matrix resulting in a high anodic current density and a high driving force for SCC. This phase was not present in the under - aged condition and present in the over - aged condition only in a small volume fraction.

2.4. Corrosion of Aluminium Alloys

2.4.1. Introduction

The susceptibility of high strength aluminium alloys such as the 7XXX and 2XXX series to corrosion is due to precipitation which results in the formation of continuous anodic paths in or close to the grain boundaries. Most forms of corrosion are electrolytic in nature and affect the internal structure of the material. In general corrosion may be classified under the following headings (115):

1. General surface attack.
2. Pitting corrosion.
3. Intercrystalline corrosion.
4. Exfoliation corrosion.

Figure 2.21 (116) shows a diagrammatic representation of the effects of corrosion.

The general surface attack results from dissolution of the protective oxide film. Pitting corrosion arises from local attack originating from point heterogeneities and forms randomly distributed pits over the surface of the material. Points of initiation can be

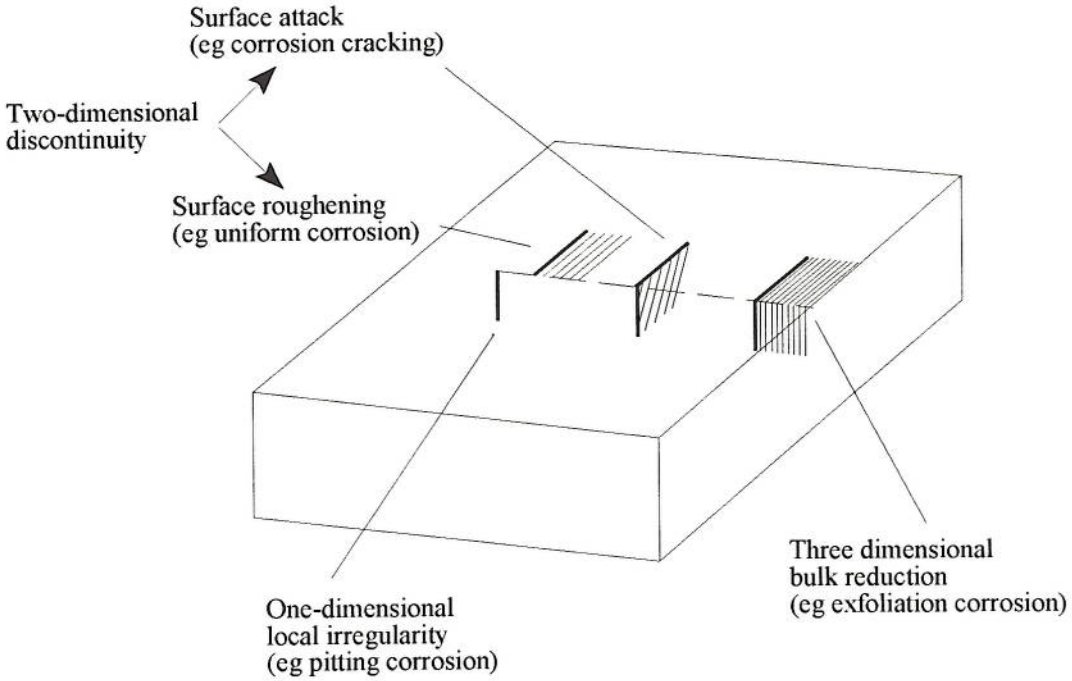

Figure 2.21. : Diagram showing the physical effects of corrosion on aircraft materials (116).

intermetallic particles in the material, defects in the protective oxide film or the prolonged exposure to droplets of moisture. Intercrystalline (intergranular) corrosion results from preferential dissolution of the metal along grain boundaries without any appreciable attack in the grains. The presence of precipitation results in the anodic paths required for this type of corrosion. Although corrosion products are formed as a result of this attack, these are not voluminous. Wetting or the presence of condensation are the basic environmental requirements for intercrystalline corrosion and the presence of halides such as chlorides accelerate the corrosion. Exfoliation or layer corrosion is a type of intercrystalline corrosion in which the metal disintegrates into layers. Attack can proceed along multiple grain paths parallel to the surface of the material. Most of the high strength, heat treatable aluminium alloys are susceptible to exfoliation corrosion. This is due to the fact that they possess a highly elongated grain structure present in rolled, extruded or forged products. The ratio of the grain length and width can be expressed

as the aspect ratio of the material and, as this increases the susceptibility to corrosion increases. Corrosion products build up along each pathway and introduce internal stresses within the structure as the products are more voluminous than the original material. These stresses cause layers of material to open like the pages of a book. Testing for exfoliation corrosion is normally carried out using NaCl containing solutions in the laboratory but corrosion also occurs in the environment. The major difference among all the above - mentioned types of corrosion in aluminium alloys is that intercrystalline and exfoliation corrosion are insidious - the depth of attack and the extent of damage within the material are not visible to the naked eye.

Exfoliation corrosion can reduce the service life of an aircraft, increase maintenance and repair costs and cause structural failures. Due to the insidious nature of this attack repair of damage is difficult and time consuming. After repair it is not always possible to tell whether all of the corrosion has been completely removed. In extreme cases where extensive repair has to be made the complete panel or area is replaced. Commercial aircraft are exposed to corrosive environments constantly and, with investments up to $100 million per unit for wide body aircraft, full scale inspections to determine structural integrity often exceed $2.5 million (116). In a dry climate corrosion takes place slowly, however, a warm, wet climate with salt water present increases the severity of attack. If any light corrosion on the aircraft is missed under inspection, the corrosion can continue very rapidly in the warmer climate.

2.4.2. Occurrence of Exfoliation Corrosion

Most of the structures that have been built from high strength aluminium alloys have suffered from exfoliation corrosion after many years of exposure to marine or polluted atmospheres. Aluminium alloys are not only used for aircraft but also military equipment, civil structures, packaging and engineering. In the extreme case exfoliation corrosion has been reported on structures such as clothes posts where an AlCuMg alloy, HE15, used as tubes for these posts suffered corrosion in ordinary atmospheric exposure conditions (117). 7075 aluminium die forgings used on the M16 rifle have been reported to suffer

from exfoliation corrosion (118). After three years in service in a hot and humid climate these forgings showed exfoliation which was due to contact with the hands of the soldier.

Although the 2XXX and 7XXX series alloys have been used in aircraft for many years the occurrence of exfoliation corrosion was not a major threat until the use of these materials in thick sections. Lifka (119) pointed out that, an increased reduction in area of the ingot produces higher grain directionality. In the thicker sections there is a greater tendency for intergranular corrosion due to slower cooling on quenching. In commercial structures the rivet or fastener holes provide favourable sites of initiation where the corrosive electrolyte can have easy access to the interior directional grain structure, and exfoliation can occur without a lengthy incubation period (120). This is a type of "end grain" attack where the ends of the grain boundaries are exposed allowing fairly rapid initiation and propagation. Exfoliation corrosion has been reported on the wing skins of the F101 Voodoo aircraft (121). The first signs of corrosion occurred after three to four years of service mainly in warm, marine environments. The main initiation points seemed to be rivets made from 2024 aluminium alloy. Action was taken to combat this problem especially after corrosion of the under wing skin threatened the structural integrity. The lower wing skins were replaced and type 305 stainless steel fasteners were used rather than those of 2024. Each fastener was coated with zinc chromate putty which seemed to reduce the corrosion problem. With the fact that the environment plays a major part in the exfoliation corrosion of aircraft materials, leaving the planes exposed on the flight deck of an aircraft carrier can cause severe problems over time (122). This is due to the combination of attack from sea spray and sulphur from exhaust fumes. Exfoliation seems to be most prevalent in alloys which are exposed to marine and industrial environments (123).

Exfoliation corrosion is by no means restricted to the outer surfaces of aircraft structures (124). Internal areas such as galley locations where liquid spillages such as coffee can cause problems, toilets and washing areas, freight holds where corrosion results from spillages from the cargo and the fuselage skin where soundproofing can absorb condensation and lie like a wet blanket against the structure. A typical list of

contaminants can be seen in table 2.2 (124).

Table 2.2. : List of Contaminants and Conditions for Corrosion Initiation (124).

Base airport and Operational Environment	Operational/Maintenance Materials and Hazards
Climate/humidity.	Oils and hydraulic fuels.
Location relative to seawater.	Cleaning materials and paint strippers.
Condensates from passengers and live stock.	Maintenance actions causing scratches and abrasions.
Airborne salts and industrial impurities.	Accidental damage during maintenance and in operation.
Sunlight and ozone affecting rubber and plastic materials.	Battery acid.
Runway salts and contaminants.	Exhaust gases.
	De - icing and de - frosting fluids.
	Toilet and galley spillages.
	In flight turbulence causing spillage.
	Cargo breakage and/or spillage.
	Contaminated fuel (kerosene).

Liang (125) showed that aluminium alloys in aircraft fuel tank compartments corrode due to condensed water. It was shown that, in some instances the relative humidity in these compartments can be as high as 100% and condensed water drips can be found on the walls. The formation of the condensed water results from the fact that the aircraft is not waterproof and moisture and rainwater can penetrate into the fuselage and to the fuel tank compartment. It was found that the condensed water contained relatively high levels of ionic chloride and sulphate which increase the corrosiveness of the corrosion medium resulting from HCl, NaCl and SO_2 which exist in the atmosphere in polluted areas. Microbial sludge can have a profound effect on the corrosion of wing tank skins (126).

It has been shown that the existence of exfoliation corrosion in an aircraft can affect the fatigue life. Shaffer et al (127) found that the existence of exfoliation corrosion reduced the fatigue strength of spar caps made from 7075 alloy. Compared to the same

components which were uncorroded this reduction amounted to 40 - 60%. It was found that as the severity of the exfoliation increased the reduction in the fatigue life increased ie there is an increased number of sites for the initiation of fatigue cracks. Work carried out at Cranfield by Morad (128) on an AlCu alloy using push - pull fatigue test equipment showed that a reduction of up to 96% in life can be achieved by severely corroding rods of the AlCu alloy in EXCO solution.

It has been shown that the surface finish can affect the corrosion on aluminium alloys (129). In this investigation specimens of 7075 with a lapped surface were compared to those with an abraded surface. In the initial stages of corrosion the abraded specimens exhibit a faster corrosion rate due to a higher surface area and flaw density resulting from higher surface roughness. As corrosion continues the reverse is experienced - lapped specimens show the faster corrosion rate due to the fact that the abraded surface breaks up the continuous path of material and corrosion slows once precipitates are preferentially dissolved. Abraded specimens show more uniformly distributed and shallower pits than exhibited on the lapped specimens.

2.4.3. Exfoliation Corrosion Testing

2.4.3.1. Laboratory Testing

Exfoliation corrosion has been known for many years now, and the first type of test was that of the salt - spray test which was developed by J. Capp (130) around 1914 in order to rapidly assess materials for use in coastal or marine environments. This, and other early laboratory tests used to identify exfoliation corrosion were deemed inconclusive due to the fact that, in the majority of cases only pitting corrosion was observed. Since then, the development of corrosion testing has led to numerous accelerated tests in the form of total immersion or cyclic salt - spray tests all of which can identify the susceptibility of aluminium alloys to exfoliation. These tests can distinguish between susceptible aluminium alloys, non - susceptible aluminium alloys and differing tempers. A suitable accelerated test normally provides fairly rapid corrosion - the total immersion test provides results within a few hours, whereas results are obtained within a few days for

salt - spray testing rather than several months for exposure to an aggressive marine environment. The cyclic test normally involves alternate immersion in 3.5% NaCl solution and the conditions are of practical importance because they simulate service conditions. This section deals with a review of some of the early efforts to develop suitable test methods for determining the susceptibility of aluminium alloys and the tests which are available today.

Liddiard et al (131) exposed an AlCuMg alloy, HE15, to intermittent salt spray exposures in neutral and acidified solutions using a humidity chamber. The main disadvantage of this testing was that of the time required to show signs of corrosion - long exposures of 80 to 100 weeks and even these did not show the type of corrosion that had occurred in marine environments. Immersion tests were also carried out in solutions containing 3% NaCl, 6% NaCl + 0.1% H_2O_2, 0.5N - NH_4Cl and tap water and no exfoliation was observed in any of the solutions even after three months of testing - only pitting corrosion occurred on the specimens. With the fact that neutral salt solutions only produce pitting attack rather than exfoliation a test was developed by Lifka and Sprowls (132) using 5% NaCl solution acidified to pH 3 using acetic acid. This type of test is commonly known as the MASTMAASIS test (Modified ASTM Acetic Acid Salt Intermittent Spray) and involves subjecting specimens in a chamber to a six hour cycle which is a three stage cycle - spraying the specimens with the 5% NaCl solution, purging and drying at a high relative humidity. One major advantage of this test is that several specimens can be tested in the cabinet at any one time. The solution in the cabinet appears as a fog as it is atomised while it passes through the nozzle and the purging stage removes this from the cabinet which allows the corrosion product to remain and harden. This product causes delamination by exerting pressure on the material. The duration of the test tended to be around two weeks for susceptible alloys such as the 2XXX and 7XXX series and longer at four weeks for less susceptible alloys such as the 3XXX and 6XXX series. This test was deemed successful in that the corrosion products form at the site of corrosion attack and not away from it as in earlier immersion testing (131). Although the standard acetic acid salt - spray test required that the pH be around 3.1 to 3.3 the concentration of acetic acid in the solution varied from 3ml/l up to 6ml/l

to maintain the pH level constant. R. C. Spooner (133) showed that the addition of a constant volume of acid produced more consistent test results. This high acetic salt - spray test (HASS) was used for anodic films, painted aluminium panels and bare aluminium alloys. This test provided a means of testing which could distinguish between tempers in alloys such as 7075 but was not really accepted as a standard test.

Later work led to the development of the SWAAT test (134) (Sea Water Acetic Acid Test) which made use of a synthetic sea water environment acidified to a pH of around 2.8 using acetic acid. This test is another salt - spray test making use of a cabinet and cyclic conditions but, unlike the MASTMAASIS test there is no drying cycle, rather a soaking at 100% relative humidity. The duration of the test tended to be around one week. One advantage of the test is that it can distinguish between small differences in susceptibility of aluminium alloys and their tempers. This test was developed for the testing of AlZnMgCu and AlCu alloys. Ketcham and Jeffrey (135) subjected 2XXX and 7XXX series alloys to the MASTMAASIS and SWAAT tests making a comparison between the two test methods. It was suggested that the MASTMAASIS test gave better reproducibility and a greater deal of exfoliation on 2024 (used as a control alloy) than did the SWAAT test whereas, in the 7XXX series alloys the SWAAT test gave the better results. In the case of the AlZnMg alloys it was suggested the variability of results produced in the MASTMAASIS test was due to the fact that, both wet and dry bottoms were used in the cabinet producing varying humidity levels. It was suggested that increasing the concentration of acetic acid might improve the reproducibility of the MASTMAASIS test.

Another type of test equivalent to MASTMAASIS is that of the sulphur dioxide salt fog test (ASTM G 85.A4-85) which utilises a high humidity, salt containing environment. The acidifying species used is that found in service from stack gases, ie sulphurous acid. This type of testing has been successfully applied to structural materials, organic coatings and avionics (122). As with the other salt - spray testing 5% NaCl is used with sulphur dioxide injected into the cabinet for one hour at six hour intervals with a nominal cabinet temperature of around 35^0C. J. Thompson (136) used this test as well as the

MASTMAASIS test on aluminium - lithium alloys and found that only pitting had occurred for both tests. These tests were effective predictors of performance for other alloys such as 7075. In this work it was concluded that the laboratory techniques did not reproduce the macroscopic behaviour of alloys which had been subjected to aircraft carrier exposure. A comparison was made between the SO_2 salt fog and MASTMAASIS tests by Parzuchowski et al (137) and showed that the MASTMAASIS test caused greater attack of bare aluminium - lithium specimens. However, 2024, used as a control alloy, showed greater corrosion when subjected to the SO_2 test.

Another test used by Thompson (136) was that of the EXCO test (ASTM G34-86) which is a constant immersion test. This test was originally used for 2XXX and 7XXX alloys as it can produce fairly reproducible results for these two alloy systems, but is also used for aluminium - lithium alloys. The test solution makes use of chloride and nitrate ions which, combined, increase the corrosivity of the corrosion medium - the composition of the solution is 4M NaCl, 0.5M KNO_3 and 0.1M HNO_3 and has an initial pH of 0.4. Testing is carried out at room temperature and the duration of the test normally lasts up to four days. The recommendation for assessing the extent of exfoliation damage is by comparing the corroded surfaces to a set of standard photographs. Ratings which are given to the exfoliated surfaces range from N (no appreciable attack) through to varying degrees of exfoliation damage (EA - ED). It has been shown (138) that the EXCO test provides a better correlation with salt water exposure than acidified salt - spray testing. Although the EXCO test is a reliable test, when it is used on alloys such as 7050 and 7150 the amount of general corrosion increases, and this reduces the ability of the test to distinguish between varying tempers. Lee and Lifka (139) modified the EXCO solution with a new composition containing 600mg\l of aluminium ions plus 4M chloride and 0.6M nitrate at pH 3.2. Another advantage of this test is that it can distinguish between susceptible and resistant materials as well as differing tempers. Alternate, constant immersion testing which can be used for alloys such as the 5XXX series is that of the ASSET test (138) which has the composition - 0.75M ammonium chloride, 0.25M ammonium nitrate, 0.01M ammonium tartrate and 10 ml\l hydrogen peroxide. The duration of the test is fast at around 24

hours as it is used at a slightly elevated temperature of 80^0C.

Above it has been shown that the EXCO test can be very reliable. However, Colvin and Murtha (140), when testing 2090 and 2091 aluminium - lithium alloys showed otherwise. In their experiments, EXCO did not accurately predict the performance of 2090 in seacoast environments, underestimated the susceptibility of 2091 and did not distinguish between samples of 2091 with different susceptibilities. As a comparison the MASTMAASIS test was used, with both wet and dry bottoms. Conditions using a wet bottom tended to be less severe than using dry bottom MASTMAASIS testing. The EXCO results were less severe only reaching a rating of EA whereas the dry bottom results suffered ratings of EC for specimens of the 2091 alloy. Similar results were found for the 2090 alloy. Although Colvin and Murtha (140) showed that MASTMAASIS produced more severe corrosion than EXCO in relation to the surface ratings these results did not demonstrate the possible difference of the extent of corrosion attack. Gray et al (141) tested 8090 in both the EXCO and MASTMAASIS tests and used the corrosion depth as a comparison. The 8090, in unrecrystallised and recrystallised form showed a higher resistance to exfoliation than did a 2024 alloy in the EXCO test but in the MASTMAASIS testing the exfoliation corrosion of 2024 was less severe than for 8090. Table 2.3 shows the results from the work of Gray et al (141). One conclusion made was that similar visual ratings can have significantly different depths of attack.

Table 2.3. : Mean Depths of Attack for the Different Accelerated Tests (141).

Alloy Type/Temper	Intergranular Test MIL-H-6088 (μm) (surface)	Exfoliation Testing (Surface)				Marine Exposure 270 days (μm)
		EXCO		MASTMAASIS		
		48 hrs (μm)	96 hrs (μm)	14 days (μm)	28 days (μm)	
8090-T8X51 (R)	70	426	591	140	285	100
8090-T8X51 (UR)	133	290	460	-	-	20
2024-T3	190	500	>1000	72	200	50

Electrochemical techniques have also been used to determine the exfoliation susceptibility of aluminium alloys. Horst and Lifka (142) used an electrochemical test which produced an electrode potential for 2XXX and 7XXX series specimens in a mixture of methyl alcohol and carbon tetrachloride. The advantages of this test were that it was very short, eliminated the visual evaluation for exfoliation and metallographic examination for SCC and it appeared to have good reproducibility. Another test of this type is electrochemical impedance spectroscopy (EIS) (143). Roberge et al (144) exposed 8090 and 2090 aluminium - lithium alloys, along with conventional 2024 and 7075, to sea water fog and full or partial immersion in sea water (testing carried out in the laboratory with natural sea water). The results of these tests were then compared with EIS. After four months of testing 2090 showed a higher resistance to corrosion than 7075 and the 8090 was more resistant than 2024. It was concluded that, although EIS is a useful technique for rapidly assessing the corrosion resistance of aluminium alloys it cannot be used to characterise the corrosion behaviour.

2.4.3.2. Outdoor Corrosion Testing

Although laboratory testing is a rapid way to assess the susceptibility to exfoliation corrosion the results do not always correlate well with corrosion experienced in service conditions. Outdoor corrosion testing on aluminium alloys is a lengthy process sometimes taking up to many years for any substantial attack to occur.

Carter (145) exposed four aluminium alloys at five different sites in Great Britain for up to six years. These sites ranged from severe industrial at Sheffield which contained varying levels of sulphur dioxide to a marine atmosphere free from industrial pollution. The specimens were exposed on racks, inclined 30^0 to the horizontal and faced in the direction of the prevailing wind. All the specimens suffered from localised surface pitting and it was shown that, the more aggressive the atmosphere the greater the severity of pitting. The rate of penetration of pits decreased with time of exposure - at the milder sites corrosion versus time curves became almost parallel to the time axis after two years and, in the more severe atmospheres the rate continued to increase for the six year

period of testing. It has been shown in detail that it is not only the skyward facing surfaces that suffer from corrosion (146) - sheltered surfaces, in some cases suffered greater corrosion due to a build up of chemical contaminants which were not cleansed by rainfall. This was also shown by S. P. Jones (147) when testing 2024, 2014 and 7075 in a rural atmosphere and 7075 in a marine atmosphere. Only the 7075 T/2 marine and 2024 T/2 specimens showed any signs of exfoliation with the other specimens suffering from varying levels of pitting. Ailor (148) tested 5XXX series alloys in half tide and full immersion for ten years. The corrosion rates were greater for the full immersion than the tidal immersion.

2.4.4. Mechanisms of Exfoliation Corrosion

As exfoliation corrosion occurs in materials with an elongated grain structure a prerequisite for this type of intergranular attack is an electrochemically active path in the grain boundary region - this can be the solid solution or anodic precipitate particles along the grain boundary. In a review on the exfoliation behaviour of aluminium alloys Summerson and Sprowls (149) listed some specific active paths giving rise to the electrochemical attack of the grain boundaries in various aluminium alloy systems and these can be seen in table 2.4.

Hunter et al (150) studied the relationship between the microstructure and corrosion attack in a 2024 alloy. It was found that, with rapid quenching, pitting occurred in high copper content solid solution but, during ageing the low copper content matrix is attacked. In the aged material precipitate particles were present which were cathodic relative to the matrix. The presence of these precipitates acted as minute galvanic cells producing the driving force for corrosion which consumed the depleted zones around precipitate particles. In slow quenching rates the type of attack became intergranular and occurred in the depleted zone adjacent to the grain boundary which is anodic to the grains. Anwar (46) found that attack in 2024 with a low Cu : Mg ratio was that of anodic dissolution of magnesium from the anodic $CuMgAl_2$ precipitate which renders them cathodic onto which copper can redeposit from surrounding areas. This enlarges the

cathodic area and increases the anodic current density at the grain boundary regions producing a larger driving force for corrosion to occur.

Table 2.4. : Identities of the Electrochemically Active Paths in Various Alloys that are Susceptible to Intergranular Corrosion (149).

Alloy Family	Active Grain Boundary Path
Unalloyed aluminium	High energy boundary due to quenched - in vacancies
AlCu, AlCuMgMn and AlCuSiMn	Cu - depleted solid solution
AlMg and AlMgMn	Closely spaced pattern of Mg_2Al_3 precipitates
AlMgSi	Closely spaced particles of Mg_2Si and/or Mg_2Si/Si solid solution
AlSi	Si depleted solid solution
AlZnMg	Closely spaced $MgZn_2$ precipitates or Zn enriched solid solution
AlZnMgCu	Cu - depleted solid solution and/or Zn - enriched solid solution
AlLi	Closely spaced Al_3Li precipitate
AlLiCu	Cu - depleted solid solution and/or closely spaced Al_2CuLi precipitates

According to Galvele (151) the determining factor for exfoliation corrosion is the relative values of the pitting potentials of the various phases present within the structure. If the pitting potential of the grain boundary is more anodic than that of the grain interior, intergranular corrosion develops, in addition to pitting corrosion. For AlCu alloys Muller and Galvele (152) showed that heat treatment affects the pitting potential because of the formation of copper depleted zones in the aged alloy. It is the formation of the $CuAl_2$ precipitate which leaves the more active, copper deleted zone along the grain boundaries which renders the alloy susceptible to intergranular corrosion where a lower pitting potential exists. As ageing increases, grain boundary pitting increases but the

matrix pitting does not. Maitra and English (153) found that the preferential anodic path was that of solute enrichment (Zn and Mg) in the vicinity of grain boundaries for a 7075 alloy. The use of anodic polarisation studies showed two breakdown potentials for the peak - aged material - an active potential for pitting of the solute enriched grain boundary and a more noble potential for the pitting of the matrix. In the peak - aged condition, precipitates form at the grain boundaries and grain interiors where intergranular attack is caused by the preferential dissolution of the grain boundary precipitates. Over - ageing reduced the pitting potentials of the grain boundaries and grain interiors so that intergranular corrosion could not be sustained.

Mattson (154) investigated the corrosion behaviour in a Al - 5%Zn -1% Mg alloy which is used for welding. In the naturally - aged condition the intermetallic α - Al (Fe,Me) Si phase (Me represents Mn, Cr, Cu, V or W) is present which was very noble compared to the surrounding matrix. The corrosion attack was transgranular in nature, with the anodic material being the Zn and Mg matrix adjacent to the cathodic α phase. It was found that, in the artificially aged condition general attack occurred which was due to the more anodic $MgZn_2$ precipitate. Reboul and Bouvaist (155) studied the corrosion of a welded 7020 alloy and found that there was two types of exfoliation corrosion according to the nature of the anodic zones. In the first case the formation of the anodic $MgZn_2$ phase at the grain boundaries where exfoliation corrosion followed the anodic path. Secondly, the secondary elements Cr and Mn inhibit recrystallisation and form cathodic intermetallic particles forming an anodic zone by depletion of the solid solution of these elements which contributes to the exfoliation corrosion. Onoro and Ranninger (156) tested 2017 AlCu and 7015 alloys and found that 2017 suffered more extensive attack than 7015 in the welded zone and in the base material. The HAZ revealed precipitates of $CuAl_2$ which promoted intergranular attack due to the electrochemical behaviour between the intermetallic and the adjacent grains which were depleted in copper. All the heat treatments studied - as received, T4 and T6 - gave poor exfoliation behaviour. Again, as with the other investigators the $MgZn_2$ precipitate caused intergranular attack in the 7015 alloy but this attack was less than that of 2017 due to a smaller potential difference between the grain boundaries and adjacent grains.

The same type of mechanisms can be found in aluminium - lithium alloys which are susceptible to exfoliation corrosion. Reboul and Meyer (157) studied the exfoliation characteristics of 8090 type alloys which were prone to exfoliation corrosion in the peak - aged condition and the attack was suppressed in the under and over - aged material. It was found that alloys which do contain copper were susceptible to intergranular and exfoliation corrosion. Copper precipitation during ageing produces the S phase at the grain boundaries and S' phase within the matrix. This precipitation shifts the corrosion potential to a more active potential. This produces a Cu depleted zone adjacent to the grain boundaries resulting in intergranular corrosion.

Corrosion behaviour in binary and ternary aluminium - lithium alloys is controlled initially by dissolution of δ, then by the matrix (54, 158, 159, 160). Niskanen (158) found that the anodic δ phase had a deleterious effect on the corrosion resistance of AlLi, AlLiMn and AlLiZr alloys in 3.5% NaCl solution. Ageing increased the corrosion susceptibility by increasing the volume fraction of the δ phase. Ways to decrease the susceptibility were additions of Mg which, on over - ageing formed Al_2MgLi and retarded δ formation or Cu which tied up the lithium in transition phases. Gregory et al (159) found that, in low concentrations δ dissolution stops when this phase is dissolved after which the matrix controls the long - term corrosion behaviour. If the volume fraction of δ is between 0 -10% then the corrosion susceptibility is improved by the depletion of lithium in the matrix. Concentrations above 10% lead to an increase in the susceptibility since dissolution of δ can continue for a long time.

Buchheit et al (67, 160) found that the corrosion mechanism in a 2090 AlLiCu alloy was that of the dissolution of the T_1 (Al_2CuLi) phase. An ingot was made from the T_1 phase and compared to solution heat treated 2090 and pure 1100 aluminium which represented the α - Al matrix and a copper depleted zone respectively. Pitting potentials showed that the T_1 specimen was more active and would corrode much quicker than a copper depleted region along a subgrain boundary. It was proposed that the dissolution of T_1 exposes the matrix which corrodes at a slower rate. Zhang et al (161) showed that the intergranular corrosion susceptibility of 8090 in the peak - aged condition was caused

by anodic dissolution of the T_2 (Al_6CuLi_3) present at the grain boundaries.

2.4.4.1. Corrosion Product Wedging

Conversion of aluminium at the grain boundaries produces a corrosion product with a greater volume than the original material. A wedging mechanism was proposed by Robinson (162). The formation of these corrosion products exerts a force on the grain boundaries lifting layers of material which gives the characteristic delamination appearance of exfoliation corrosion. The mechanism of exfoliation corrosion was thought to be stress corrosion driven. Measurement of forces generated by the corrosion product was carried out on a compression rig. A load cell could measure the transmitted force produced by a propagating blister. The limiting value of the wedging force is governed by compressive stress on the strained specimen. The force reached a maximum when compressive stresses overcame the propagation of exfoliation. Figure 2.22 shows corrosion product stringers and how they affect the tensile stress at the corrosion tip. Stress from a second stringer compresses the corrosion tip and prevents propagation. Liddiard and Whittaker (163) tested HE10 (AlMg) and HE15 (AlCuMg) in atmospheric corrosion tests and showed that the compressive stresses were relieved with the delamination of the surface layer of grains for the HE15 alloy which suffered severe exfoliation corrosion.

2.4.4.2. Mathematical Modelling

Mathematical modelling of exfoliation corrosion was put forward by Robinson (164) based on the formation of blisters. The effects of heat treatment and grain shape on corrosion susceptibility were investigated. Blister formation is the result of intergranular penetration and the wedging force produced from the corrosion product. Figure 2.23 represents the cross section showing the intergranular corrosion through the grains of a wrought high strength aluminium alloy. If the corrosion is constant then the attack will penetrate the same distance in all directions no matter whether the pathway is tortuous or not. The initial point of attack occurs at O, with D being the depth of attack, L the blister diameter and AB, AC and AE the intergranular pathways. The exfoliation damage

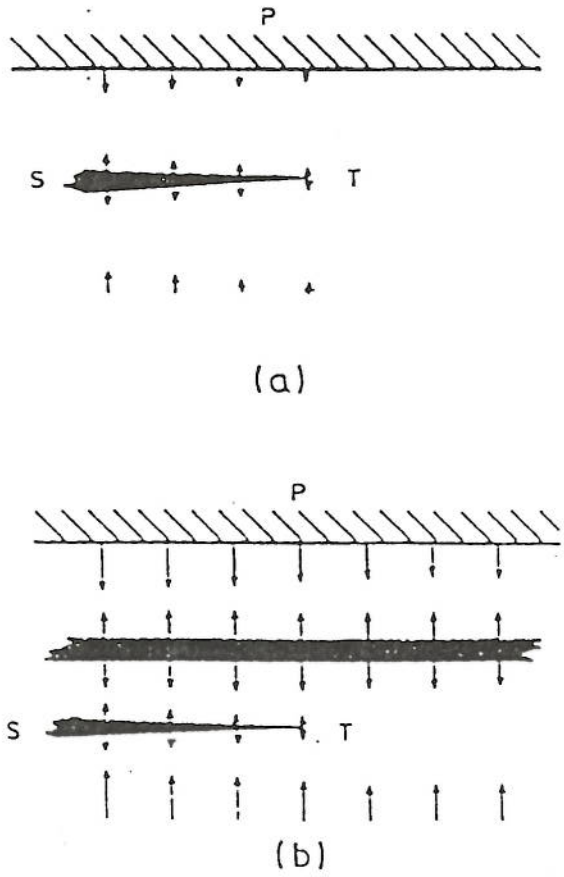

Figure 2.22. : Diagram showing - a) development of a corrosion product stringer, S, with a tensile stress, T, and, b) further stringers produce large compressive stresses reducing the tensile stress at the corrosion tip (162).

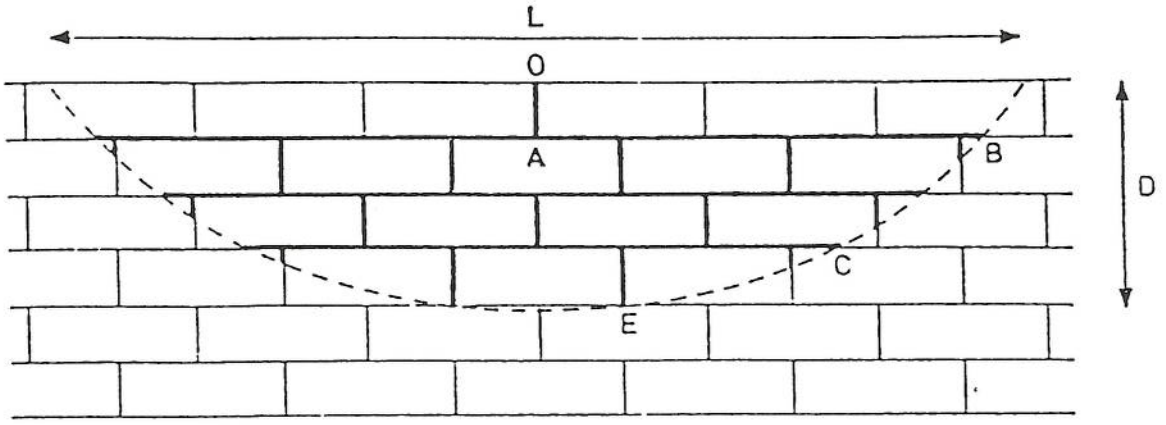

Figure 2.23. : Diagram showing the model for intergranular attack for an aluminium alloy (164).

is assessed by the formation of these blisters and may be reduced by minimising the grain aspect ratio or over - ageing the material. As a blister grows there comes a point when the strain in the skin exceeds the fracture strain of the alloy which is in the order of 11%. The effects of heat treatment and aspect ratio can be seen in figures 2.24 through to 2.27. Heat treatment changes the grain boundary sensitivity, for example over - ageing reduces the sensitivity and the corrosion product aspect ratio, A'. The numbers 6 through to 20 shown in figures 2.24 and 2.25 equate to different corrosion product aspect ratios. A grain boundary becomes more sensitive as the corrosion product aspect ratio increases. As can be seen from figure 2.25 higher corrosion product ratios produces blisters with larger diameters. In terms of the grain aspect ratio effect, for a higher ratio the blister strain takes longer to reach the strain in the alloy and a larger blister develops. For a smaller aspect ratio spalling, flaking or powdering of the surface occurs.

2.4.5. The Effect of Heat Treatment and Microstructure on Exfoliation Corrosion

The most common alloying elements can be classified into two groups - soluble elements which can be retained in solid solution or precipitated under controlled conditions and low solubility elements which are present in elemental form or intermetallic compounds. Soluble elements such as copper, magnesium and zinc form precipitates which differ in their electrochemical activity from that of the solid solution. Low solubility elements such as Si, Fe, Mn, Cr and Zr are present in intermetallic precipitates dispersed throughout the structure. The corrosion behaviour can also be influenced by these intermetallics but to a lesser degree.

The addition of copper to the aluminium - magnesium alloy HE10 (131, 163) was thought to confer some resistance to the exfoliation corrosion. An increase in the copper content of a binary AlCu alloy increased the pitting potential of the alloy (152). However, it has been shown that an increase in the copper content for aluminium - lithium alloys increases corrosion. Moore et al (109) showed that increasing copper from 5% to 6.3% increased the corrosion rate and greater pit depths were observed for the alloy containing 6.3% copper. The addition of copper was found to increase the exfoliation

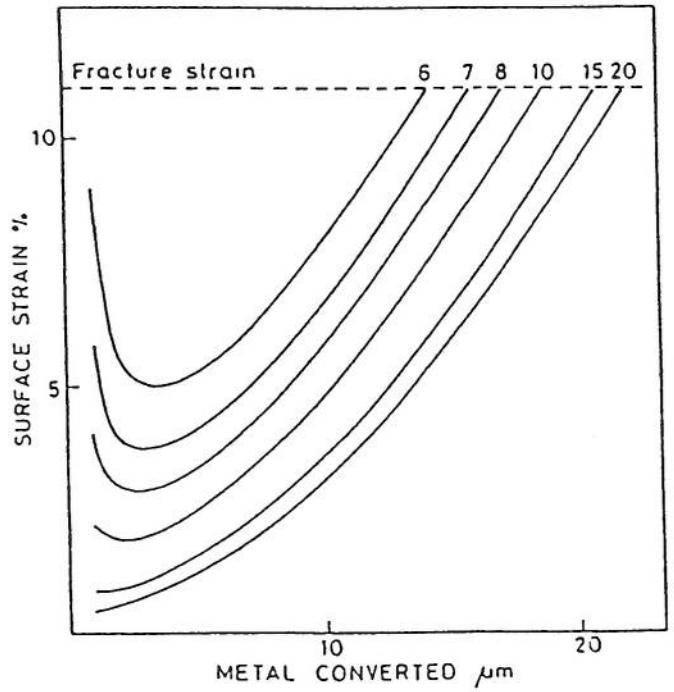

Figure 2.24. : Graph showing the theoretical effect of grain sensitivity on development of surface strain during exfoliation corrosion where 6, 7, 8, 10, 15 and 20 represent different corrosion product aspect ratios (164).

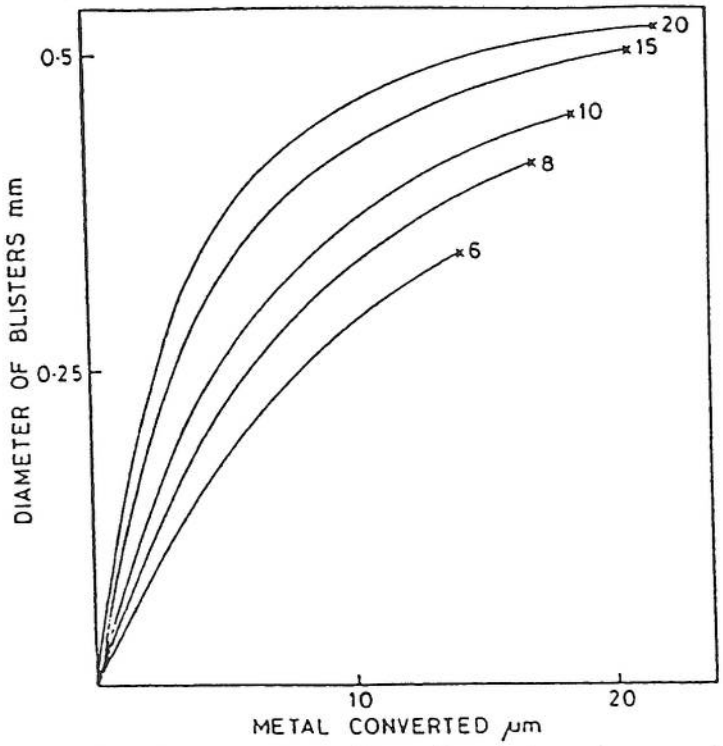

Figure 2.25. : Graph showing the theoretical effect of grain boundary sensitivity on blister diameter during exfoliation corrosion where 6, 8, 10, 15 and 20 represent different corrosion product aspect ratios (164).

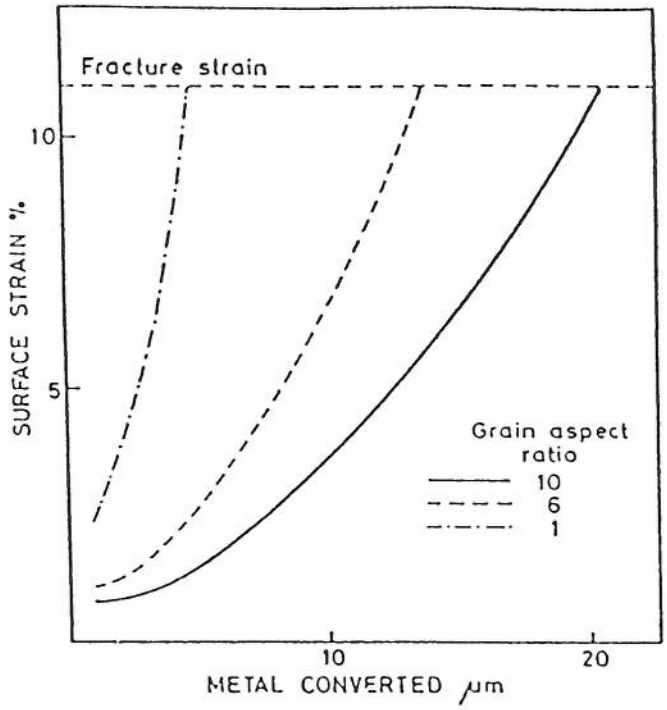

Figure 2.26. : Graph showing the theoretical effect of grain aspect ratio on development of surface strain during exfoliation corrosion (164).

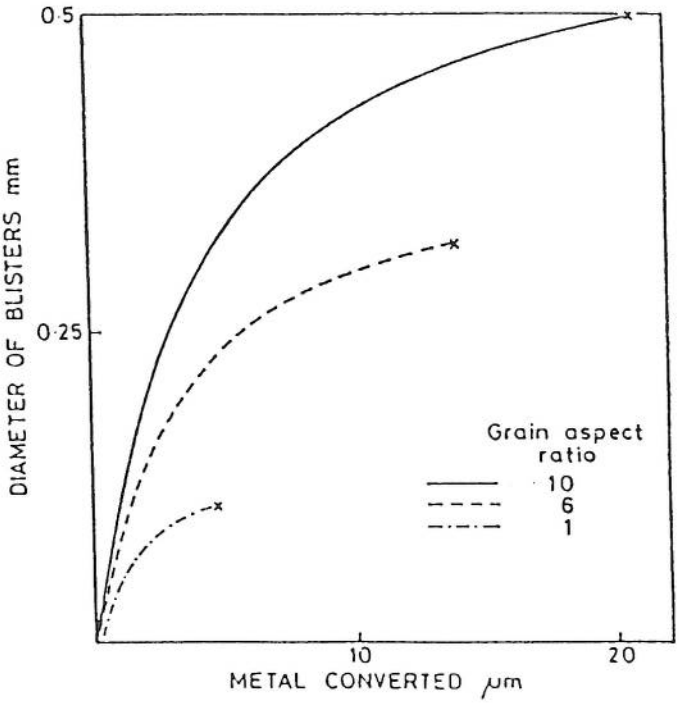

Figure 2.27. : Graph showing the thoeretical effect of grain aspect ratio on blister diameter during exfoliation corrosion (164).

corrosion attack of a AlLiMg alloy (165). This, together with ageing to the peak - aged condition increased the corrosion susceptibility but over - ageing decreased the susceptibility. The ternary AlLiMg alloy was shown to be resistant to exfoliation corrosion in all the under -, peak - and over - aged tempers. Moran et al (166) showed that the addition of magnesium to aluminium - lithium alloys increases the resistance to exfoliation corrosion. Prevention of corrosion in the under - aged temper was due to magnesium's stopping the formation of the T_1 phase.

The addition of minor elements such as chromium to a AlMg alloy improved the corrosion resistance (167). This is due to the fact that a more uniform distribution of precipitates is present in the grains which minimises the potential difference between the precipitate free regions and the solid solution. The T4 temper was shown to be more susceptible to T6. The localised corrosion in the T6 temper was reduced by minimising the potential difference between the solid solution and precipitates.

In a review by Lifka and Sprowls (168) various heat treatments and tempers were investigated together with their effects on corrosion of 2XXX and 7XXX type aluminium alloys. Rapid quenching in AlCu type alloys in the naturally - aged tempers (T3 and T4) produces a high resistance to corrosion. Artificially ageing a 2024 - T351 alloy to the T851 temper the alloy is still susceptible to intergranular attack but not to exfoliation corrosion. Over - ageing to the T7X tempers in an AlZnMgCu alloy imparts a high degree of resistance to exfoliation and SCC, for example the T73 temper is immune to exfoliation. Heat treatment in HE10 and HE15 alloys (131) rendered some resistance to exfoliation due to an increase in subgrain boundary precipitation which created less attack at the grain boundaries. In an AlCuMg alloy Lee and Pyun (98) aged specimens in the T4 and T6 tempers. It was shown that, for the under - aged specimen potentials became more anodic and the corrosion rate increased with ageing time. In the over - aged specimen the corrosion rate initially decreased and then became constant which was due to negligible precipitation.

In the three heat treatment conditions Ohsaki et al (169) found three types of attack

in a 8090 alloy. The under - aged state suffered from preferential dissolution of the Cu - depleted zone along the margin of the subgrain and grain boundary. Ageing to the peak - aged condition increased the pitting potential between the grain boundary and grains, where dimple type pitting occurred associated with heterogeneous precipitates of the T_1 phase which facilitated intergranular corrosion. In the over - aged condition general corrosion was found to occur. Over - ageing was found to have a detrimental effect on the pitting resistance in a AlLiCuMgZr alloy (170) - an increase in the ageing time increases the E_{PIT} value. The higher the E_{PIT} then the more resistant the material is to pitting initiation. The pitting resistance decreased in the order UA > PA > OA1 > OA2. The increased susceptibility to pitting in the over - aged state was due to microstructural changes where the formation and coarsening of the undesirable δ' phase occurred. For the aluminium - lithium 2090 alloy it has been shown (140) that the under - aged condition is most susceptible when exposed to natural seacoast environments and the peak - aged material exhibited excellent corrosion resistance. However, work carried out at RAE in Farnborough (171) showed that the peak - aged material showed the greatest susceptibility to exfoliation whereas, both the under and over - aged conditions improved the resistance to attack. Zhang et al (161) showed that pitting, intergranular and exfoliation corrosion were worst for the peak - aged material and corrosion susceptibility followed the order naturally - aged < under - aged < over - aged < peak - aged where the depth of penetration reached 153μm for peak - ageing : far worse than the other heat treatments.

2.4.6. The Effect of Environment on Exfoliation Corrosion

The corrosion rate of aluminium alloys can be altered by changing the corrosive environment. Changes such as a decrease in the pH, the addition of sulphate or nitrate ions, temperature can increase the corrosion rate and, in atmospheric conditions pollution can decrease the life of a component.

Maitra and English (172) showed that changes in the environment had significant effects on the localised corrosion of a 7075 alloy. For example, the addition of nitrates

to an aqueous NaCl solution increased the difference between the pitting potentials of the grains and grain boundaries. Nitrates caused intergranular corrosion of 7075 plate in the T7351 temper which, in the absence of applied stress, had not occurred in solutions without the nitrate ion. The addition of sulphates and an increase in the pH from 4.5 to 7 altered the corrosion rate but to a lesser degree than the change associated with the nitrate ions. It was concluded that intergranular corrosion of 7075 - T7351 would occur in urban environments as they contain both nitrates and chlorides. Nitrate ions, when present in seawater can accelerate the intergranular corrosion of 7075 alloy (173). Also, by increasing the temperature of the artificial seawater environment to 60^0C the severity of attack was increased. The corrosion susceptibility of 8090, 2091 and 2014, used as a comparison, was found to be a function of the chloride ion concentration (174). Localised attack was found to increase as the chloride ion increased. It was shown that the corrosion rate increased as the chloride ion concentration increased up to 3.5%. For the 8090 - T6 alloy the corrosion rate decreased as the chloride ion concentration increased above 3.5% NaCl. The 2091 and 2014 alloys were also found to exhibit a slower corrosion rate for chloride concentrations between 3.5% and 7% but this rate increased slightly for concentrations above 7%. However, other work by Ambat and Dwarakadasa (175) showed that the corrosion rates for 2014 and 8090 increased with increasing chloride ion concentration with no apparent decrease for either alloy as the concentration increased.

It has also been shown, in an investigation by Srivatsan et al (176) that the pH of the solution influences the corrosion behaviour. For pH values which are more acidic (ie pH<7) the corrosion rate was very high indicated by a large weight loss. In neutral, pH7 solutions there was also evidence of weight loss but an order of magnitude less than in the acidic conditions. For solutions which are basic (ie pH>7) the corrosion rate increased again as compared to the neutral environment but was less than in acidic conditions. Testing was carried out under constant immersion conditions and, as the test duration increased the pH of the solution changed as a result of the reaction between the material and the environment. In the acidic solutions a rapid initial increase in the pH was observed during the first few hours of immersion after which it remained fairly

constant. In the basic conditions there was an initial decrease in the pH which again levelled off to a constant value. A change in the corrosion rate was observed which was as a direct result of this change in pH. For example, in the acidic environment the initial corrosion rate was very high, and decreased as the immersion time increased when the pH altered to higher values. Ambat and Dwarakadasa (175) showed that the corrosion rates of 8090 and 2014 were higher for pH 2 and 11 than at pH 6. Changes in the corrosion rates were attributed to the stability of the oxide film. In acidic and alkaline conditions the oxide film is soluble whereas, at pH 6 the film is stable. The dissolution equilibria for all three pH values are as follows:

pH 2 : $Al = Al^{3+} + 3e^{-}$

pH 6: $Al^{3+} + H_2O = AlOH^{2+} + H^{+}$

$Al^{3+} + 2H_2O = Al(OH)_2^{+} + 2H^{+}$

$Al^{3+} + 3H_2O = Al(OH)_3 + 3H^{+}$

pH11: $Al^{3+} + 4H_2O = Al(OH)_4^{-} + 4H^{+}$

For acidic and alkaline conditions, Al^{3+} and AlO_2^{-} (equivalent to $Al(OH)_4.2H_2O$) exist in solution respectively, and in near neutral conditions aluminium hydroxide protects the alloy surface thus reducing the corrosion rate.

Changes in the environment alter the corrosion rate of aluminium alloys. In a review of various weather factors that can influence the corrosion in the environment, Sereda (177) concluded that the time of wetness is a very important factor. Here, the conditions of relative humidity can result in the formation of an adequate film of water on a metal surface and facilitate the electrochemical reaction for corrosion. A comparison (122) was made between corrosion on alloys which had been exposed to an aircraft carrier environment and a number of natural environments. Corrosion rates were higher on board the aircraft carrier due to the levels of sulphur dioxide from fuels that were present in the atmosphere. A sea coast location is less severe when compared to a ship at sea. In the extreme case, very severe conditions were found in the Indian Ocean especially during the months of May to August. During this time there are a lot of monsoons which

produce high humidity - up to 100% at night producing a continuous salt mist in the air. A study on the effects of three different environments was carried out by Sheldon and William (178). Results showed that an industrial environment produced severe corrosion. An urban - coastal environment and a high chloride containing marine environment showed lower rates of corrosion with the marine site being the least damaging. It was concluded that carbon containing particles provided a more potent agent for corrosion of aluminium alloys than did the coupling of a high airborne salt content and high humidity found in a marine atmosphere.

2.5. Summary

The literature has shown that developments over the years have produced tempering treatments through extended heat treating, various quenching conditions and thermomechanical pretreatments which can reduce the susceptibility to exfoliation corrosion. New alloys available today are of the aluminium - lithium series which have greater resistance to corrosion than the conventional 2XXX and 7XXX series alloys. Research into these new lithium containing alloys have gained wide acceptance and these alloys are now being used in a number of areas in aerospace.

SCC and exfoliation corrosion are similar in that they both follow an intergranular pathway and rely upon the microstructure and grain morphology within the structure of aluminium alloys. For example, the greater the length of the grains the faster the rate of attack. Microstructural changes in various alloy systems alter the nature of attack - copper containing phases cause exfoliation corrosion in aluminium - lithium alloys, copper depleted solid solution influences the corrosion characteristics in AlCuMg type alloy and the $MgZn_2$ precipitates present along the grain boundaries in AlZnMg alloys. These changes affect the pitting potential between the grain boundaries and the matrix which alters the susceptibility of a material to exfoliation corrosion and SCC. Artificially heat treating the alloy alters this potential difference - at the peak - aged condition this potential difference is at its maximum which imparts maximum susceptibility to a material. In the under - aged and over - aged conditions the potential difference is lower so the

resistance of an alloy to exfoliation corrosion and SCC is increased.

The exfoliation corrosion which occurs on aluminium alloys in the environment can be achieved in the laboratory with total immersion such as the EXCO test and salt - spray testing such as the MASTMAASIS test. These tests accelerate the time for exfoliation corrosion to occur from years in service to hours and weeks in the laboratory.

Bearing in mind the conditions under which corrosion and SCC occur the following work has been performed to study the effects of heat treatment and grain shape on the exfoliation corrosion of various aluminium alloys. AlCuMg alloys were used in plate form which exhibits a change in the grain shape through the cross - section of the plate and aluminium - lithium alloys were used to study the effects of heat treatment.

CHAPTER THREE

3.0. MATERIAL CHARACTERISATION

3.1. Materials

The test programme was carried out on two 2XXX series alloys supplied in plate form and two aluminium - lithium alloys - 8090 and 2091 both of which were supplied in sheet form. All of the material specifications can be seen in table 3.1. The 2XXX plate and aluminium - lithium alloys were supplied by Defence Research Agency, Farnborough.

Table 3.1. : Specifications for the Supplied Materials.

Alloy	Temper	Thickness (mm)
2014	T651	42
2024	T351	42
2091	T351	1.6
8090	T351	1.6

3.1.1. Alloy Composition

The composition for each alloy was evaluated by optical emission spectrometry. The 2014 and 2024 alloys were determined at International Combustion, Derby and the aluminium - lithium alloys determined at Coleshill Laboratories, Birmingham. The compositions for each alloy can be seen in table 3.2.

3.1.2. Heat Treatments

Both the 8090 and 2091 were supplied in the T351 (solution heat treated) condition so that suitable heat treatments could be performed in the laboratory. Each material was aged to the under -, peak - and over - aged conditions. The heat treatment conditions are summarised in table 3.3. It is known that the susceptibility of exfoliation corrosion increases up to peak - aged and then decreases with further ageing up to the over - aged condition so these heat treatments were carried out to establish how much the ageing

condition affects corrosion on these alloys.

Table 3.2. : Compositions for all Material Tested.

Element	Alloy			
	2014	2024	2091	8090
Li	-	-	1.67	2.24
Cu	4.09	4.37	1.89	1.05
Mg	0.43	1.35	1.3	0.59
Mn	0.66	0.62	<0.01	<0.01
Si	0.63	0.11	0.044	0.04
Fe	0.32	0.18	0.06	0.07
Zr	-	-	0.08	0.1
Zn	0.05	0.04	0.01	0.02
Ti	0.034	0.035	0.03	0.03
Pb	0.01	0.01	<0.01	<0.01
Sn	0.01	0.01	<0.01	<0.01
Ni	0.003	0.005	0.01	0.01
Al	Bal.	Bal.	Bal.	Bal.

Table 3.3. : Heat Treatments for the 8090 and 2091 Alloys.

Alloy	Temp. (^{0}C)	Time (hours)		
		Under	Peak	Over
8090	150	8	24	96
2091	138	8	24	96

Heat treatment was also performed for the 2024 alloy. This was heat treated to the peak (190^{0}C for 12 hours) and over (210^{0}C for 12 hours) aged conditions. As the 2014 was supplied in the T651 condition (peak - aged) it was not deemed necessary to carry out any heat treatment on this alloy.

3.1.3. Hardness Measurements

Hardness measurements were taken on the Vickers hardness test for the 2024, 8090 and 2091 alloys. This was done to evaluate the variation of hardness with ageing time (ie the under -, peak - and over - aged conditions) for the three materials. In each case five measurements were taken to obtain an average value and this was plotted against the ageing time. For the 2024 alloy a plot against the three ageing conditions can be seen in figure 3.1. Figures 3.2 and 3.3 represent the plots of hardness against ageing time for the 8090 and 2091 alloys respectively. As can be seen from each plot the hardness reaches a maximum for the peak - aged condition which then decreases on over - ageing.

3.2. Grain Aspect Ratio Determination

3.2.1. Introduction

Many wrought aluminium alloy products have highly directional grain structures. A typical grain structure can be seen in figure 3.4 which exhibits flat, pancake - shaped grains, elongated parallel to the rolling direction. The letters L, T and ST represent the longitudinal, transverse and short transverse directions respectively. The length of these grains tends to increase toward the centre of the plate. Exfoliation corrosion follows an intergranular pathway around these elongated grains in aluminium alloys so an understanding of grain shape and size is useful in understanding the distance to which the attack has penetrated into these materials.

3.2.2. Procedure

Characterisation of the 2XXX and aluminium - lithium alloys was carried out by metallography using extreme value statistics to give the most significant values of the grain aspect ratio. The two 2XXX plate alloys were sectioned as follows:

1) Surface, quarter - section (T/4) and mid - plane (T/2) from the longitudinal orientation.
2) Surface, T/4 and T/2 sections from the transverse orientation.

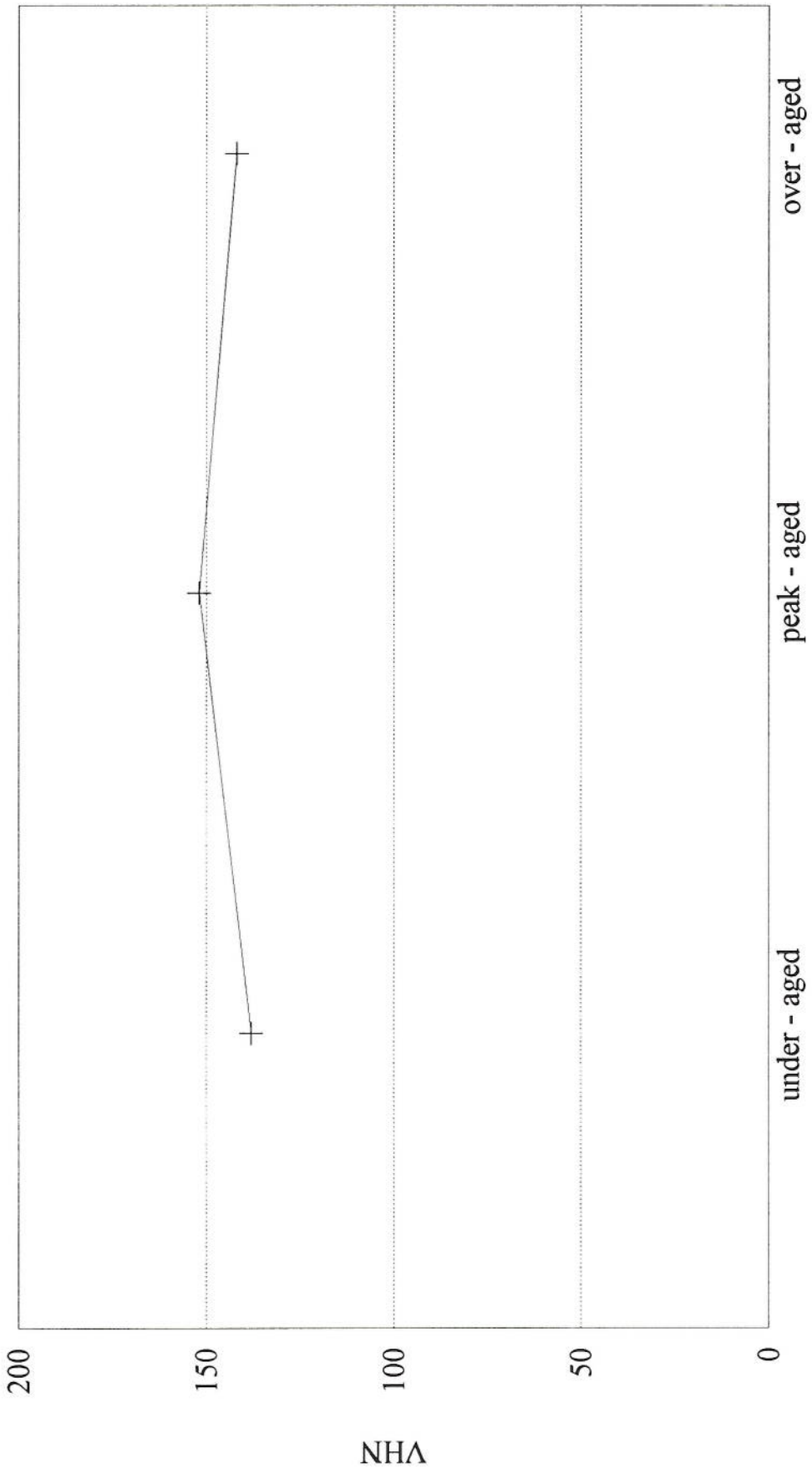

Figure 3.1. : Variation of Vickers hardness number with heat treatment for 2024 plate.

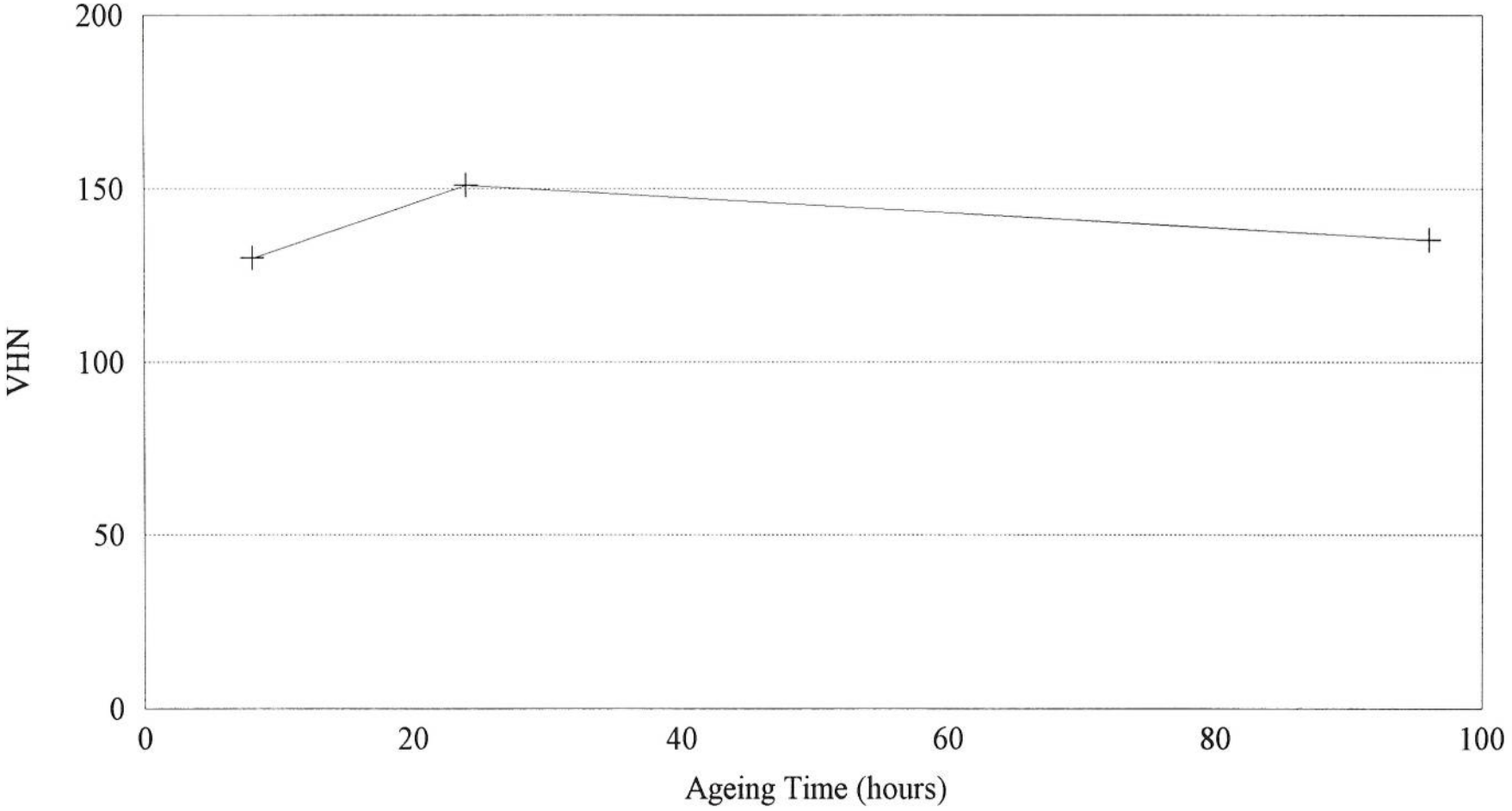

Figure 3.2. : Variation of Vickers hardness number with ageing time for 8090 sheet.

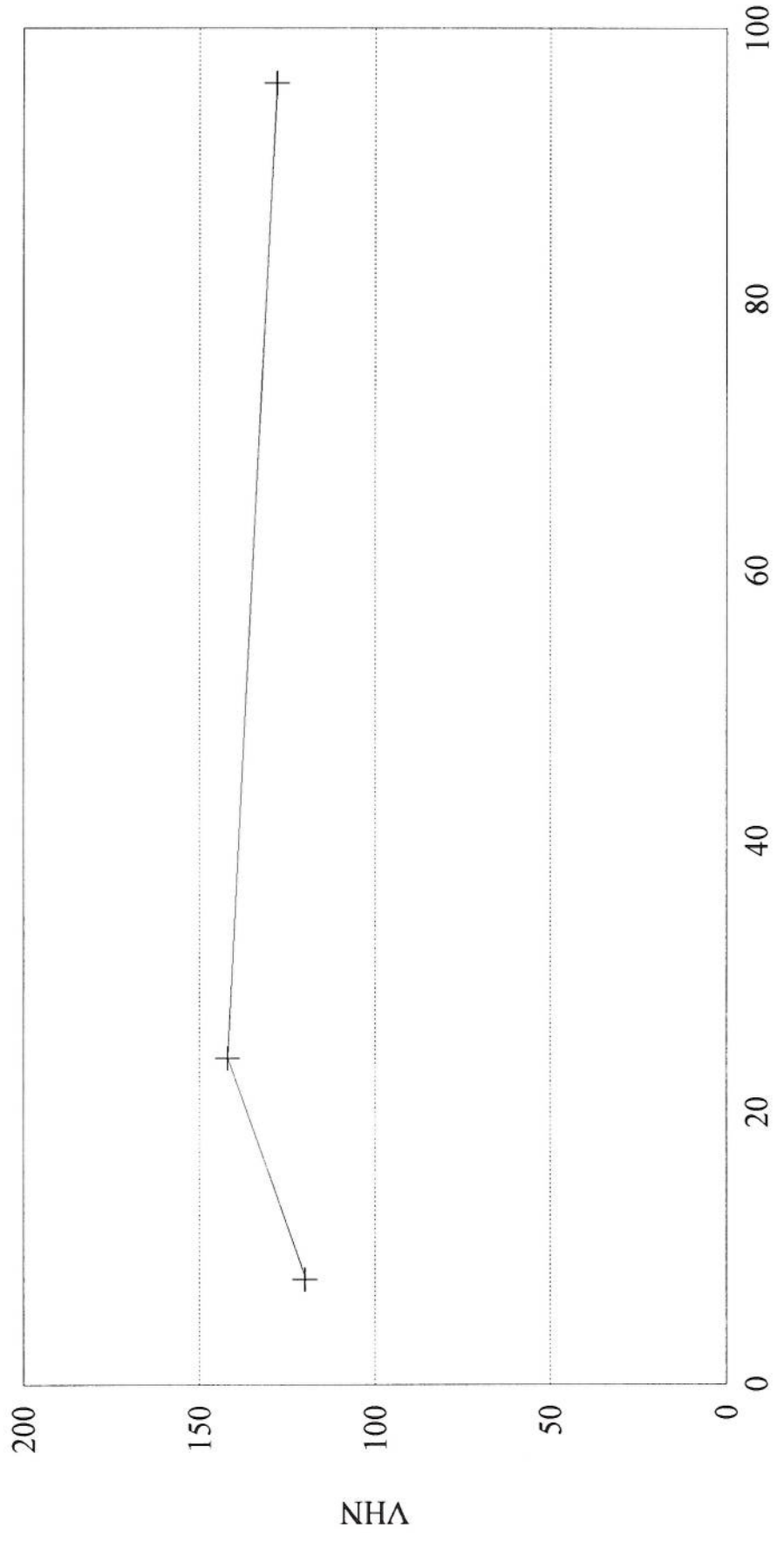

Figure 3.3. : Variation of Vickers hardness number with ageing time for 2091 sheet.

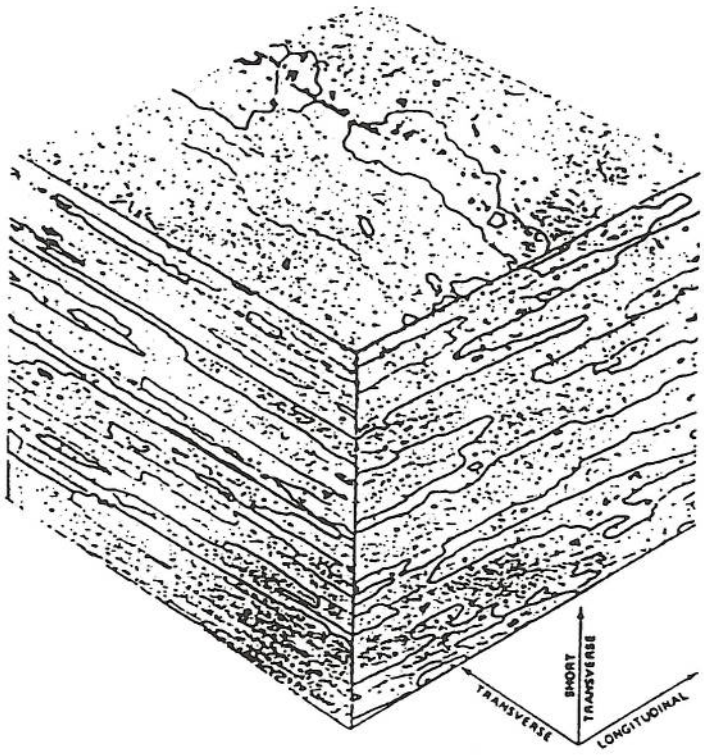

Figure 3.4. : Typical wrought aluminium alloy grain structure.

Each section was mounted in Bakelite, polished to a one micron finish and then etched with Kellers etch to expose the grain structure. Measurements of the grain length and width for both the longitudinal and transverse orientations were carried out using a Joyce Loebl Image Analyser. A population of approximately 160 grains was measured for each section, from which the top 10% of these values were taken to comply with the extreme value model (179). This model involved plotting graphs of $-\ln(-\ln F_{imax})$ against grain length (or width), where F_{imax} represents the probability of any grain not exceeding the selected grain size. A line of best fit was drawn through the points on the graph from which the gradient and intercept were obtained. These values were then used to calculate the most probable grain length and width, assuming the largest grain size observed approximated to the true grain size. The grain aspect ratio was then determined by the ratio of grain length to grain width for each section. A more detailed description of this method can be seen in appendix three.

3.2.3. Results for Aspect Ratios

The 2014 and 2024 alloys both showed recrystallised grains at the surface of each plate with more elongated, 'pancake - shaped' grains towards the centre of the plate which is typical for wrought aluminium alloys in plate form. The 8090 and 2091 sheet alloys tended to show a recrystallised grain structure. Optical micrographs showing the grain structure in the longitudinal direction can be seen in figures 3.5, 3.6 and 3.7 for the 2014, 8090 and 2091 alloys respectively. Figure 3.8 illustrates the grain structure for the T/2, T/4 and surface sections of the 2024 plate material. The grain aspect ratio values are shown in table 3.4.

Table 3.4. : Grain Aspect Ratios for all Alloys Tested.

Alloy	Orientation	Section	Length (μm)	Width (μm)	Aspect Ratio
2014 Plate	Longitudinal	T/2	362±50	30±9	12.1±5.8
		T/4	294±41	34±10	8.6±4.1
		Su	136±17	28±4	4.9±1.3
	Transverse	T/2	177±15	29±3	6.1±1.2
		T/4	137±20	33±6	4.2±1.6
		Su	86±14	25±4	3.4±1.1
2024 Plate	Longitudinal	T/2	221±30	18±3	12.4±3.8
		T/4	234±25	25±6	9.4±3.4
		Su	169±30	24±4	7±2.5
	Transverse	T/2	136±21	16±8	8.5±7.4
		T/4	149±18	27±5	5.5±1.8
		Su	118±15	25±5	4.7±1.6
2091 Sheet	Longitudinal		39±4	2.7±1	14.2±7.9
	Transverse		10.7±2	2.9±0.5	3.7±1.4
8090 Sheet	Longitudinal		76.4±12	13.7±3	5.6±2.2
	Transverse		32.5±4	11.2±2	2.9±0.9

Figure 3.5. : Micrograph showing grain structure for the longitudinal orientation of 2014 T/2 (x50).

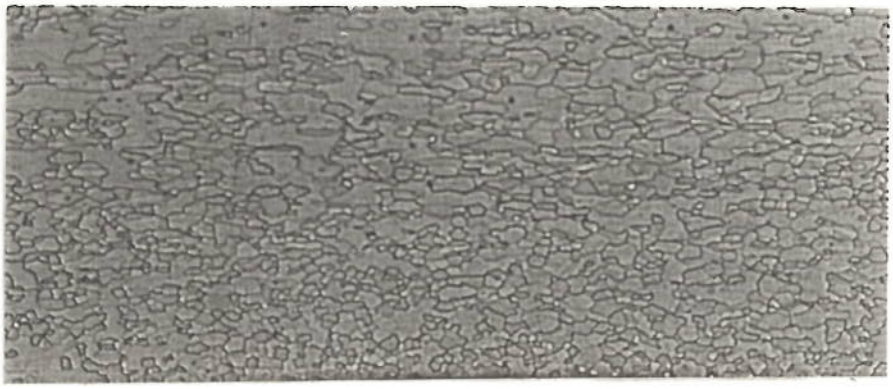

Figure 3.6. : Micrograph showing grain structure for the longitudinal orientation of 8090 sheet (x50).

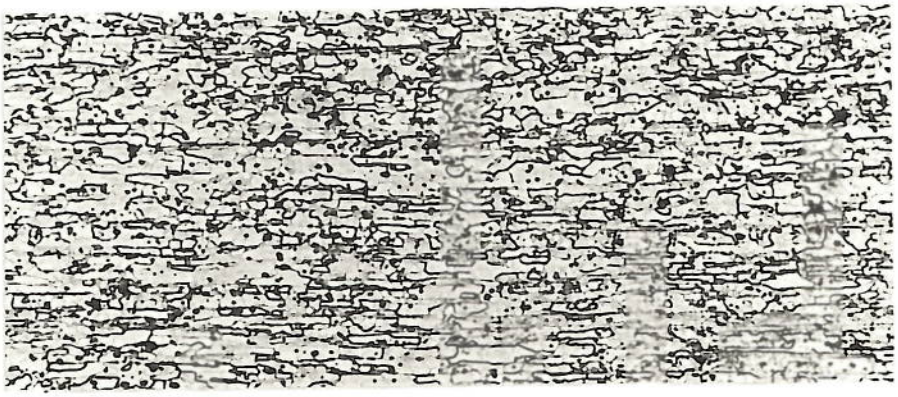

Figure 3.7. : Micrograph showing grain structure for the longitudinal orientation of 2091 sheet (x50).

a)

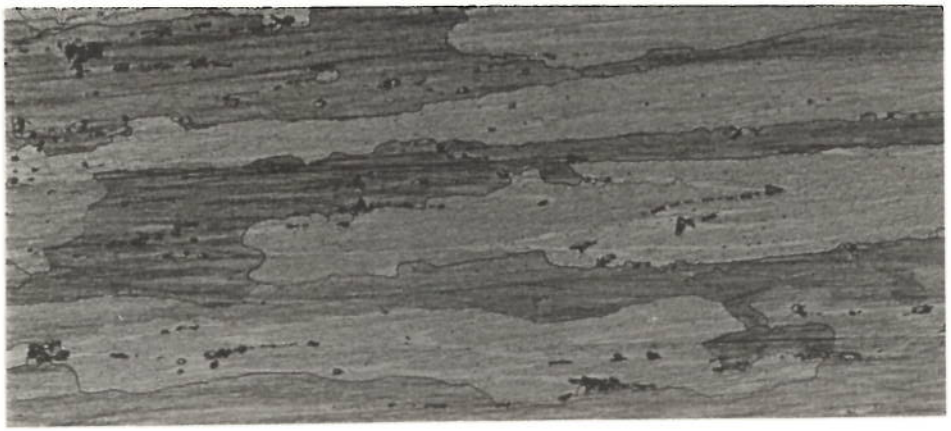

b)

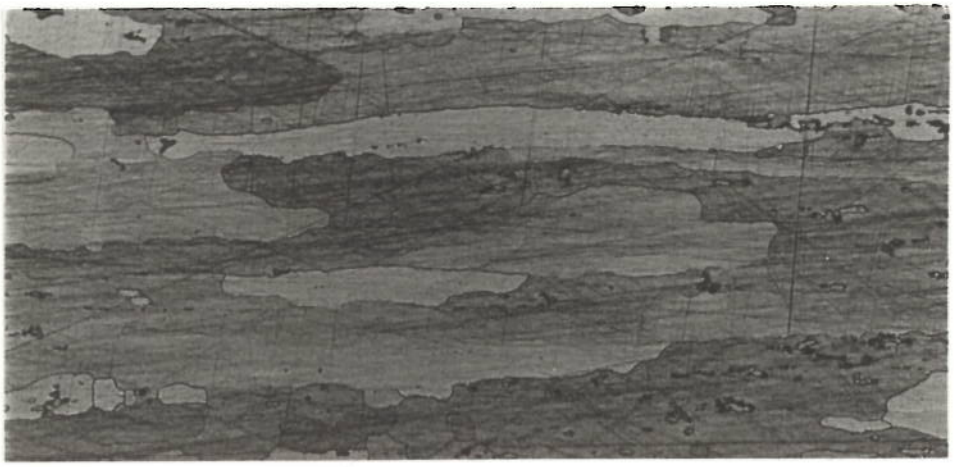

c)

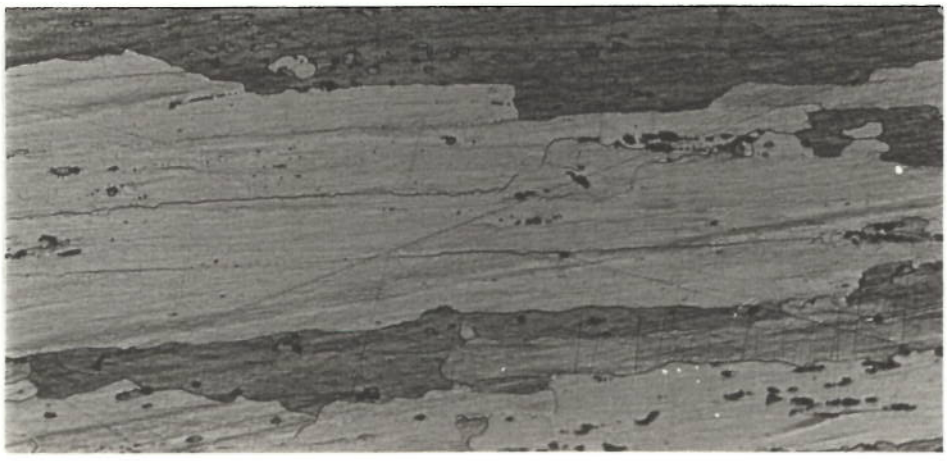

Figure 3.8. : Micrographs showing grain structure for the longitudinal orientation of 2024 plate where a, b and c represent the T/2, T/4 and surface sections respectively (x150).

For both the longitudinal and transverse orientations the general trend in the 2014 and 2024 alloys was for the aspect ratio to be higher in the centre and decreased in the order T/2 > T/4 > surface. In general it is expected that the grain length would be the greatest at the centre of the plate due to the rolling process. In the 2024 alloy the T/4 section exhibits longer grain lengths than the T/2 section which could be caused by a degree of cross - rolling during processing of the ingot. In this alloy the difference between the lengths of the T/4 and T/2 sections does not alter the fact that the grain aspect ratio is larger in the T/2 section due to the fact that the T/4 section has a much larger grain width. In fact, for each case the T/4 section exhibited a greater width than the other two sections through the plate - this could be due to a) the grain size in the original ingot being greater in the T/4 section and this difference was retained during processing, or b) a degree of cross - rolling during processing. The magnesium and zinc present in these two alloys form fine intermetallic particles which pin grain boundaries helping to keep the elongated grain structure present towards the centre of the plate. The 2091 exhibited a greater aspect ratio than that obtained for the 8090 alloy. With the 2091 and 8090 provided in sheet form there are no variables with the aspect ratio assumed to be constant through the thickness. The emphasis during testing on these alloys was placed between the different heat treatments.

Ideally, if each specimen had been sectioned from the same position within the plate, each section would exhibit the same grain width for both the longitudinal and transverse orientations. For the measurements reported in table 3.4 it can be seen that the widths are very similar for the two orientations. The specimens from each section used for the aspect ratio determination were taken from different areas in the plate giving rise to the slight discrepancy between the longitudinal and transverse values.

CHAPTER FOUR

4.0. EXFOLIATION CORROSION TESTING

4.1. Bend Rig Testing

Exfoliation corrosion is an insidious form of attack. This a major problem for an engineer in that if corrosion has occurred on any part of an aircraft, he does not know how deep the attack has penetrated into the material or how much damage has occurred within the structure. This loss in thickness reduces the load bearing capacity of any component on an aircraft. One method of determining the loss in thickness is that of four - point bend testing first reported by E.A.G. Liddiard et al (131) in 1960. In this method the changes in deflection characteristics over time are used as an effective measure of the loss in thickness. The four - point bend test is a useful mode of testing and preferred to any other such as three - point testing. This is due to the larger amount of material that experiences the maximum stress in four - point loading.

4.1.1. The Four - Point Bend Rig

A four - point bend rig was designed to determine the effective remaining thickness of plate and sheet specimens after periods of exfoliation corrosion. The deflection of any material is a function of the dimensions and, by recording the changes in deflection, the change in cross - section can be determined. This can be done for a number of loads depending upon the thickness of the specimen. The deflection, δ, under four - point loading is given by:

$$\delta = \frac{Wa}{48EI}(3L^2 - 4a^2) \qquad (1)$$

Where W = load (N)

E = modulus of elasticity

I = moment of inertia

L = distance between outer fulcrums

a = distance between inner fulcrums

The specimens used in this work were rectangular in cross - section and for rectangular shaped objects the moment of inertia is:

$$I=\frac{bd^3}{12} \tag{2}$$

Where b = specimen width (30mm).

d = specimen thickness (3mm).

Therefore the deflection, after combining equations (1) and (2), becomes:

$$\delta=\frac{Wa(3L^2-4a^2)}{4Ebd^3} \tag{3}$$

It was decided that the best four - point configuration was that of 180mm and 90mm for the outer and inner fulcrums respectively which maximised the testing area on specimens used for corrosion testing. It can be seen that, from equation (3) the elastic deformation is proportional to $1/d^3$ providing a sensitive means of measuring small changes in depth of attack after periods of corrosion. To prevent exceeding the elastic limit of these aluminium alloys, especially after the specimens had been thinned by periods of corrosion, it was necessary to evaluate the load at which this would occur. In order to determine the maximum load it was necessary to evaluate the radius of curvature and maximum deflection of a specific thickness of material which was 3mm. The radius of curvature, R, can be given by:

$$R=\frac{Ey}{\sigma} \tag{4}$$

Figure 4.1 shows a schematic diagram of the deflection on a specimen where BB represents the distance between the fulcrums, θ the angle of deflection, H the maximum

deflection, O the centre point of deflection and A the original position of the specimen. The maximum deflection can be obtained as follows:

$$H = R - OB\cos\theta \tag{5}$$

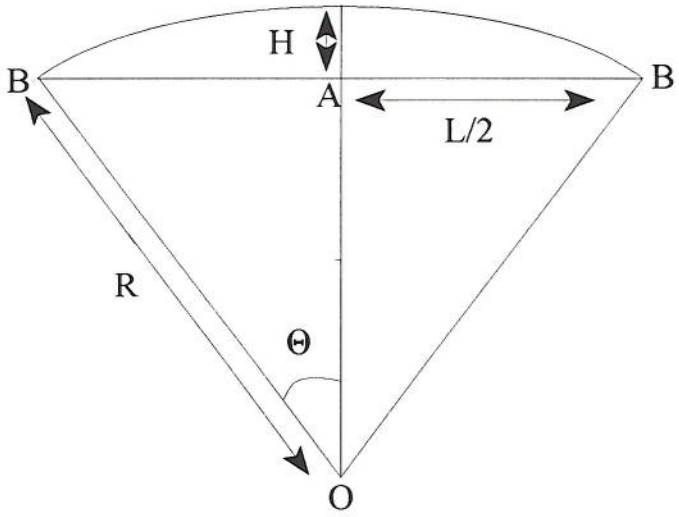

Figure 4.1. : Schematic diagram representing the deflection caused on a specimen subjected to loading on the four - point bend rig.

The maximum load can then be obtained through equation (3). Table 4.1 shows typical values of the maximum load that can be applied to specimens over a range of thicknesses. As the specimen thickness decreased during periods of corrosion it was decided comparatively lower loads should be used for testing so yield would not be reached. Figure 4.2 shows the general arrangement of the four - point bend rig. The rig consists of two outer and two inner fulcrums between which the specimen can be placed. An end stop was used in the bend rig to enable the specimen to be positioned so that the same area was tested every time. The method used was to load each specimen by placing different weights on the load plate which acted through the two upper fulcrums and caused the specimen to deflect. The load used was that of 48.2 Newtons. The deflection

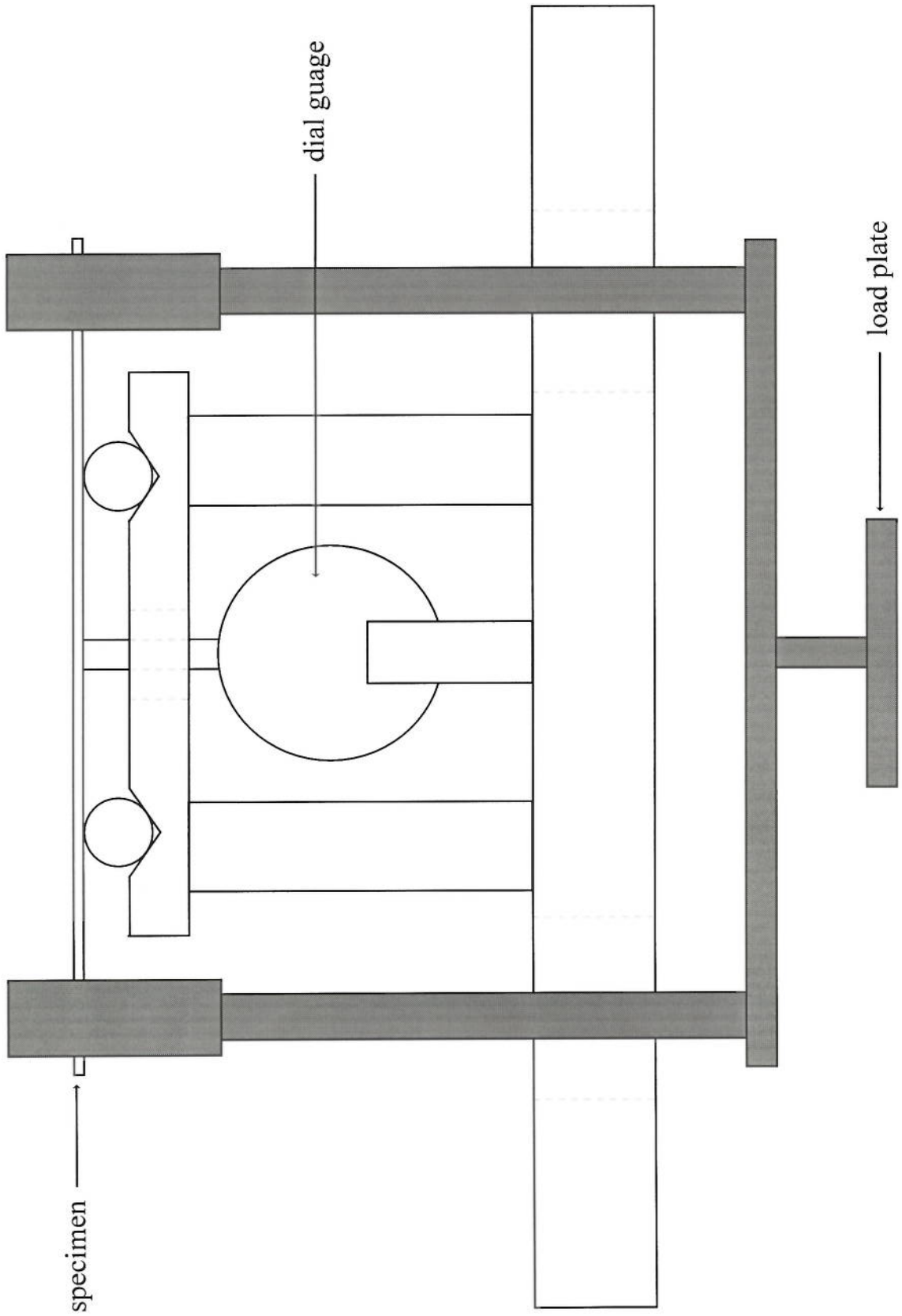

Figure 4.2. : General arrangement of the four point bend test (not to scale).
Load plate and attachments are shown in grey.

of the specimen was measured on the dial gauge and the change in thickness could be obtained through equation (3).

Table 4.1. : Maximum Loads that can be used for Testing Specimens of Varying Thickness.

Specimen Thickness (mm)	δmax (mm)	Maximum load (N)
3	2.8	124.44
2.9	2.9	116.42
2.8	3	108.42
2.7	3.1	100.45
2.6	3.2	92.59
2.5	3.4	87.45
2.4	3.5	79.6
2.3	3.66	73.3
2.2	3.8	66.6
2.1	4	60.98
2	4.22	55.57

4.2. Corrosion Testing

Accelerated corrosion testing was carried out on the 2XXX series, 8090 and 2091 materials in order to determine their corrosion susceptibility. The materials were corroded in the MASTMAASIS (Modified ASTM Acetic Acid Salt Intermittent - ASTM B117 - 64) test using an Ascott salt spray cabinet with a dry bottom (the dry bottom is considered to be a more corrosive environment). The test environment is that of 5% NaCl solution acidified to a pH of 3. A description of the test can be seen in appendix four. The MASTMAASIS test gives a good correlation between outdoor exposure testing in that the conditions are similar to in service conditions that an aircraft would experience. This testing was carried out on the 2024, 8090 and 2091 for the various heat treatment conditions and the 2XXX series alloys in the T/2, T/4 and surface sections with varying aspect ratios. It is expected that, as the heat treatment condition increases to peak - aged,

the exfoliation susceptibility increases, and then decreases on over - ageing. Also, as the aspect ratio increases exfoliation should increase.

4.2.1. Experimental Procedure

4.2.1.1. Specimen Preparation

Specimens were machined from the T/2, T/4 and surface planes within the plate of the 2014 and 2024 alloys, and cut from the sheet of the 8090 and 2091 alloys. These specimens were rectangular in shape with dimensions 200mm in length, width 30mm and thickness 3mm. The thickness of each specimen was measured accurately using a micrometer. For each section two specimens were used, one for testing on the four - point bend rig and the other was used for metallographic assessment by means of cutting a small sample after each successive test interval. As machining had left a rough surface, the surface of each specimen was lightly polished down to 1200 grit using silicon carbide paper and then degreased in propanol. In the aluminium - lithium alloys the surface usually shows a lithium depleted zone during heat treatment due to selective oxidation of lithium, hence removal of this zone required polishing. The surface was then cleaned using a two - stage process:

1) Placed in a 5% NaOH solution for approximately two minutes.
2) Desmutted in concentrated nitric acid for approximately one minute.

The specimens were then washed with distilled water, dried and coated with lacomit varnish. The back, sides and ends were coated leaving the top surface exposed to corrosion. The specimens were then placed in the MASTMAASIS cabinet with the exposed area facing upwards at an angle of 45^0 for periods of testing. After each test duration the specimens were removed and cleaned with distilled water. One specimen was tested on the bend rig and the other cut for metallographic assessment which included measuring the depth of attack, visual assessment and photographic evidence of the morphology of attack.

4.2.1.2. Depth of Attack Measurements

Metallographic examination gives more reliable information about the extent of exfoliation damage as there is not always a clear correlation between surface appearance (assessed visually using the ASTM, STP G34-79 standard) and the depth of attack. The specimens used for metallographic examination were removed from the salt - spray cabinet after periods of corrosion and cut into smaller, more manageable sections which showed a cross - section of the attack. These sections were mounted in epoxy resin which preserved the attack, and polished to a one micron finish. With the aid of an optical travelling microscope the depth of attack was measured at ten points of attack across each specimen. The average and maximum depths of attack were recorded. The morphology of attack appeared to show a difference between the varying aspect ratios through the 2014 and 2024 plate materials - the lower the aspect ratio the more localised the attack. The depths of attack measurements were then compared to those obtained from the four - point bend testing.

4.2.2. Intergranular Corrosion Velocity

It is assumed that the wrought alloy has an idealised grain structure. Intergranular velocities were calculated by making use of the depth of attack, the grain dimensions and the time over which the attack takes place. Intergranular corrosion velocities give an indication how susceptible a material is to intergranular corrosion - the higher the velocity the higher the susceptibility. Corrosion velocities were calculated for all materials and conditions tested. The maximum depths of attack that were measured are those in which the corrosion pathway takes the most direct route around the grains in the material which gives the fastest intergranular velocities. The total distance of the path travelled by corrosion can be obtained using the depth of penetration. By assuming a "half - brick" model, the total length of the pathway and, subsequently the velocity, can be calculated as follows:

Length of grain boundary corrosion = $(|N| \times L/2) + (N \times W)$

Where $N = \left(\frac{\text{depth of attack}}{\text{width of grain}}\right)$ = number of grains penetrated

L = length of grain (μm)

W = width of grain (μm)

Intergranular velocity $V_{IG} = \frac{\text{length of G.B. corrosion}}{\text{time}}$

The intergranular velocities are quoted in ms^{-1} so the length was converted into metres and the time measured in seconds.

4.3. Experimental Results for the 2XXX Series Alloys

4.3.1. Visual Assessment

The degree of corrosion was established visually by ranking each specimen using photographs of standard ASTM exfoliated specimens. Tables 4.2 and 4.3 represent rankings for 2014 and 2024. These results are also represented in bar chart form which can be seen in figures 4.3 and 4.4 for 2014 and 2024 respectively. The MASTMAASIS test showed that 2014 and 2024 were susceptible to exfoliation corrosion to some degree. In both cases the susceptibility was relatively easy to establish using the ASTM visual classification. As expected, in both cases the degree of attack was greatest in the T/2 section due to the grains exhibiting a higher aspect ratio in the centre part of the plate, while the attack on the T/4 and surface sections was not as extensive. In the 2014 alloy the degree of attack reached a ranking of EA+ for the T/2 with the T/4 and surface sections reaching EA and EA- respectively, whereas in the 2024 alloy the ranking was EC+ for T/2, EB+ for T/4 and EB- for the surface section. The ranking was higher in the 2024 alloy than 2014 which was due to the higher aspect ratios. Photographs of the surfaces can be seen in figure 4.5.

In each case blisters appeared over a shorter period of time for the T/2 section than for the T/4 and surface sections. Alloy 2024 was faster to show signs of exfoliation than 2014 where small blisters were visible during the first 70 hours of testing. These blisters tended to grow gradually throughout the duration of the test and little metal loss occurred until about 100 hours when these blisters tended to burst open. At longer times

Table 4.2. : Results of MASTMAASIS Test for 2014.

Time (hours)	Surface	T/4	T/2
70	N	N	N
144	N/P	P	P
189	P	P	P/EA-
319	P	P	EA-
391	P	P/EA-	EA-/EA
439	P/EA-	EA-	EA-/EA
487	P/EA-	EA-	EA
535	EA-	EA	EA
583	EA-	EA	EA
631	EA-	EA	EA+
679	EA-	EA	EA+

Table 4.3. : Results of MASTMAASIS Test for 2024.

Time (hours)	Surface	T/4	T/2
70	P	EA-	EA-
144	P/EA-	EA-	EA
189	EA-	EA	EA+
319	EA-	EA	EA+
391	EA	EA+	EB-
439	EA+	EA+/EB-	EB
487	EA+	EB-	EB
535	EA+/EB-	EB-	EB+
583	EB-	EB+	EC-
631	EB-	EB+	EC+

Where N = no appreciable attack

P = pitting

EA = superficial corrosion

EB = moderate corrosion

EC = severe corrosion

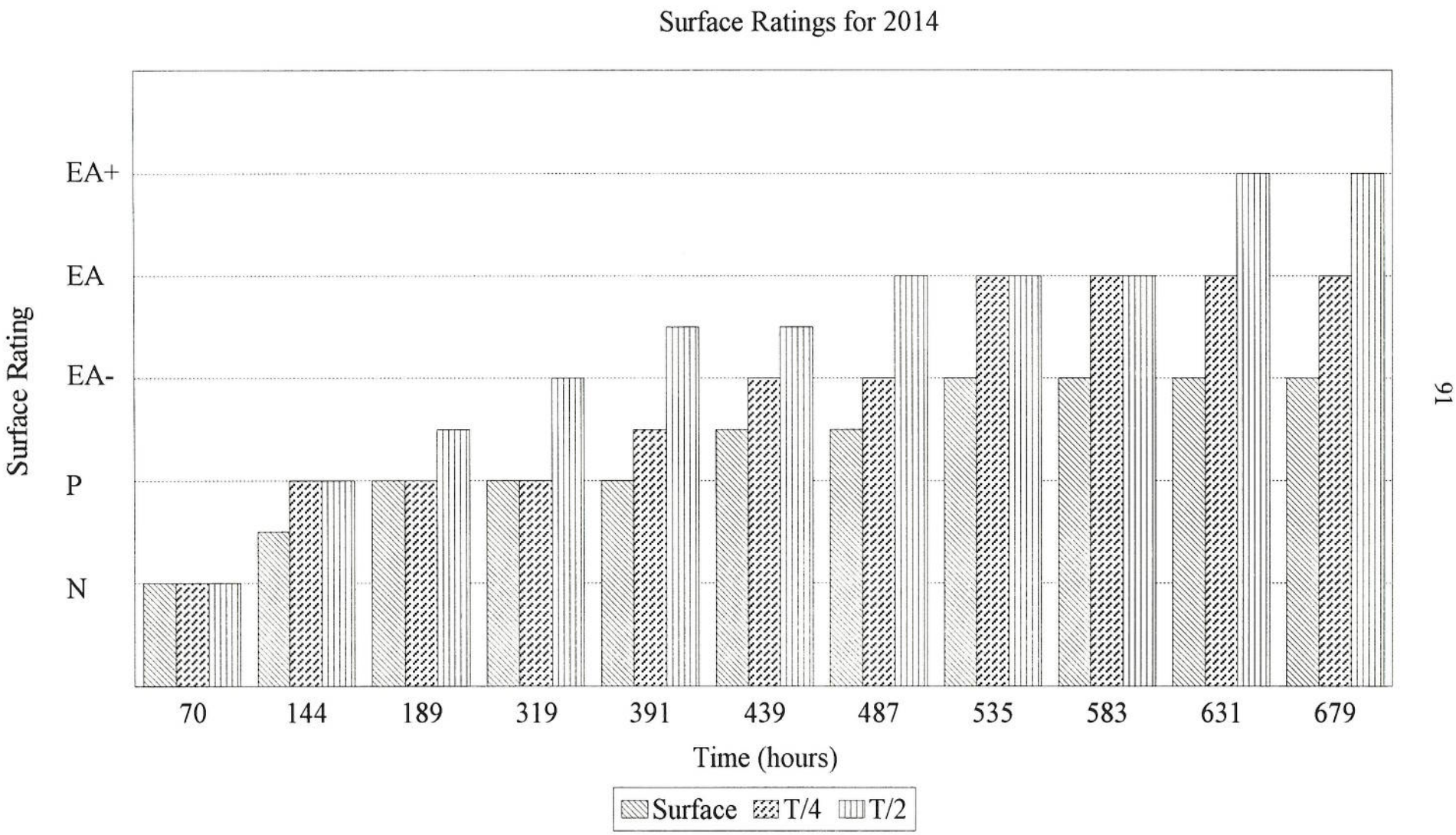

Figure 4.3. : Bar chart representing surface ratings for MASTMAASIS testing of 2014.

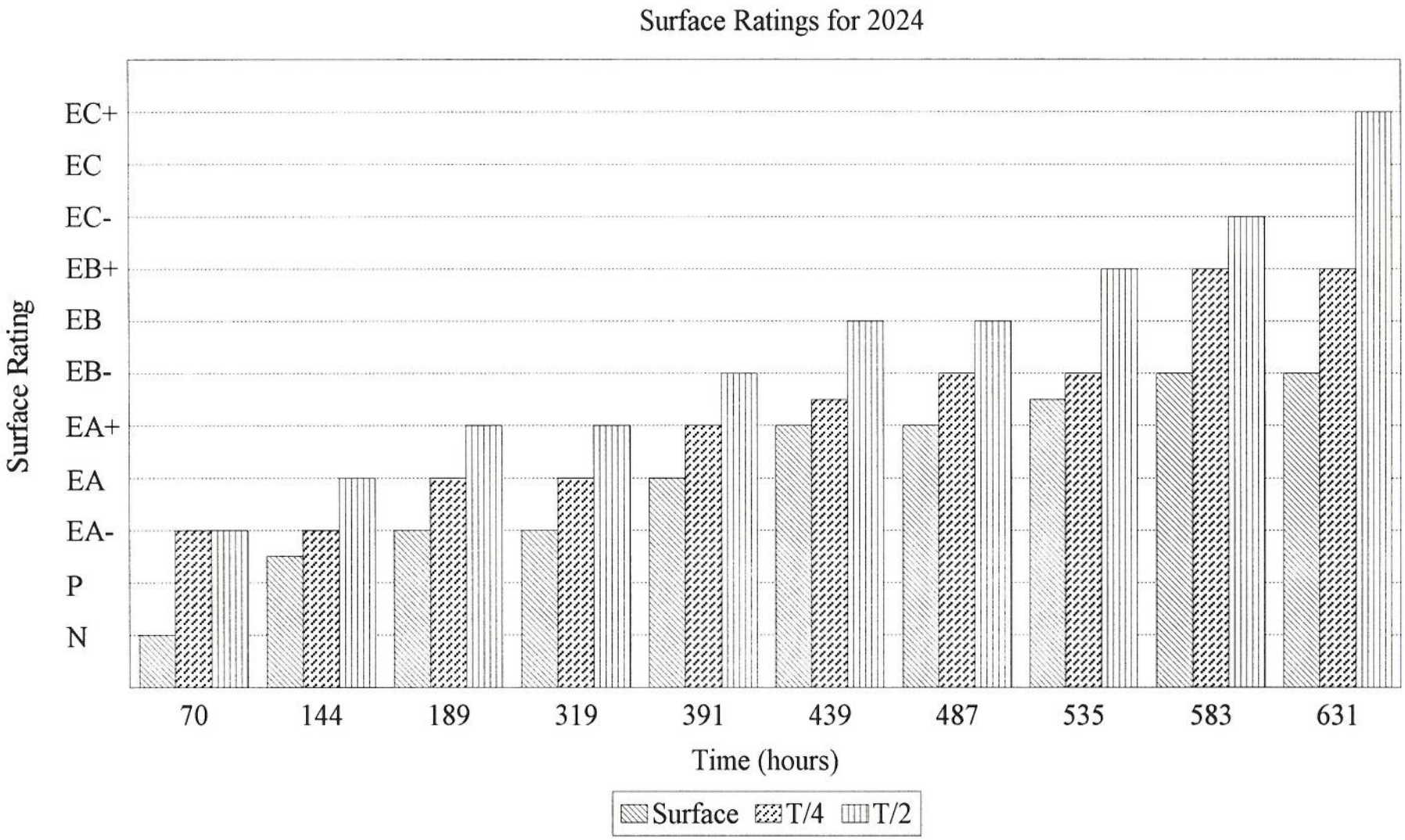

Figure 4.4. : Bar chart representing surface ratings for MASTMAASIS testing of 2024.

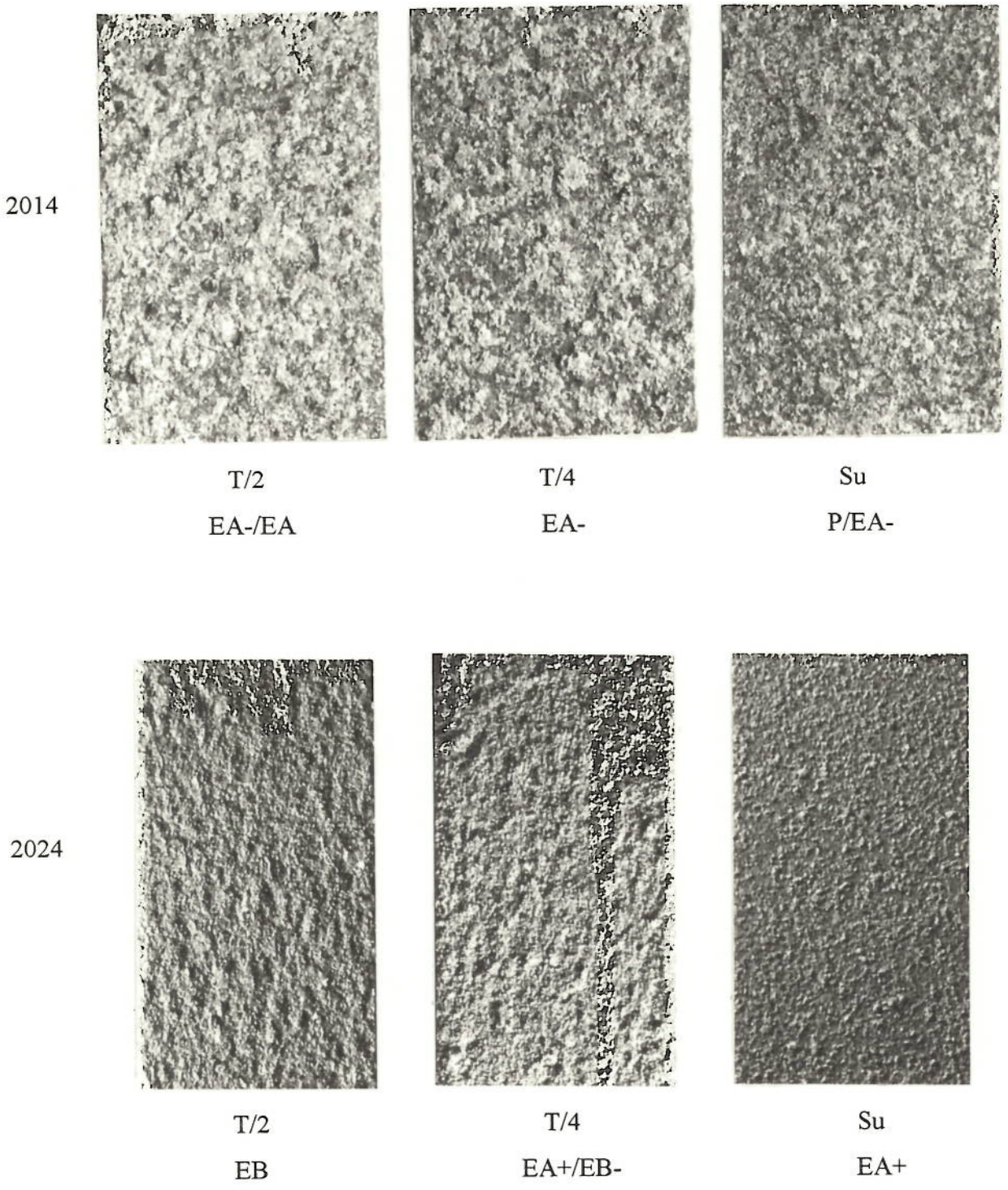

Figure 4.5. : Photographs showing the surface attack on 2014 and 2024 after 439 hours of MASTMAASIS testing (x2).

metal flaked from the surface of the specimen making classification of the degree of attack a little more difficult. Blisters in the 2014 alloy were more rounded in shape and tended to take longer to form. No metal loss occurred and the degree of attack did not increase a great deal throughout the duration of the test, only reaching EA+ in the extreme case even after almost 700 hours.

4.3.2. Depth of Attack Measurements

4.3.2.1. Bend Test Measurements

When each specimen was positioned on the bend rig, the load plate and attachments (marked in figure 4.2) acted as a separate load of 10N. This was useful when positioning the specimens and zeroing the dial gauge but it caused a small deflection on the specimen. The size of this initial deflection caused by this "preload" was obtained by plotting a graph of deflection against load, an example of which can be seen in figure 4.6. By extrapolating the straight line, the point of intersect on the Y axis was obtained which represented the initial deflection and this was taken into consideration in the final calculation to provide the true depth of attack. The combination of this preload and weights used was less than the maximum load allowed before exceeding the elastic limit of these aluminium alloys so no permanent deformation was detected in the specimens. The depths of attack obtained through four - point bend testing can be seen in figures 4.7 through to 4.12 representing the T/2, T/4 and surface sections of the 2014 and 2024 alloys. An example calculation can be seen below where the deflection represents the combination of preload and the weight used for testing:

Alloy 2014 T/2 after 631 hours:

Initial thickness	(d_O) = 2.97mm	L = 180mm
Load	(W) = 48.2N	a = 90mm
Deflection	(δ) = 1.47mm	E = 8 x 10^{10}Nmm^{-2}

Where d = thickness after 631 hours.

$$\delta = \frac{Wa(3L^2 - 4a^2)}{4Ebd^3}$$

Rearranging:

$$d = \sqrt[3]{\frac{Wa(3L^2 - 4a^2)}{4Eb\delta}}$$

$$d = \sqrt[3]{\frac{48.2x90x10^{-3}(3x(180x10^{-3})^2) - (4x(90x10^{-3})^2)}{4x8x10^{10}x0.03x1.47x10^{-3}}}$$

$$= \sqrt[3]{\frac{0.281}{14112000}}$$

$$= 2.71\text{mm}$$

Hence the depth of attack is:

$$2.97 - 2.71 = 0.26\text{mm}$$

4.3.2.2. Metallographic Assessment

The average and maximum depths of attack measured through metallographic assessment were compared to the depths of attack obtained through bend rig testing and are shown in the plots of depth of attack against time in figures 4.7 through to 4.12. In both alloys the attack seems to be fairly linear but the longer the test duration there seems to be a slight decrease in the rate of attack. This may be due to the corrosion having to follow a more tortuous path as the attack penetrates further into the material. As expected the depth of attack increases in the order surface < T/4 < T/2, ie the higher the aspect ratio the greater the depth.

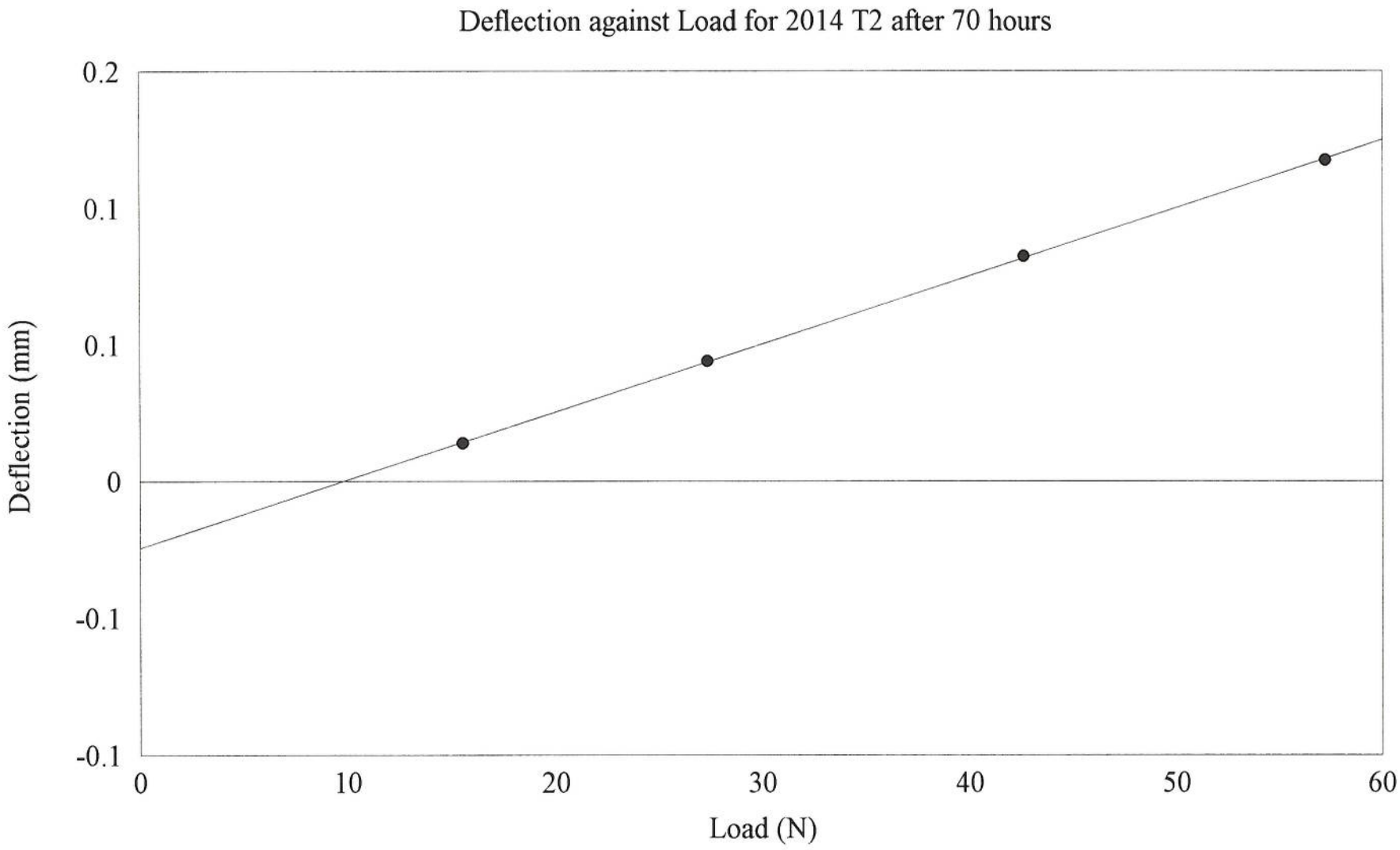

Figure 4.6. : Graph showing straight line of deflection against load for 2014 T/2.

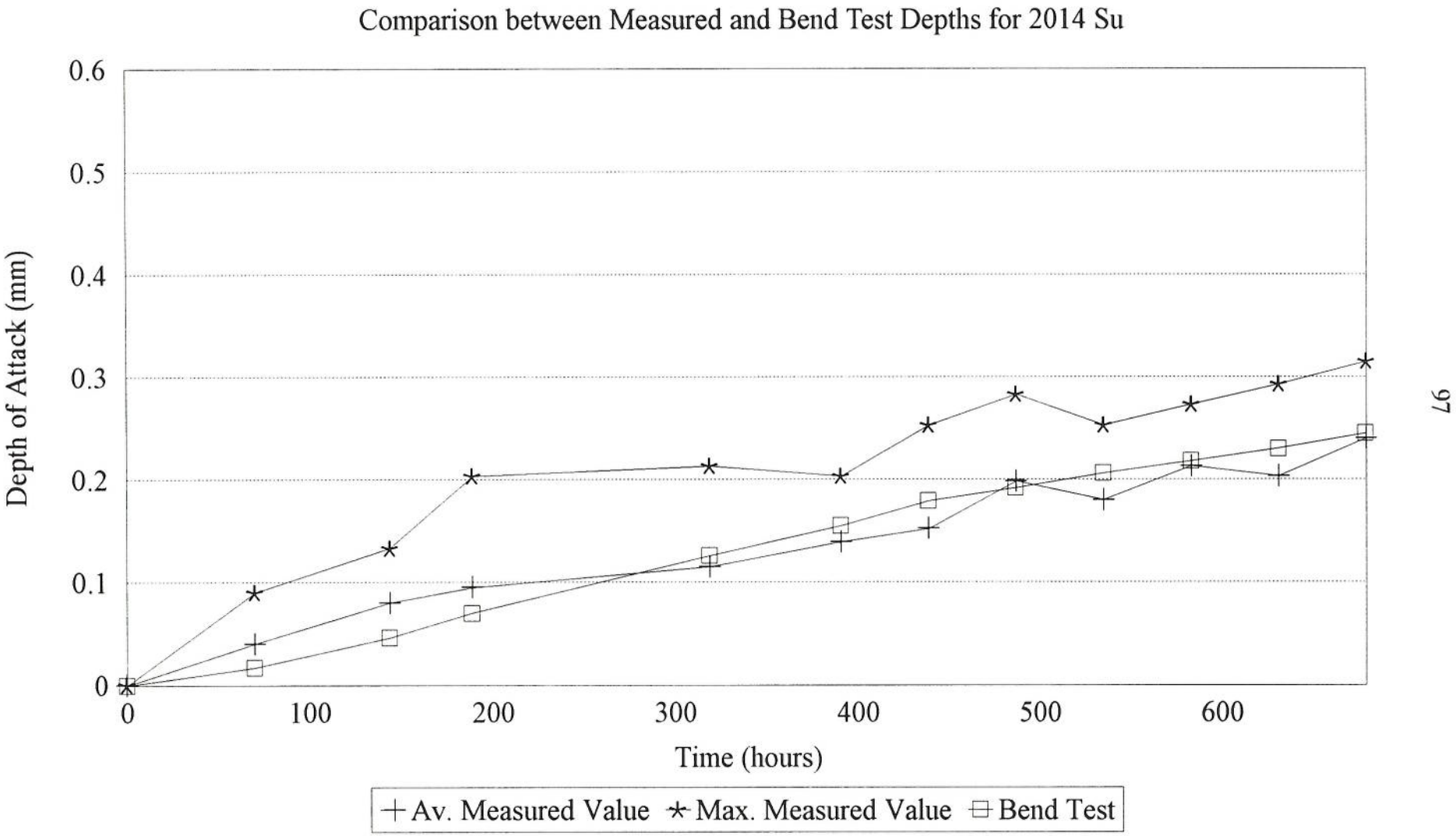

Figure 4.7. : Graph of depth of attack against time for 2014 Surface.

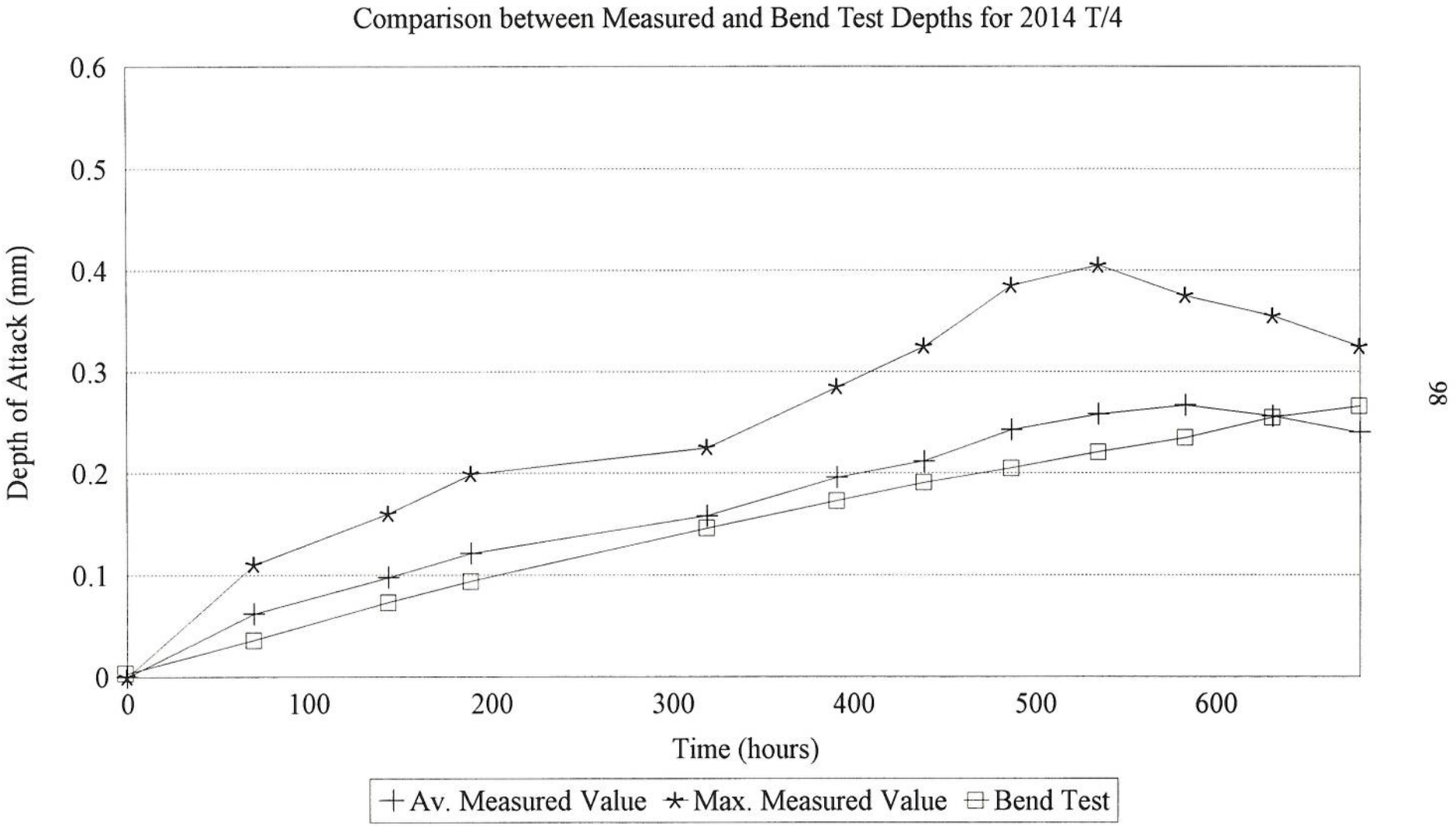

Figure 4.8. : Graph of depth of attack against time for 2014 T/4.

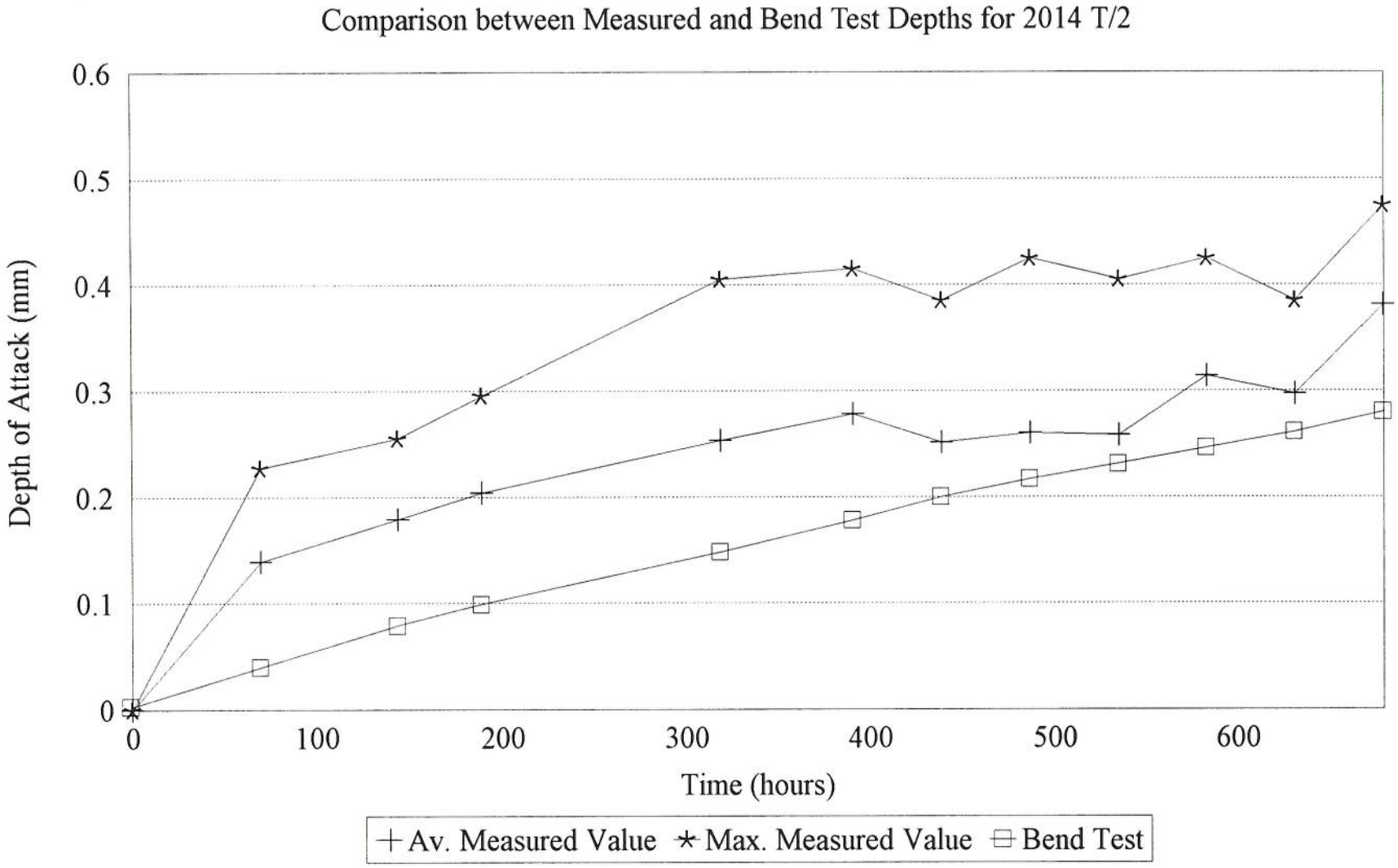

Figure 4.9. : Graph of depth of attack against time for 2014 T/2.

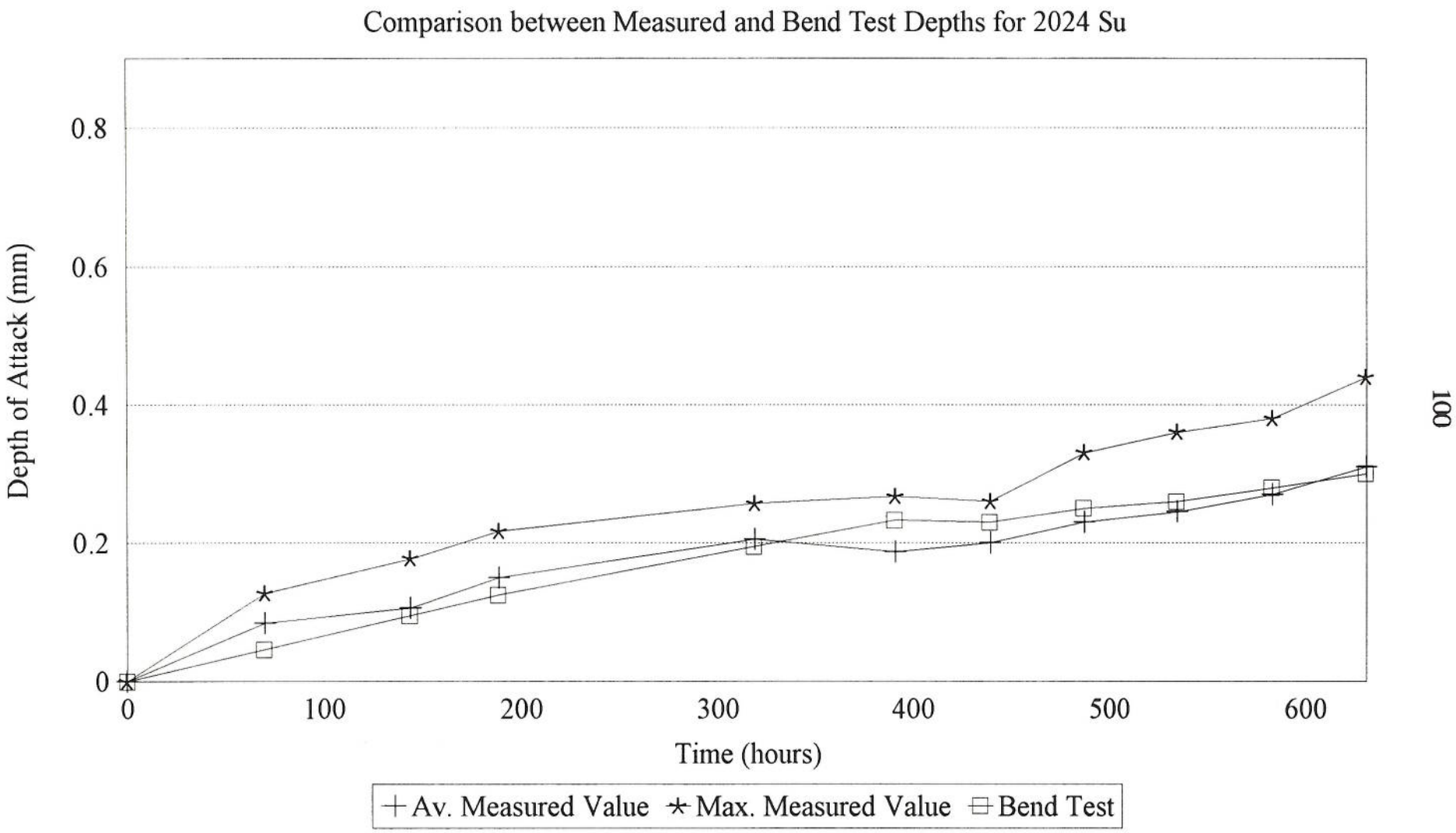

Figure 4.10. : Graph of depth of attack against time for 2024 Surface.

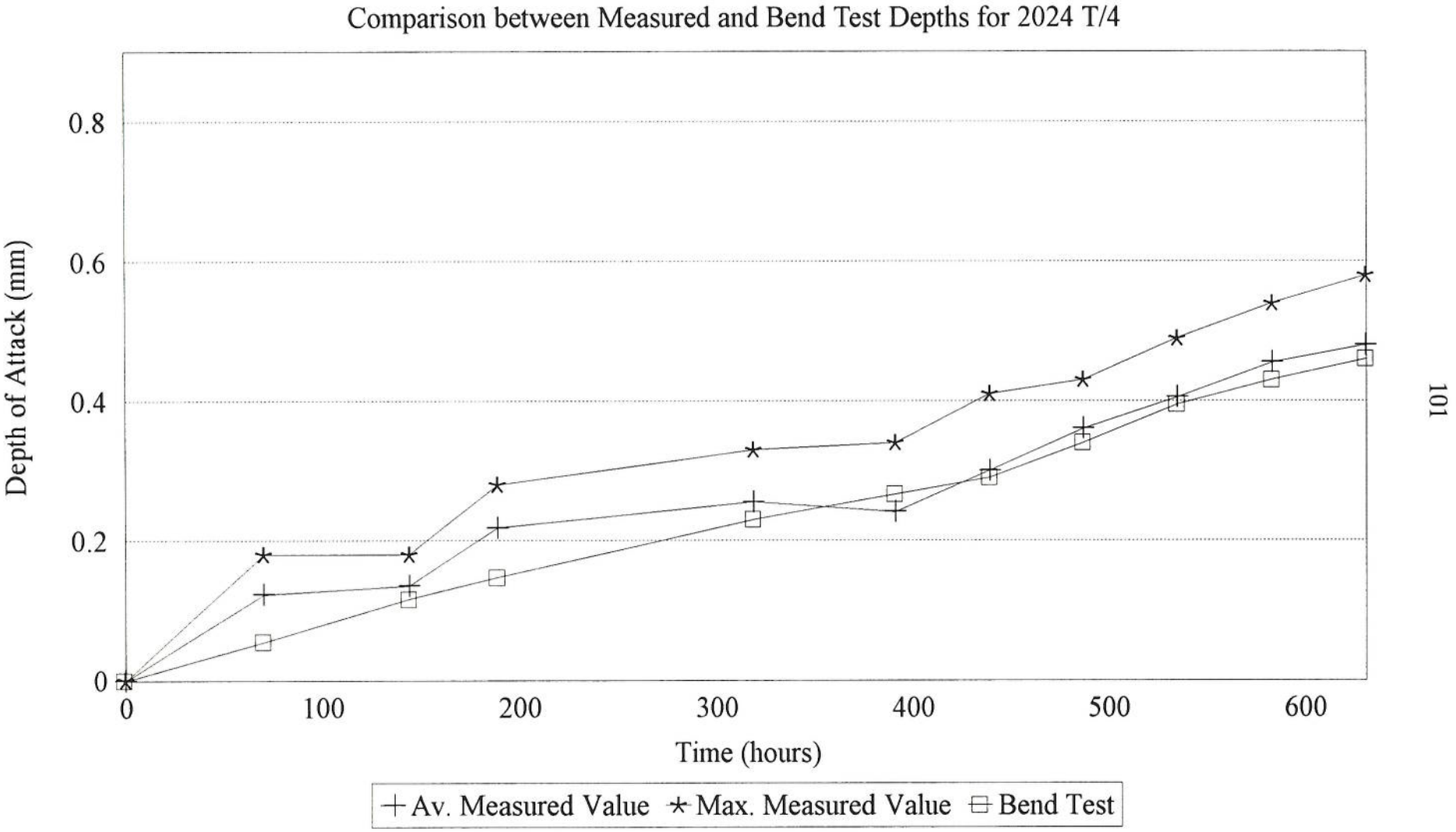

Figure 4.11. : Graph of depth of attack against time for 2024 T/4.

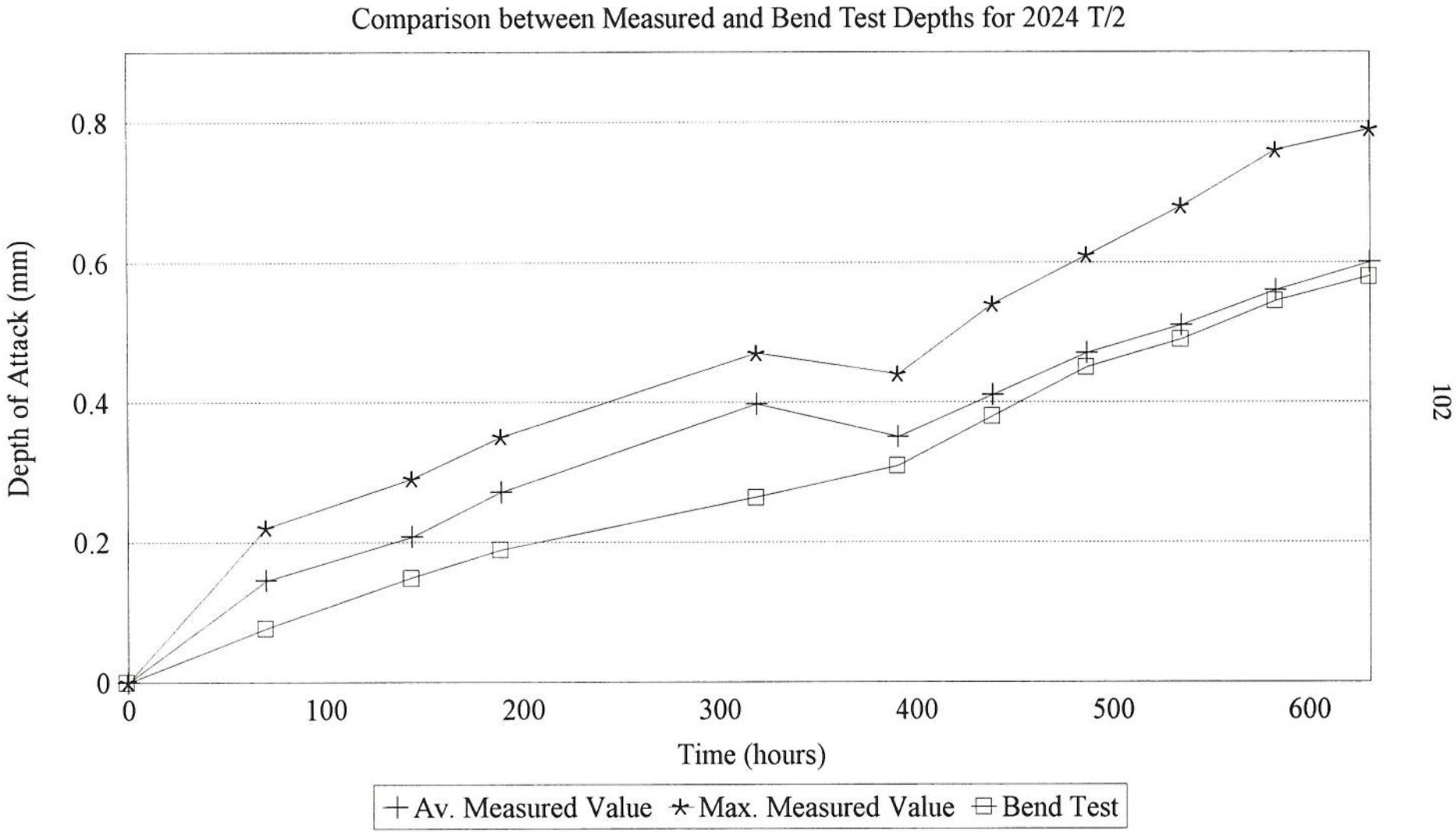

Figure 4.12. : Graph of depth of attack against time for 2024 T/2.

It is interesting to note that the bend test values are lower than the average measured depths. As the test duration increases the bend test value approaches that of the average depth of attack. It appears that the depths of attack agree with the surface ratings. The surface rating worsens in the order surface < T/4 < T/2 as does the depth of attack which is greatest in the T/2 section of the plate.

Figure 4.13 shows the morphology of attack for the 2XXX alloys. The morphology exhibited blistering where some of these blisters were close to bursting suggesting exfoliation corrosion. The width of the attack appeared to increase from the surface through to the T/2 section. As the test duration increased the attack tended to spread outwards forming a network under the surface.

4.3.2.3. Intergranular Corrosion Velocity

The calculated intergranular velocities can be seen in tables 4.4 and 4.5 for 2014 and 2024. The higher velocities suggest that the 2024 alloy is more susceptible to corrosion than 2014. It can be seen that the velocity increases toward the centre of the plate and is higher in the 2024 alloy compared to the velocity of the 2014 alloy hence increasing the corrosion susceptibility.

4.3.3. Heat Treatment for 2024

The depths of attack can be seen in figures 4.14 through to 4.19 for the peak and over - aged conditions for the 2024 alloy. Again, as in the under - aged alloy the bend test values appear to be lower than those obtained through metallographic assessment. The peak - aged material appears to be more susceptible to attack than the over - and under - aged materials and the susceptibility increases in the order over - aged < under - aged < peak - aged. Figure 4.20 represents a bar chart comparing the depths of attack between the three heat treatment conditions.

a)

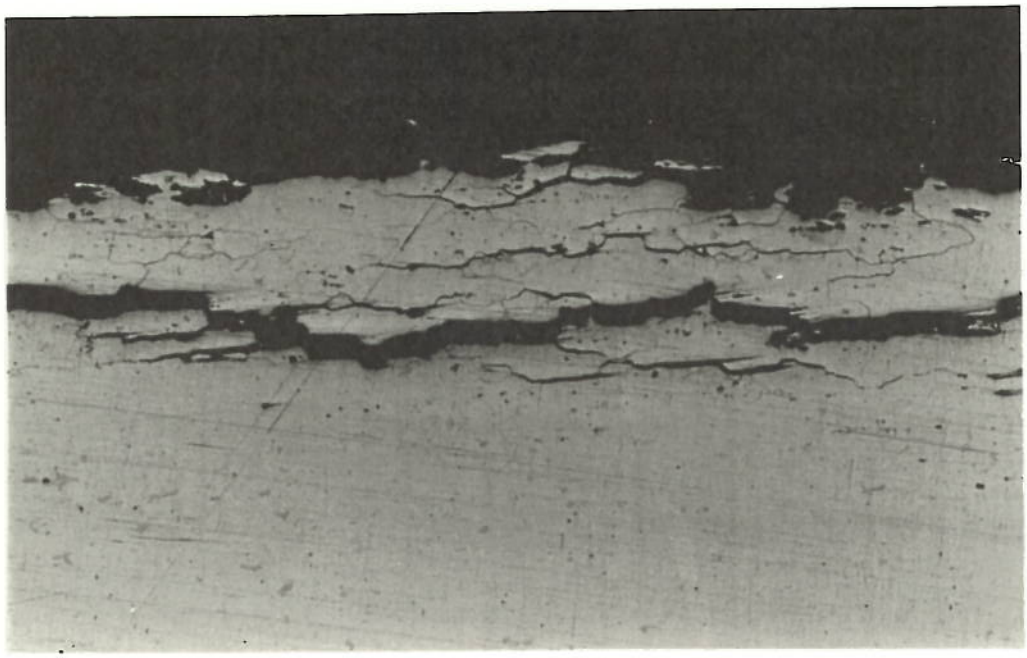

b)

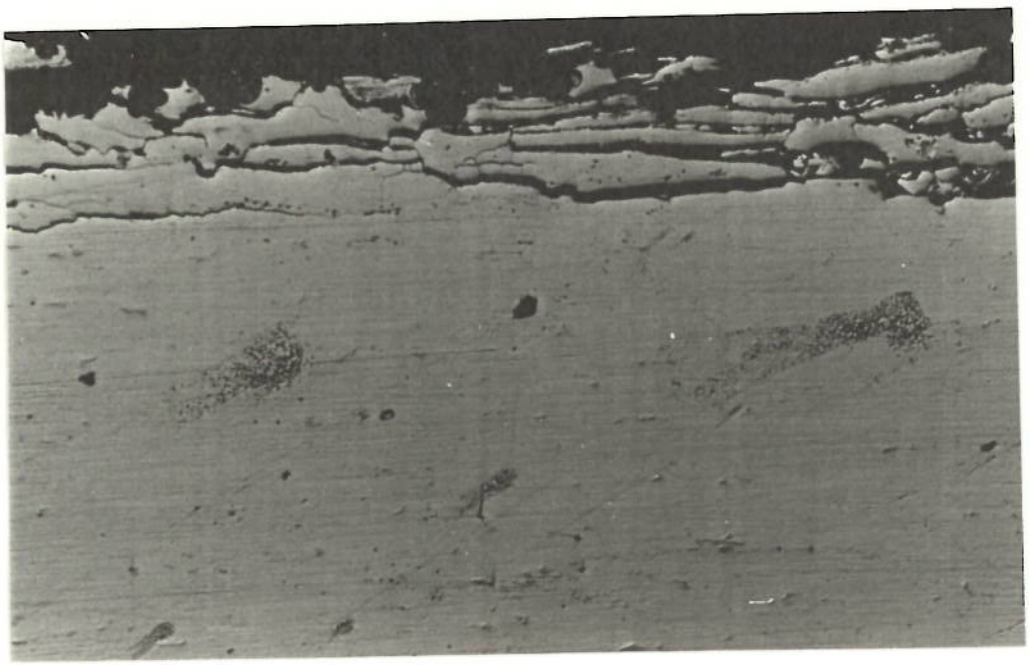

Figure 4.13. : Cross - sections showing attack for 2024 after 319 hours of MASTMAASIS testing where a and b represent the T/2 and T/4 sections respectively (x100).

Table 4.4. : Intergranular Velocities for 2014.

Time (hours)	Intergranular Velocity (ms^{-1})		
	Surface ($x10^{-10}$)	T/4 ($x10^{-10}$)	T/2 ($x10^{-10}$)
70	4.29±0.57	8.3±1.53	34.3±0.56
144	4.17±0.55	7.56±1.34	21±0.34
189	4.4±0.58	8.27±1.42	18.9±0.31
319	3.38±0.44	6.5±1.12	14.8±0.24
391	3.41±0.44	6.62±1.13	13.6±0.22
439	3.12±0.4	6.93±1.17	10.7±0.17
487	3.86±0.5	7.26±1.22	9.7±0.16
535	3.1±0.4	6.69±1.14	8.9±0.14
583	3.28±0.43	6.18±1.05	10.1±0.16
631	2.99±0.39	5.66±0.96	8.5±0.14
679	3.21±0.42	5.19±0.87	10.5±0.16

Table 4.5. : Intergranular Velocities for 2024.

Time (hours)	Intergranular Velocity (ms^{-1})		
	Surface ($x10^{-10}$)	T/4 ($x10^{-10}$)	T/2 ($x10^{-10}$)
70	13.4±2.3	23.5±0.32	41±0.57
144	8.57±1.5	13.9±0.18	27.5±0.39
189	9.67±1.7	16.9±0.22	28.4±0.4
319	7.68±1.3	12.4±0.16	24.7±0.34
391	5.54±0.96	9.2±0.12	17.4±0.24
439	5.55±0.97	10.8±0.14	18±0.25
487	5.66±1	14.1±0.15	19.1±0.28
535	5.7±0.98	11.8±0.15	18.7±0.26
583	5.73±1	12±0.16	19±0.26
631	5.84±1.02	11.9±0.15	18±0.26

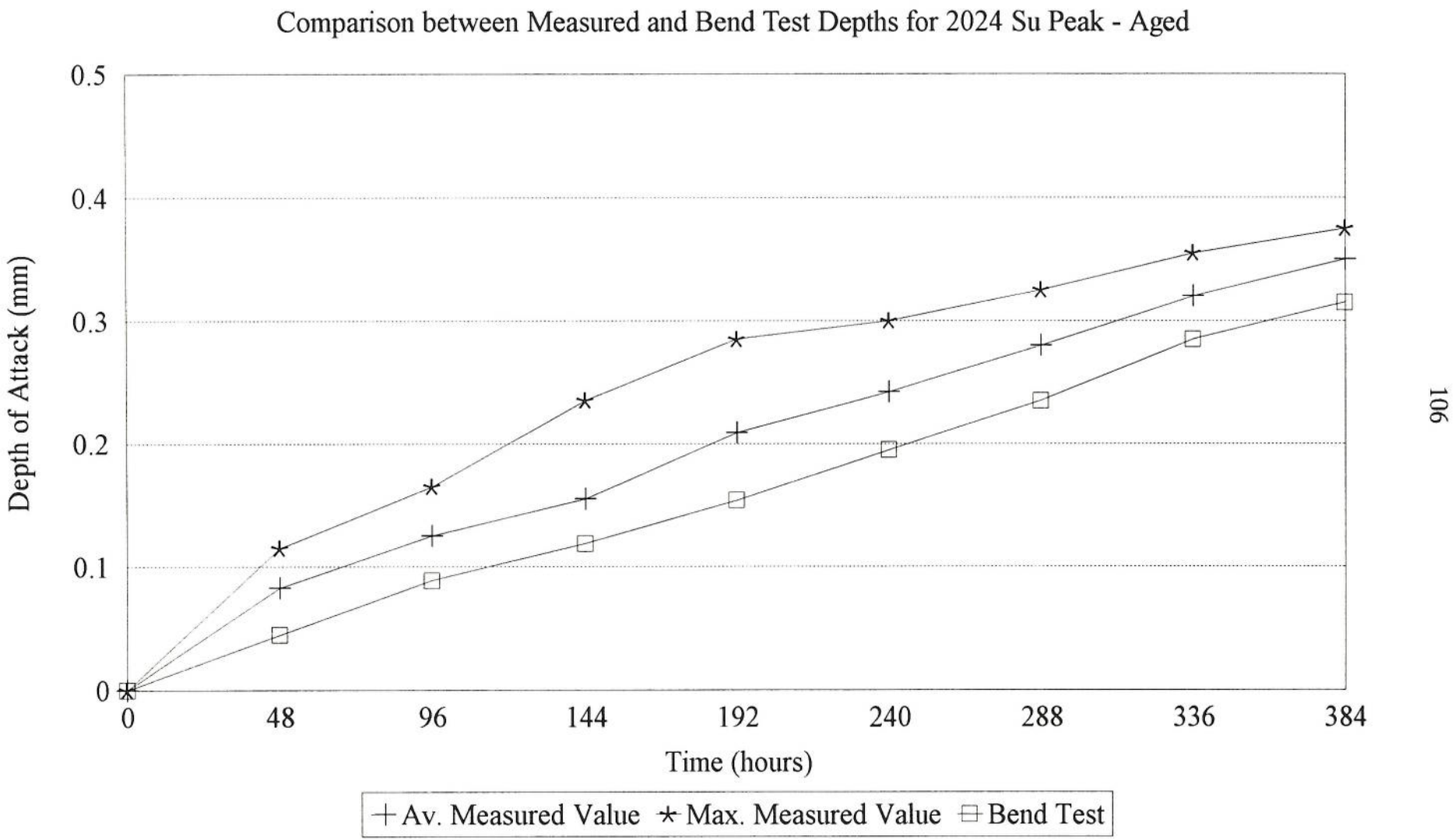

Figure 4.14. : Graph of depth of attack against time for 2024 surface peak - aged.

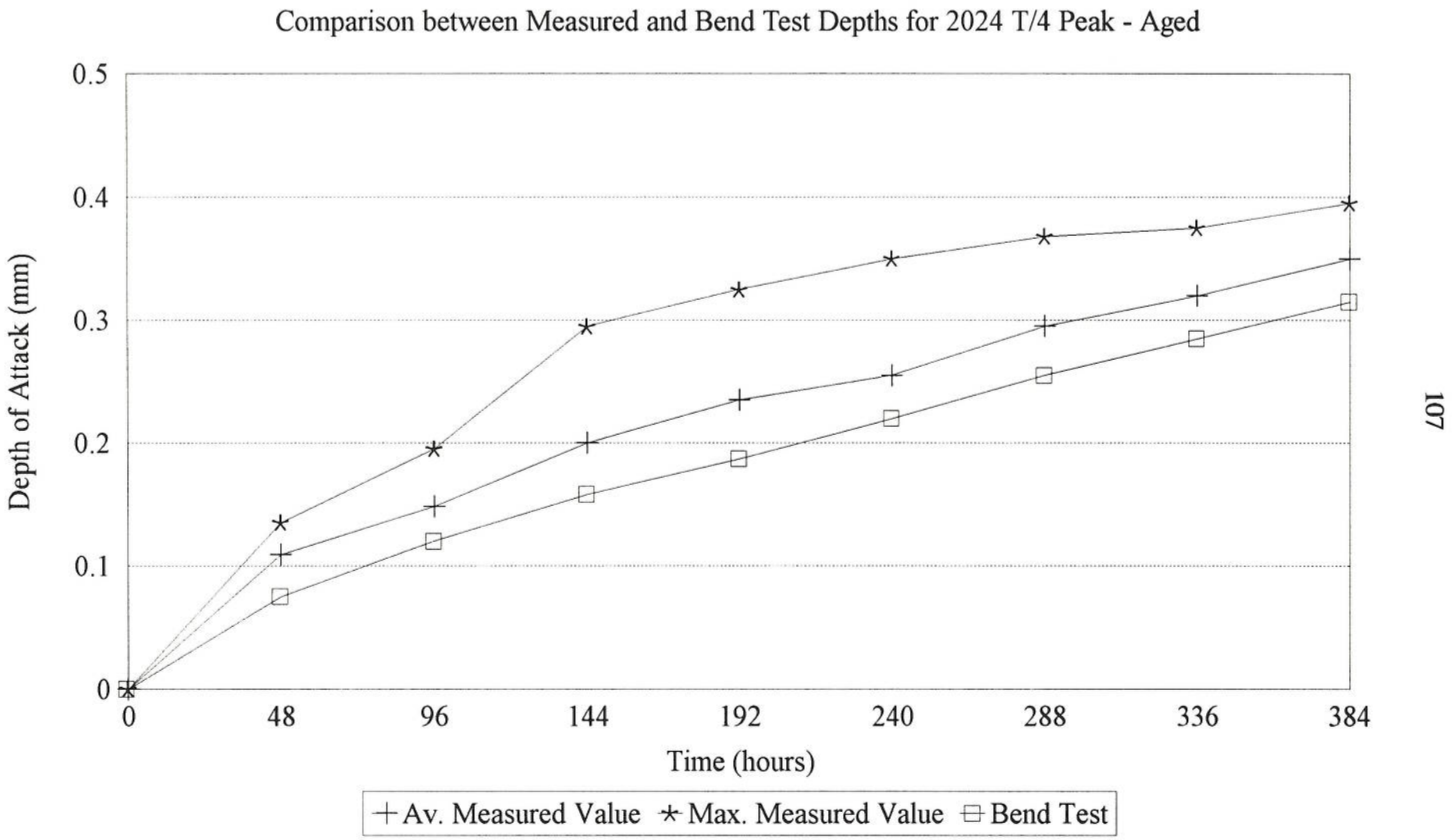

Figure 4.15. : Graph of depth of attack against time for 2024 T/4 peak - aged.

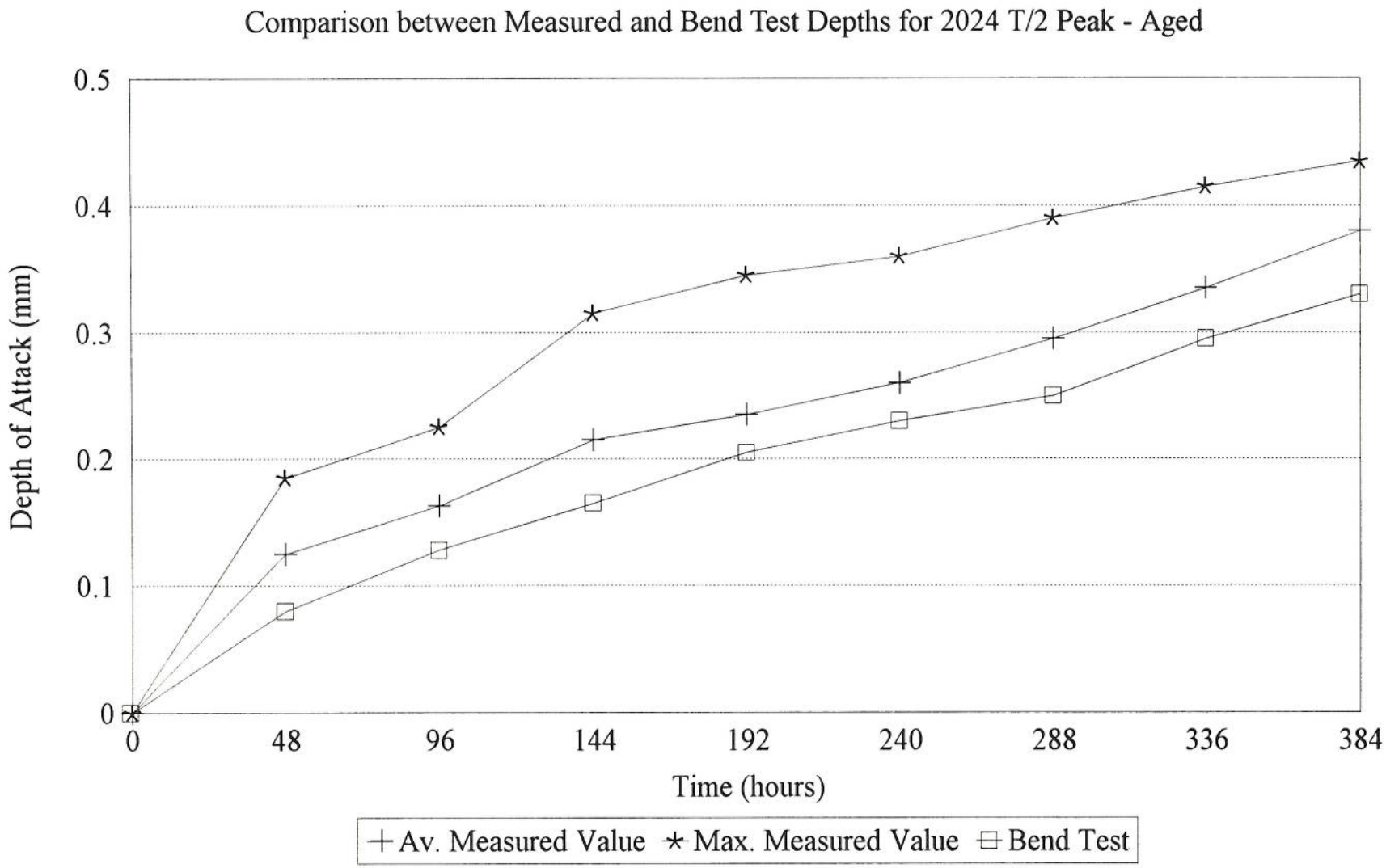

Figure 4.16. : Graph of depth of attack against time for 2024 T/2 peak - aged.

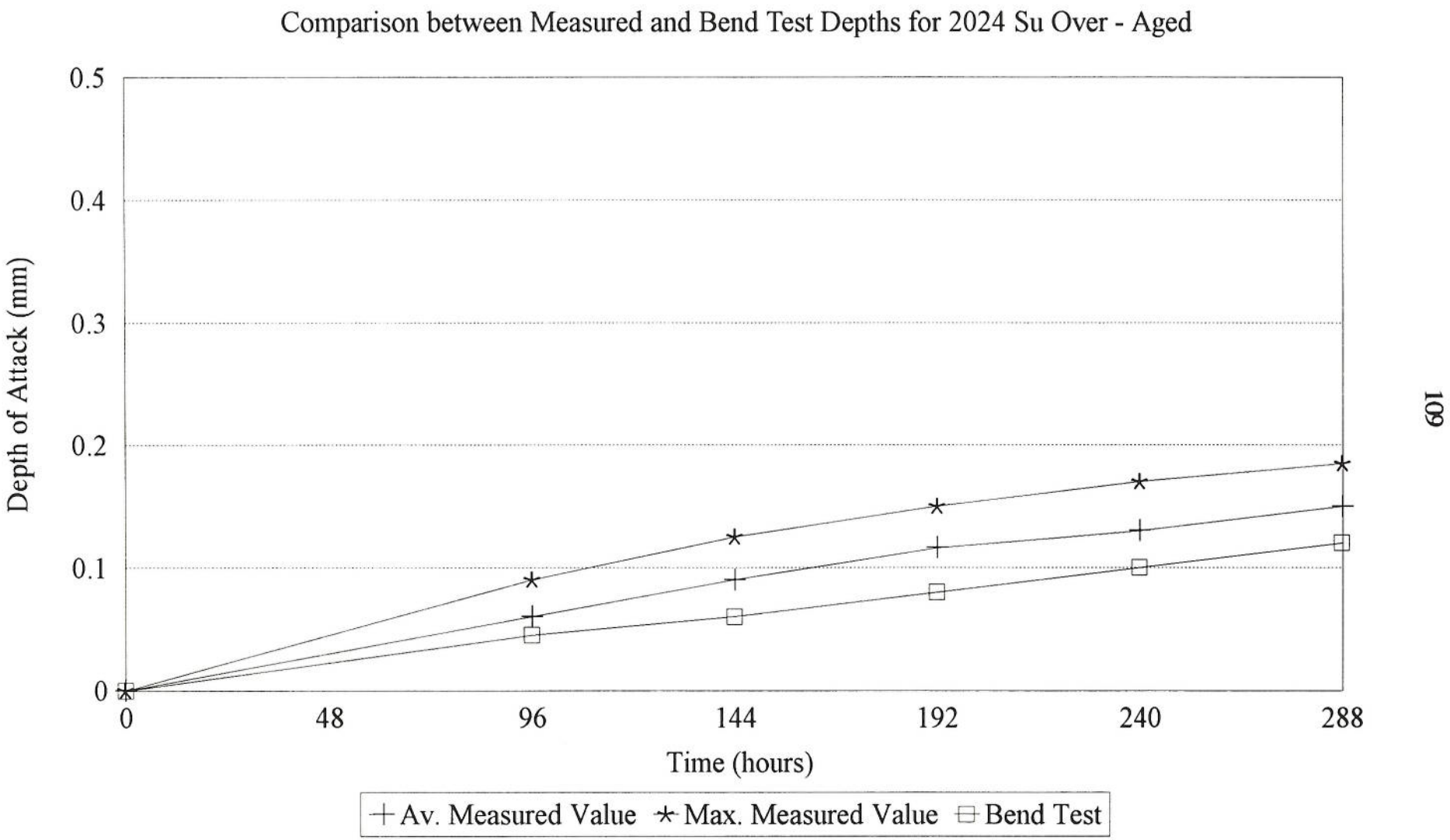

Figure 4.17. : Graph of depth of attack against time for 2024 surface over - aged.

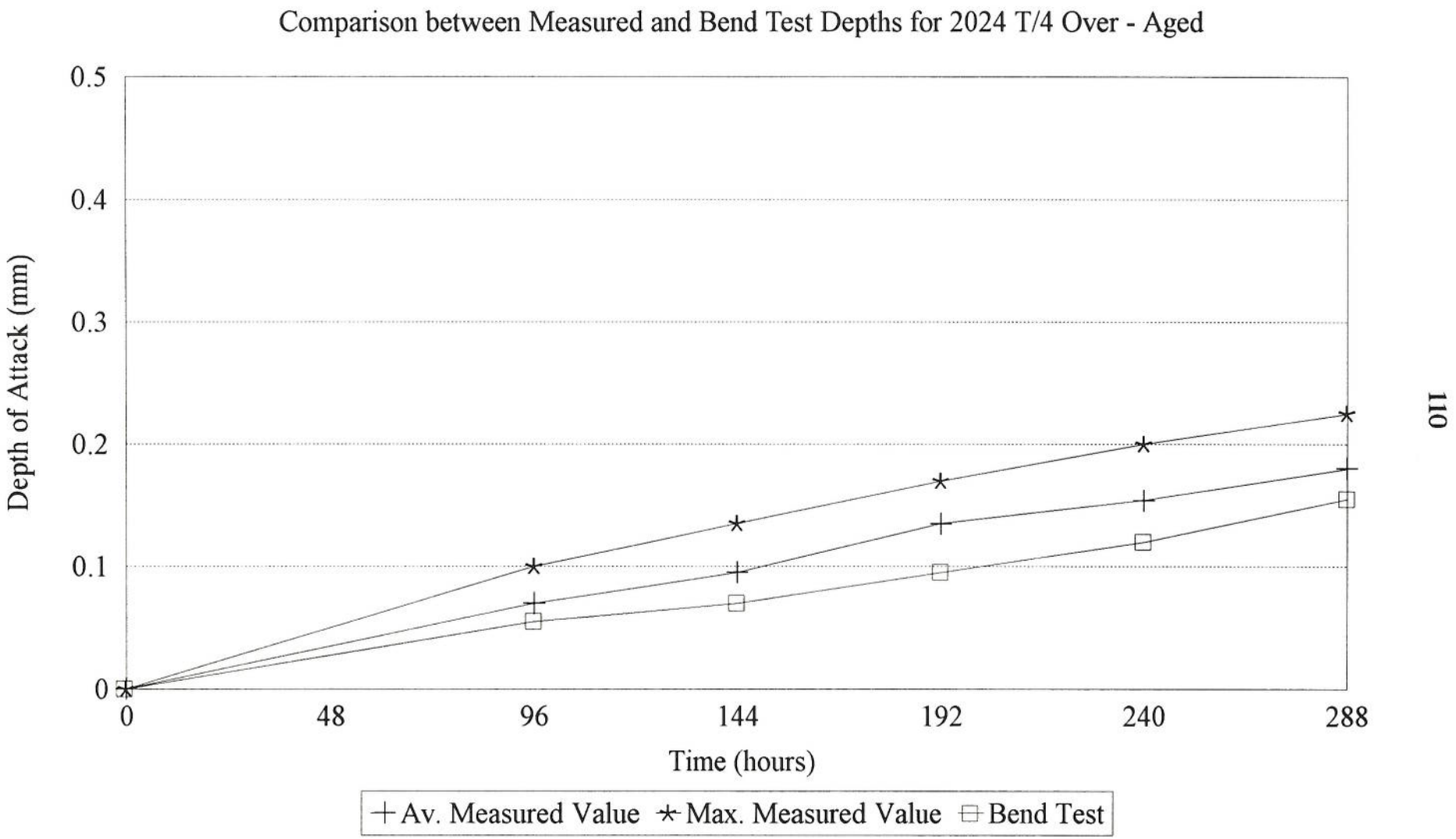

Figure 4.18. : Graph of depth of attack against time for 2024 T/4 over - aged.

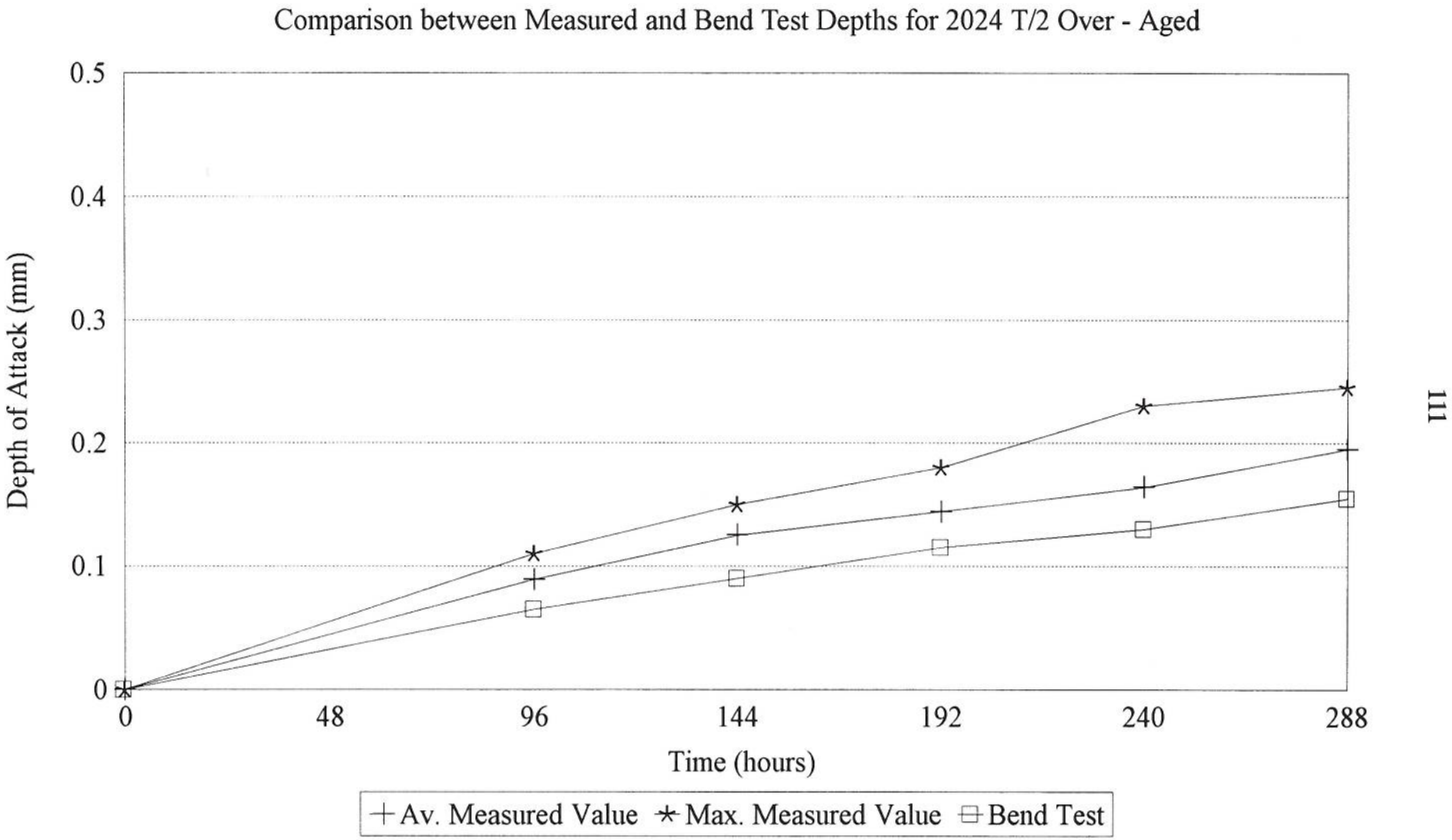

Figure 4.19. : Graph of depth of attack against time for 2024 T/2 over - aged.

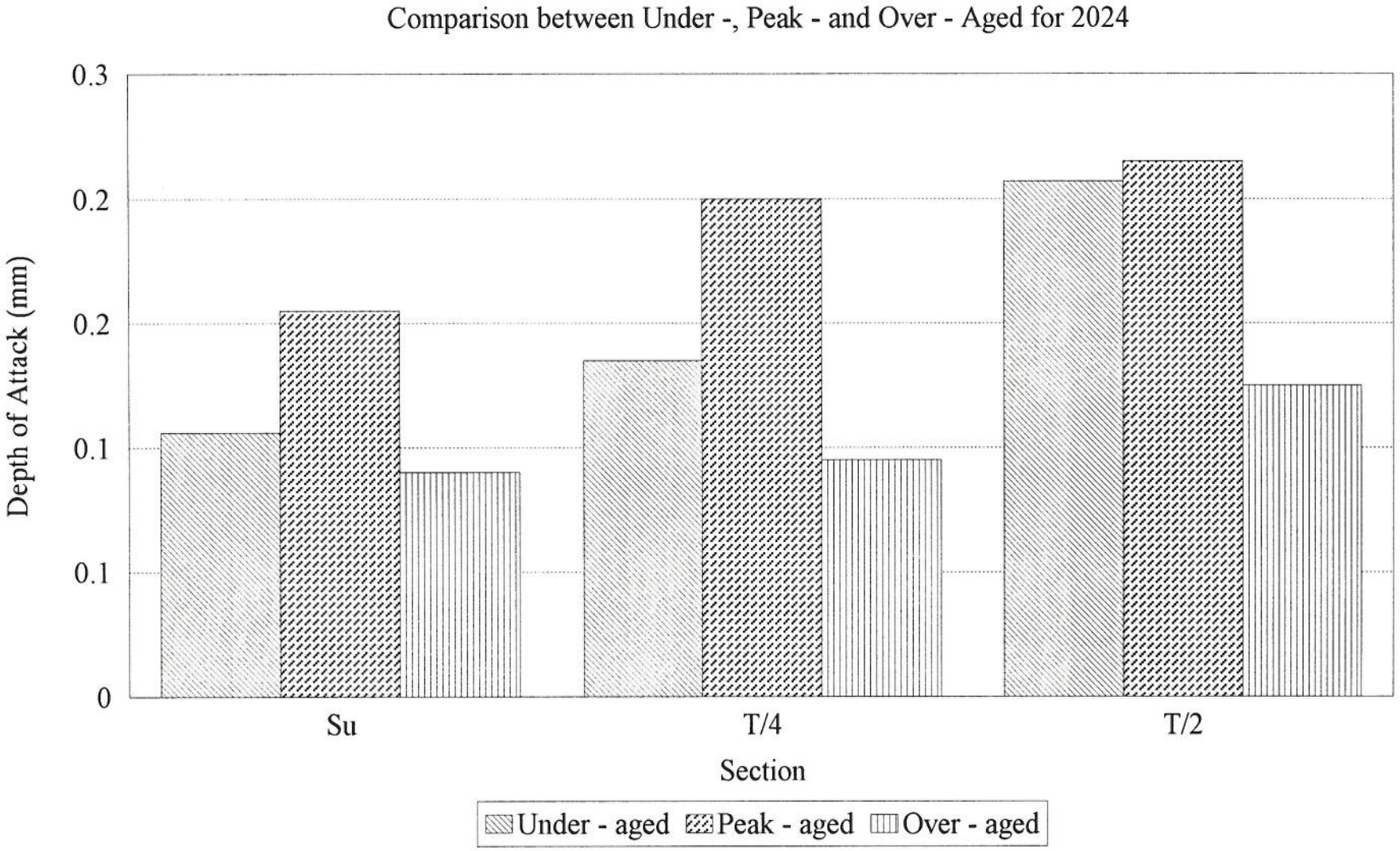

Figure 4.20. : Bar chart representing under -, peak - and over - aged conditions for 2024 after 144 hours.

4.4. Experimental Results for the Aluminium - Lithium Alloys

4.4.1. Visual Assessment

The degree of corrosion was ranked for the 8090 and 2091 alloys and can be seen in table 4.6. Surface ratings do not differ greatly between the under -, peak - and over - aged conditions for both the alloys. The under - aged condition for the 2091 alloy showed a slightly more favourable rating than the peak - and over - aged conditions, whereas the over - aged condition was more favourable for the 8090 alloy. Figures 4.21 and 4.22 represent the surface ratings in bar chart form. After 336 hours the degree of attack reached a surface rating of superficial corrosion for the peak - aged in both the 8090 and 2091 alloys. During the early stages of attack the surfaces showed varying degrees of pitting with large areas of material unattacked. As the duration of the test increased and corrosion continued, the density of pits increased and, eventually, the formation of blisters gave rise to increasing signs of exfoliation corrosion. In some cases these blisters had or were about to burst. The 2091 alloy, with the higher aspect ratio did show slightly worse surface ratings than 8090. Photographs of the surfaces can be seen in figure 4.23.

Table 4.6. : Results of MASTMAASIS Test for 8090 and 2091.

Time (hours)	8090			2091		
	Under	Peak	Over	Under	Peak	Over
48	N	N	N	N	N	N
96	N/P	N/P	N	N	P	N
144	N/P	P	N/P	N/P	P	N/P
192	P	P	N/P	P	P/EA-	P
240	P	P/EA-	P	P	P/EA-	P
288	P/EA-	EA-	P/EA-	P/EA-	EA-	P/EA-
336	P/EA-	EA	P/EA-	P/EA-	EA	EA

4.4.2. Depth of Attack Measurements

Figures 4.24 through to 4.29 represent a comparison between the maximum and average measured depths of attack and the bend test results. Again, as with the 2XXX

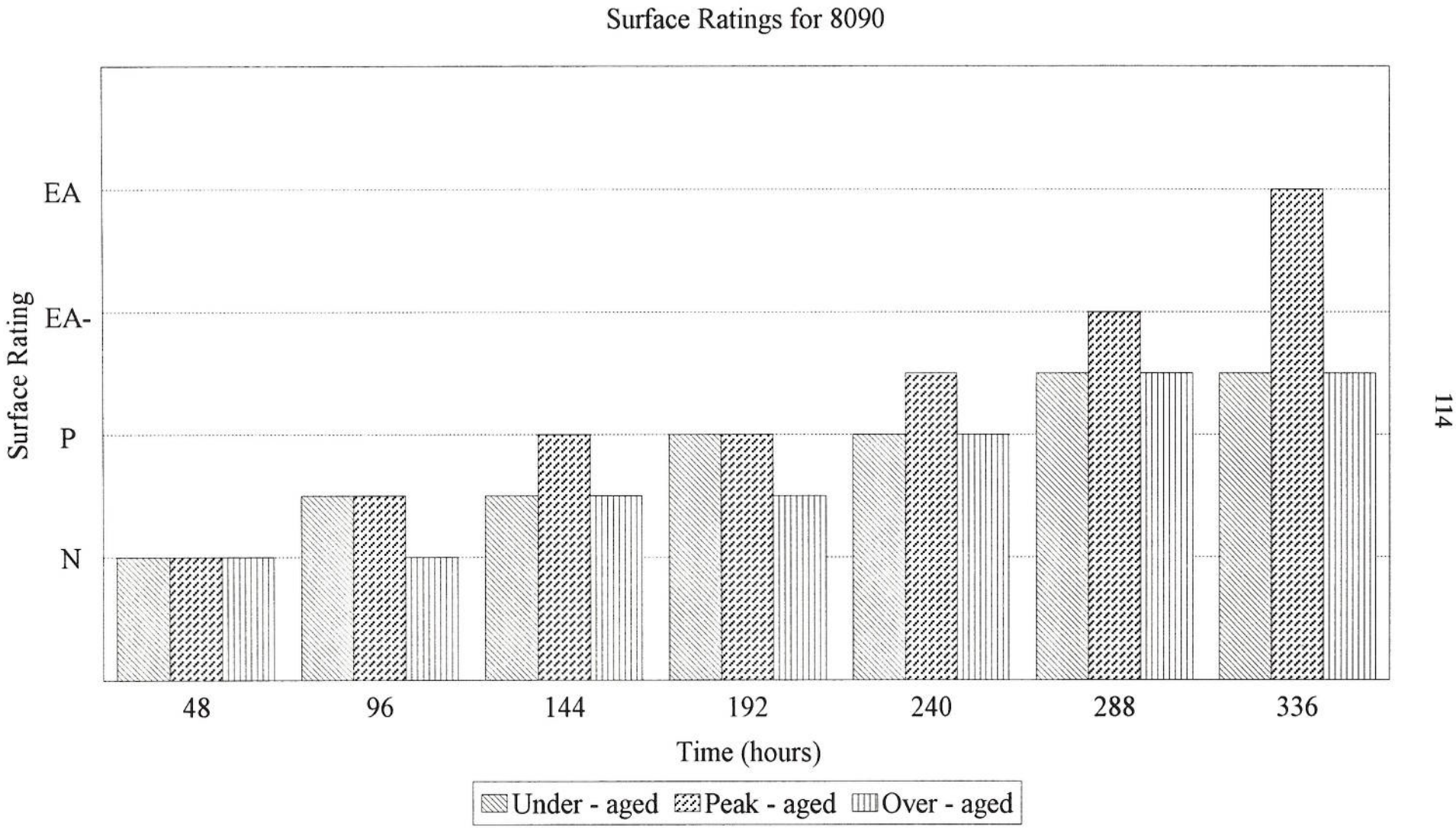

Figure 4.21. : Bar chart representing surface ratings for MASTMAASIS testing of 8090.

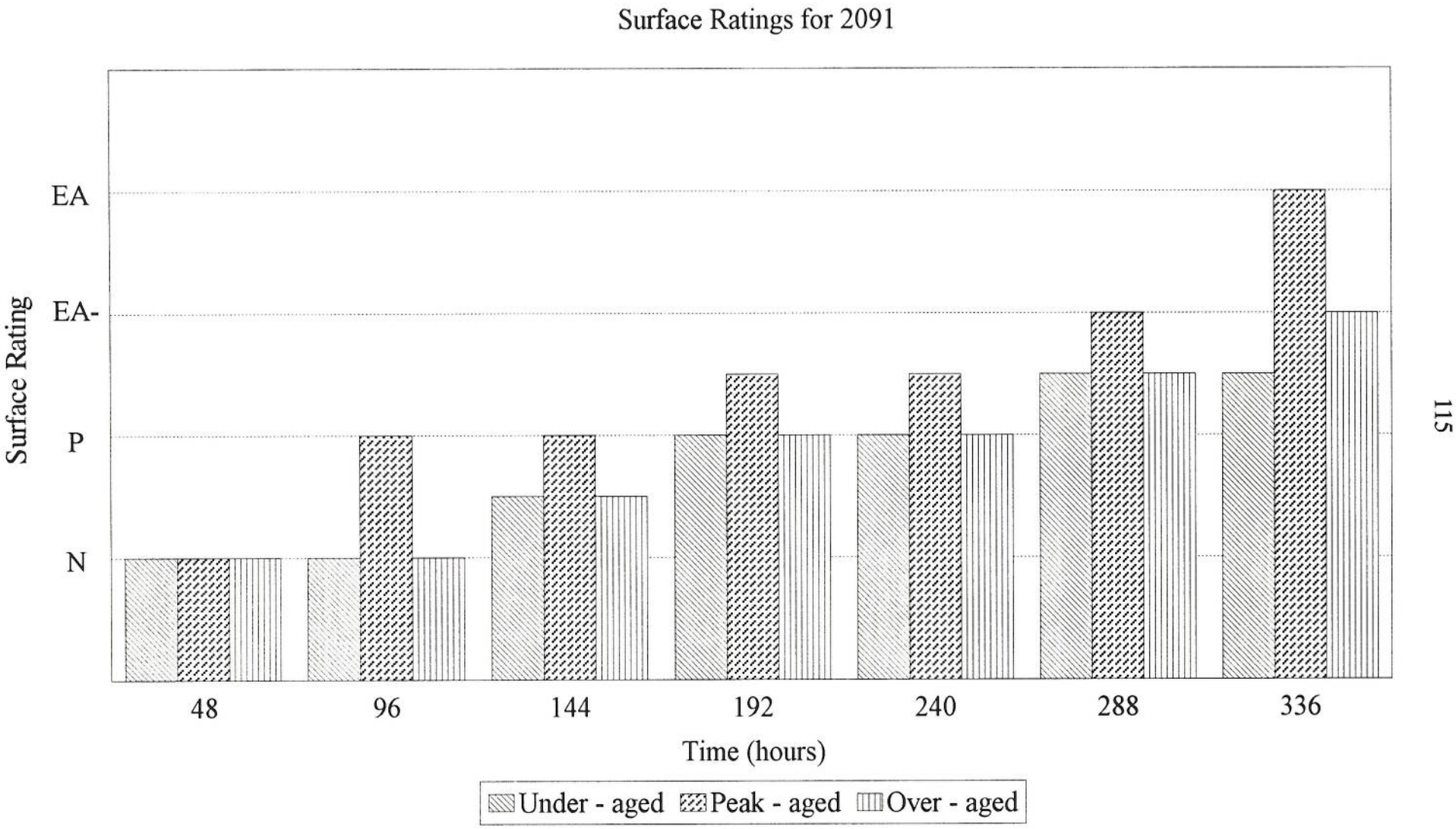

Figure 4.22. : Bar chart representing surface ratings for MASTMAASIS testing of 2091.

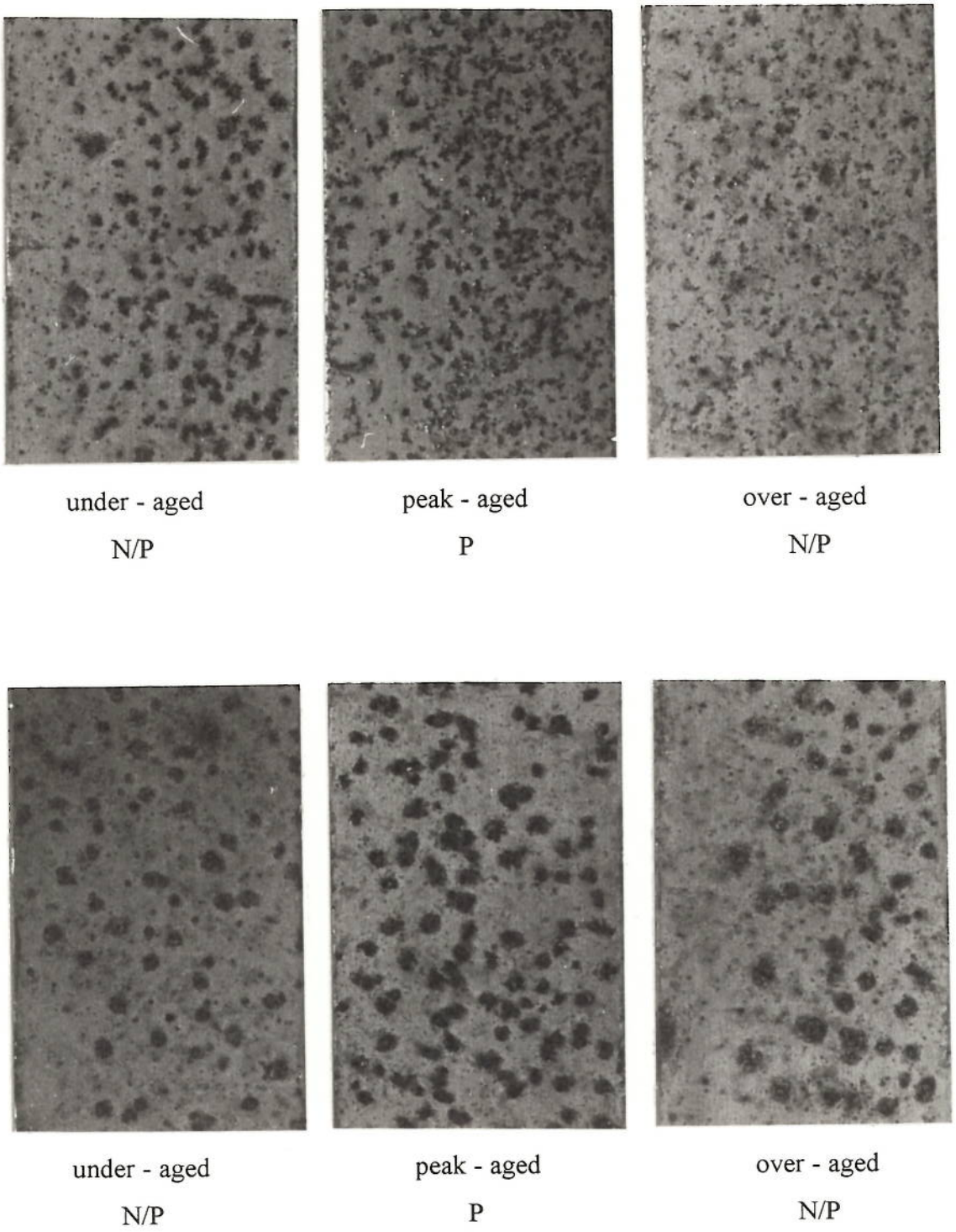

Figure 4.23. : Photographs showing the surface attack on 8090 and 2091 after 144 hours of MASTMAASIS testing (x2).

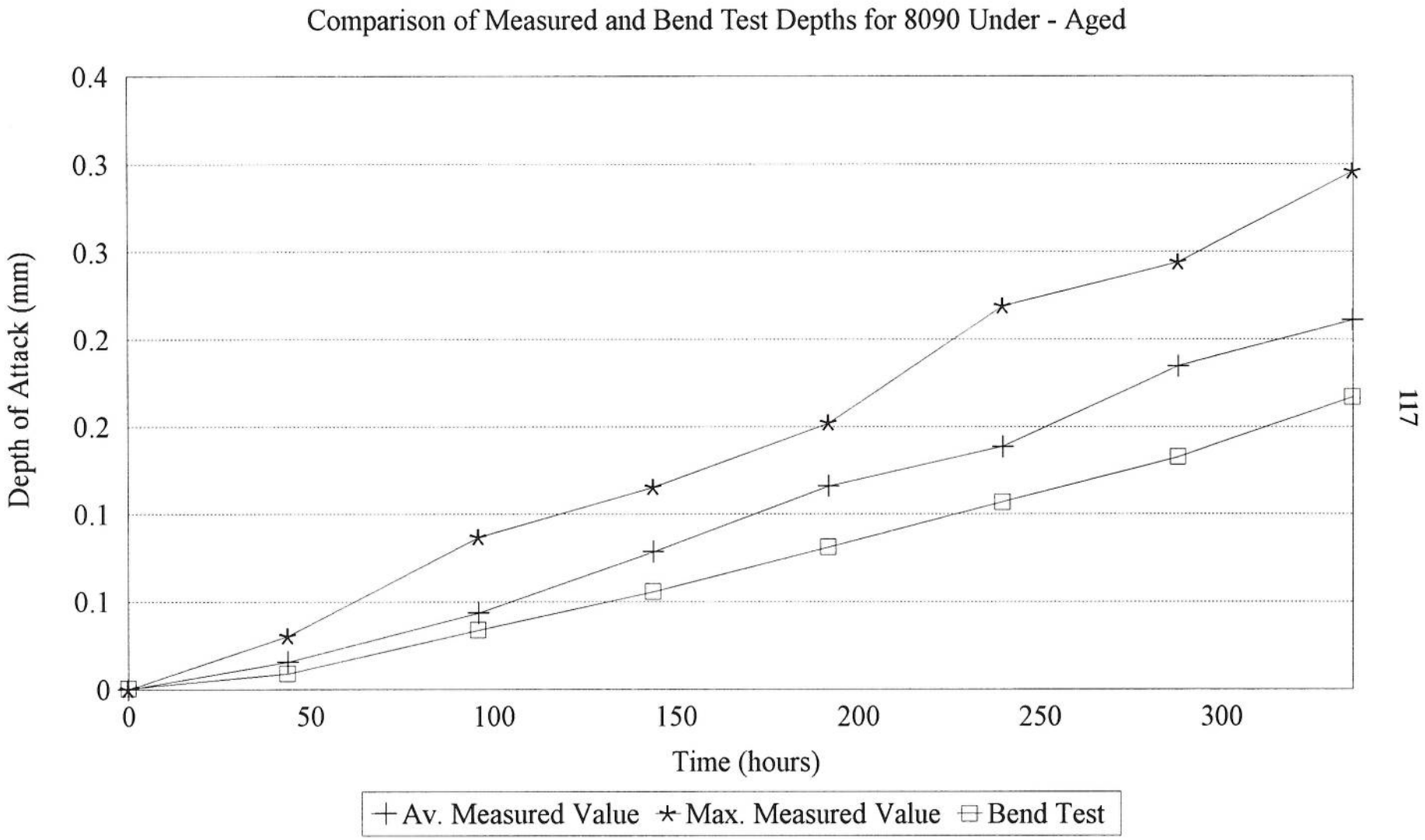

Figure 4.24. : Graph of depth of attack against time for 8090 under - aged.

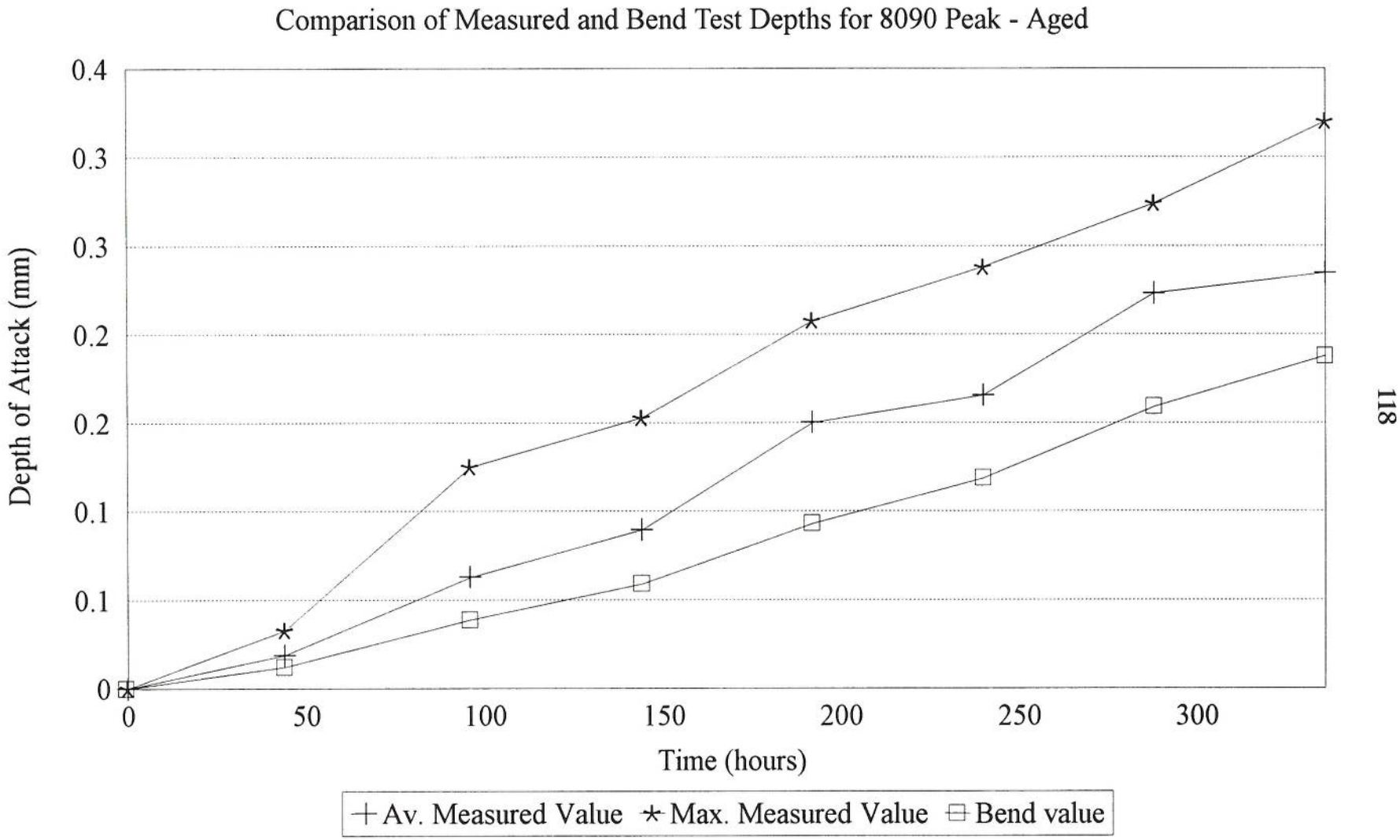

Figure 4.25. : Graph of depth of attack against time for 8090 peak - aged.

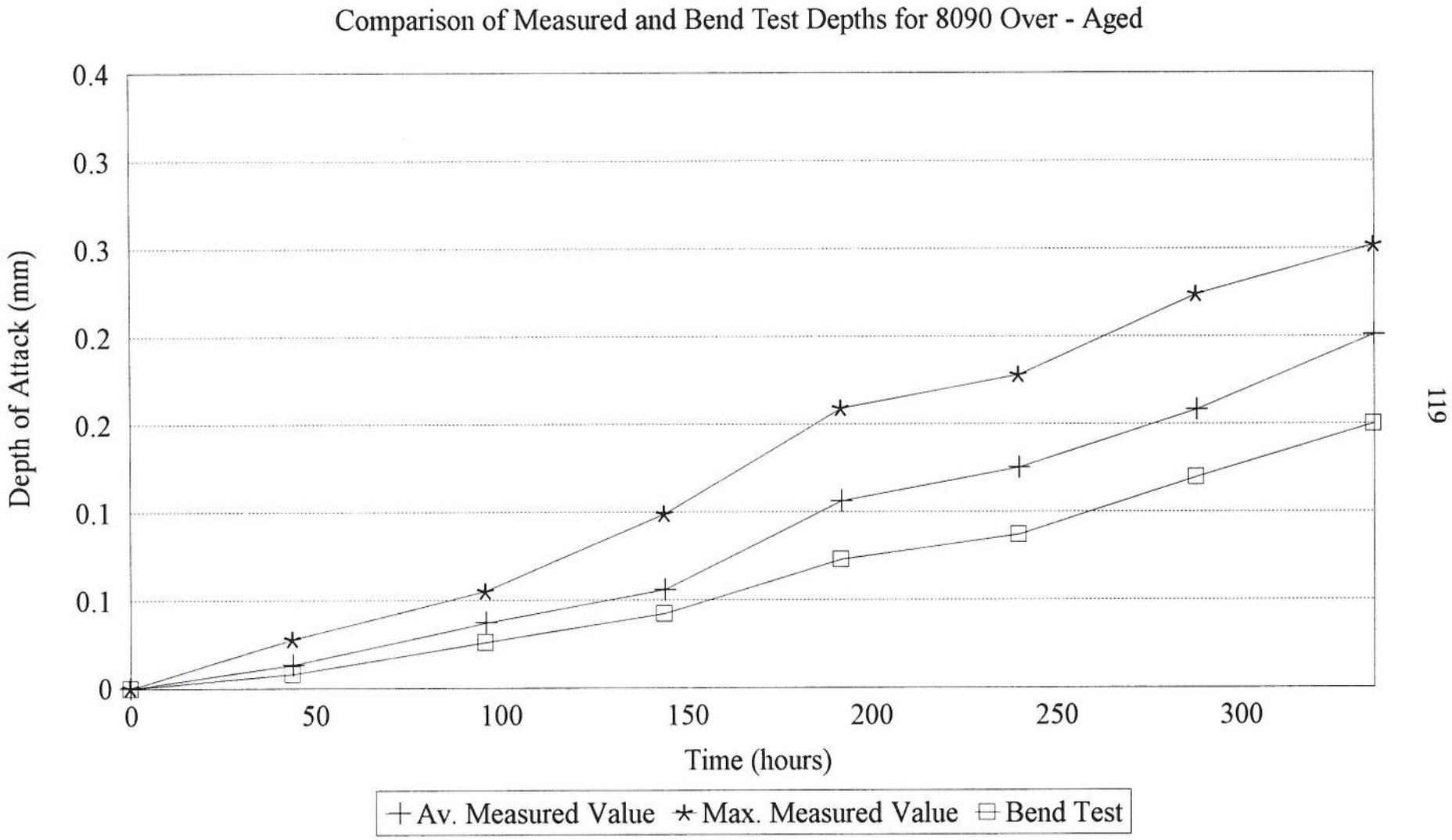

Figure 4.26. : Graph of depth of attack against time for 8090 over - aged.

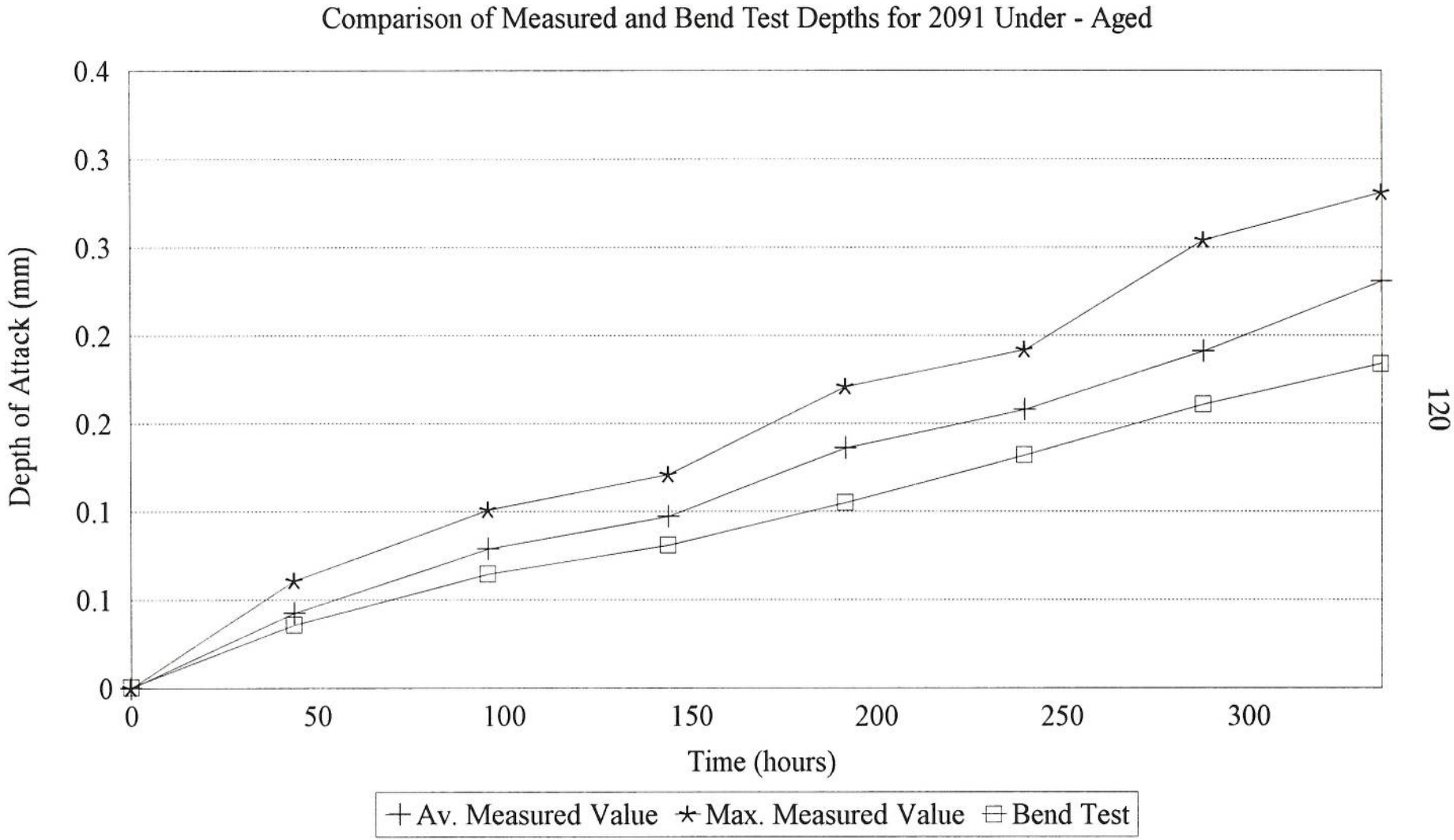

Figure 4.27. : Graph of depth of attack against time for 2091 under - aged.

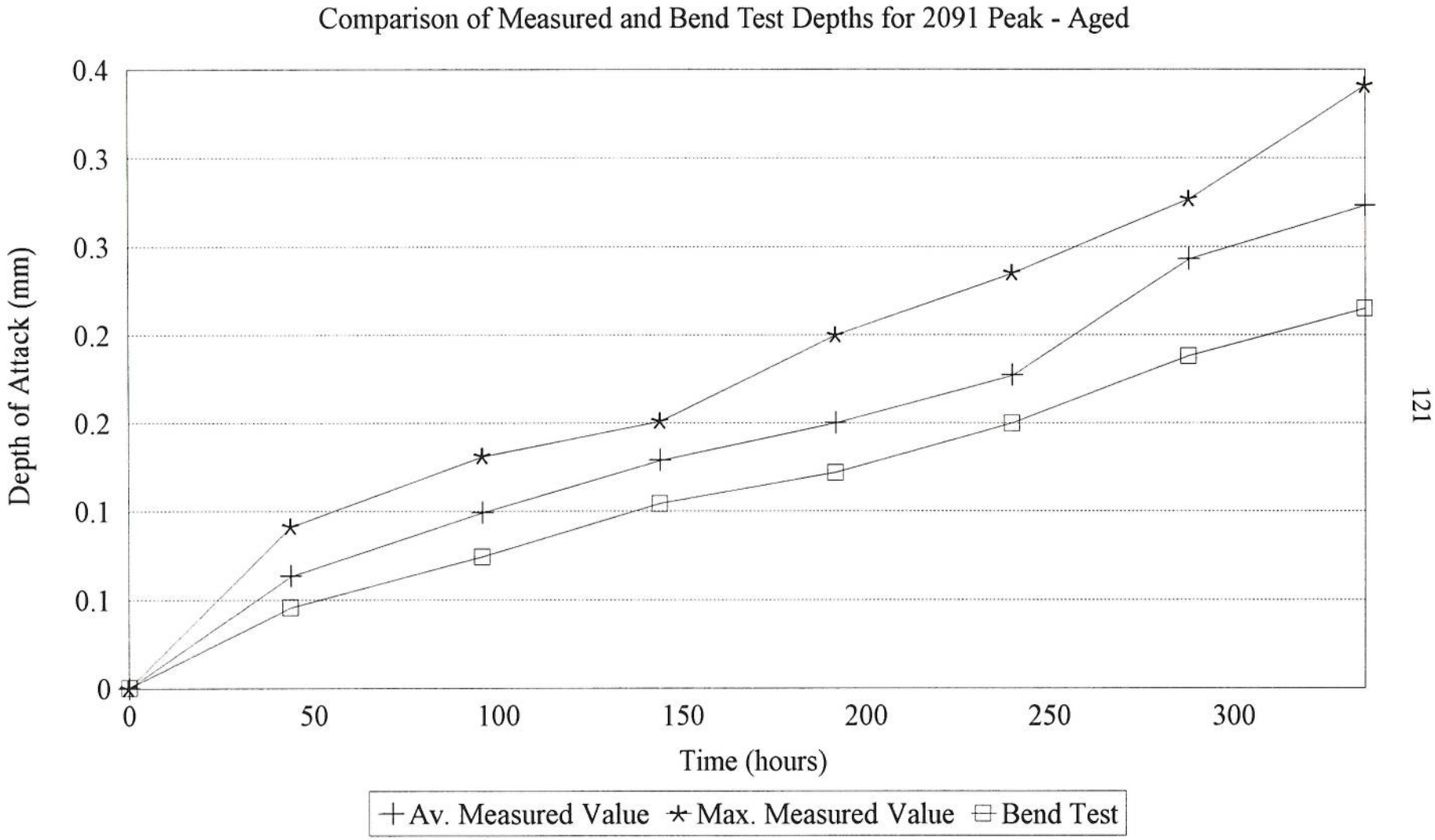

Figure 4.28. : Graph of depth of attack against time for 2091 peak - aged.

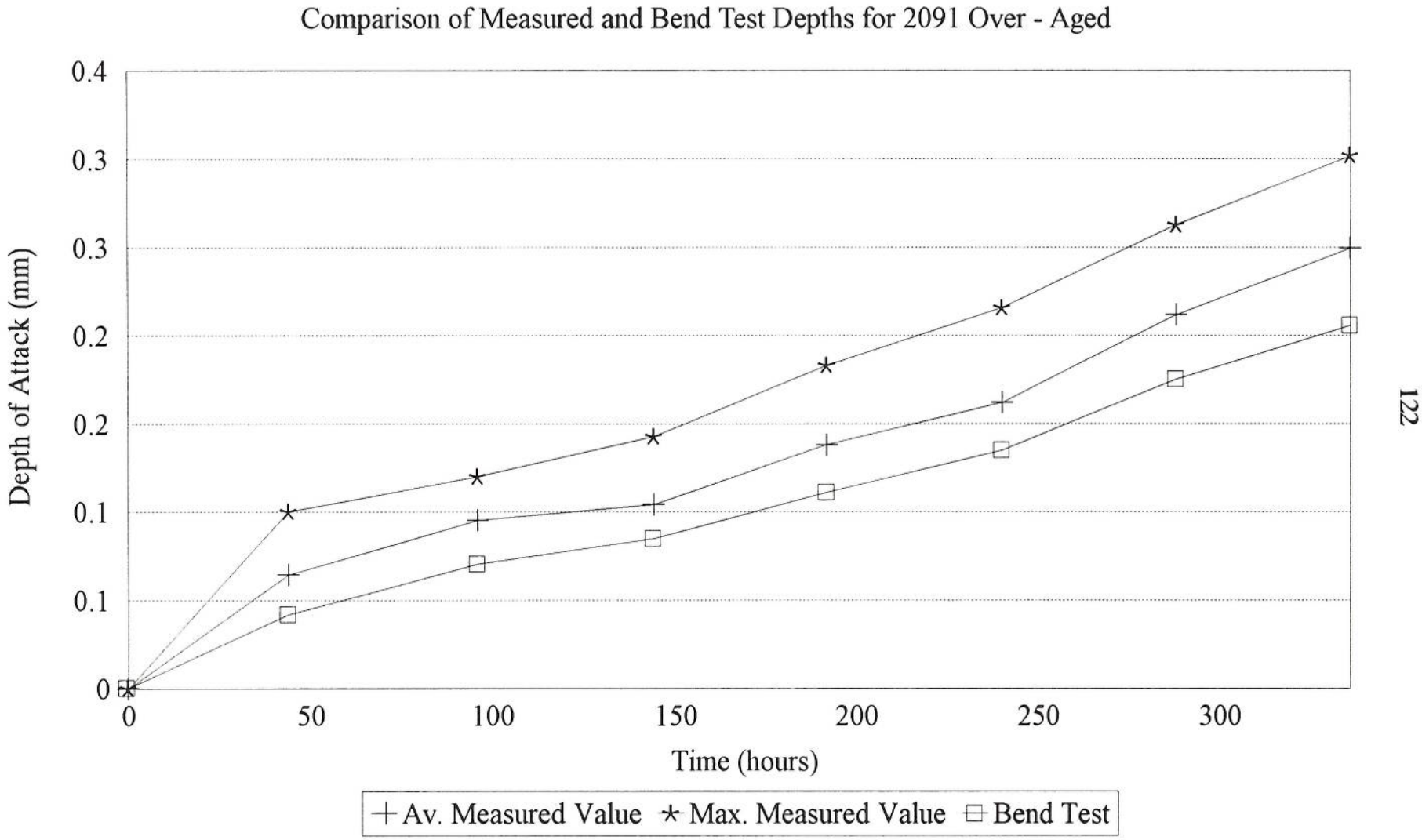

Figure 4.29. : Graph of depth of attack against time for 2091 over - aged.

series alloys the bend test values are lower than the average and maximum depths obtained through metallographic assessment. The surface ratings appear to be in agreement with the depths of attack for both materials - the depth of attack and the surface rating are greater in the peak - aged condition for both alloys than both the under - and over - aged conditions. For the 2091 alloy the under - aged condition showed a lower depth of attack than the over - aged condition whereas in the 8090 alloy the over - aged condition showed the lowest depth of attack. 2091 showed a greater depth of attack than the 8090 alloy due to a higher aspect ratio. It may be significant that 2091 has grains with a higher aspect ratio although, clearly there are other factors to be considered as the two alloys have different compositions.

Figures 4.30 and 4.31 show cross - sections of attack for the 8090 and 2091 alloys respectively for the peak - aged condition. It can be seen that the morphology for 8090 is that the attack follows the grain boundaries clearly defining the grains within the structure. In 2091 deep pitting was observed with some intergranular attack. For both alloys the peak - aged condition shows the greatest depth of attack which is expected following the work by Spiedel (70). The under - aged specimen showed fewer areas of attack than the peak and over - aged specimens for 2091 and 8090. The order of decreasing susceptibility was that of peak - aged > under - aged > over - aged for 8090 and peak - aged > over - aged > under - aged for 2091.

4.4.3 Intergranular Corrosion Velocity

The calculated corrosion velocities for 8090 and 2091 can be seen in tables 4.7 and 4.8. The 2091 is more susceptible to exfoliation corrosion than 8090 due to a higher intergranular corrosion velocity. The velocity was greatest in the peak - aged condition for both alloys indicating a higher degree of susceptibility of attack than in the under - and over - aged conditions.

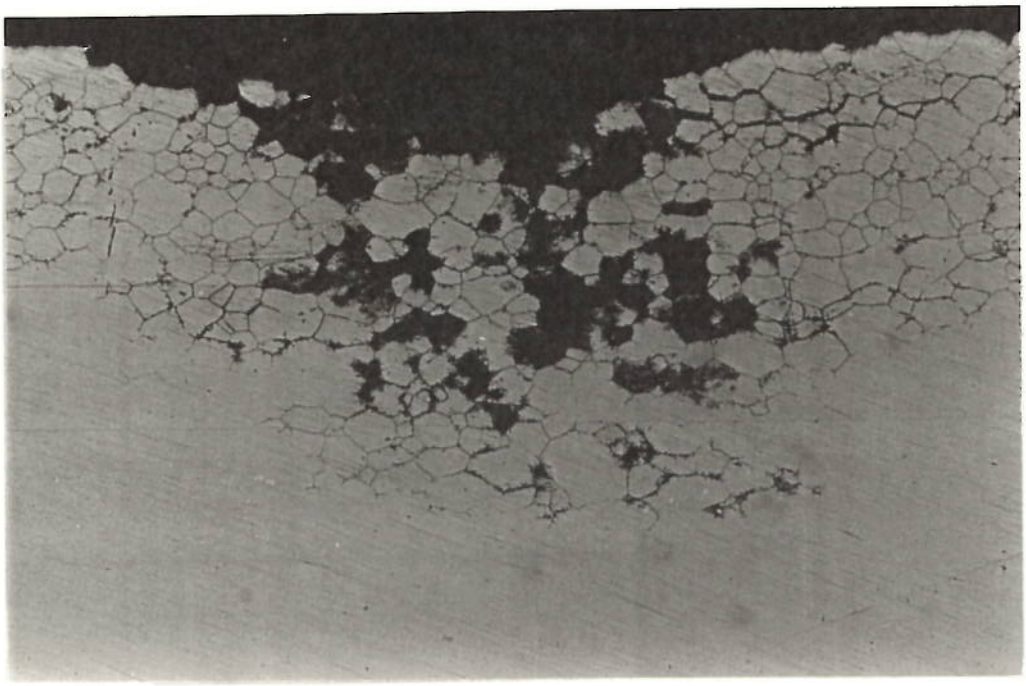

Figure 4.30. : Cross - section showing attack for 8090 peak - aged after 336 hours of MASTMAASIS testing (x200).

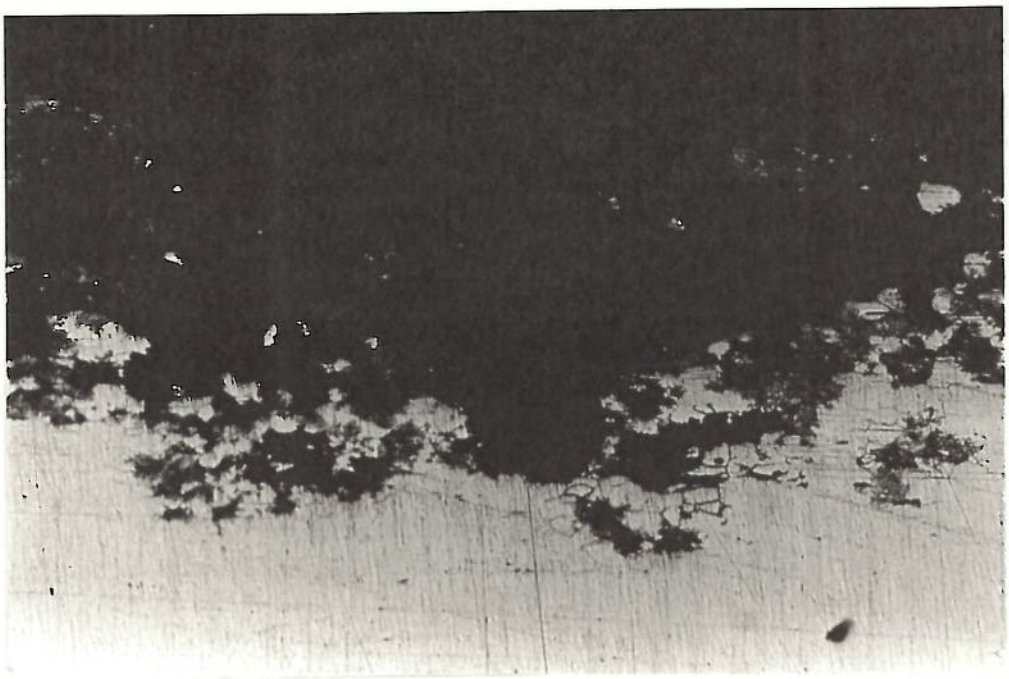

Figure 4.31. : Cross - section showing attack for 2091 peak - aged after 144 hours of MASTMAASIS testing (x200).

Table 4.7. : Intergranular Velocities for 8090.

Time (hours)	Intergranular Velocity (ms^{-1})		
	Under ($x10^{-10}$)	Peak ($x10^{-10}$)	Over ($x10^{-10}$)
48	3.4±0.6	3.59±0.64	2.99±0.52
96	4.58±0.8	6.24±1.1	3.28±0.58
144	5.19±0.9	6.15±1.1	4±0.7
192	6.1±1.1	7.69±1.3	5.4±0.9
240	6±1	7.21±1.2	5.43±0.95
288	6.57±1.1	8.05±1.4	5.57±0.97
336	6.48±1.1	7.31±1.3	6.08±1.1

Table 4.8. : Intergranular Velocities for 2091.

Time (hours)	Intergranular Velocity (ms^{-1})		
	Under ($x10^{-10}$)	Peak ($x10^{-10}$)	Over ($x10^{-10}$)
48	21.1±0.29	32.3±0.3	32.4±0.4
96	18.7±0.25	23.1±0.31	22.5±0.3
144	15±0.2	20±0.27	16.3±0.23
192	16±0.2	17.7±0.24	16.4±0.22
240	14.9±0.2	16.7±0.2	15.4±0.2
288	15±0.2	19.3±0.26	16.7±0.2
336	15.6±0.21	18.5±0.25	16.9±0.23

4.5. Discussion on the 2XXX Series Alloys

It has been shown that the degree of attack is dependent on the grain shape. In susceptible alloys, corrosion proceeds along multiple paths in the material structure and the formation of a corrosion product with a higher volume than that of the material forms, exerting a wedging action. This results in the formation of blisters, flaking or delamination at the surface of the material and can be rated in accordance to standard ASTM exfoliated specimens. As the grain aspect ratio increased from the surface to the

central (T/2) section of the plate, the surface rating became more severe for both the 2014 and 2024 alloys. Rating became more difficult for the 2024 alloy over the duration of the test as material which had been attacked at the surface of the specimen became more brittle and metal loss occurred by means of the surface grains flaking away leaving the underlying grains exposed to attack. Thus, the surface ratings after a period of exfoliation for 2024 was several grains below the original surface. This loss in material was evident in the T/2 and T/4 sections of the 2024 alloy where attack reached the rating of moderate / severe exfoliation. According to Ketcham and Shaffer (123) an increase in the length of the grain increases the development of exfoliation which leads to higher surface ratings. However, the 2024 T/4 section exhibited a slightly larger grain length than the T/2 section with a lower rating of EB+ compared to EC+ for T/2. This suggests that one of the major contributors affecting the surface appearance and susceptibility to exfoliation corrosion is the grain aspect ratio.

The blisters formed during testing were due to the lifting of the grains caused by the formation of corrosion products and the size of these blisters are governed by the aspect ratio of the material. Alloy 2014 which has the lower grain aspect ratio exhibited smaller, more rounded grains which was in agreement with the mathematical model put forward by Robinson (164). In this model it was demonstrated that smaller blisters would be observed for a material with a lower aspect ratio. The formation of larger blisters at an earlier stage in corrosion for 2024 meant that these could burst due to the pressure exerted by the greater volume of the corrosion products thus exposing the underlying material to attack hence, the greater surface ratings. This method of rating the surface attack suffers one problem in that the interpretation of results can differ greatly. The morphology of exfoliation corrosion is so variable depending on the susceptibility of the particular material. This makes rating difficult to the operator in that he has to find the standard photograph which bears the closest resemblance to the particular exfoliated surface.

Metallographic examination of the corroded material provides more reliable information about the extent of damage than the ASTM ranking method. The attack initially shows

the formation of pits which widen and become deeper leaving less material unattacked. At the onset of exfoliation a network of intergranular pathways appear at the base of these pits where the corrosion has proceeded along grain boundaries. As the grains become more elongated toward the centre of the plate, these intergranular networks become more extensive enabling a greater formation of corrosion products. These corrosion products have a volume of three times that of the original material producing a wedging effect which lifts and breaks the elongated grains, hence the more severe ratings achieved with the more elongated grains in the 2024 alloy. The surface ratings can be related to the depths of attack and are shown in figure 4.32 representing a plot of depth of attack against surface rating for 2014 and 2024. The 2014 tends to exhibit a lower surface rating for the same depth of attack than that of the 2024 alloy. For example, a depth of 0.29mm was recorded coupled with a rating of P/EA- for 2014 whereas the same depth of approximately 0.29mm was associated with EA+ for 2024. The results for the 2014 alloy tended to be more scattered than that for the 2024 alloy which fell into a narrower band. It should be noted that these visual assessment / depth of attack results do not indicate the rates of exfoliation for the two alloys. In each case the 2024 alloy suffered the more rapid exfoliation corrosion, even if this was not suggested by the surface appearance. In this work 2014 was found to exhibit smaller blisters than those found on 2024. However, it was shown by Anwar (46) that 2014 developed large blisters in comparison to 2024 which burst open to give the impression of severe exfoliation corrosion. On metallographic examination the 2024 alloy was more susceptible to exfoliation corrosion producing a greater reduction in the section thickness. The attack on the 2024 alloy was found to be more insidious in nature than the 2014 alloy making the corrosion more difficult to detect.

The four - point bend test calculations for depth of attack are lower than the depths obtained through metallographic assessment in the early stages of corrosion with the values converging in the later stages of corrosion. This is probably due to the fact that, in the early stages of corrosion only discreet pits were observed and the bend test measured all of these pits including the unattacked areas over the whole of the specimen whereas the metallographic sections were measured over the width of the specimen which

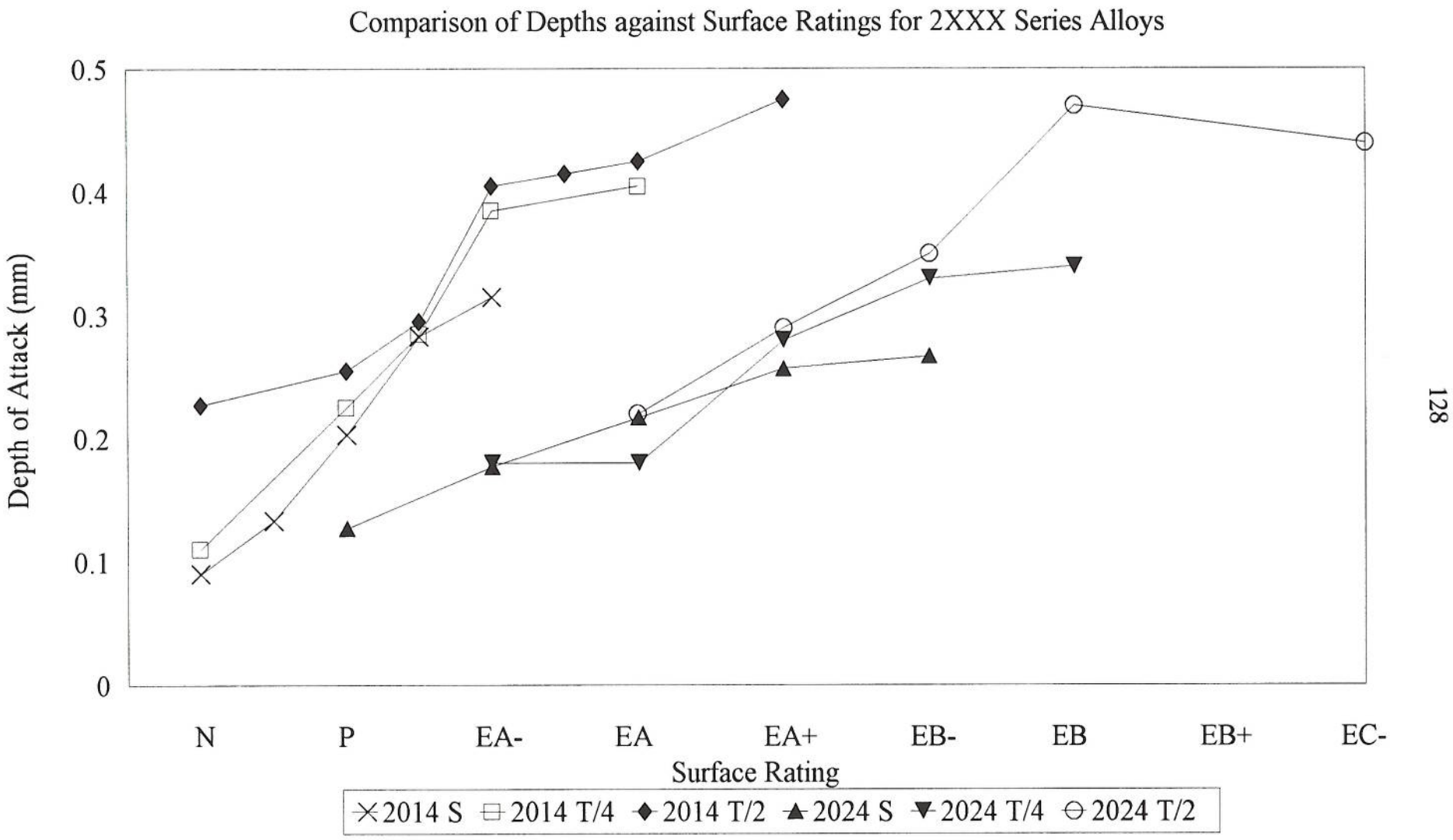

Figure 4.32. : Graph showing relationship between surface rating and depth of attack for 2014 and 2024.

reduced the possibility of unattacked areas being measured. At longer times the severity of exfoliation increased, decreasing the unattacked areas where, in bend testing a more realistic value of the depth was obtained over the whole of the specimen. The maximum depth was taken from the deepest point of attack which was a simple and straightforward method. The average depth of attack was taken from ten measurements along the width at equally spaced intervals. Clearly, this method would produce some scatter amongst the results as is evident in the two alloys. One difficulty of obtaining average depth of attack measurements is that the observer may discriminate inadvertently between the attacked and unattacked areas of the surface. If the most significant depths of corrosion are selected then the average value will be high and approach the maximum value. If, however, the measurements are made at equally spaced intervals without regard to the appearance of the corrosion then a more accurate value for the depth of attack is obtained. This can be illustrated in figures 4.33 and 4.34. With the more uniform attack during the later stages of corrosion, depths (D1 to D10) can be taken over equal spacings and, hence a more realistic set of results can be obtained.

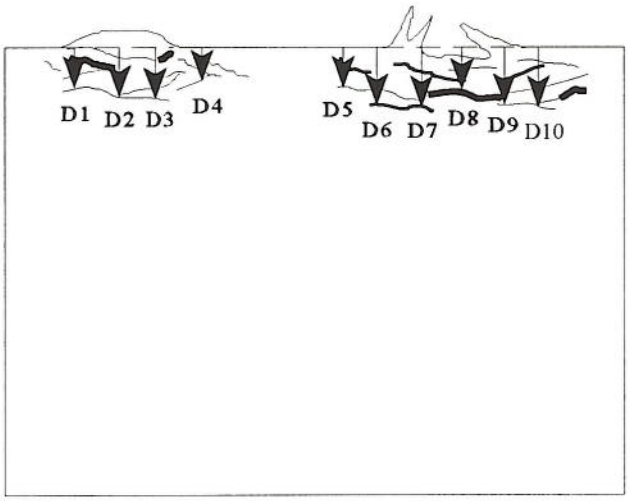

Figure 4.33. : Diagram of cross - section during the early stages of corrosion.

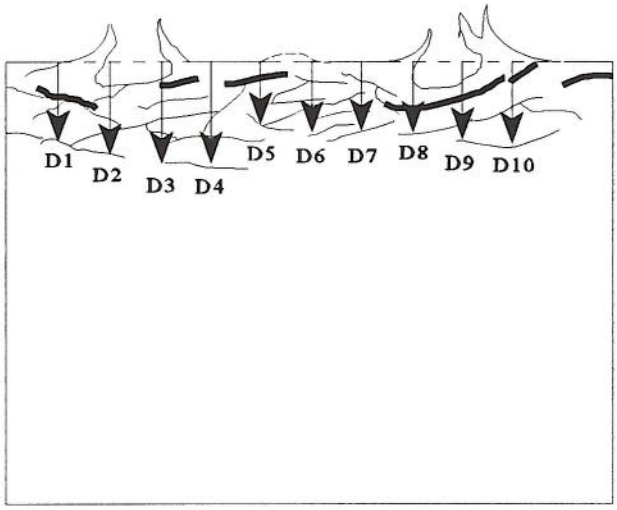

Figure 4.34. : Diagram of cross - section as corrosion develops during time.

In the work carried out by Liddiard et al (131) it was shown that the corrosion rate on the specimen with a machined face was linear, but with an as - extruded face there were three parts to the curve for thick plates - a slow incubation period associated with a thick recrystallised skin, a second, rapid linear attack where the skin is lifted and final slowing down in comparison to the second stage where the highly directional grains encounter the corrosion. The graphs for 2014 and 2024 in figures 4.7 through to 4.12 all show a linear rate of attack for the surface, T/4 and T/2 sections through the plate material. As the surface of each specimen had been machined and polished prior to MASTMAASIS testing the recrystallised skin had been removed so there is no apparent incubation period for the corrosion to develop. The attack appeared to remain constant up to the final depths of attack reached at the end of the test. With the fact that exfoliation has been shown to be slower at the surface of wrought aluminium alloys compared to the interior it can be expected that the surface specimens would corrode at a slower rate than the T/4 and T/2 specimens. These recrystallised grains at the surface of thick plate material exhibit a lower grain aspect ratio hence the slow rate of attack found by Liddiard et al (131).

The intergranular corrosion velocities were seen to have greater values for the 2024 alloy than those of 2014 and increase towards the T/2 section of the plate in the order Su < T/4 < T/2 indicating a higher degree of susceptibility to intergranular attack. As the aspect ratio for the two alloys increased through the plate, the intergranular corrosion velocity increased. The intergranular corrosion velocities reported for the 2XXX series alloys show that the rate of attack in the 2024 alloy is approximately double the rate shown for 2014. As the aspect ratio does not differ significantly between 2014 and 2024, microstructural changes could play a more important role in affecting the corrosion rate. There is also a large difference in the corrosion rate between the surface, T/4 and T/2 sections through the plate which can be explained by cooling during processing. The cooling rate is important in determining the microstructure of the material where different precipitates form. The distribution and size of precipitates depends on the rate of cooling. For thick plate material the cooling rate is slower at the centre than at the surface.

The increase in the aspect ratio toward the centre of the plate does not explain the large differences in the results obtained between the surface, T/4 and T/2 sections. Rapid cooling produces a supersaturated solid solution at room temperature together with a high vacancy concentration. On slow cooling, precipitation from the solid solution starts at the grain boundaries during quenching leading to the formation of second phase precipitates. These precipitates have a different electrochemical behaviour from the adjacent matrix and are preferentially corroded. Thus maximum resistance to corrosion could be obtained by rapid quenching. The relationship between quench rate and corrosion susceptibility of 2024 can be seen in figure 4.35 (168) where the resistance to intergranular corrosion and stress corrosion cracking can be improved by rapid quenching at 277^{0}C/s. The significance of the T62 (or T8) temper improves the resistance to exfoliation but susceptibility to intergranular corrosion is not eliminated. Rapid quenches can only be achieved for thin sheet materials whereas, for a plate material the midsection does not quench as rapidly as the surface which results in varying corrosion susceptibilities through the thickness of the plate. W. G. J. 't Hart et al (36) investigated the relationships between quench rate, corrosion properties and microstructure of 2024 and 7075 by means of a Jominy end quench test. The quench rate decreased along the length of the Jominy end piece

allowing easier formation of grain boundary precipitates and the material was more susceptible to corrosion. This suggests there may be more precipitates present at the mid - plane of the plate where the electrochemical differences between the grain boundary precipitates and the grains are larger than at the surface providing a large driving force for corrosion to occur. In particular, differences in precipitation between the surface and the T/4 and T/2 sections of the plate may explain the differences in exfoliation susceptibility in these regions.

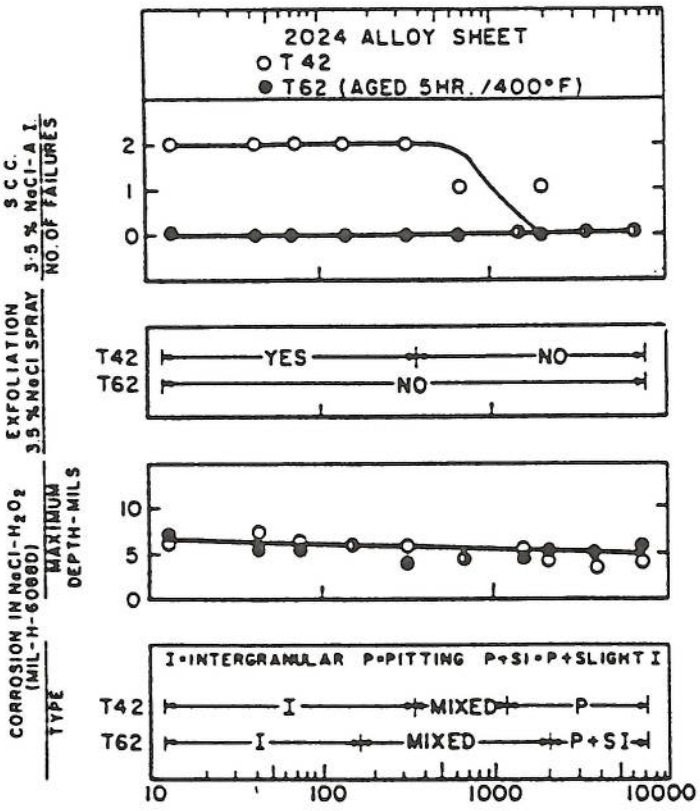

Figure 4.35. : Comparative effects on the corrosion and stress corrosion resistance of 2024-T42 and T62 tempers of sheet as influenced by quenching rate (168).

As there is not a great deal of difference in the aspect ratios for the 2014 and 2024 alloys, the large difference in the intergranular velocities, depths of attack and surface ratings can also be due to compositional differences. Electrochemical effects have a strong influence on the corrosion resistance in these alloys due to the fact that copper influences

both the corrosion potential of the aluminium solid solution and the presence of the copper rich second phase precipitates. As the corrosion continues, copper ions are plated out on the aluminium surface which creates a myriad of small galvanic cells on the alloy surface which intensifies pitting around each copper particle. The major difference between the two alloys is their Cu : Mg ratio - 9 : 1 for 2014 and 3 : 1 for 2024 resulting in different phases being present. 2014 has a low magnesium content with the $CuAl_2$ phase being predominant whereas 2024 has a higher magnesium content with the $CuMgAl_2$ phase being predominant. The higher susceptibility to exfoliation corrosion in the 2024 alloy is due to this more anodic, $CuMgAl_2$ phase. Anwar (46) found initiation attack in 2024 due to preferential dissolution of magnesium in the $CuMgAl_2$ precipitate with copper depositing onto the precipitate. This leaves the matrix around the precipitate depleted in copper which is anodic relative to the grains hence vulnerable to attack. Liddiard et al (131) tested HE10 for comparative purposes against an AlCuMg alloy and the increase in copper content was thought to confer some resistance to exfoliation corrosion.

The heat treatments conveyed onto the 2024 alloy had an effect on the susceptibility to corrosion. The peak - aged material showed the highest susceptibility to corrosion, whereas in the under - and over - aged conditions there was an increase in resistance to exfoliation corrosion. Precipitation hardening is of paramount importance. Alloys usually become susceptible to corrosion with increasing precipitation hardening, reaching a maximum before peak strength. M.O. Speidel (70) has shown that peak - aged material exhibits the least resistance to corrosion. In this condition the electrochemical difference between the precipitates and the grains is at its maximum. An increase in the distribution of the $CuMgAl_2$ phase gives rise to a larger number of galvanic cells along the grain boundaries which increases the driving force for corrosion. Galvele and De Micheli (151) have shown that this difference in the pitting potentials for the grains and grain boundaries was the cause for intergranular corrosion in Al-Cu alloys. In the under - and over - aged conditions the amount of copper in solid solution diminishes hence the electrochemical difference is minimised by the presence of fewer precipitates which renders some resistance to exfoliation corrosion, in fact more so in the over - aged condition

which showed the most resistance.

4.6. Discussion on the Aluminium - Lithium Alloys

In the case of the 8090 and 2091 aluminium - lithium alloys the material was supplied in sheet form which appeared to be partially recrystallised. The fact that the material was 1.6mm thick sheet meant that the grain aspect ratio remained constant through the thickness and could not be altered so heat treatment (under -, peak - and over - aged conditions) was the major factor for a comparison for exfoliation susceptibility in each material. There was a difference in the aspect ratio between the two materials which did affect the corrosion resistance. Compositional differences which were brought about by the different heat treatments affected the susceptibility of the material to corrosion.

The surface ratings did not differ greatly between the heat treatments and the two alloys reaching the rating of superficial corrosion with large areas of material unattacked after a two week period. This has been reported in other work where general pitting / superficial corrosion on all aluminium - lithium alloys in the MASTMAASIS test was observed. R. Braun (102) showed that, after four to five weeks of exposure time in the MASTMAASIS test, 8090 alloy only experienced slight corrosion attack with a rating of P/EA. Work carried out at DFVLR (180) showed that all three ageing conditions (under -, peak - and over - aged) produced a rating of P/EA for the 2091. This can be emphasised in this work in that both materials reached a surface rating of pitting / superficial corrosion for all three heat treatment conditions after two weeks of testing. The appearance of corrosion on the surface of 2091 is similar to 8090. In these two alloys there is not a good correlation between the surface rating and the depth of attack where 2091 exhibits greater depths than 8090. For example, both the 8090 and 2091 show a rating of EA in the peak - aged condition after 336 hours of testing but the 2091 alloy has a greater depth of attack of 0.273mm compared to that of 0.235mm in 8090. In fact both alloys exhibited a deep pitting attack with some sections of grains having been lifted by the formation of some corrosion products. The greater depths found in alloy 2091 can be attributed to the fact that 2091 has a larger grain aspect ratio of

14.2 than 8090 with a ratio of 5.6. For the material with the greater aspect ratio there are a number of paths the corrosion can proceed around a grain but, due to the depths obtained for the 2091 alloy the attack may also "short - circuit" down the transverse path as well as longitudinal around each grain resulting in higher depths. The fact that 2091 shows a higher susceptibility to corrosion than 8090 can also be seen by the difference between the intergranular corrosion velocities. In all three heat treatment conditions the corrosion velocities are higher for 2091 than 8090.

The peak - aged condition showed the greatest depth for both alloys with the under - aged showing the greatest resistance for 2091 and the over - aged showing the greatest resistance for 8090 which is in direct contrast to Ramu et al (170) where the study of pitting potentials for an 8090 alloy produced the order of under - aged > peak - aged > over - aged, indicating that the over - aged alloy was the most susceptible with the under - aged condition being the least susceptible. However D. Kelly (181) showed that, for partially recrystallised 8090 sheet material, the heat treatment condition which showed the greatest susceptibility was that of the under - aged condition and the susceptibility decreased on ageing through peak - to over - aged. This increased susceptibility to pitting and exfoliation corrosion is due to microstructural changes during ageing. Corrosion mostly initiates at, and propagates at grain boundaries which means that the microstructure in the grain boundaries is important. Over - ageing results in the increased formation of δ' (Al_3Li) precipitates (undesirable heterogeneous grain boundary precipitation) and large precipitate free zones associated with δ' precipitates in AlLiCuMgZr alloys. Niskanen et al (54) suggested that over - ageing produces a δ (AlLi) phase which is detrimental to pitting corrosion resistance. However Zhang Yun et al (161) showed that the corrosion resistance of the over - aged condition is increased while pitting corrosion generally takes place within the grains. Zhang Yun et al (161) suggested that corrosion resistance may not be influenced by fine dispersoid phases such as δ', but may be controlled by the presence of coarse precipitates such as particles of the T_2 (Al_5CuLi_3) phase present in the grain boundaries. Clearly, there are important differences between exfoliation corrosion which follows an intergranular path and pitting which occurs predominantly within the grains.

The nature of the attack changes between the different heat treatment conditions. For the under - aged condition a fine heterogeneous distribution of S precipitates along with δ' and T_1 phases are present which provides a continuous anodic path resulting in a favourable pathway for corrosion to occur. A precipitate free zone depleted in copper appears as a result of copper being tied up with the S and T_1 phases producing an anodic area. This copper depleted zone becomes more anodic as ageing continues up to the peak - aged state and, together with more precipitation, the driving force required for corrosion to continue increases by virtue of increasing the potential difference between the grain boundaries and the grains.

CHAPTER FIVE

5.0. ATMOSPHERIC CORROSION TESTS

5.1. Introduction

The susceptibility to corrosion, and particularly to exfoliation corrosion, of aluminium - lithium sheet in the under -, peak - and over - aged conditions and the 2XXX plate materials was determined by a two - year exposure to atmospheric conditions in outdoor corrosion tests. It is generally considered that aluminium alloys have good resistance to corrosion in atmospheric exposure. Testing in a marine atmosphere similar to the one that an aircraft would experience is the most representative of service conditions. A comparison of the results between outdoor testing and laboratory tests can be used as a calibration for the MASTMAASIS cabinet. The times experienced for corrosion in the accelerated laboratory test can be related to months or years of testing in atmospheric conditions.

5.1.1. Procedure

All the alloys were tested at Eastney in Hampshire for the evaluation of a coastal marine atmosphere. The preparation for etching and covering the sides and back of each specimen was the same as that reported in chapter four for MASTMAASIS testing. All the specimens were placed on a wooden rack at an angle of 45^0 just like in the MASTMAASIS test and were held using ceramic holders at the ends of each specimen so that they were facing due south and subjected to a maximum of 24 months of testing. After six monthly periods all the alloys were removed from the rack and tested at Cranfield. Small sections were cut from each specimen, mounted and subjected to metallographic assessment and the visual appearance of each specimen was recorded. A second set of specimens was tested on the four - point bend test. Photographs were taken to show the morphology of attack and the appearance of corrosion on the surface of each specimen. After these sections were cut, each specimen was sent back to Eastney for further exposure.

5.2. Results

5.2.1. Visual Assessment

The 2XXX series alloys have been exposed for two years, the 8090 exposed for 18 months and the 2091 exposed for one year due to the time each particular material was received during the test programme. The results for the visual appearance can be seen in table 5.1.

Table 5.1. : Surface Ratings for the Coastal Specimens.

Alloy	Section/Heat treatment	Surface Ratings			
		6 months	12 months	18 months	24 months
2014	T/2	P	-	EA-	EA
	T/4	N	-	P/EA-	EA-
	S	N	-	P	EA-
2024	T/2	P/EA-	-	EA-	EA+
	T/4	P	-	P/EA-	EA
	S	N	-	P/EA-	EA-
8090	Under	-	P	P	-
	Peak	-	P	P	-
	Over	-	P	P	-
2091	Under	P	P	-	-
	Peak	P	P/EA-	-	-
	Over	P	P	-	-

For the 2XXX series alloys the surface ratings increase in the order surface < T/4 < T/2 showing an increase in corrosion susceptibility as the aspect ratio increases and there is no difference between the ratings for 8090 and 2091. Figure 5.1 shows an example of the type of attack experienced on the 2XXX series alloys where the attack has reached moderate exfoliation with relatively small areas of material unattacked. For the aluminium - lithium alloys there is a number of pits evident as shown in figure 5.2 with large areas of material unattacked. With the 2XXX series alloys all the sections experienced varying degrees of exfoliation susceptibility after two years of exposure. Although

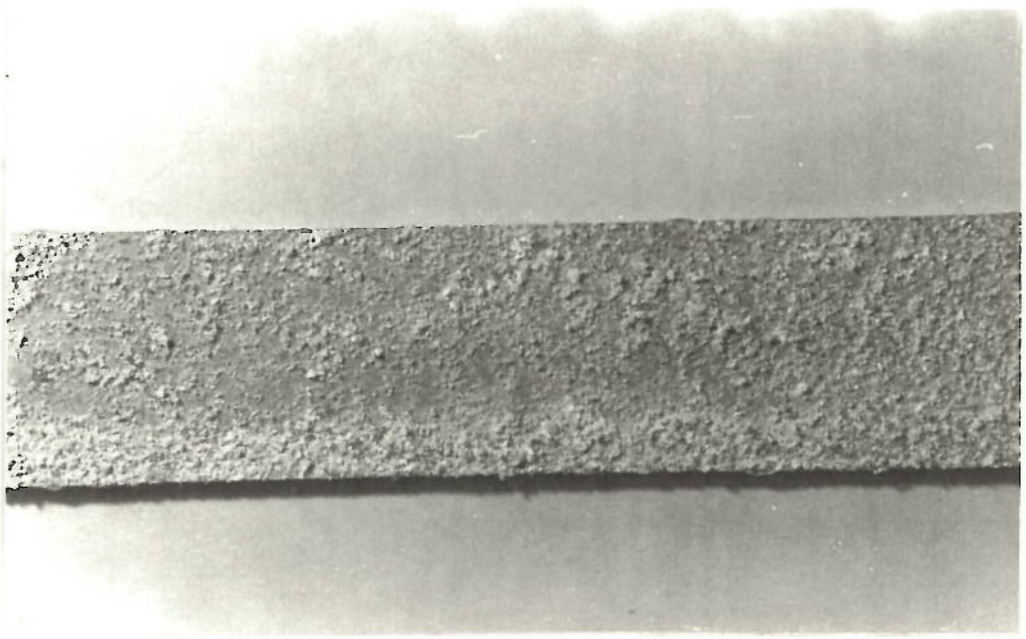

Figure 5.1. : Photograph showing the surface attack on 2024 T/2 after two years in a coastal marine atmosphere (x1).

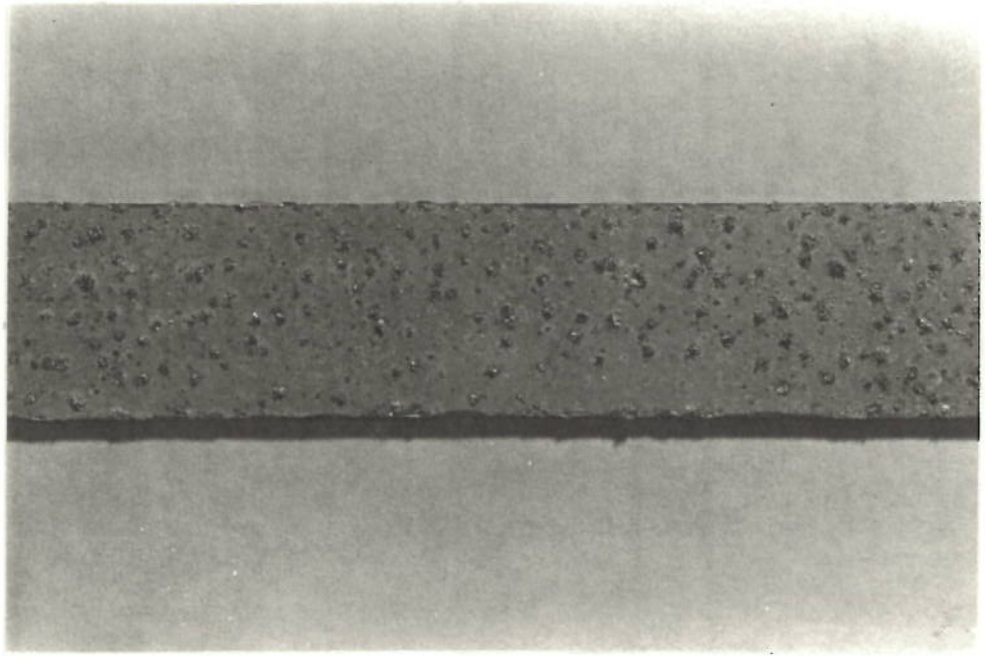

Figure 5.2. : Photograph showing the surface attack on 2091 peak - aged after one year in a coastal marine atmosphere (x1).

the 2014 and 2024 alloys are represented with P or EA there appears to be small patches over some specimens, especially in the 2024 alloy, where the attack seems to be in the form of large blisters, some of which have, or are about to, burst. These areas tend to be around the ends where the specimens were held using the ceramic holders. There could have been a build up of water at these areas or the formation of an occluded cell increasing the rate of attack. These large blisters also appear at the centre of some specimens especially in the 2024 T/2 and T/4 sections. In general, there is not a great difference in the surface appearance at the longer exposure times. The 8090 and 2091 exhibit localised pitting attack which increases in density only slightly during the duration of the test in which case there is a small increase in the size of the pits. In the case of the 2091 peak - aged specimen, signs of blistering was observed after one year of exposure. As with the 2XXX series alloys, the aluminium - lithium alloys also show areas where the surface appearance seems to be greater. These areas showing the higher surface rating appear towards the edge of the specimen. These results can be compared to those obtained through the MASTMAASIS testing but the depths of attack give a better comparison.

The lower surface of some specimens especially in the 2024 alloy, even though this was protected from exposure with clear tape and lacomit, exhibited greater attack than the exposed, upper surface which was washed periodically with rain. With this periodic washing, corrosion products washed away from the top may have penetrated the edges of each specimen lifting the clear tape and corroding the bottom surface. As the exposure time increased the corrosion increased at the bottom surface. This phenomenon can be seen in figures 5.3 and 5.4 showing photographs of the upper and lower surfaces respectively for comparison.

The morphology of attack is similar to that found in the MASTMAASIS testing of the 2XXX and aluminium - lithium alloys. For the 2014 and 2024 alloys the attack initiates as pits which grow to form large blisters which, after longer times, burst open with loss of material. At the base of these pits a network of intergranular pathways form which increase in size and width leaving less material unattacked as the exposure time

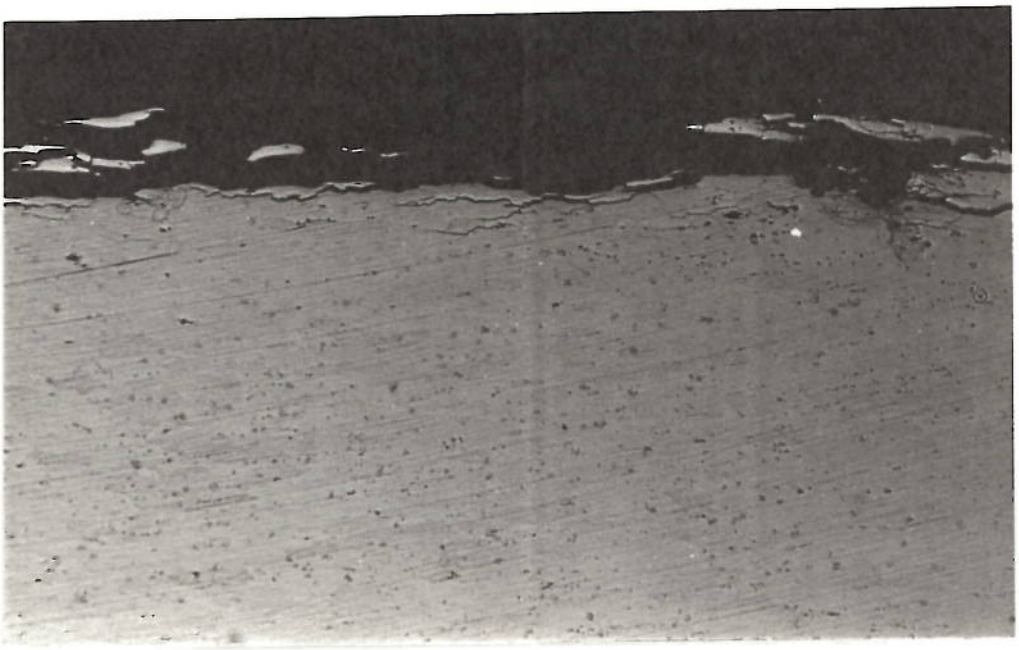

Figure 5.3. : Cross - section showing morphology of attack for the upper surface of 2024 T/2 after two years in a coastal marine atmosphere (x100).

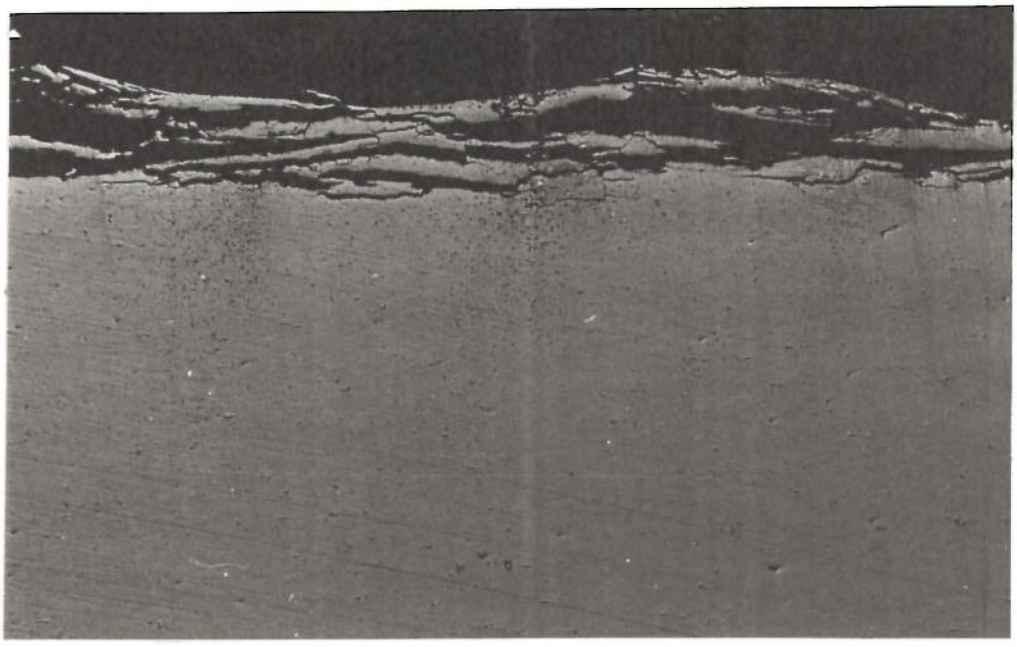

Figure 5.4. : Cross - section showing morphology of attack for the lower surface of 2024 T/2 after two years in a coastal marine atmosphere (x100).

increases. The size and width of these intergranular pathways increase as the aspect ratio increases towards the centre of the plate. In the case of the 8090 and 2091 alloys, pits initiated on the surface of each specimen with 2091 exhibiting the greater number of pits. For both alloys, the peak - aged condition appeared to have a greater density of pits on the surface than the under - and over - aged conditions. As the duration of the test increased, these pits increased in number and depth with some evidence of intergranular attack extending from the base of pits, which suggested signs of exfoliation corrosion. The network of intergranular pathways are present mainly on the peak - aged specimens but also, to a smaller extent appear on the under - and over - aged specimens.

5.2.2. Depth of Attack Measurements

The results obtained from bend rig testing on specimens exposed for the total period of exposure (24 months for 2014 and 2024, 18 months for 8090 and 12 months for 2091) are compared to the maximum and average depths measured metallographically in tables 5.2 and 5.3 for the 2XXX series and aluminium - lithium materials respectively.

As with the MASTMAASIS testing the order of greatest depth remains the same for each alloy with the order for the 2XXX being T/2 > T/4 > surface due to the higher aspect ratios seen for the mid - section of the plate. The over - aged condition for both the 8090 and 2091 alloys tended to be more beneficial than the peak and under - aged conditions.

The depths of attack measurements were not in agreement with the surface ratings in that the 8090 and 2091 alloys showed the greater depths with the least severe surface rating. When comparing the average measured depths between the different alloys it can be seen that the 2024 alloy is more susceptible than 8090, 2091 and 2014. This result does not typify those found in the MASTMAASIS test in that 2091 seemed to be the most susceptible. It must be noted that the depths reported for each alloy in tables 5.2 and 5.3 have not been measured over the same duration of time with the fact that the 2XXX series alloys have been tested over two years, 8090 over 18 months and the 2091

alloy only for one year. The depths in the 8090 and 2091 alloys were larger than in the 2XXX series during the earlier months but as the duration of the test increased, and as exfoliation corrosion developed, the attack in the 2024 alloy was more extensive than in 8090 and 2091.

Table 5.2. : Depths of Attack for the 2XXX Series Coastal Specimens.

Alloy	Time months	Measurement	Depth of Attack (mm)		
			T/2	T/4	Su
2014	24	max.	0.197	0.18	0.16
		av.	0.144	0.13	0.11
		bend	0.13	0.11	0.08
2024	24	max.	0.28	0.22	0.18
		av.	0.21	0.19	0.15
		bend	0.17	0.155	0.126

Table 5.3. : Depths of Attack for the 8090 and 2091 Coastal Specimens.

Alloy	Time months	Measurement	Depth of Attack (mm)		
			Under	Peak	Over
8090	18	max.	0.23	0.24	0.2
		av.	0.153	0.19	0.13
		bend	0.11	0.13	0.095
2091	12	max.	0.17	0.17	0.16
		av.	0.14	0.155	0.13
		bend	0.09	0.12	0.1

For the 2XXX series alloys the depth increased in the order surface < T/4 < T/2 and for both the 8090 and 2091 alloys the peak - aged material showed the greater depth, decreasing in the order of peak - aged > under - aged > over - aged. This is in direct contrast to the MASTMAASIS testing in that the order of susceptibility for the 2091 alloy showed that the under - aged condition was the least susceptible to exfoliation corrosion. It appears that the 2014 alloy is the least susceptible to marine corrosion and

the susceptibility follows the order 2024 > 8090 > 2091 > 2014. As with the MASTMAASIS testing the depths of attack obtained through the four - point bend test are all lower than the maximum and average measured depths.

5.2.3. Intergranular Corrosion Velocity

The calculated intergranular velocities for all the alloys tested can be seen in table 5.4. The intergranular velocity gives a better indication of the corrosion susceptibility of each material. Susceptibility increases as the velocity increases. The trend of maximum susceptibility supported that found in the surface ratings and depths of attack in that the susceptibility increased towards the centre of the plate for the 2XXX series alloys in the order surface < T/4 < T/2 and the peak - aged condition was the most susceptible for 8090 and 2091.

Table 5.4. : Intergranular Velocities for all Coastal Specimens.

Alloy	Section/Heat Treatment	Intergranular Velocity (ms^{-1})			
		6 months	12 months	18 months	24 months
2014	T/2	$1.47x10^{-11}$	-	$1.34x10^{-11}$	$1.37x10^{-11}$
	T/4	$1.25x10^{-11}$	-	$7.94x10^{-12}$	$1.14x10^{-11}$
	Su	$7.38x10^{-12}$	-	$5.9x10^{-12}$	$6.07x10^{-12}$
2024	T/2	$3.37x10^{-11}$	-	$2.4x10^{-11}$	$2.26x10^{-11}$
	T/4	$2.73x10^{-11}$	-	$1.8x10^{-11}$	$1.6x10^{-11}$
	Su	$2.07x10^{-11}$	-	$9.51x10^{-12}$	$1.04x10^{-11}$
8090	Under	-	$1.64x10^{-11}$	$1.21x10^{-11}$	-
	Peak	-	$1.97x10^{-11}$	$1.45x10^{-11}$	-
	Over	-	$1.31x10^{-11}$	$9.9x10^{-12}$	-
2091	Under	$5.25x10^{-11}$	$3.59x10^{-11}$	-	-
	Peak	$6.25x10^{-11}$	$4.01x10^{-11}$	-	-
	Over	$4.97x10^{-11}$	$3.38x10^{-11}$	-	-

The 2091 alloy exhibited the greatest intergranular velocity suggesting that this alloy

was more susceptible to corrosion in the marine atmosphere. The susceptibility decreases in the order 2091 > 2024 > 8090 > 2014. This is the same trend that was shown in MASTMAASIS testing with the exception that the 2014 T/4 and T/2 sections showed faster intergranular velocities than those for the 8090 alloy in the MASTMAASIS test.

5.3. Discussion

As with the MASTMAASIS testing it appears that the aspect ratio of the different sections and alloys affects the corrosion susceptibility. This is shown by the fact that the most severe exfoliation rating was achieved with the T/2 section in both the 2014 and 2024 alloys with the higher aspect ratios than the T/4 and surface sections. Even though there was a limited number of blisters on the surface of the specimens and the fact that they had not burst, the 2XXX series alloys were deemed to have displayed moderate exfoliation on the surface of each specimen. Given that the corrosion rate is slower in the marine exposure testing than in the MASTMAASIS test, the formation of corrosion products and, therefore, the wedging force is not as large. It can be seen from table 5.2 that the depths of attack are greater for the mid - section of the plate material. A comparison can be made between the surface rating and depth of attack for the 2014 and 2024 alloys which can be seen in figure 5.5. The 2014 alloy exhibited a lower surface rating for the same depth of attack than that for 2024. The fact that 2024 shows greater signs of exfoliation than 2014 is supported by higher intergranular corrosion velocities for the surface, T/4 and T/2 sections through the plate. The corrosion velocity increases through the plate as the aspect ratio increases. As with MASTMAASIS testing the difference in velocities between the two alloys is approximately a factor of two which is not reflected by the aspect ratios. The $CuMgAl_2$ phase present in 2024 differs from $CuAl_2$ in 2014 due to a higher magnesium content in the former. $CuMgAl_2$ precipitates are more anodic relative to the grains than the $CuAl_2$ precipitate which increases the potential difference between the precipitates and grains providing a greater driving force for corrosion to take place.

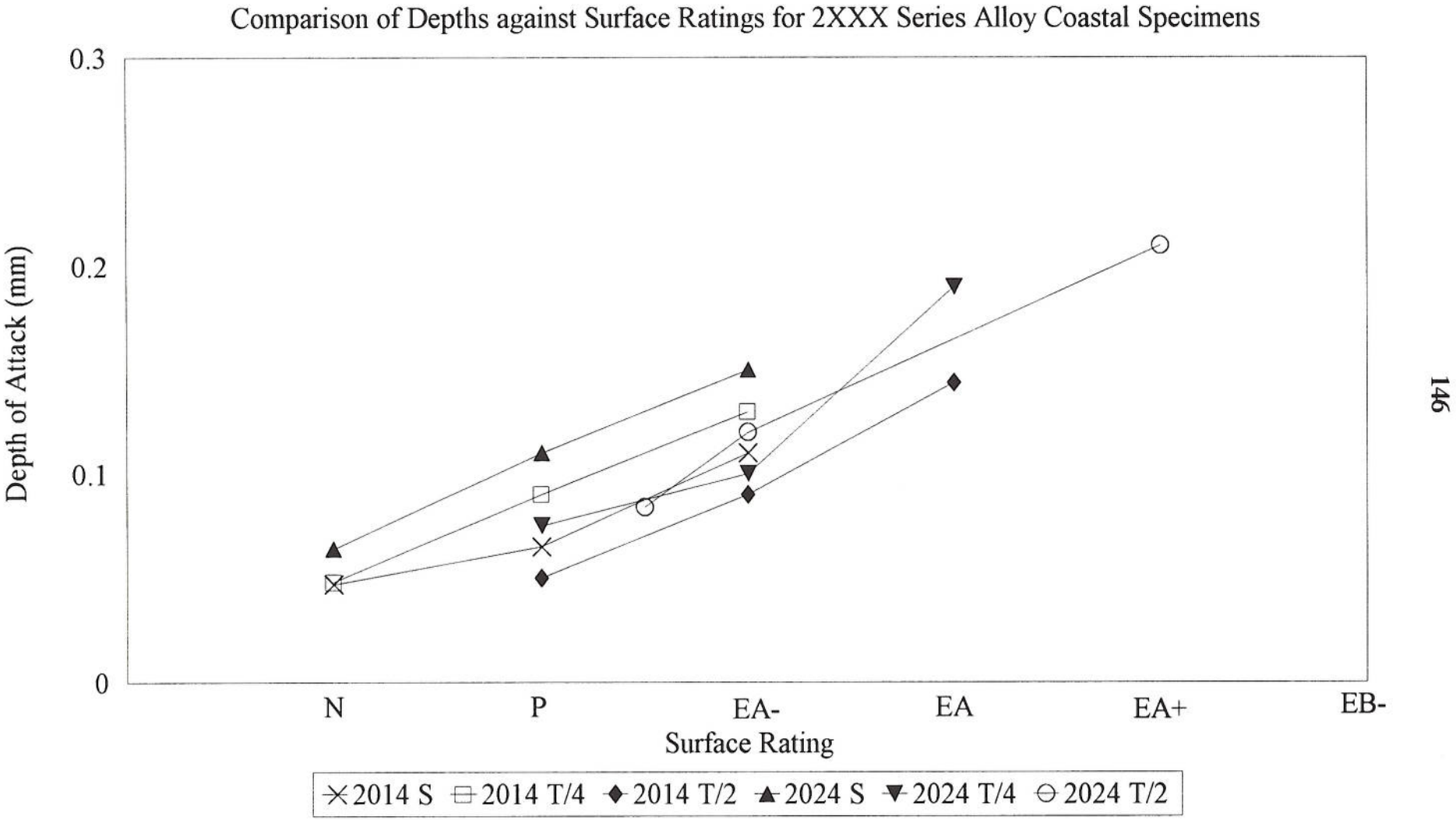

Figure 5.5. : Graph showing relationship between surface rating and depth for 2014 and 2024 coastal specimens.

In the case of the aluminium - lithium alloys all the specimens for the heat treatment conditions displayed only pitting with the exception of 2091 peak - aged where small blisters appeared after one year of exposure attributed to the early stages of exfoliation corrosion. Although pitting was prevalent on the surface of the aluminium - lithium alloys, the attack showed the same type of morphology as the 2XXX series alloys - ie pits with a network of intergranular pathways. These intergranular pathways were not as advanced as those found for 2014 and 2024. P. R. Roberge et al (144) reported the appearance of corrosion on 2024, 7075, 2090 and 8090 after four months of testing and noted that, although pitting was more severe on the 2024 alloy, deep pits appeared on the 2090 alloy. Evidence of deep pits for 8090 and 2091 can be seen in this work. The depths were greater for the 8090 alloy coupled with the rating of pitting which suggests that the attack in the marine atmosphere was more insidious than first suggested. For example, in the 8090 peak - aged specimen a 15% reduction in thickness from the original 1.6mm thick sheet was reported. This could cause a problem in service for this type of aluminium - lithium alloy sheet in that the load bearing capacity of the material would be significantly reduced. The over - aged specimen exhibited the lowest depth of attack for both 8090 and 2091 and also showed fewer areas of attack than the peak - and under - aged conditions possibly due to S and δ' being more finely distributed. Although 8090 exhibited greater depths than 2091 for the same surface rating, intergranular corrosion velocities showed that 2091 was more susceptible to exfoliation corrosion. For example, 2091 peak - aged had a velocity of $4x10^{-11}ms^{-1}$ for the first year of exposure compared to $1.97x10^{-11}ms^{-1}$ for 8090 peak - aged. The reason for 2091 showing a higher susceptibility to attack in the marine atmosphere is a greater grain aspect ratio than 8090.

The 2091 appeared to be the most susceptible alloy of all the materials tested with the 8090 and 2024 showing fairly comparable rates and the 2014 being the least susceptible. Although there are major compositional differences among all the four alloys it may be significant that the 2091 should exhibit the greatest susceptibility due to the fact that it has the largest grain aspect ratio. This seems to be in direct contrast to L. Schra et al (182) and S. P. Jones (147) where they showed that 2XXX series alloys were more susceptible to atmospheric corrosion than aluminium - lithium alloys. In their

study the 2091 alloy appeared to be relatively insusceptible to corrosion but the susceptibility increased with increasing ageing time up to the peak - aged condition. As another comparison L. Schra (182) found that plate materials tended to be less corrosion resistant to atmospheric corrosion than sheet materials. In this study the 2091 sheet material was found to have a fast initiation time for corrosion which may have been due to over polishing and etching during preparation. It is known (183) that copper containing phases provide the initiation sites for corrosion, and that the solute depleted layer at the surface of these aluminium - lithium alloys imparts resistance to exfoliation attack. This layer is very thin and over polishing may have eliminated the layer exposing these copper containing phases thus decreasing the initiation time.

From figures 5.3 and 5.4 it can be seen that the under surface has corroded more than the upper surface. This has been reported by other authors where there has been a considerable difference between the depths measured on the downward and skyward surfaces. Figure 5.6 represents work carried out by F. L. McGeary et al (146) at several different test sites within the United States and the downward surface has a greater depth of corrosion at each particular site. It was concluded that accumulation of chemical contaminants and corrosion products on the downward surface could not be cleansed by rainfall whereas the upper surface is cleansed by periodic rainfall.

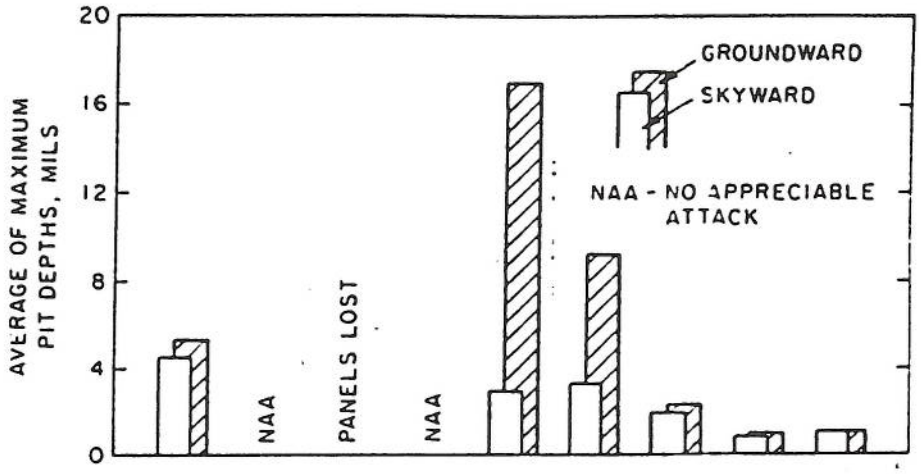

Figure 5.6. : Comparison of corrosion on the groundward and skyward surfaces of specimens subjected to atmospheric corrosion (146).

The fact that corrosion had occurred on both surfaces probably affected the depth of attack results obtained through four - point bend testing. It was shown the average measured depths for MASTMAASIS testing were higher due to the bend test measuring the whole of the specimen including the unattacked areas. Since there were large areas of unattacked material on the specimens exposed to the marine atmosphere the bend results would be expected to be significantly lower than the average measured depths. However, this was not the case as the bend test depths were close to the measured value. The bend test measured attack on both the top and bottom surfaces which probably gave a higher result than expected. Although the four - point bend test was used, no significant importance was given to the results as the marine exposure trials were carried out to see whether the MASTMAASIS test was a suitable test to compare to in - service conditions that an aircraft would experience. The major use of the bend test was to determine the effective remaining thickness of specimens after periods of exfoliation corrosion when subjected to the MASTMAASIS test.

The initial weather conditions and the weather throughout the duration of testing in a marine atmosphere plays an important role on the corrosion of aluminium alloys. As noted in this investigation the corrosion rate tends to decrease with time. V. E. Carter et al (184) reported that the depth of corrosion tended to level off after two years of exposure, although the rate of corrosion, which was measured by weight loss measurements, remained fairly constant for the six - year period of testing. Environmental factors that influence the initial rate of pitting attack may have a very marked effect on the depth of pitting observed even after long periods of exposure. V. E. Carter (185) suggested that corrosion occurring on specimens exposed initially during the summer is approximately the same as on specimens exposed initially during the winter. The 2014 and 2024 alloys were sent in October 1992, the 8090 sent out in May 1993 and the 2091 was sent out in September 1993. The differences in the depths of attack recorded are probably due to the time for which the specimens carried a reasonably continuous film of moisture during the first few weeks or months of exposure. Initial exposure of 8090 to the relatively high temperatures during summer would mean that the specimens would dry off quickly if any moisture was present on the surface of the specimen. The lower

temperatures during September and October would result in the specimens drying more slowly.

5.3.1. Comparison Between Atmospheric and MASTMAASIS Testing

In the earlier laboratory tests the susceptibility to exfoliation corrosion was assessed using the MASTMAASIS intermittent salt - spray test for both the 2XXX plate and aluminium - lithium sheet materials. A valid accelerated test should be able to predict exfoliation resistance in natural environments that are encountered in service, and also determine the exfoliation performance between alloys and tempers. A comparison between the two tests can be seen in table 5.5 by making use of the final surface ratings observed for the duration of each test on all four alloys. It can be said that the MASTMAASIS test gave a correct prediction of the behaviour of the 2014 alloy. For all the surface, T/4 and T/2 sections the surface rating showed the same signs of exfoliation corrosion between the two tests. In the case of the 2024 alloy laboratory testing overestimated the corrosion behaviour in that superficial corrosion was found on the specimens after two years of outdoor exposure whereas, severe corrosion occurred during MASTMAASIS testing. This is probably due to the fact that a dry bottom was used in the MASTMAASIS cabinet which provides a severe corrosion environment and more so than would be found for the particular environmental conditions used for outdoor testing. The MASTMAASIS test discriminated between the 2014 and 2024 alloys and all the sections, whereas the difference in outdoor exposure was not so obvious. For the aluminium - lithium alloys both the MASTMAASIS and outdoor exposure tests failed to discriminate between the alloys and the different heat treatment conditions. Both of the tests showed the same morphology of attack in the 2XXX series alloys where pits were observed in the initial stages of attack followed by a network of intergranular pathways which grew as the duration of testing increased. The morphology for 8090 and 2091 in the MASTMAASIS test showed that the attack followed the grain boundaries clearly defining grains within the structure. For outdoor testing deep pits were evident in the 8090 and 2091 alloys where there was some evidence of intergranular attack.

Table 5.5. : Comparison of Corrosion Attack for MASTMAASIS and Outdoor Testing.

Alloy	Type of Test	
	MASTMAASIS	Outdoor Exposure
2014 surface	EA-	EA-
2014 T/4	EA	EA-
2014 T/2	EA+	EA
2024 surface	EB-	EA-
2024 T/4	EB+	EA
2024 T/2	EC+	EA+
8090 under	P/EA-	P
8090 peak	EA	P
8090 over	P/EA-	P
2091 under	P/EA-	P
2091 peak	EA	P/EA-
2091 over	EA-	P

Even though the intergranular velocities differ greatly between the two tests the depths of attack can be compared. For example, alloy 2024 exhibits a maximum corrosion depth of 0.28mm for the T/2 section after two years of exposure which is equivalent to approximately one week of testing in the MASTMAASIS cabinet. The maximum depth on the 2014 alloy after exposure for two years was 0.197mm which was also equivalent to around one week of testing in the laboratory. For the 8090 alloy the results from the outdoor testing seem to correlate to around 240 hours of testing in the MASTMAASIS cabinet, whereas one year of atmospheric exposure for the 2091 alloy correlates to around 192 hours of testing.

CHAPTER SIX

6.0. END GRAIN ATTACK IN 2XXX SERIES ALLOYS

6.1. Introduction

Exfoliation corrosion in wrought aluminium alloys is intergranular in nature where the corrosion propagates around the elongated grains. At the junction of a grain there are a number of pathways the direction of attack can proceed. Major factors that will affect the direction of attack are the length and width of the grains. The attack may follow the longitudinal path or "short - circuit" down the transverse path. Figure 6.1 shows an elongated grain with longitudinal and transverse directions of attack.

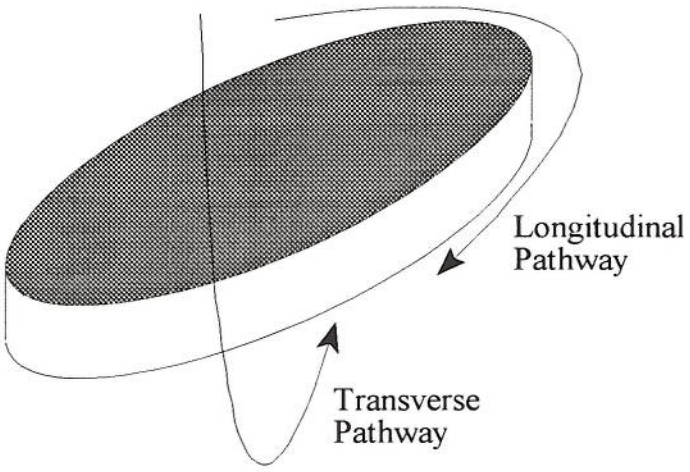

Figure 6.1. : Schematic diagram showing attack along the longitudinal and transverse directions around a typical elongated grain.

From the results of the exfoliation tests carried out on the 2XXX series alloys (see chapter four) it is not clear which path around the elongated grains the corrosion has followed to produce the observed depths of attack. The aim of this experiment is to determine the pathway which attack has followed, whether longitudinal, transverse or a combination of the two during exfoliation of 2014 and 2024 to provide further

information about the mechanism of attack. This end grain attack was carried out by exposing the edges of specimens to corrosion, measuring depths of attack for both the longitudinal and transverse orientations. From these depth measurements the mean corrosion velocities were calculated for each time interval. If the corrosion were to follow a longitudinal path the intergranular velocity would need to be much higher than in the transverse direction. A comparison can be made between the two orientations by comparing the ratios of the longitudinal and transverse velocities to the ratios of the grain dimensions to obtain the preferred pathway for attack during exfoliation corrosion of the T/2, T/4 and surface sections for the 2014 and 2024 alloys.

6.1.1. Procedure

Specimens from the T/2, T/4 and surface sections of the 2014 and 2024 alloys were subjected to the MASTMAASIS test. The specimen sizes were the same as those used in the MASTMAASIS testing (see chapter 4.2.1.). The sides and edges of each specimen from each section were lightly polished down to 1200 grit using silicon carbide paper and then etched in 5% NaOH and desmutted in concentrated nitric acid. The top and bottom surfaces were coated as an effective means of masking the specimens. Three different coatings were used which provided varying degrees of protection against corrosion. These were:

1. Coating the upper and lower surfaces of each specimen with lacomit to prevent corrosion.
2. Coating the upper and lower surfaces with epoxy resin.
3. Coating the upper and lower surfaces with Scotchweld structural adhesive.

The edges and sides were exposed to attack as this revealed the end grains which provided rapid initiation for attack. The specimens were placed in the MASTMAASIS cabinet for corrosion testing then removed after different time intervals and sectioned at the corners such that the end grain attack could be measured. Figure 6.2 shows the point from where the specimens were sectioned for measuring end grain attack.

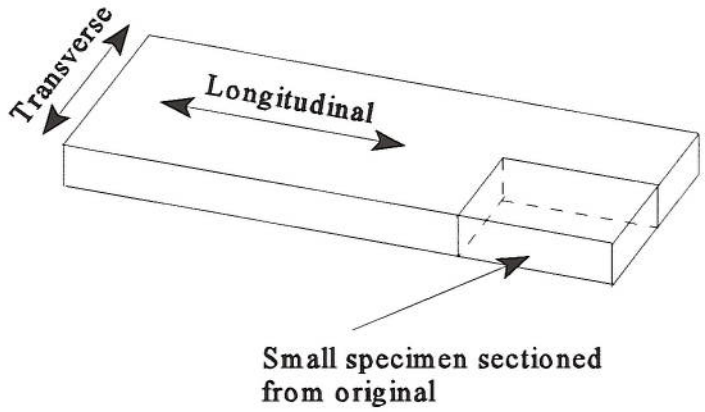

Figure 6.2. : Diagram showing the position from which specimens were sectioned.

In the first approach small sections were cut from the longitudinal and transverse orientations and mounted in epoxy resin. To determine the end grain depth of attack, ten to fifteen measurements were taken under an optical microscope for both orientations and the average was obtained from which intergranular corrosion velocities were calculated. For the second approach the original specimens were sectioned and the corners were mounted in purpose made square section mounts, designed so that the two perpendicular faces of the specimen were polished for metallographic examination. In this approach it was possible to measure attack which had initiated at the same point on the edge for both the longitudinal and transverse orientations. The third method made use of extreme value statistics where the extreme end grain depth of attack was obtained.

A fourth approach was used in order to determine whether or not internal stresses within the material have an effect on the intergranular corrosion rate. If there is enough stress in the material to constrain attack there would be a specific corrosion profile over the cross - section. The centre of the material exhibits greater stresses increasing the constraint hence decreasing the corrosion rate which would produce small depths of attack. These depths should increase toward the top and bottom surfaces where the

constraint is smaller. In this method four cubes each 20mm by 20mm by 20mm were machined from the original material for both the 2014 and 2024 alloys. One of the longitudinal faces was polished and etched leaving the remaining faces covered with Scotchweld structural adhesive and lacomit. This left the polished face exposed to attack in the MASTMAASIS cabinet. Each cube was removed after 1000 hours of testing (up to a maximum of 4000 hours for the two alloys) and cut in half along the centre line exposing the entire cross section. As this approach concentrated on the internal stresses within each alloy, measurements were taken in the longitudinal orientation. The maximum depth of attack measured for every 2mm across the cross - section was recorded.

6.1.2. Statistical Analysis

For the statistical approach several sections were cut from the longitudinal and transverse orientations and approximately 160 depths of attack were measured for each direction for the surface, T/4 and T/2 sections. From the measurements obtained, the top 10% were taken and used to calculate the most probable depth of attack. The method of extreme value statistics involved plotting graphs of $-\ln(-\ln F_{(Imax)})$, the cumulative distribution function, against the depth of attack. A line of best fit can be produced from which the gradient and intercept were obtained and used to calculate the maximum depth of attack. This is a more accurate approach in that more depths are recorded and that the measurements do not discriminate between attacked and unattacked areas on the edge.

6.2. Results

6.2.1. Effect of Specimen Preparation

6.2.1.1. Depth of Attack Measurements

The method of coating the specimens with Scotchweld structural adhesive combined with the use of extreme value statistics provided more accurate depths of attack. This was due to the fact that the lacomit and epoxy resin used for coating the specimen surfaces did not provide sufficient protection. In these two cases, attack not only occurred at the edges but also on the surfaces, therefore it was concluded that the

results did not solely represent end grain depth of penetration but also exfoliation from the surfaces. Measurements were taken across the cross - section of each specimen and included this attack occurring at the top and bottom surfaces. This resulted in the average depths being greater than expected for both the longitudinal and transverse orientations. A higher degree of protection was obtained using the Scotchweld structural adhesive as only end grain attack occurred and there was no evidence of attack along the surfaces. The depths obtained in the statistical approach were all lower than the maximum depths measured in the other two methods. It was assumed that in each case the corrosion occurred at the start of exposure testing and the initiation time was not significant. The depths of attack obtained through the statistical approach for the 2014 and 2024 alloys can be seen in tables 6.1 and 6.2. These results represent the most probable depth of attack obtained statistically from the 160 directly measured depths.

Table 6.1. : Maximum End Grain Depths of Attack for 2014.

Time hours	Depth of Attack (mm)					
	T/2		T/4		Su	
	Long.	Trans.	Long.	Trans.	Long.	Trans.
336	0.29	0.17	0.27	0.14	0.25	0.12
504	0.42	0.25	0.392	0.21	0.36	0.2
700	0.521	0.32	0.5	0.3	0.45	0.25
868	0.68	0.39	0.632	0.37	0.538	0.32
1012	0.725	0.428	0.69	0.45	0.613	0.39

Table 6.2. : Maximum End Grain Depths of Attack for 2024.

Time hours	Depth of Attack (mm)					
	T/2		T/4		Su	
	Long.	Trans.	Long.	Trans.	Long.	Trans.
336	0.35	0.22	0.4	0.24	0.28	0.16
504	0.48	0.375	0.52	0.321	0.4	0.25
700	0.65	0.458	0.69	0.465	0.54	0.34
868	0.78	0.519	0.81	0.53	0.65	0.42
1012	0.85	0.55	0.89	0.57	0.743	0.458

All the measurements made in the longitudinal direction were greater than those made in the transverse direction. Clearly, it is evident from the tables that, for both the alloys the corrosion had travelled further in the longitudinal direction. In the 2014 alloy the depths were greater in the mid - section and in the order T/2 > T/4 > surface due to a higher aspect ratio in the centre of the plate. It is surprising that the T/4 should have a greater depth of attack than the T/2 section in the 2024 alloy. Although the T/2 section has a higher aspect ratio than T/4, the length and width of the grains in the T/4 section are greater than in T/2. The difference in depths may also be due to a difference in precipitate distribution within the plate from which the specimens were machined.

The end grain attack appearance tended to be of small pits increasing in number and size as the duration of the test increased. For the morphology, attack tended to be a mixture of fissures initiating at the edges and intergranular attack. In general this intergranular attack either appeared at the end of these fissures or initiated at the end of each specimen. An example of end grain attack can be seen in figure 6.3 showing intergranular attack penetrating along the grain boundaries into the material. It can be seen that this type attack could have a very damaging effect on the structure of the material. The width of this network of intergranular attack increases as corrosion develops further from wedging caused by corrosion products.

Figure 6.3. : Cross - section showing end grain attack for 2024 after 2000 hours (X50).

6.2.1.2. Intergranular Corrosion Velocity

The intergranular velocities were calculated by making use of the depth of attack and the time taken in seconds. These velocities for 2014 and 2024 can be seen in tables 6.3 and 6.4. The longitudinal direction exhibits a greater intergranular velocity than the transverse direction for all test times which suggests that the longitudinal orientation is more susceptible to attack than the transverse orientation. For the 2014 alloy the velocities increased in the order surface < T/4 < T/2 for both the longitudinal and transverse directions. In 2024 the T/4 section exhibited the greater rate of attack followed by the T/2 and surface sections.

Table 6.3. : End Grain Intergranular Velocities for 2014.

Time hours	Intergranular Velocity (ms^{-1})					
	T/2 ($x10^{-10}$)		T/4($x10^{-10}$)		Su ($x10^{-10}$)	
	Long.	Trans.	Long.	Trans.	Long.	Trans.
336	2.4	1.4	2.15	1.16	1.9	0.99
504	2.3	1.38	2.2	1.4	1.9	1.1
700	2.1	1.26	1.98	1.19	1.78	0.99
868	2.17	1.25	2.02	1.18	1.72	1
1012	1.99	1.17	1.89	1.14	1.68	0.97

Table 6.4. : End Grain Intergranular Velocities for 2024.

Time hours	Intergranular Velocity (ms^{-1})					
	T/2($x10^{-10}$)		T/4($x10^{-10}$)		Su($x10^{-10}$)	
	Long.	Trans.	Long.	Trans.	Long.	Trans.
336	2.89	1.81	3.3	1.98	2.3	1.32
504	2.64	1.93	2.2	1.8	2.2	1.38
700	2.57	1.8	2.74	1.85	2.14	1.3
868	2.5	1.7	2.59	1.7	2.08	1.34
1012	2.33	1.5	2.44	1.56	2.04	1.26

6.2.2. Effect of Internal Stresses

The diagram shown in figure 6.4 indicates how the cubes were sectioned and measured. The measurements were taken from the cross - section AA. The maximum measurements taken from the cross - section are represented in bar chart form and can be seen in figure 6.5. The measurements were not taken from the very edge of the cube as the Scotchweld structural adhesive coating overlapped the edges to prevent any attack occurring along the surfaces which would have resulted in inaccurate results. From figure 6.5 it can be seen that there is no specific corrosion profile over the cross - section which seems to suggest that any internal stresses present within the material do not have any effect on the corrosion.

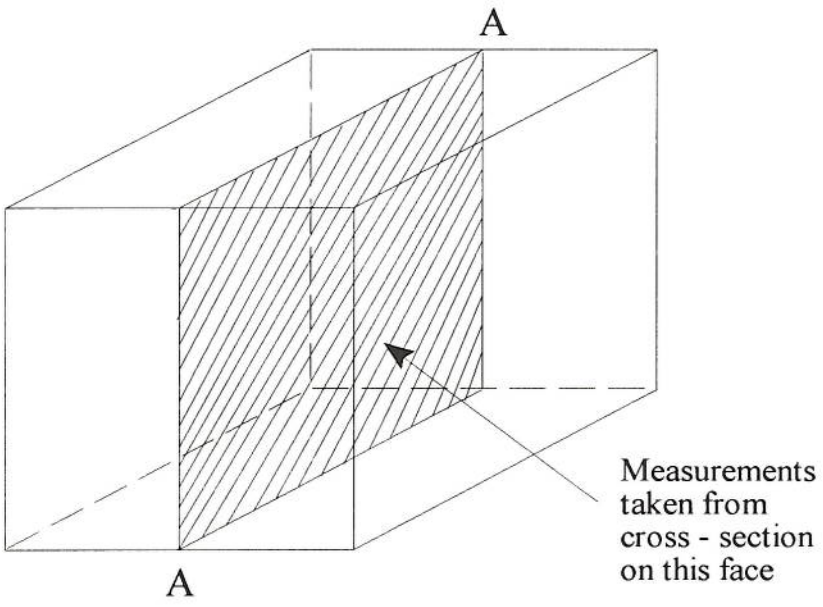

Figure 6.4. : Diagrammatic representation of the sections cut from the original cube.

6.3. Discussion

During the initial stages of attack the surface appearance was the same as in the MASTMAASIS testing where a uniform distribution of small pits appeared over the surface of the specimens with large areas of material unattacked. In the MASTMAASIS

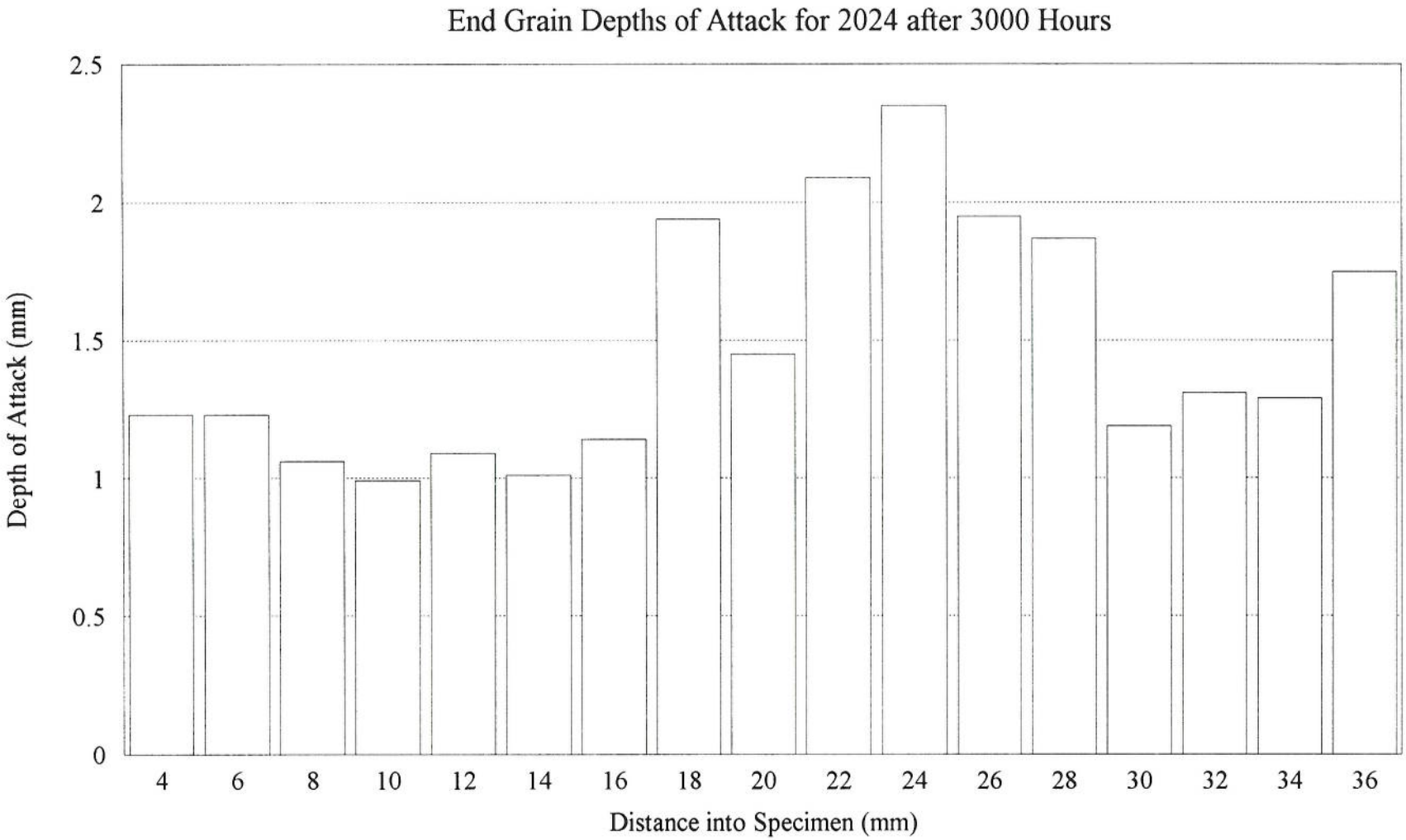

Figure 6.5. : Maximum end grain depths of attack for 2024 after 3000 hours.

testing the pits grew into large blisters and ruptured causing lifting of the grains due to wedging stresses caused by the build up of corrosion products. As the time increased in the end grain test the pits grew in number and size until deep fissures were seen protruding into the specimen. At longer times these fissures widened possibly relieving any stresses present in the material. The attack was intergranular in nature with an increasing number of intergranular networks growing from the large fissures as the duration of the test increased. In general the intergranular attack initiated at the end of the pits but, in some areas initiated at the end of each specimen. This could be due to the fact that these sites are more active than the surrounding area. L. S. Anwar (46) described the initiation of intergranular attack from the end of the specimen through "active grains" present within the structure. It appears that the depth of penetration associated with the initiation of intergranular attack from these "active grains" is greater than depths obtained from the surrounding areas.

The statistical approach was the most reliable test in obtaining the true end grain depths of attack. With the lacomit the maximum depth reached 1.51mm after 288 hours whereas from statistical analysis of the results the maximum depth only reached 0.89mm after 1012 hours. This is due to the fact that as corrosion increased, the lacomit and epoxy resin lifted from the top and bottom exposing these surfaces to attack. The large difference in depths between the tests was caused by the fact that, in the specimens coated with lacomit and epoxy resin, measurements did not distinguish between end grain attack and attack which may have initiated at the top and bottom edges and spread along each surface faster than it would have in the centre of the specimen. Wedging stresses which increased over the duration of testing probably caused the lacomit and epoxy resin to lift at the top and bottom edges of the specimen. The Scotchweld structural adhesive is stronger than the lacomit and epoxy resin withstanding higher wedging stresses so the coating did not lift from the surface and was protected during the entire duration of the test.

The velocities obtained from the end grain depths of attack are shown in tables 6.3 and 6.4 and represent the same trend in the MASTMAASIS testing. Alloy 2024, with

the larger grain aspect ratios exhibits the greater intergranular velocities than 2014 for all sections. In the 2014 alloy the velocity increases toward the mid section of the plate in the order surface < T/4 < T/2 whereas, for 2024 the T/4 section shows the fastest rate of attack followed by the T/2 and surface sections respectively. For determining the orientation of the intergranular pathway for each section in the two alloys the velocities and grain dimensions were used. The diagram shown in figure 6.6 represents typical end grain attack around elongated grains in an aluminium alloy showing the intergranular velocity for the longitudinal (V_L) and transverse (V_T) directions. The preferred corrosion path was then determined by comparing the ratio of the corrosion rates in the longitudinal and transverse pathways, V_L/V_T, with the ratio of the grain dimensions in these directions, L/T.

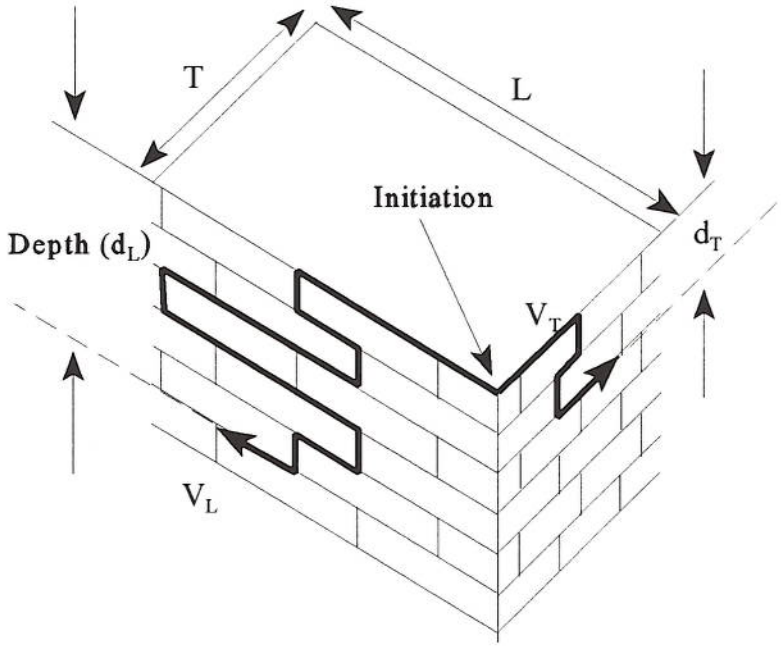

Figure 6.6. : Diagram showing the end grain attack around elongated grains.

There are three possible cases to consider:

If $\frac{V_L}{V_T} > \frac{L}{T}$ then the attack follows the longitudinal path.

If $\frac{V_L}{V_T} < \frac{L}{T}$ then the attack follows the transverse path.

If $\frac{V_L}{V_T} \approx \frac{L}{T}$ then both the longitudinal and transverse paths contribute to the attack.

The values for L and T which are the grain lengths and widths respectively can be seen in table 3.4 (section 3.2.3) and are shown in figure 6.7.

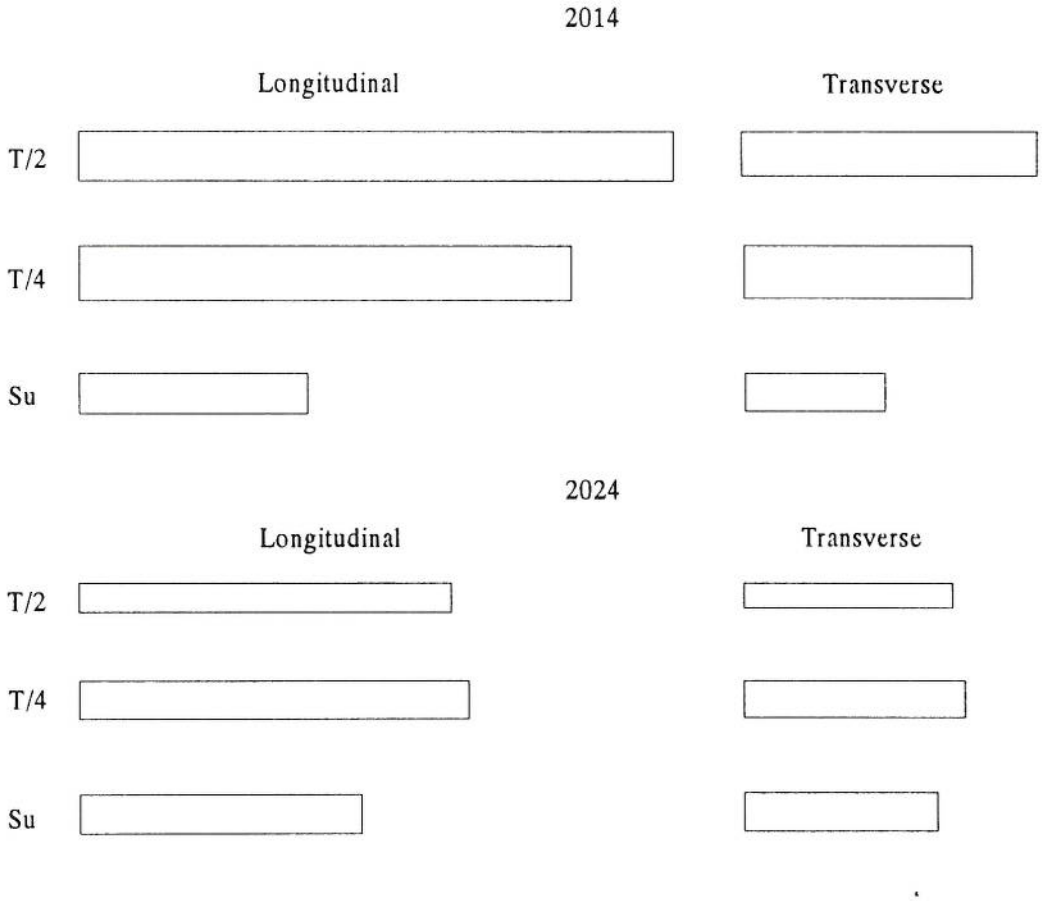

Figure 6.7. : Diagrammatic representation of grain aspect ratios for 2XXX series alloys.

The ratios of the velocities and the intergranular pathways can be seen in tables 6.5. and 6.6.

Table 6.5. : Comparison of Ratios for 2014.

Time	V_L / V_T			L / T		
hours	T/2	T/4	Su	T/2	T/4	Su
336	1.71	1.85	1.91	2.04	2.15	1.58
504	1.67	1.57	1.72			
700	1.67	1.66	1.79			
868	1.74	1.7	1.68			
1012	1.71	1.52	1.7			

Table 6.6. : Comparison of Ratios for 2024.

Time	V_L / V_T			L / T		
hours	T/2	T/4	Su	T/2	T/4	Su
336	1.59	1.67	1.74	1.63	1.57	1.44
504	1.37	1.61	1.59			
700	1.43	1.48	1.65			
868	1.47	1.52	1.55			
1012	1.54	1.56	1.62			

There seems to be no trend for which pathway the attack follows between the sections for the two alloys. For the 2014 alloy the velocity ratio tends to be lower than the ratio of the intergranular pathways for the T/2 and T/4 sections which seems to suggest that the direction of attack follows the transverse path whereas, in the surface section the velocity ratio is higher suggesting that corrosion follows the longitudinal path around the elongated grains. With the surface section showing a longitudinal pathway for attack the grain boundaries provide an unbroken path for attack to propagate along horizontally and not short circuit around the grains. For T/2 and T/4, although they have longer grains than the surface section the preferred direction of attack is to "short - circuit" around the transverse pathway providing the greater depths of attack found in MASTMAASIS testing. In the 2024 alloy the ratio of the velocities is similar to that of the intergranular pathway for the T/4 and T/2 sections suggesting a combination of attack

from both the longitudinal and transverse orientations. This suggests that, for the 2024 T/2 and T/4 sections, once a grain boundary junction is met the attack can proceed in any direction - downwards, upwards or continue laterally. From the depths of attack obtained during MASTMAASIS testing it is evident that the attack does not continue upwards but downwards providing deep penetration which resulted in the greater depths shown in chapter four. The surface section for the 2024 alloy exhibits a higher intergranular pathway ratio than that for the intergranular velocities with attack prevailing longitudinally around the grains.

CHAPTER SEVEN

7.0. STRESS CORROSION CRACKING

7.1. Introduction

Stress corrosion cracking and exfoliation corrosion are believed to be related in that they both require a tensile component of stress at the developing corrosion tip. In the case of stress corrosion cracking the stress is generally applied through an external load, whereas in exfoliation corrosion the stress arises from the wedging effect caused by the build up of voluminous corrosion products. These corrosion products are three times the volume of the original material causing the lifting of grains. For stress corrosion cracking to occur three conditions need to be satisfied; first, the alloy must be susceptible; second, there must be a specific environment (water or salt water for aluminium alloys) and; third, there must be a tensile stress. The environment must be aggressive enough to promote stress corrosion failure otherwise intergranular corrosion dominates and stress corrosion cracking does not occur.

The aim of this experiment was to compare the stress corrosion and exfoliation susceptibilities of the 2091 in different heat treatment conditions and 2014 and 2024 alloys in the different grain morphology conditions to provide further understanding of the failure mechanism. For a material having an elongated grain structure, the orientation of the major grain boundary to the direction of applied stress becomes an important factor in determining stress corrosion susceptibility. Both exfoliation and stress corrosion cracking propagate along the elongated grains within each material and it is clearly important therefore that the stress corrosion cracking specimens be stressed in the short transverse direction. The elongated grain structure provides an easy path for corrosion to take place and the stress involved accelerates this corrosion. Previous work with rolled aluminium plate (93) has shown that susceptibility is maximum for specimens stressed in this direction rather than the longitudinal direction. In specimens stressed in the short transverse direction, the cracks can propagate with very little deviation along grain boundaries perpendicular to the direction of applied stress.

7.2. Experimental

7.2.1. Specimen Design

Testing was carried out for the 2091 alloy in the under -, peak - and over - aged conditions and the T/2, T/4 and surface sections for the 2014 and 2024 alloys. Discs were machined from the 2091 sheet and the 2XXX series plate materials. The dimensions for 2091 were 19mm diameter, 1.6mm thickness (the gauge of the sheet) with a circumferential notch giving an internal diameter of 4.7mm and a cross - sectional area of 17mm^2. In the 2XXX series alloys the dimensions were 19mm diameter, 5mm thickness with an internal diameter of 4mm and a cross - sectional area of 12.6mm^2. The internal diameter in the 2XXX series alloys was machined with an included, angled notch of 60^0 that acted as a stress raiser promoting fast initiation of stress corrosion. The specimens used can be seen in figure 7.1.

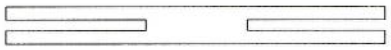

Specimen for 2091

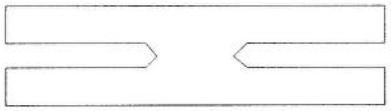

Specimen for 2014 and 2024

Figure 7.1. : Diagram of specimens used for stress corrosion testing.

7.2.2. Procedure

Each disc was given a light polish on both sides and cleaned before being attached between two mild steel holders. These holders were necessary in order for the specimens

to be held in the constant load testing machine which had a 10:1 lever arm. The mild steel holders were coated with lacomit for corrosion protection and to prevent the set up of a galvanic cell in the testing environment. Each disc was attached to the holders by using a two - part Scotchweld structural adhesive, type 9323B/A supplied by 3M which is an aerospace adhesive and possesses a tensile strength of 37MPa at 25^{0}C. This adhesive has a curing time of 48 hours, and as the whole arrangement needed to be collinear, vee blocks were used to prevent any misalignment during the curing period. This avoided any shear stresses being placed on the specimen during testing. Using an adhesive with such a high tensile strength was necessary so that the specimen would fail before the adhesive. The larger area of material bonded to the adhesive and the smaller area to carry the load also ensured that the specimen would fail first.

A small cell was placed around the specimen and holders before placing them in the testing machine. A small amount of silicon sealant was used to hold the cell in place and to prevent any leakages of the testing solution. The general arrangement of the specimen, holders and cell can be seen in figure 7.2. After loading, the test solution was added to the cell. Three solutions were used - those of 3.5% NaCl solution, 3.5% NaCl acidified to pH3 with acetic acid and EXCO. Only the 3.5% NaCl solution was used for testing the 2091 whereas the 2XXX series alloys were also tested in the other two solutions. It is known that the test solution affects the resistance to stress corrosion cracking - the EXCO environment is very aggressive and this was expected to reduce the time to failure significantly. The stress used for the 2XXX series alloys was 190MPa which represents approximately 48% of the yield strength of the alloys. The load pan of the test machine was carefully loaded using these loads and released so that the specimen was not loaded with shock. The time was measured up to the point of fracture using a timing device attached to the cell such that when the specimen failed the circuit to the timer was broken and the clock stopped. After the specimen had failed, it was taken from the test solution, removed from the holders and washed thoroughly. Examination of the surfaces was undertaken using a scanning electron microscope. Times to failure and the initial stress were the measurements of interest.

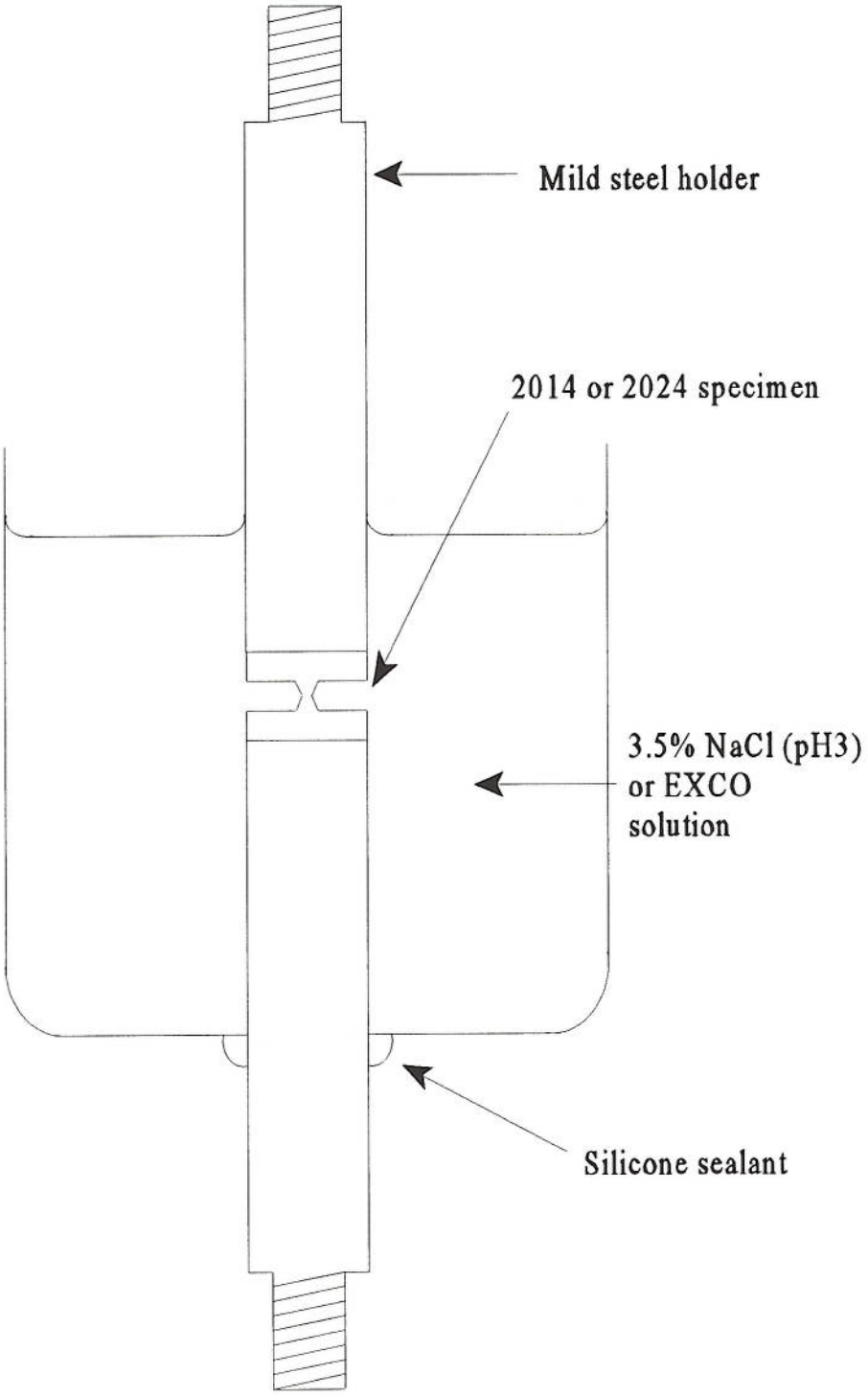

Figure 7.2. : Diagram showing the arrangement of the specimen holders, specimen and the cell used for stress corrosion cracking (not to scale).

7.3. Results

Due to the relatively low susceptibility of the 2091 in neutral 3.5% NaCl solution each test took a long time for the specimens to fail with only two results recorded - those for the under and peak - aged conditions. Each disc failed in shear rather than in tension. The time to failure for the two tests was 990 hours for the under - aged condition and 770 hours for the peak - aged condition. Although the mode of failure was undesirable, this result seems to suggest that the peak - aged material was more susceptible to stress corrosion than the under - aged material.

The dimensions of the 2014 and 2024 specimens were used so that the specimens would not fail in shear. An increase in the thickness to 5mm and the included angle of 60^0 in the internal diameter (which acts as a stress raiser) reduced the likelihood of failure in shear mode. Initially the specimens were tested in the 3.5% NaCl solution acidified to pH3 which was thought to be a more aggressive environment than neutral NaCl solution but each section showed very low susceptibility in this environment and no failure was recorded in more than one month testing for each specimen. It would appear that the initiation time was very long in this environment. The times to failure were significantly reduced in the more aggressive environment of the EXCO solution. The results for the 2014 and 2024 alloys can be seen in tables 7.1 and 7.2. It can be seen that the susceptibility to stress corrosion increases toward the centre of the plate in the order surface < T/4 < T/2. The times to failure ranged from two days for the 2024 T/2 section to just under a week for the 2014 surface section. The failure times were lower in the 2024 alloy for all the sections due to the higher aspect ratio in each case. Included in each table is a comparison between the velocities from the MASTMAASIS corrosion testing and the stress corrosion tests. The stress corrosion velocity is a mean value and assumes that SCC initiates immediately. Corrosion and the presence of corrosion products obscured the fracture face of failed specimens. Using scanning electron microscopy to study the fracture faces it was assumed that a crack had travelled around 2mm into the specimen before failure. The velocities were then calculated by making use of the assumed crack length and the time to failure. Velocities were greater in the stress

corrosion testing possibly due to applied stress.

Table 7.1. : Stress Corrosion Results for 2014.

Section	Intergranular Velocity (ms^{-1})	Time to Failure (hours)	SCC Velocity (ms^{-1})
Surface	$3.19x10^{-10}$	140	$3.96x10^{-9}$
T/4	$6x10^{-10}$	96	$5.78x10^{-9}$
T/2	$8.16x10^{-10}$	66	$8.42x10^{-9}$

Table 7.2. : Stress Corrosion Results for 2024.

Section	Intergranular Velocity (ms^{-1})	Time to Failure (hours)	SCC Velocity (ms^{-1})
Surface	$6.45x10^{-10}$	114	$4.87x10^{-9}$
T/4	$1.1x10^{-9}$	76	$7.31x10^{-9}$
T/2	$1.81x10^{-9}$	49	$1.13x10^{-8}$

7.4. Discussion

It was shown that the 2091 was fairly insusceptible to stress corrosion in the neutral NaCl solution. The peak - aged material showed an increase in susceptibility over the under - aged material. Due to the failure mode of the 2091 specimens - in shear rather than tension - the over - aged condition was not tested. It was assumed that the over - aged material would have been less susceptible than the peak - aged material. Marsac et al (185) tested 2091 T8X and 2091 T851 alloys and showed that the peak - aged T851 had a greater stress corrosion susceptibility in NaCl solution than the T8X under - aged material, in fact the T8X temper was unsusceptible. Moran (186) et al explained the low stress corrosion susceptibility in NaCl by the aggressive nature of this solution, which promoted relatively large, blunted pits and inhibited the nucleation of stress corrosion cracks.

Balasubramaniam et al (89) showed that the stress corrosion susceptibility in an

AlLiCu alloy increases up to a maximum at the peak - aged condition. They stated that alloys in the over - aged condition appear to be at least as susceptible to stress corrosion as the peak - aged material, due to a reduction in the stress corrosion crack initiation resistance of the material. This may be explained by the fact that ageing of AlLiCu type alloys leads to the precipitation of the metastable δ' (Al_3Li) phase which imparts strength to the alloy. After longer ageing times, δ' transforms to δ (AlLi) which lowers the crack resistance of the alloy. In contrast Meletis (107) found that the over - aged condition in 2090 resulted in poor stress corrosion resistance. Wang et al (114), finding the peak - aged material more susceptible, suggested a model of preferential dissolution of the T_2 (Al_6CuLi_3) phase which precipitated at grain boundaries and subgrain boundaries. This T_2 phase is anodic in relation to the matrix. There is a large volume fraction of the T_2 phase in the peak - aged condition resulting in a high anodic current density, which provides a large driving force for the dissolution of the T_2 phase. In the over - aged condition the potential difference between the grain boundary and the matrix is reduced, due to a lower volume fraction of T_2 hence reducing the driving force for anodic dissolution. In aluminium alloys the strength maximum corresponds to a ductility minimum under peak - aged conditions.

For the 2XXX series alloys the stress corrosion susceptibility increased towards the centre of the plate which exhibits the more elongated grains. As with the 2091 alloy the susceptibility was very low in the NaCl solution with no failures recorded. Sharp cracks cannot be sustained in this environment causing blunt intergranular fissures. It was shown that increasing the aggressiveness of the solution promoted stress corrosion failure. Work carried out by H. F. De Jong et al (187) showed that reducing the pH of the solution did promote failure in aluminium alloys but increased general corrosion, pitting and/or intergranular corrosion in the material. W. Gruhl (73) stated that AlCuMg type alloys do not truly stress corrosion crack, but rather exhibit intergranular corrosion, which can occur without stress but is accelerated under stress. Indeed, in NaCl solutions intergranular corrosion produces crack branching which decreases the stress intensity (the driving force for crack extension) and a low susceptibility is observed. This explains the fact that the EXCO environment produces a greater susceptibility to stress corrosion

cracking. As the susceptibility increases, the time to failure decreases, limiting the propagation of intergranular corrosion. In EXCO, voluminous corrosion products are formed rapidly due to the aggressive nature of the solution which increases the stress intensity producing a large driving force for cracking to occur. The EXCO environment produced failures at the times shown in tables 7.1. and 7.2. R. Braun (101) tested 2014 and 2024 under constant immersion stress corrosion tests and found similar times to failure. For the 2024 alloy the times to failure were in the range of 50 to 120 hours and, for the 2014 alloy the times were 90 to over 200 hours. The results follow the same trend shown for MASTMAASIS testing in that the susceptibility increased as the aspect ratio increased in the order surface < T/4 < T/2 for both the alloys. This can be seen in the times to failure as they decrease into the plate with the T/2 section showing 66 hours for 2014 and 49 hours for 2024 - lower than the other sections. The results exhibited lower times to failure for 2024 than 2014 with the lower grain aspect ratio. In structures exhibiting more elongated grains the susceptibility is increased due to a more direct corrosion path. Braun (188) showed that the 3.5% NaCl solution caused severe corrosion on the fracture surfaces, especially in the 2014 alloy which failed at longer times. In fact stress corrosion cracking could not be inferred due to the severe corrosion on the fracture surfaces.

The main difference between the two alloys is their Cu : Mg ratios resulting in different phases - $CuAl_2$ in 2014 and $CuMgAl_2$ in 2024. Preferential precipitation of these phases along grain boundaries creates copper depleted solid solution regions along these boundaries. In a corrosive medium the anodic copper depleted regions corrode preferentially causing intergranular attack and stress corrosion cracking. The results obtained here contradict the findings of K. Urushino (76) where he stated that "the susceptibility to stress corrosion cracking decreases with Mg content of the alloy". The 2024 has a higher Mg content than 2014 but shows a greater susceptibility. This may be caused by a higher volume fraction of precipitates present at the grain boundaries in the 2024 alloy resulting in a high anodic current density and a large driving force for the dissolution of the $AlCuMg_2$ phase.

CHAPTER EIGHT

8.0. GENERAL DISCUSSION

8.1. Comparison of Results

Exfoliation corrosion in wrought, high strength aluminium alloys can be attributed to the combined effects of an elongated grain structure and susceptibility to intergranular corrosion. The use of the MASTMAASIS test, environmental exposure and the constant load test were used to rank the susceptibility of the 2014 and 2024 alloys to exfoliation corrosion. Results obtained such as the intergranular corrosion velocity and time to failure give an indication of the resistance of a material to exfoliation and stress corrosion cracking respectively. Shown in table 8.1 is a summary of the results from the total duration of each test for the 2014 and 2024 alloys. The total testing time was 679 and 631 hours for 2014 and 2024 respectively in the MASTMAASIS cabinet and two years of outdoor exposure for both alloys. Similarly, table 8.2 shows a summary of results for the 8090 and 2091 alloys obtained through MASTMAASIS and environmental testing.

Table 8.1. : Comparison of Results for 2014 and 2024.

Alloy		MASTMAASIS Test			Outdoor Exposure			Stress Corrosion	
		Surface Rating	Depth of Attack (mm)	IG.C.V. (ms^{-1})	Surface Rating	Depth of Attack (mm)	IG.C.V. (ms^{-1})	Time to Failure (hours)	Velocity (ms^{-1})
2014	Su	EA-	0.24	$3.2x10^{-10}$	EA-	0.11	$6.1x10^{-12}$	140	$4x10^{-9}$
	T/4	EA	0.24	$5.2x10^{-10}$	EA-	0.13	$1.1x10^{-11}$	96	$5.8x10^{-9}$
	T/2	EA+	0.38	$1.1x10^{-9}$	EA	0.144	$1.4x10^{-11}$	66	$8.4x10^{-9}$
2024	Su	EB-	0.31	$5.8x10^{-10}$	EA-	0.15	$1.1x10^{-11}$	114	$4.9x10^{-9}$
	T/4	EB+	0.48	$1.2x10^{-9}$	EA	0.19	$1.6x10^{-11}$	76	$7.3x10^{-9}$
	T/2	EC+	0.6	$1.8x10^{-9}$	EA+	0.21	$2.3x10^{-11}$	49	$1.1x10^{-8}$

For the MASTMAASIS testing of the 2XXX series alloys the trend is that as the surface rating worsens, the depth of attack and the intergranular corrosion velocity increases - sections showing severe corrosion exhibit deep intergranular attack and the sections which show moderate exfoliation have shallower depths of intergranular

Table 8.2. : Comparison of Results for 8090 and 2091

Alloy	Heat Treatment	MASTMAASIS Test			Outdoor Exposure		
		Surface Rating	Depth of Attack (mm)	IG.C.V. (ms^{-1})	Surface Rating	Depth of Attack (mm)	IG.C.V. (ms^{-1})
8090	Under	P/EA-	0.21	$6.5x10^{-10}$	P	0.15	$1.2x10^{-11}$
	Peak	EA	0.235	$7.3x10^{-10}$	P	0.19	$1.5x10^{-11}$
	Over	P/EA-	0.2	$6.1x10^{-10}$	P	0.13	$9.9x10^{-12}$
2091	Under	P/EA-	0.23	$1.6x10^{-9}$	P	0.14	$3.6x10^{-11}$
	Peak	EA	0.273	$1.8x10^{-9}$	P/EA-	0.15	$4x10^{-11}$
	Over	EA	0.25	$1.7x10^{-9}$	P	0.13	$3.4x10^{-11}$

penetration. This is not so apparent for 8090 and 2091 where the ratings do not differ very much between the two alloys and the different heat treatment conditions. Although the visual assessment results indicate the susceptibility of exfoliation corrosion in these alloys, this method is not reliable on its own. The use of metallographic examination to obtain the depth of attack and intergranular velocities provide, to a greater extent, how susceptible a material is to exfoliation. Laboratory testing should be able to reproduce the exfoliation that can be found in service in a short period of time and it has been shown that the MASTMAASIS test is a valid, accelerated test in determining the corrosion susceptibility of aluminium alloys. Although the attack was not as advanced in outdoor corrosion testing, similar morphologies of attack were found between outdoor testing and the MASTMAASIS test for all the alloys tested. It would be expected that for corrosion to penetrate to the depth of attack found on the specimens subjected to the MASTMAASIS cabinet, aluminium alloys would have to be exposed to the environment for several years. The test discriminated between the different sections of the plate for the 2XXX series alloys more so than the heat treatment conditions for 8090 and 2091. The stress corrosion testing exhibited the highest intergranular velocities in 2014 and 2024. Although it must be taken into consideration that the stress corrosion testing was carried out in a more aggressive solution, that of EXCO, the introduction of stress increases the intergranular corrosion rate. Once started, the attack tends to

continue along the grain boundaries. The exfoliation corrosion of aluminium alloys may proceed as a stress corrosion mechanism - in stress corrosion an external stress is applied for the mechanism to proceed and, for exfoliation corrosion, the formation of corrosion products exert stresses on the internal structure of the material. If the volume of these corrosion products exceed the volume of the material from which they form then wedging stresses arise which provide the force required for lifting the surface grains of the material.

The use of the four - point bend test to establish the depth of penetration seemed to underestimate the depth by virtue of the whole specimen being measured. This included the unattacked areas which lowered the result when compared to metallographic assessment. The bend test may have measured the pits which had formed during corrosion but not the intergranular penetration extending into the material which was evident through metallography. The maximum depths seen are the measurements of the maximum intergranular penetration. To obtain greater accuracy in the average measured depth of attack, and hence a better comparison with the bend test, extreme value statistics (see appendix three) can be used where approximately 100 measurements were taken metallographically to obtain the true depth. Taking a large number of measurements along the specimen reduces any discrimination by the observer between attacked and unattacked areas, so reducing the scatter which was evident in the results from chapter four. A graph of depth of attack against time can be seen in figure 8.1 representing statistical and bend test depths for 2014 T/2. Here the depths obtained through bend testing lie between the average and maximum measured values compared to being lower than the average depth as reported in chapter four. The fact that four - point bend testing does not underestimate the depth of attack shows that the deflection method for determining the depth is a useful test.

8.1.1. The Effect of Grain Aspect Ratio

For the determination of the grain aspect ratio the assumption that all the grains in the structure have the same shape was made. The grains which show the greatest dimensions are those which are sectioned through the centre of the grain and these would

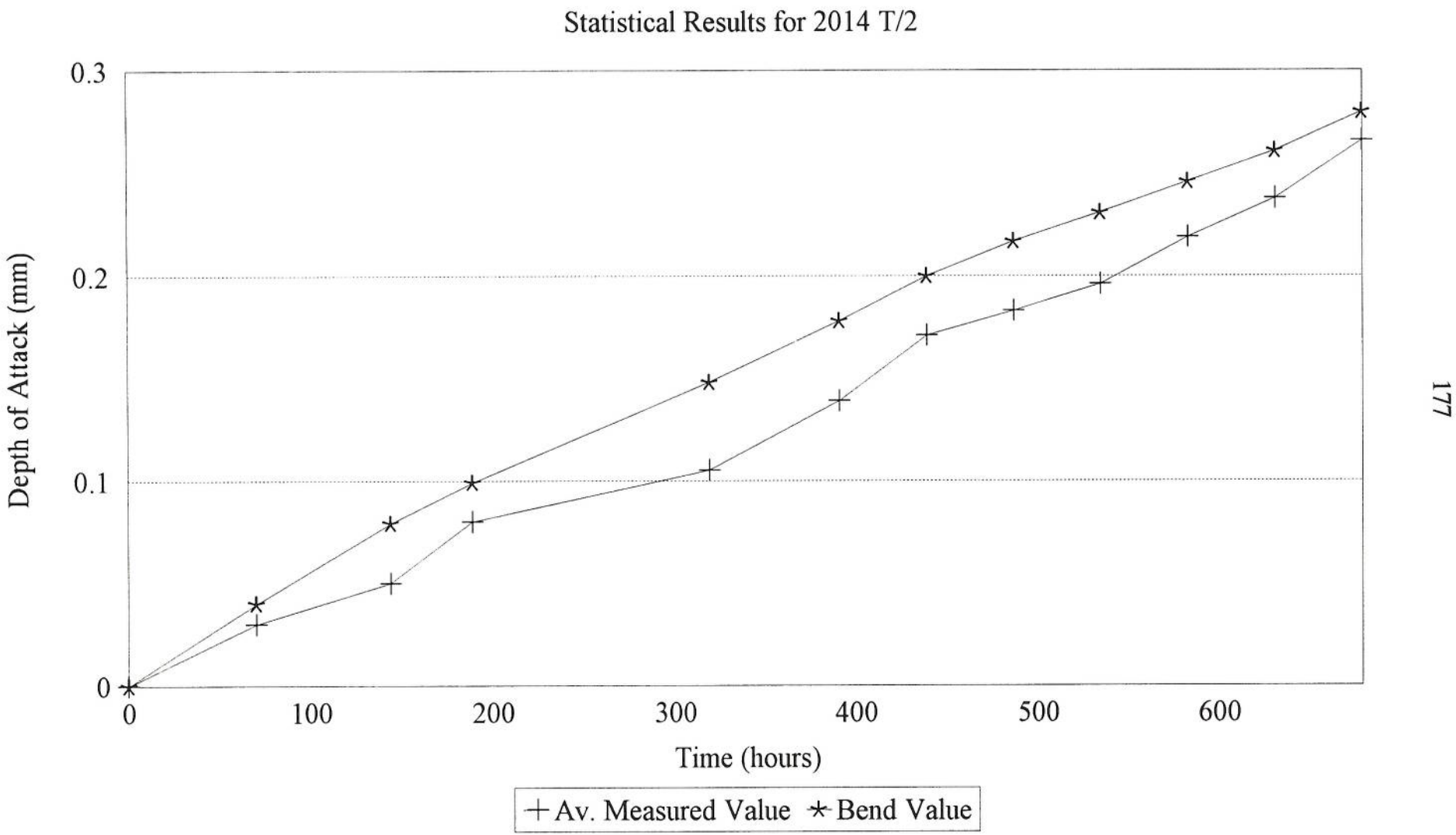

Figure 8.1. : Graph of depth of attack against time showing statistical results for 2014 T/2.

approximate to the true grain length and width. The results showed that the grains become more elongated toward the centre of the plate due to rolling during processing of the plate and resulting in a higher grain aspect ratio for the T/2 section. The grains at the surface are equiaxed with the smallest aspect ratio. There was no large difference between the aspect ratios for the two alloys where both had similar elongated structures.

It has been shown that the grain shape does alter the exfoliation susceptibility of aluminium alloys. Corrosion developed readily for the 2014 and 2024 surface, T/4 and T/2 sections where, over a period of time, blisters formed and burst to give the characteristic of exfoliation. The 2024 T/2 section exhibited the worst attack where large blisters formed and burst giving rise to a rating of severe exfoliation. This was expected due to the aspect ratio for this section being the largest. The formation of large blisters has been attributed to a more elongated grain structure (164). Here, the grain boundary sensitivity is larger for higher aspect ratios which results in a slow build up of strain in the blister skin. In materials with a more equiaxed grain structure the surface strain develops rapidly leading to the formation of small blisters or general spalling. Blister growth continues until the strain in the skin of the blister exceeds the fracture strain of the material at which point it will break open. In fact, as the aspect ratio increased toward the centre of the plate the surface rating, depth of attack and intergranular velocity increased showing a higher susceptibility to corrosion for the T/2 section in both alloys.

Although the grain aspect ratio influences the extent of attack, for materials which possess similar aspect ratios, the intergranular velocity is the dominant factor. A graph of intergranular velocity against aspect ratio can be seen in figure 8.2 for the 2014 and 2024 surface, T/4 and T/2 sections. The intergranular velocity increases with grain aspect ratio, and evidence from the graph suggests that this increase is linear. It can be seen that 2024 exhibits higher corrosion velocities than 2014 for all sections which results in a greater susceptibility to exfoliation corrosion. The stress corrosion testing showed the same trend as that for corrosion testing. The times to failure decreased as the grain aspect ratio increased in the order surface > T/4 > T/2 indicating higher susceptibility

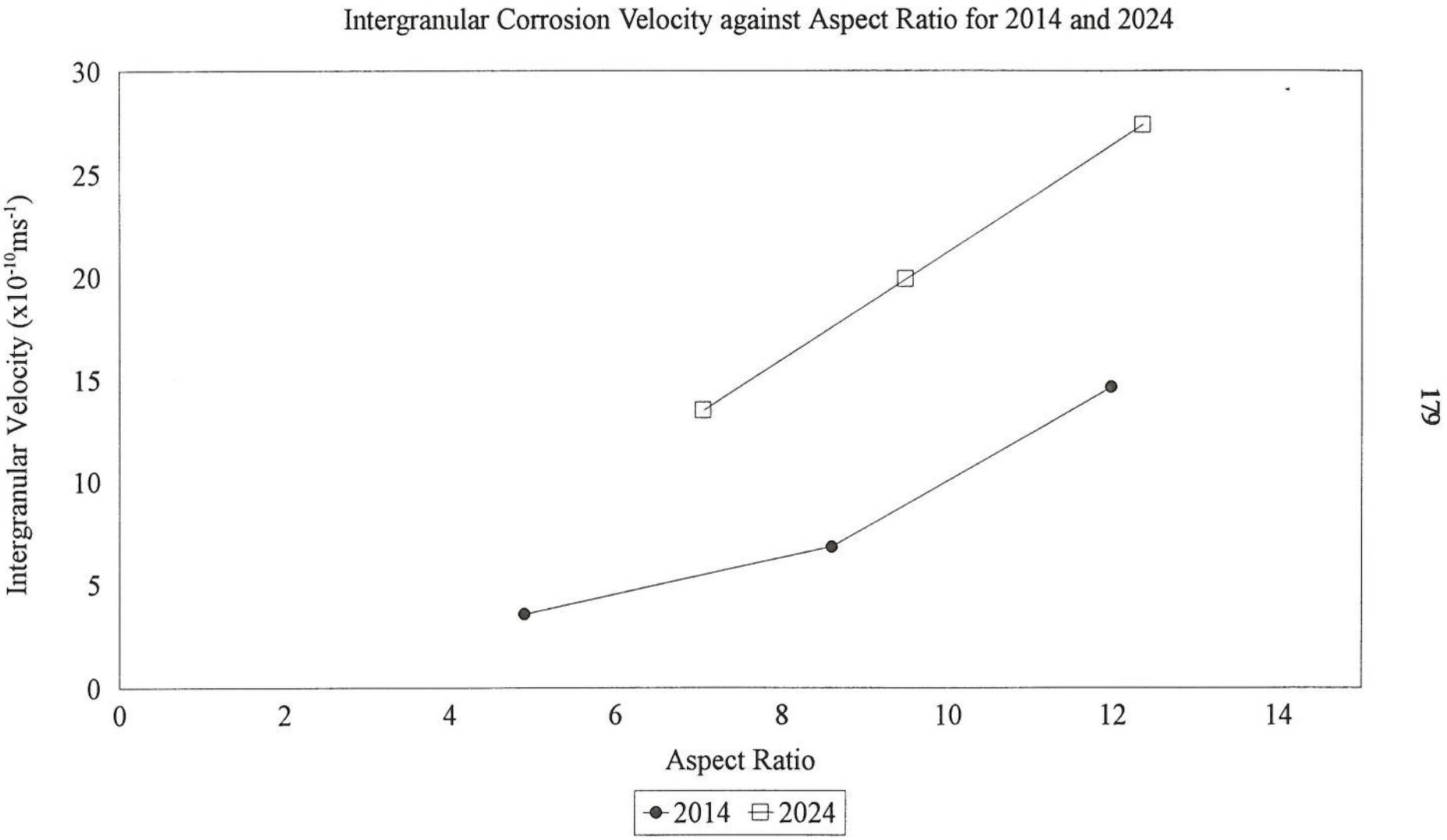

Figure 8.2. : Graph showing relationship between intergranular corrosion velocity and aspect ratio for 2014 and 2024.

to stress corrosion in the centre of the plate.

Although other research work has shown that the depth of penetration of exfoliation corrosion is unrelated to the shape of the grains (189), a greater depth of attack will occur if the grain boundaries are more susceptible to penetration which is the case between different alloys. This can be seen in this work where the depths of penetration for 2024 are larger than in 2014. It has been demonstrated that the greater depths exhibited for the 2024 alloy could be due to the intergranular pathway in which the attack proceeds. The T/2 and T/4 sections of the 2024 alloy, with the more susceptible grain boundaries, showed attack following both the longitudinal and transverse orientations. The precipitate distribution may be the same for both orientations and the attack proceeds in the two directions into the material providing greater penetration. For the depths of penetration exhibited in these sections the intergranular velocity must be high for the attack to travel a long distance around the elongated grains which was demonstrated in the end grain and MASTMAASIS testing. The length of the intergranular attack for the 2024 T/2 section was 2453μm showing that the attack had to travel a long distance around the grains. The T/4 and T/2 sections of the 2014 alloy showed attack "short - circuiting" around the transverse path of the elongated grains. In the surface sections attack proceeded longitudinally at a slower rate where the boundaries may be less susceptible to penetration and show the lowest depths of attack in both the alloys.

Even though the aluminium - lithium alloys were supplied in sheet form in order to study the effects of heat treatment there was a difference in the aspect ratios. A comparison can be made between the two alloys assuming that the grain boundary sensitivity remains constant for each heat treatment. The 2091 alloy has a ratio double that of 8090 and this was reflected in the MASTMAASIS testing which showed a greater susceptibility to exfoliation corrosion by virtue of the greater intergranular corrosion.

As the difference between the aspect ratios does not reflect the large differences in intergranular velocities for any of the sections between the two alloys, compositional effects must play an important role in determining their susceptibility. These compositional

differences give rise to differing precipitates present within the microstructure of each alloy. One prerequisite for intergranular attack is that an active path is present along the grain boundaries along which these precipitates reside. 2XXX series alloys become more susceptible to intergranular corrosion when their grain boundaries are sensitised by precipitation and attack proceeds by anodic dissolution of anodic metallurgical features adjacent to the grain boundaries. There is a potential difference between the grain bodies and grain boundaries due to these precipitates which provides the driving force for attack. The deeper penetration shown for 2024 over 2014 is due to the fact that the grain boundaries are more susceptible to attack. Precipitates which are more anodic relative to the surrounding area such as $CuMgAl_2$ present in 2024 preferentially dissolve leaving a copper depleted zone in the surrounding matrix which becomes vulnerable to attack. The higher susceptibility shown for the centre of the plate could be due to a greater distribution of precipitates present along the grain boundaries. It has already been mentioned that this may be true where slower cooling rates toward the centre provides easier formation of precipitates rendering the boundaries more susceptible.

8.1.2. The Effect of Heat Treatment

In conventional aerospace alloys the susceptibility to exfoliation corrosion can be controlled by an appropriate ageing treatment which imparts resistance to intergranular corrosion. Heat treatment affects the exfoliation corrosion susceptibility by virtue of altering the precipitation at the grain boundaries. It has been shown that the peak - aged condition for the 2024 alloy is the most susceptible to exfoliation corrosion. The under and over - aged conditions exhibited lower susceptibilities with over - ageing being the most beneficial. Peak - ageing exhibited the maximum strength and it is known (70) that the susceptibility to exfoliation corrosion and stress corrosion reaches its peak just before maximum strength and further ageing beyond peak hardness reduces the susceptibility. As ageing continues the amount of copper in solid solution diminishes leading to a lower electrochemical difference between the grains and grain boundaries reducing the susceptibility to corrosion. Precipitates at the grain boundaries that are readily attacked or dissolved such as $CuMgAl_2$ will expose fresh aluminium for reaction, and show faster

intergranular corrosion velocities for increased precipitation at the grain boundaries. The magnitude of the effect of heat treatment on exfoliation corrosion can be seen in figures 8.3 and 8.4 which represent graphs of intergranular velocity against aspect ratio for the under, peak and over - aged conditions and intergranular velocity against heat treatment respectively. These both represent the surface, T/4 and T/2 sections of the 2024 alloy. It can be seen that the velocities do not differ greatly between under and peak - aged but the over - aged condition shows a significant drop in corrosion rate for all sections through the plate. Although the aspect ratio has an effect on exfoliation corrosion, it seems that heat treatment has a greater effect showing that the grain boundary microstructure is a very important factor in the exfoliation process.

For the aluminium - lithium alloys the heat treatment also affected the susceptibility to exfoliation corrosion. For both alloys peak - ageing showed the greatest susceptibility to corrosion. In the 8090 alloy the over - aged condition showed the highest resistance and for 2091 the under - aged condition was beneficial. It has already been shown that the microstructure plays an important role for corrosion in these alloys. Buchheit et al (67) showed that the T_1 phase was an important factor in the intergranular corrosion behaviour in 2090. Intergranular corrosion occurred by virtue of dissolution of the T_1 precipitates present along the subgrain boundaries, followed by matrix dissolution due to an acidic environment being developed. Other precipitates present within the microstructure such as δ' (54) and T_2 (161) are thought to influence the intergranular corrosion in these alloys. The initiation of attack occurs at constituent particles such as the noble Al-Fe-Cu precipitate (67) present in the matrix leading to aggressive pit solutions. The precipitate spacing is smaller in the peak - aged condition which provides a more active path for intergranular corrosion to occur by virtue of an increased potential difference between the grain boundary precipitates and the matrix. For 8090 this precipitate spacing increases on over - ageing reducing the driving force for corrosion which is shown by reduced intergranular corrosion velocities. The S phase appears as heterogeneous precipitates in the under - aged condition and is known to become homogeneously distributed in the peak - aged condition (190) which increases the potential difference, and hence the susceptibility. Over - ageing results in the formation of δ at the grain boundaries and

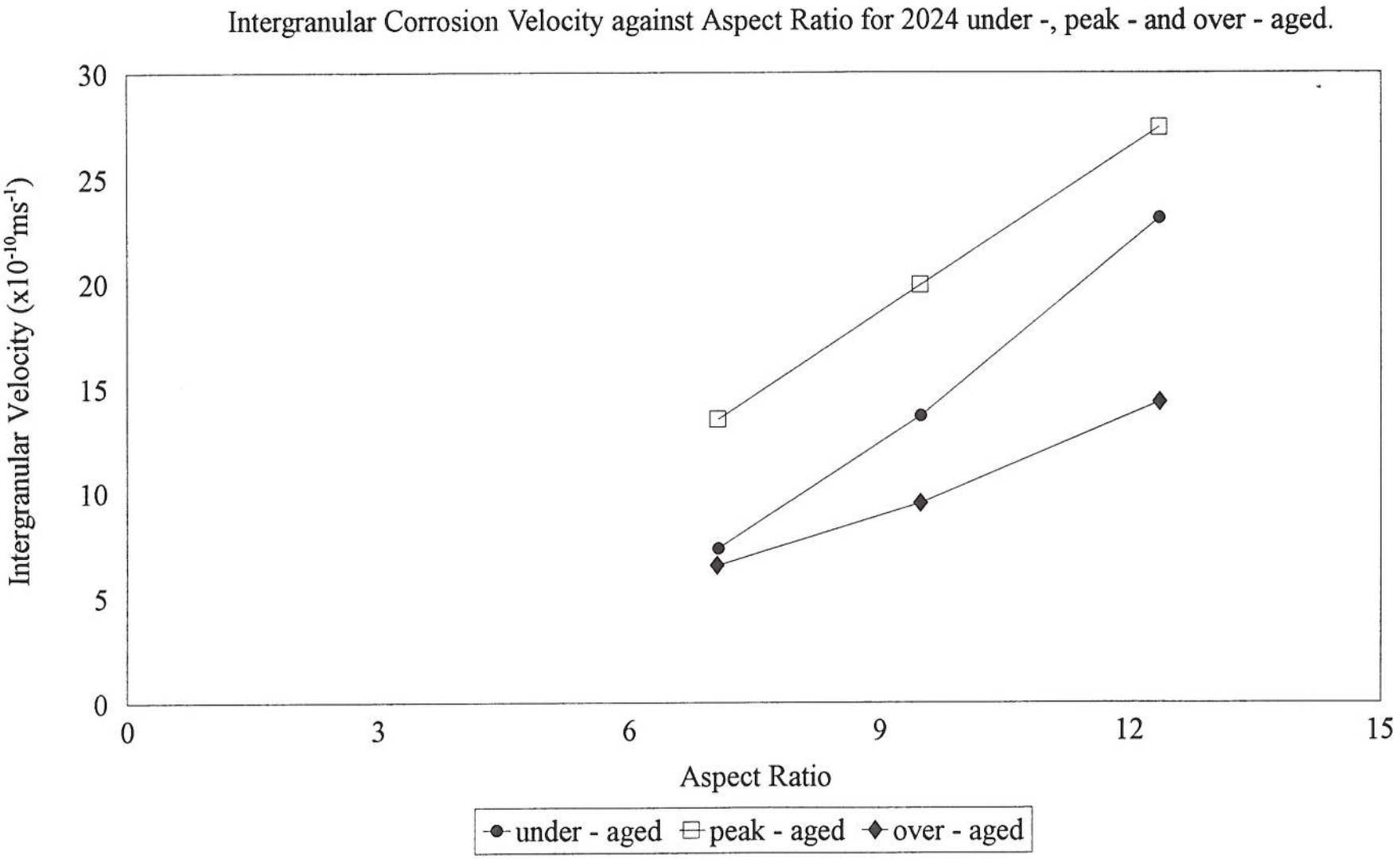

Figure 8.3. : Graph showing relationship between intergranular corrosion velocity and aspect ratio for 2024.

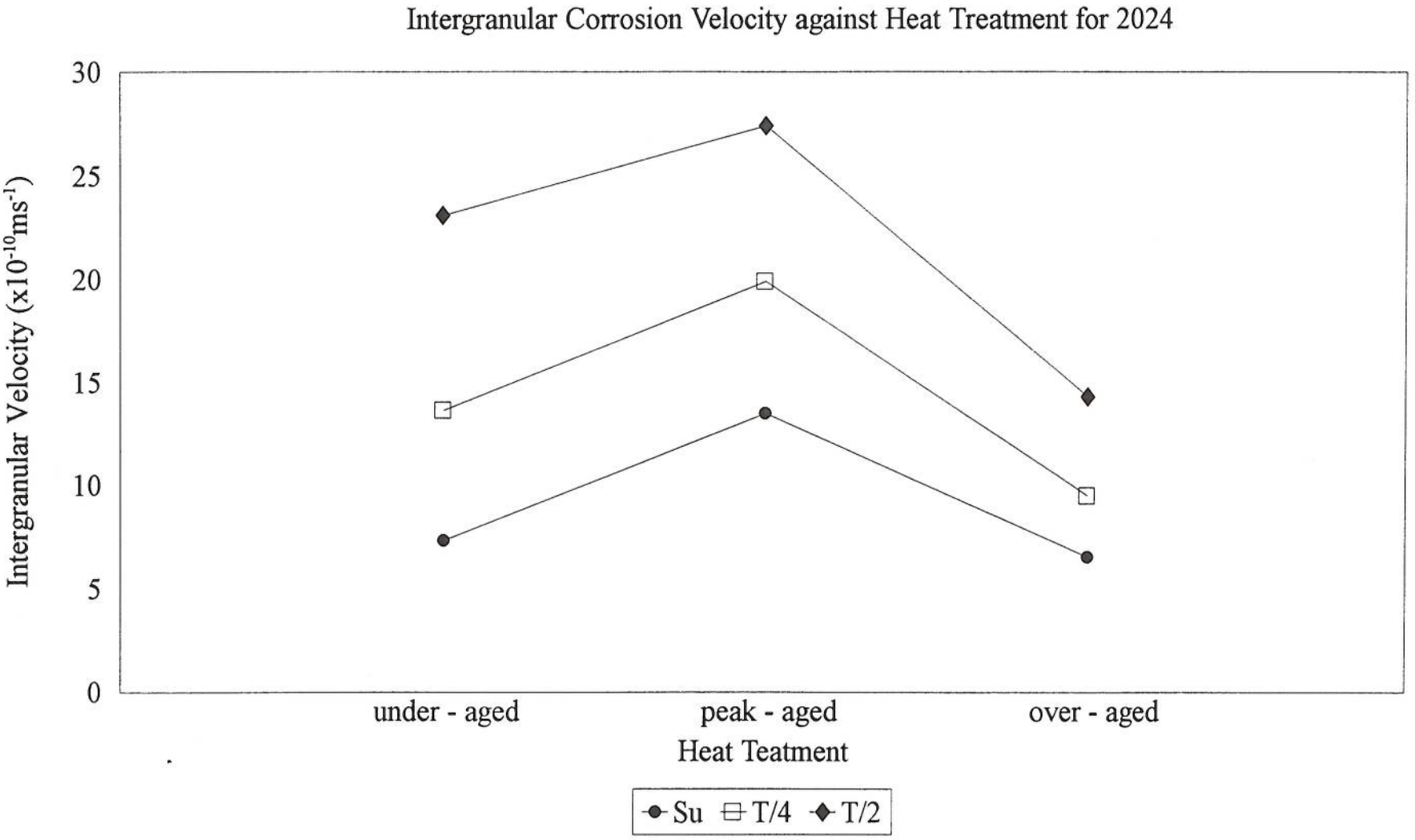

Figure 8.4. : Graph showing relationship between intergranular corrosion velocity and heat treatment for 2024

matrix which lowers the potential difference.

8.1.3. The Effect of Environment

It has been shown by the stress corrosion tests that increasing the aggressiveness of the environment increases the susceptibility. In a neutral NaCl solution no stress corrosion failures were recorded for the 2014, 2024 and 2091 alloys. Reducing the pH of the solution normally increases the susceptibility of a material to stress corrosion and exfoliation corrosion. It has been shown that the solution pH influences the corrosion behaviour by reducing the stability of the oxide film (175). At low pH values the oxide film is unstable which reduces the initiation time for attack. Susceptibility increased when the 2014 and 2024 alloys were subjected to the EXCO solution which is an aggressive environment by virtue of its low pH. The environmental conditions are different in this solution which results in larger volumes of corrosion product formed. In normal NaCl solutions the initial corrosion product, which is thought to be gelatinous $Al(OH)_3$ (46) may have formed very slowly in these tests. The duration of the test was not sufficient to promote the formation of enough corrosion product to maintain the crack tip stress intensity and induce failure. The corrosion product forms rapidly in an EXCO environment which increases the crack tip intensity at an earlier stage. This probably results in the high intergranular velocities exhibited by the 2XXX series alloys. The corrosion products which form have a volume of three times that of the original material. This exerts a force on the material and reduces the time to failure.

8.2. Mechanism of Exfoliation Corrosion

All the testing and discussion have shown that aluminium alloys are susceptible to exfoliation corrosion in differing ways. The actual mechanism for attack involves many of the above observations and can be divided as such - initiation, spread of intergranular attack, formation of blisters, rupture of these blisters to expose the underlying material to attack and the lifting of layers of material.

For aluminium - lithium alloys the presence of intermetallic particles such as $FeAl_3$ which are known to act as favourable sites for pitting corrosion (191) will tend to accelerate the initiation process and may increase the number of sites where corrosion starts. Other possible initiation sites are noble Al-Cu-Fe particles (67) and T_2 precipitates (161). In 2014 initiation starts in the precipitate free zone around the $CuAl_2$ precipitates and initiation in 2024 occurs at the $CuMgAl_2$ precipitates. The pitting attack around the $CuMgAl_2$ precipitates can be attributed to coupling between the matrix and a copper depleted region around the precipitate. In 2024 it is known that pitting initiation can be attributed to other sites such as iron rich precipitates of the type Al_3FeMn (192). From the morphologies shown in chapter four it was evident that the attack was intergranular in nature where precipitation leads to susceptible grain boundaries along which the attack proceeds. As is evident from the end grain testing the presence of "active grains" can promote deep intergranular attack in these alloys. The precipitate distribution around these grains may be higher which increases their susceptibility. The formation of the corrosion products from this intergranular attack promotes the appearance of blisters on the surface of the material. The main anodic reaction which occurs during the corrosion of aluminium is as follows:

$$Al \rightarrow Al^{3+} + 3e^-$$

The Al ions diffuse away from the anodic sites and in chloride solutions the formation of $AlCl_3$ and other transitionary forms such as $AlCl_4^-$ increase the acidity within pits. It is the formation of aluminium hydroxides which occupy the large volumes required to produce blister formation. If the blister formation is inhibited then the rate of exfoliation corrosion slows down. It was shown in the end grain testing that any constraint in the material does not really have an effect on corrosion. This was demonstrated by the fact that very deep intergranular pathways were seen which can lead to stress corrosion cracking. When the strain in the skin of the blister exceeds the fracture strain of the material then these blisters burst and localised corrosion begins on a larger scale. The underlying material is exposed to attack and corrosion initiates at new phases where the corrosion cycle starts all over again.

8.3. Summary

The 2024 alloy exhibits a greater susceptibility to exfoliation corrosion than 2014 in both laboratory, outdoor corrosion and stress corrosion testing by virtue of a greater aspect ratio and the presence of more anodic precipitates along the grain boundaries. It appears that the peak - aged condition shows the greatest susceptibility to exfoliation corrosion for all the 2024, 8090 and 2091 alloys. The under and over - aged conditions show less susceptibility than peak - ageing by virtue of differing precipitation at the boundaries. Aircraft manufacturers and operators are well aware of the problems caused by exfoliation corrosion and the fact that it is difficult to detect, and when detected it is costly to repair.

It has been shown here and in other work (46) that the laboratory testing does reproduce the exfoliation found in service albeit in a shorter period of time. Work carried out on specimens taken from an aircraft after 16 years in service (19043 flights) showed extensive pitting of the surface (193). Extensive intergranular corrosion had increased the thickness of the specimen by 10% due to the lifting of layers of material. The remaining, intact thickness of the material is reduced which impairs the load bearing capacity of the component. Twelve years of service resulted in insignificant corrosion where specimen edges were free from cracks and the specimen thickness did not increase possibly due to low amounts of corrosion product. Cracks appeared at the edges after 14 years and it was concluded that 12 years in service was a threshold in the evolution of intergranular corrosion. It may be that the corrosion exhibited on the marine specimens would relate to these times and catastrophic corrosion could become very probable after 16 years in service, should the protective coating be damaged.

Environmental effects both in the air and on the ground are important factors in the ability of a structure to withstand corrosive attack. In - service conditions can affect the corrosion rate therefore altering the lifespan of an aircraft. Ideally an aircraft should have a lifespan in excess of 20 years provided that regular inspections are made and the initial preventative treatments such as coatings to provide corrosion protection are adequate. In

dry conditions corrosion progresses very slowly. However, in conditions of a warm, wet climate with salt water nearby, light corrosion, if untreated, can become very severe in a short period of time thereby reducing the lifespan of the aircraft. The problems arise when an aircraft takes off and climbs through industrially polluted air and rain, cruises at very low temperatures and lands where the climate may be hot and humid. During these phases of flight, moisture condenses and airborne salts accumulate on the skin. These phases are simulated by the use of the MASTMAASIS test enabling the prediction of in service exfoliation. As this type of attack is insidious in nature regular inspections must be made but if any areas of attack are missed then this can lead to severe corrosion thereby reducing the load bearing capacity of the component in question. The morphology of attack produced from the MASTMAASIS test does not differ from that found in natural environments and this information can be used to predict the way exfoliation is going to develop in a specific alloy. The rate of blistering and the insidious nature of the attack will aid the inspector in detection of exfoliation damage and also provide a guideline into how much material is involved in the attack. Although the attack seen on the specimens exposed to the marine atmosphere seemed to be of moderate corrosion and the pits were deep for the time period involved, in true life materials used for aircraft are protected using various pretreatments and protective coatings which isolate the metal component from the atmosphere (194). Sometimes problems arise from the initiation of exfoliation corrosion from areas adjacent to fasteners particularly in countersink holes which expose the end grains to attack. End grain attack can occur very rapidly and depends upon the susceptibility of the grain boundaries resulting in deep penetration and the formation of large amounts of corrosion products which increase the wedging force acting on the material. Inspection methods by visual assessment may detect defects such as surface flaws or slight bulging of the skin caused by corrosion and NDT methods used on these areas would identify any intergranular attack and how deep it may be. Various repairs can then be made ranging from removal of the detected areas to the depth of the intergranular attack to the extreme case of changing the entire component.

CHAPTER NINE

9.0. CONCLUSIONS

1. The MASTMAASIS test was able to produce representative exfoliation corrosion for the 2XXX series alloys and aluminium - lithium alloys. Metallographic examination which provides depth of attack measurements and intergranular corrosion velocities gives a better indication of exfoliation corrosion than the surface ratings provided by the EXCO standard photographs.

2. The four - point bend test used to determine the effective remaining thickness of specimens subjected to the MASTMAASIS test showed that the deflection method was a useful way of determining the depth of attack.

3. The use of extreme value statistics was found to be a suitable method in determining the grain aspect ratio and demonstrated quantitatively the increase in grain elongation toward the centre of the plate in the 2XXX series alloys.

4. The severity of exfoliation corrosion was shown to be related to the grain aspect ratio in the 2XXX series alloys. It was shown that the susceptibility increased toward the mid - section of the plate material and ranked in the order T2 > T/4 > surface.

5. Differences in the microstructure between 2014 and 2024 contributed to the susceptibility to exfoliation corrosion. The Cu : Mg ratio differs in these alloys where the ratio is 9 : 1 for 2014 and 3 : 1 for 2024. 2014 has a low magnesium content where the $CuAl_2$ phase is predominant and 2024 has a higher magnesium content with the $CuMgAl_2$ phase predominant. This $CuMgAl_2$ phase is more anodic which provides a higher susceptibility to exfoliation corrosion.

6. The intergranular corrosion velocity was found to be a useful parameter for assessing the susceptibility to exfoliation corrosion. An increase in the velocity

increases the susceptibility to exfoliation corrosion. The rate of attack was shown to be greater in the mid - section of the plate and decreased in the order T/2 > T/4 > surface.

7. The rate of intergranular corrosion on the aluminium - lithium alloys was determined by their heat treatment condition and was most advanced on the peak - aged material. Under - ageing was beneficial in reducing the exfoliation susceptibility for 2091 and the over - aged condition was beneficial for 8090.

8. Outdoor corrosion testing gave the same morphology of attack as laboratory testing albeit on a smaller scale and over a longer period of time. The severity of exfoliation corrosion that the specimens exhibited in the MASTMAASIS test would equate to several years in a marine atmosphere.

9. End grain testing showed that the preferred pathway for intergranular attack in the 2XXX series alloys predominantly followed the shorter transverse path around the elongated grains.

10. The rate of intergranular corrosion was higher in stress corrosion cracking than in exfoliation corrosion. The stress corrosion susceptibility was affected by the grain shape where the susceptibility increased in the order surface < T/4 < T/2.

11. All the 2091, 2014 and 2024 alloys displayed a very high resistance to stress corrosion in a neutral NaCl solution with no failures recorded for each alloy. The times to failure were significantly reduced when testing in the more aggressive EXCO environment.

ACKNOWLEDGEMENTS

I would like to express my sincere gratitude to my supervisor, Dr. M. J. Robinson for his guidance, depth of knowledge, advice and ease of approach during the course of this work.

I would like to thank the following people for their help:-

Dr. C. J. E. Smith and Dr. B. Evans from RAE Farnborough for their support of this work and useful advice.

Mrs. T. Roberts, Mrs. C. Kimpton and Mr. C. Matthews for their assistance and advice in all the metallographic and photographic work.

Mr. R. Hardwicke for his technical help and advice.

Mr. A. Baldwin and the workshop staff for their machining of specimens and for building the four - point bend rig.

Mrs. S. Skevington for help with the diagrams.

Mr. F. Robinson for machining the stress corrosion specimens.

Staff and students from buildings 56 and 57 for their help and encouragement throughout my stay at Cranfield University.

Thanks to my parents for their encouragement and support during my time spent in education. I would also like to thank my father's secretary, Miss. A. Scott for her help with some of the typing and photocopying.

REFERENCES

1. E. J. Lavernia, B. Pogialli, I. Servi, J. Clark, F. Fatrak and N. J. Grant, Journal of Metals, Vol. 37, (11), 1985, pp. 35-38.
2. D. S. Thompson and S. A. Levy, Light Metal Age, Vol. 35, (7-8), 1977, pp. 11-15.
3. A. Perrone and O. Lotti, Aluminium Alloys in the Aircraft Industry, Proc. Symposium, Turin, Oct. 1-2 1976, pp. 21-30.
4. M. Hunt, Materials Engineering (Cleveland), Vol. 107, (8), 1990, pp. 27-30.
5. J. T. Staley, Encyclopedia of Physical Science and Technology, 2nd Edition, Vol. 1, ed. by R. E. Meyers, Academic Press, San Diego, California, 1992, pp. 591-598.
6. J. T. Staley, Canadian Aeronautics and Space Journal, Vol. 31, (1), 1985, pp. 14-29.
7. H. Y. Hunsicker, Philosophical Transactions, Series A, Vol. 282, Plate 23, 1976, pp. 359-376.
8. J. T. Staley, H. Y. Hunsicker and R. Schmidt, AIME, TMS Paper F71-7, 1971.
9. E. A. Starke, Jr., Materials Science and Engineering, Vol. 29, (2), 1977, pp. 99-115.
10. R. Woodward, Materials and Design, Vol. 10, (5), 1989, pp. 248-254.
11. E. S. Balmuth and R. Schmidt, Proc. 1st International Aluminium - Lithium Alloy Conference, eds. T. H. Sanders Jr. and E. A. Starke Jr., TMS-AIME, Stone Mountain, Georgia, May 19-21, 1980, pp. 69-88.
12. E. H. Spuhler, A. H. Knoll and J. F. Kaufman, Metal Progress, Vol. 77, (6), 1960, pp. 80-82.
13. K. K. Sankaran and N. J. Grant, as ref. 11, pp. 205-227.
14. E. A. Starke Jr. and H. G. F. Wilsdorf, Thermal Structures and Materials for High Speed Flight, Vol. 140, C. 23, pp. 113-139.
15. J. S. Ekvall, J. E. Rhodes and G. G. Wald, Design of Fatigue and Fracture Resistant Structures, ASTM STP 761, 1982, pp. 328-341.
16. T. H. Sanders Jr. and E. A. Starke Jr., Foote Prints, Vol. 44, (1), 1981, pp. 11-17.
17. R. Grimes, A. J. Cornish, A. S. Miller and M. A. Reynolds, Metals and Materials, Vol 1, (6), 1985, pp. 357-363.
18. R. C. Dorward and T. R. Pritchet, Materials and Design, Vol. 9, (2), 1988, pp. 63-69.

19. W. E. Quist, G. H. Narayanen and A. L. Wingert, Proc. 2nd International Aluminium-Lithium Alloy Conference, TMS-AIME, Warrendale, Pennsylvania, 1981, pp. 313-334.
20. H. F. De Jong, Report LR 406, Delft University of Technology, January 1984.
21. C. J. Peel, B. Evans and D. S. McDarmaid, Metals and Materials, Vol. 3, (8), 1987, pp. 449-455.
22. C. J. Peel, B. Evans and D. S. McDarmaid, Proc. 3rd International Aluminium - Lithium Alloy Conference, eds. C. Baker, P. J. Gregson, S. J. Harris and C. J. Peel, Institute of Metals, London, 1986, pp. 26-36.
23. P. E. Bretz and R. R. Sawtell, ibid, pp. 47-56.
24. P. E. Bretz, Proc. 4th International Aluminium - Lithium Alloy Conference, eds. G. Champier, B. Dubost, D. Miannay and L. Sabetay, Paris, France, Journal de Physique, No. NC3, September 1987, pp. 25-31.
25. A. Schofield, Proc. 6th International Aluminium - Lithium Alloy Conference, eds. M. Peters and P. J. Winkler, Deutsche Gesellschaft fur Metallkunde, Garmisch - Partenkirchen (FRG), 1991, pp. 1293-1298.
26. A. F. Smith, ibid, pp. 1305-1311.
27. J. R. Pickens, US Patent 5, 032, 359, July 16, 1991.
28. L. W. Loechel and E. F. Scholz, as ref. 25, pp. 1299-1305.
29. C. Suryanarayana and M. Hanumantha, Journal of Materials Science Letters, Vol. 6, (3), 1987, pp. 317-320.
30. Aluminium and its Alloys, ed. by F. King, J. Wiley and Sons, New York, 1987, pp. 92-103.
31. R. B. Nicholson, G. Thomas and J. Nutting, Journal of the Institute of Metals, Vol. 87, August, 1959, pp. 429-438.
32. M. J. Starink and P. Van Mourik, Metallurgical Transactions A, Vol. 22A, (3), 1991, pp. 665-674.
33. T. S. Srivatsan, D. Lanning Jr. and K. K. Soni, Journal of Materials Science, Vol. 28, (12), 1993, pp. 3205-3213.
34. E. P. Butler, N. J. Owen and D. J. Field, Materials Science and Technology, Vol. 1, (7), 1985, pp. 531-536.

35. J. A. Walsh, K. V. Jata and E. A. Starke Jr., Acta Metallurgica, Vol. 37, (11), 1989, pp. 2861-2871.
36. W. G. J. 't Hart, H. G. Kolkman and L. Schra, NLR Technical Report 80102U, November 1980.
37. W. A. Anderson, Precipitation from Solid Solution, ed. by R. F. Mehl, ASM, Cleveland, Ohio, 1959, pp. 150-207.
38. A. K. Jenna, A. K. Gupta and M. C. Chaturvedi, Acta Metallurgica, Vol. 37, (3), 1989, pp. 885-895.
39. V. Radmilovic, G. Thomas, G. J. Shiflet and E. A. Starke Jr., Scripta Metallurgica et Materialia, Vol. 23, (7), 1989, pp. 1141-1146.
40. Jin Yan, Li Chunzhi and Yan Minggao, Journal of Materials Science Letters, Vol. 9, 1990, pp. 421-424.
41. A. K. Gupta, P. Gaunt and M. C. Chaturvedi, Philosophical Magazine A, Vol. 55, (3), 1987, pp. 375-387.
42. Jin Yan, Journal of Materials Science Letters, Vol. 10, (10), 1991, pp. 591-593.
43. N. Sen and D. R. F. West, Journal of the Institute of Metals, Vol. 97, (3), 1969, pp. 87-92.
44. Jin Yan, Li Chunzhi, Li Chunyu and Yan Minggao, Acta Metallurgica Sinica (English Edition), Series A, Vol. 4, (4), 1991, pp. 225-230.
45. S. Singh and D. B. Goel, Journal of Materials Science, Vol. 25, (9), 1990, pp. 3894-3900.
46. L. S. Anwar, Exfoliation Corrosion of AlCuMg Alloys, Ph.D. Thesis, Cranfield University, 1982.
47. R. K. Wyss and R. E. Sanders Jr., Metallurgical Transactions A, Vol. 19A, (10), 1988, pp. 2523-2530.
48. R. N. Wilson, Journal of the Institute of Metals, Vol. 97, (3), 1969, pp. 80-86.
49. M. C. Chaturvedi, A. K. Gupta and A. K. Jena, Materials Science and Engineering, Vol. A110, 1989, pp. 187-192.
50. H. M. Flower, Proc. Conference on High Performance Materials, "Hipermat 89", City Conference Centre, London, September 27-28 1989, pp. 173-192.

51. M. J. Kaufman, A. A. Morrone and R. E. Lewis, Scripta Metallurgica et Materialia, Vol. 27, (9), 1992, pp. 1265-1270.
52. E. A. Starke Jr., Proc. 15th Congress on the International Council of the Aeronautical Sciences, Vol. 2, London, September 7-12 1986, pp. 934-943.
53. J. M. Silcock, Journal of the Institute of Metals, Vol. 88, 1959-1960, pp. 357-364.
54. P. Niskanen, T. H. Sanders Jr., J. G. Rinker and M. Marek, Corrosion Science, Vol. 22, (4), 1982, pp. 283-304.
55. D. B. Williams, R. Levi-Setti, J. M. Chabala, Y. L. Wang, D. E. Newbory and K. K. Soni, Proc. 5th International Aluminium - Lithium Alloy Conference, eds. T. H. Sanders, Jr. and E. A. Starke, Jr., Williamsburg, Virginia, March 1989, p. 605.
56. D. B. Williams, as ref. 11, pp. 89-100.
57. T. H. Sanders Jr., as ref. 11, pp. 63-67.
58. J. Lendvai and H. J. Gundludt, Zeitschrift fur Metallkunde, Vol. 84, (4), 1993, pp. 242-247.
59. E. A. Starke Jr. and G. Lutgering, Fatigue and Microstructure, ed. by M. Meshii, ASM, Metals Park, Ohio, 1979, pp. 205-240.
60. T. H. Sanders Jr. and E. A. Starke Jr., as ref. 55, pp. 1-37.
61. K. Dinsdale, S. Harris and B. Noble, as ref. 11, pp. 101-118.
62. M. J. Birt, R. A. Hafley, J. A. Wagner and W. B. Lisagor, Scripta Metallurgica and Materialia, Vol. 28, 1993, pp. 919-923.
63. D. M. J. Wilkes, Y. Li and H. Jones, Material Science and Engineering, Vol. A179/A180, 1994, pp. 681-687.
64. E. J. Lavernia and N. J. Grant, Journal of Materials Science, Vol. 22, 1987, pp. 1521-1529.
65. P. S. Pao, K. K. Sankaran and J. E. O'Neal, as ref. 11, pp. 307-323.
66. M. H. Tosten, A. K. Vasudevan and P. R. Howell, Metallurgical Transactions A, Vol. 19A, (1), 1988, pp. 51-66.
67. R. G. Buchheit, J. P. Moran and G. E. Stoner, Corrosion, Vol. 46, (8), 1990, pp. 610-617.
68. N. J. Kim, Materials Science and Engineering, Vol. A158, 1992, pp. 103-110.

69. B. P. Gu, G. L. Liedl, T. H. Sanders Jr. and K. Welpmann, Materials Science and Engineering, Vol. 76, 1985, pp. 147-157.
70. M. O. Spiedel, Metallurgical Transactions A, Vol. 6A, (4), 1975, pp. 631-651.
71. H. L. Logan, Journal of Research of the National Bureau of Standards, Vol. 48, (2), 1952, pp. 98-105.
72. M. S. Hunter, G. R. Frank and D. L. Robinson, Proc. of the 2nd International Congress on Metallic Corrosion, Houston, Texas, NACE, 1963, pp. 102-108.
73. W. Gruhl, Zeitschrift fur Metallkunde, Vol. 75, (11), 1984, pp. 819-826.
74. G. Wenzel, G. Knornschild and H. Kaesche, Werkstoffe und Korrosion, Vol. 42, (9) 1991, pp. 449-454.
75. K. Sugimoto, K. Hoshino, M. Kageyama, S. Kageyama and Y. Sawada, Corrosion Science, Vol. 15, 1975, pp. 709-720.
76. K. Urushino and K. Sugimoto, Corrosion Science, Vol. 19, 1979, pp. 225-236.
77. J. G. Rinker, M. Marek and T. H. Sanders Jr., Materials Science and Engineering, Vol. 75, 1984, pp. 203-221.
78. A. Buis and J. Schijve, Corrosion, Vol. 48, (11), 1992, pp. 898-909.
79. J. B. Lumsden and A. T. Allen, Corrosion, Vol. 44, (8), 1988, pp. 527-532.
80. G. Disson, M. Reboul and C. Fiaud, as ref. 55, pp. 1261-1269.
81. T. D. Burleigh, Corrosion, Vol. 47, (2), 1991, pp. 89-98.
82. R. J. Gest and A. R. Troiano, Corrosion, Vol. 30, (8), 1974, pp. 274-279.
83. Jin Yan, Li Chunzhi, Ru Jigang and Yan Minngao, Materials Letters, Vol. 12, (5), 1991, pp. 376-380.
84. G. H. Koch, Corrosion, Vol. 35, (2), 1979, pp. 73-79.
85. Wu-Yang Chu, Yan-Bin Wang and Chi-Mei Hsiao, Corrosion, Vol. 38, (11), 1982, pp. 561-570.
86. M. Baumgartner and H. Kaesche, Corrosion, Vol. 44, (4), 1988, pp. 231-239.
87. Hong-Pyo Kim, Rak-Hyun Song and Su-Il Pyun, British Corrosion Journal, Vol. 23, (4), 1988, pp. 254-258.
88. J. Chene, I. M. Bernstein and A. W. Thompson, Metallurgical Transactions A, Vol. 21A, (2), 1990, pp. 455-464.

89. R. Balasubramaniam, D. J. Duquette and K. Rajan, Acta Metallurgica, Vol. 39, (11), 1991, pp. 2597-2605.

90. F. Zeides and I. Roman, Materials Science and Engineering, Vol. A125, 1990, pp. 21-30.

91. E. N. Pugh, Corrosion, Vol. 41, (9), 1985, pp. 517-526.

92. A. Turnbull, British Corrosion Journal, Vol. 27, (4), 1992, pp. 271-289.

93. G. M. Ugiansky, L. P. Spolnick and S. W. Steifel, Corrosion, Vol. 25, (2), 1969, pp. 77-86.

94. D. O. Sprowls and R. H. Brown, Proc. Conference on Fundamental Aspects of Stress Corrosion Cracking, eds. R. W. Staehle, A. J. Forty and D. Van Rooyen, NACE, 1969, pp. 466-506.

95. M. O. Speidel, The Theory of Stress Corrosion Cracking in Alloys, NATO Science Committee Research Evaluation Conference, ed. by J. C. Scully, NATO, 1971, pp. 291-344.

96. J. Blain, J. Masounave and J. I. Dickson, Corrosion Science, Vol. 24, 1, 1984, pp. 1-12.

97. R. C. Dorward, K. R. Hasse and W. J. Helfrich, Journal of Testing and Evaluation, Vol. 6, (4), July 1978, pp. 268-275.

98. M. S. Kang-Wan Lee and S. L. Pyun, Metall., Vol. 36, (3), 1982, pp. 280-283.

99. S. Maitra, Corrosion, Vol. 37, (2), 1981, pp. 98-103.

100. N. J. H. Holroyd, A. Gray, G. M. Scamans and R. Hermann, as ref. 22, pp. 310-320.

101. R. Braun, Werkstoffe und Korrosion, Vol. 43, (9), 1992, pp. 453-458.

102. R. Braun, Werkstoffe und Korrosion, Vol. 40, (11), 1989, pp. 661-668.

103. R. Braun, as ref. 25, pp. 697-702.

104. D. Kelly and M. J. Robinson, Corrosion, Vol. 49, (10), 1993, pp. 787-795.

105. S. Maitra, Corrosion, Vol. 37, (3), 1981, pp. 125-131.

106. D. A. Hardwick, A. W. Thompson and I. M. Bernstein, Metallurgical Transactions A, Vol. 14A, (12), 1983, pp. 2517-2526.

107. E. I. Meletis and Weiji Huang, Materials Science and Engineering, Vol. A148, 1991, pp. 197-209.

108. G. Hongbin and L. Reshun, Scripta Metallurgica et Materialia, Vol. 31, (10), 1994, pp. 1431-1436.

109. K. Moore, T. J. Langan, F. H. Heubaum and J. R. Pickens, as ref. 55, pp. 1281-1291.

110. B. Sarkar, M. Marek and E. A. Starke Jr., Metallurgical Transactions A, Vol. 12A, (11), 1981, pp. 1939-1943.

111. C. Zailiang, Q. Yourong and X. Shuyi, Proc. 10th International Congress on Metallic Corrosion, Vol. 3, Sessions 10-13, November 7-11 1987, pp. 2081-2087.

112. R. C. Dorward and K. R. Hasse, Corrosion, Vol. 44, (12), 1988, pp. 932-941.

113. A. Gray, as ref. 24, pp. 891-904.

114. W. Zhengfu, Z. Ziyong, K. Wei, Z. Yun and H. Zhuangqi, Acta Metallurgica Sinica (English Edition), Series B, Vol. 5B, (5), 1992, pp. 391-395.

115. F. G. Lewis, Report AARC ACA-65, Australian Aeronautical Research Committee, July 1965.

116. M. L. Baucio, Corrosion in the Aircraft Industry, Metals Handbook, 9th Edition, Corrosion, Vol. 13, ASM, Metals Park, Ohio, 1987, pp. 1019-1055.

117. W. A. Bell and H. S. Campbell, Journal of the Institute of Metals, Vol. 89, 1960 - 1961, pp. 464-471.

118. J. V. Rinnovatore, K. F. Lukens and J. D. Corrie, Corrosion, Vol. 29, (9), 1973, pp. 364-372.

119. B. W. Lifka, D. O. Sprowls and J. G. Kaufman, Corrosion SB11A, Vol. 23, (11), 1967, pp. 335-342.

120. D. P. Lahiri and A. V. Reddy, Transactions of the Indian Institute of Metals, Vol. 35, (5), 1982, pp. 456-460.

121. D. R. Klang and W. L. Peters, Materials Protection, Vol. 3, (4), 1964, pp. 16-24.

122. S. J. Ketcham and E. J. Jankowsky, Laboratory Corrosion Tests and Standards, ASTM STP 866, eds. G. S. Haynes and R. Baboian, ASTM, Philadelphia, !985, pp. 14-23.

123. S. J. Ketcham and I. S. Schaffer, Localised Corrosion - Causes of Metal Failure, ASTM STP 516, ASTM, 1972, pp. 3-16.

124. R. G. Mitchell, Industrial Corrosion, 1983, Vol. 1, (5), pp. 11-17.

125. Z. D. Liang, Corrosion, Vol. 48, (6), 1992, pp. 514-517.

126. C. B. Ward and B. Cohen, Light Metal Age, Feb 1966, pp. 16-19.

127. R. N. Miller, Materials Protection, MAPRA, Vol. 16, (2), 1967, pp. 55-58.

128. T. A. Morad, MSc Thesis, Effect of Environment and Surface Conditions on Fatigue Crack Initiation in an Aluminium Alloy, Cranfield, 1980.

129. Tair I. Wu and Jiann Kuo. Wu, Scripta Metallurgica et Materialia, Vol. 27, (7), 1992, pp. 875-880.

130. J. A. Capp, Rational Test for Metallic Protective Coatings, Proc. ASTM, 14, V2, 1914, p. 474.

131. E. A. G. Liddiard, J. A. Whittaker and H. K. Farmery, Journal of the Institute of Metals, Vol. 89, 1960-1961, pp. 377-384.

132. B. W. Lifka and D. O. Sprowls, Corrosion, Vol. 22, (1), 1966, pp. 7-15.

133. R. C. Spooner, Plating, Vol. 56, (9), 1969, pp. 1047-1048.

134. H. B. Romans, Materials Protection and Standards, Vol. 9, (11), 1969, pp. 31-34.

135. S. J. Ketcham and P. W. Jeffrey, Localised Corrosion - Cause of Metal Failure, ASTM STP 516, ASTM, 1972, pp. 273-302.

136. J. J. Thompson, New Methods for Corrosion Testing of Aluminium Alloys, ASTM STP 1134, ASTM, 1992, pp. 70-81.

137. M. J. Parzuchowski, E. J. Tuegel and K. K. Sankaran, as ref. 25, pp. 777-782.

138. D. O. Sprowls, J. D. Walsh and M. B. Shumaker, Localised Corrosion - Cause of Metal Failure, ASTM STP 516, ASTM, 1972, pp. 38-65.

139. S. Lee and B. W. Lifka, New Methods for Corrosion Testing of Aluminium Alloys, ASTM STP 1134, 1992, pp. 1-19.

140. E. L. Colvin and S. J. Murtha, as ref. 55, pp. 1251-1260.

141. A. Gray, C. J. Newton and M. Alexander, as ref. 25, pp. 691-696.

142. R. L. Horst and B. W. Lifka, Corrosion, Vol. 26, (3), 1970, pp. 111-117.

143. J. De Damborenea and I. Martin, Progress in the Understanding and Prevention of Corrosion, Vol. 2, eds. J. M. Costa and A. D. Mercer, Published by the Institute of Materials, University Press, Cambridge, 1993, pp. 061-967.

144. P. R. Roberge, E. Halliop, D. R. Lenard and J. G. Moores, 3rd Int. SAMPE Metals Conference, October 20-22 , 1992, pp. 51-64.

145. V. E. Carter, Metal Corrosion in the Atmosphere, ASTM STP 435, ASTM, 1968, pp. 257-270.

146. F. L. McGeary, T. J. Summerson and W. H. Ailor, Jr., ASTM STP 435, ASTM, pp. 141-174.

147. S. P. Jones, Stress Corrosion and Exfoliation of High Strength Aluminium Alloys, Ph.D. Thesis, Cranfield University, 1989.

148. W. H. Ailor, Corrosion in Natural Environments, ASTM STP 558, ASTM, 1974, pp. 117-134.

149. T. J. Summerson and D. O. Sprowls, Aluminium Alloys - Physical and Mechanical Properties, Vol. 3, eds. E. A. Starke, Jr. and T. H. Sanders, Jr., University of Virginia, Charlottsville, Virginia, June 15-20, 1986, pp. 1575-1661.

150. M. S. Hunter, G. R. Frank, Jr. and D. L. Robinson, Proc. 2nd International Congress on Metallic Corrosion, NACE, 1963, pp. 102-108.

151. J. R. Galvele and S. M. De Micheli, Corrosion Science, Vol. 10, 1970, pp. 795-807.

152. I. L. Muller and J. R. Galvele, Corrosion Science, Vol. 17, 1977, pp. 179-193.

153. S. Maitra and G. C. English, Metallurgical Transactions, Vol. 12A, (3), 1981, pp. 535-541.

154. E. Mattson, L. O. Gullman, L. Knutsson, R. Sundbery and B. Thundal, British Corrosion Journal, Vol. 6, (3), 1978, pp. 73-83.

155. M. C. Reboul and J. Bouvaist, Werkstoffe und Korrosion, Vol. 30, 1979, pp. 700-712.

156. J. Onoro and C. Ranninger, British Corrosion Journal, Vol. 28, (2), 1993, pp. 137-141.

157. M. Reboul and P. Meyer, as ref. 24, pp. 881-889.

158. P. Niskanen, T. H. Sanders, Jr., M. Marek and J. G. Rinker, as ref. 11, pp. 347-376.

159. J. K. Gregory, P. J. Meschter and J. E. O'Neal, as ref. 149, pp. 1227-1231.

160. R. G. Buchheit and G. E. Stoner, as ref. 55, pp. 1347-1356.

161. Zhang Yun, Lui Yulin, Zhao Hongen, Hu Zhuangqi, Zhu Zhiyong and Wand Zhenfu, Acta Metallurgica Sinica, Vol. 5B, (1), pp.53-59.

162. M. J. Robinson, Corrosion Science, Vol. 23, (8), 1983, pp. 886-899.

163. E. A. G. Liddiard and J. A. Whittaker, Journal of the Institute of Metals, Vol. 89, 1960-1961, pp. 423-428.

164. M. J. Robinson, Corrosion Science, Vol. 22, (8), 1982, pp. 775-790.

165. T. Sheppard and N. C. Parson, Materials Science and Technology, Vol. 3, (5), 1987, pp. 345-352.

166. J. P. Moran, E. A. Starke, Jr., G. E. Stoner and G. L. Cahen, Jr., Corrosion, Vol. 43, (6), 1987, pp. 374-382.

167. Z. Ahmad and A. Aleem, Journal of Materials Engineering and Performance, Vol. 2, (5), 1993, pp. 739-744.

168. B. W. Lifka and D. O. Sprowls, Localised Corrosion - Cause of Metal Failure, ASTM STP 516, ASTM, 1972, pp. 120-144.

169. S. Ohsaki, T. Sato and T. Takahashi, Aluminium, Vol. 66, (6), 1990, pp. 569-572.

170. S. Ramu, Bulletin of Electrochemistry, Vol. 4, (1), 1988, pp. 7-10.

171. P. L. Lane, J. A. Gray and C. J. E. Smith, RAE TR 85092, 1985.

172. S. Maitra and G. C. English, Metallurgical Transactions, Vol. 13A, (1), 1982, pp. 161-166.

173. J. F. McIntyre and T. S. Dow, Corrosion, Vol. 48, (4), 1992, pp. 309-319.

174. R. Ambat and E. S. Dwarakadasa, British Corrosion Journal, Vol. 28, (2), 1993, pp. 142-148.

175. R. Ambat and E. S. Dwarakadasa, Journal of Applied Electrochemistry, Vol. 24, (9), 1994, pp. 911-916.

176. T. S. Srivatsan, G. E. Bobeck, T. S. Sudarshan and P. A. Molian, as ref. 55, pp. 1237-1249.

177. P. J. Sereda, Corrosion in Natural Environments, ASTM STP 558, ASTM, 1974, pp. 7-22.

178. S. W. Dean and W. H. Anthony, Degradation of Materials in the Atmosphere, ASTM STP 965, ASTM, 1988, pp. 191-205.

179. T. Shibata, Journal of Research of the National Institute of Standards and Technology, Vol. 99, (4), 1994, pp. 327-336.

180. K. Welpmann, H. Buhl, R. Braun and M. Peters, as ref. 24, pp. 677-683.

181. D. J. Kelly, Exfoliation and Stress Corrosion Cracking of the Aluminium Alloy 8090, Ph.D. Thesis, Cranfield, 1991.

182. L. Schra, W. G. J. t' Hart and J. A. M. Boogers, National Aerospace Laboratory, Amsterdam, NLR TP 90272 U, August 1991.

183. P. L. Lane, J. A. Gray and C. J. E. Smith, as ref 22, pp. 273-281.

184. V. E. Carter and H. S. Campbell, Metal Corrosion in the Atmosphere, ASTM STP 435, ASTM, 1968, pp. 39-42.

185. S. Marsac, G. Mankowski and F. Dabosi, British Corrosion Journal, Vol. 27, (1), 1992, pp. 50-58.

186. J. P. Moran and G. E. Stoner, as ref. 55, pp. 1187-1196.

187. H. F. De Jong and J. W. G. Berkelaar, Report LR 433, Delft University of Technology, April 1984.

188. R. Braun, Werkstoffe und Korrosion, Vol. 44, 1993, pp. 73-82.

189. L. S. Anwar, Msc Thesis, Exfoliation Corrosion of Aluminium Alloys, Cranfield, 1979.

190. H. M. Flower and P. J. Gregson, Materials Science and Technology, Vol. 3, (2), 1987, pp. 81-89.

191. G. A. W. Murray, H. J. Lamb and H. P. Goddard, British Corrosion Journal, Vol. 2, 1967, pp. 216-218.

192. T. J. Warner, M. P. Schmidt, F. Sommer and D. Bellot, Zeitschrift fur Metallkunde, Vol. 86, (7), 1995, pp. 494-501.

193. V. Y. Vasilev, A. G. Kukolkin, V. Y. Bayankin, M. S. Gromov and V. A. Volkov, Protection of Metals, Vol. 31, (1), 1995, pp. 11-14.

194. C. J. E Smith, UK Corrosion, Manchester, 13 - 15 October 1992, Vol. 3, pp. 1-9.

APPENDIX ONE

The American Association Designation for Aluminium Alloys

Alloy Designation

Aluminium alloys groups are normally identified by a four digit numerical system. There are several groups with differing alloying elements and are outlined below:

Series	Major Alloying Element
1XXX	None
2XXX	Copper
3XXX	Manganese
4XXX	Silicon
5XXX	Magnesium
6XXX	Magnesium - silicon
7XXX	Zinc
8XXX	Other than above

The 1XXX series are based on 99% aluminium or greater where the last two digits represent the minimum aluminium percentage and the second digit represents modification to the impurity level. For the 2XXX to 8XXX series the last two digits distinguish between alloys in the group and the second digit represents modifications to the alloy. There are several temper designations for aluminium alloys of which the basic tempers are outlined below.

Temper	Description
F	As fabricated : applies to wrought products that gain some temper from shaping processes where no special control is used over thermal conditions or strain hardening. For wrought products there are no mechanical property limits.

Temper	Description
O	Annealed : applies to wrought products that are annealed to obtain the lowest strength temper.
H	Strain hardened : applies to wrought products where strain hardening increases the strength.
W	Solution heat treated : an unstable temper applicable only to alloys that spontaneously age at room temperature. This designation is specified only when the period of natural - ageing is indicated.
T	Thermally treated to produce stable tempers. Applies to wrought products that are heat treated with or without supplementary cold working. The T temper is normally followed by one or more digits where the numerals 1 to 10 indicate specific sequences of treatment. There are several subdivisions of the basic T temper.

Symbol	Description
T1	Cooled from high temperature processing and naturally - aged to a substantially stable condition.
T2	Cooled from high temperature processing, cold worked and naturally - aged to a substantially stable condition. Improves ductility and increases dimensional stability of casting.
T3	Solution heat treated, cold worked and naturally - aged to a substantially stable condition. Applies to products that are cold worked to improve strength.
T4	Solution heat treated and naturally - aged to a substantially stable condition. Applies to products that are not cold worked after heat treatment.
T5	Artificial ageing - applies to products that are artificially aged after high temperature processing to improve strength.

Symbol	Description
T6	Solution heat treated and artificially aged. Applies to products that are not cold worked after solution heat treatment, or in which the effect of cold work in flattening or straightening may not be recognised in mechanical property limits.
T7	Solution heat treated and over - aged. Applies to products that are solution heat treated and artificially aged beyond the condition of maximum strength providing properties such as improved corrosion resistance.
T8	Solution heat treated, cold worked and then artificially aged. Applies to products that are cold worked to improve strength.
T9	Solution heat treated, artificially aged and then cold worked.
T10	Cooled from high temperature processing, cold worked and then artificially aged.

Variations in heat treatment on the above temper designations are indicated by additional digits. The following designations are assigned to stress - relieved tempers of wrought products:

Symbol	Description
T-51	Stress relieved by stretching. Applies directly to plate and rolled or cold finished rod or bar. Plate is normally stretched 0.5 - 3% and rod, bar and other shapes 1 - 3%. These products have no further straightening after stretching.
T-510	Products that receive no further straightening after stretching.
T-511	Products that receive minor straightening after stretching to meet standard tolerance specifications.
T-52	Stress relieved by compression.
T-53	Stress relieved by thermal treatment.
T-54	Stress relieved by a combination of stretching and compression.

The following temper designations are assigned to some wrought aluminium products that are heat treated:

Symbol	Description
T42	Solution heat treated.
T62	Solution heat treated and artificially aged.

Use of the W temper designation

Symbol	Description
W	This is an unstable temper where spontaneous ageing occurs at room temperature.
W51	Solution heat treated and controlled stretching.
W52	Solution heat treated and stress relieved by compression.
W53	Solution heat treated and stress relieved by stretching and compression.

APPENDIX TWO

BRITISH STANDARD : AEROSPACE SERIES 2L.93 (2014)

This standard sets out the specification for plate of aluminium - copper - magnesium - silicon - manganese alloy (solution heat treated, controlled stretched and precipitation treated). It covers plate, including that which has been forged at an intermediate operation, which is finished by hot or cold rolling.

Chemical Composition

The composition of the material is shown in table 2.1 where the specific limits of alloying elements are given.

Table 2.1. : Chemical Composition Limits for 2L.93

Element	Percentage	
	Minimum	Maximum
Copper	3.9	5.0
Magnesium	0.2	0.8
Silicon	0.5	0.9
Iron	-	0.5
Manganese	0.4	1.2
Nickel	-	0.2
Zinc	-	0.2
Lead	-	0.05
Tin	-	0.05
Titanium plus Zirconium	-	0.2
Chromium	-	0.1
Aluminium	-	bal.

Condition

The material is supplied solution heat treated, controlled stretched to a permanent extension of not less than 1.5% nor more than 2.5% and precipitation treated.

Heat Treatment

The material shall be heat treated as follows:

1. Solution treat by heating at a temperature of $505\pm5^{0}C$ and quenching in water at a temperature not exceeding $40^{0}C$.
2. Precipitation treat by heating uniformly for the requisite period at a temperature between $160^{0}C$ and $190^{0}C$.

The following temperatures and times given in table 2.2 have been found appropriate.

Table 2.2. : Heat Treatments for 2L.93

Temperature (^{0}C)	Time (hours)
165	12 to 18
175	9 to 12
185	3 to 6

Mechanical Properties

The mechanical properties obtained from test pieces selected and prepared in accordance with the relevant requirements of British Standard L.100 shall be no less than those seen in table 2.3.

Table 2.3. : Minimum Mechanical Property Requirements for 2L.93

Nominal Thickness (mm)		Direction	0.2% Proof Stress (N/mm2)	Tensile Strength (N/mm2)	Elongation on Gauge Length of	
Over	Up to and Including				50 mm %	5.65 $\sqrt{S_o}$ %
6	12.5	LT	410	460	7	–
12.5	25	LT	410	460	–	6
25	40	L	410	450	–	6
		LT	400	450	–	5
		ST	360	420	–	2.5
40	63	L	400	430	–	6
		LT	390	430	–	5
		ST	360	420	–	2.5
63	90	L	400	430	–	6
		LT	390	430	–	4
		ST	360	420	–	2.5
90	115	L	380	430	–	6
		LT	370	420	–	4
		ST	340	410	–	2.5
115	140	L	360	420	–	6
		LT	350	410	–	4
		ST	340	400	–	2.5

BRITISH STANDARD : AEROSPACE SERIES 2L.97 (2024)

This standard sets out the specification for plate of aluminium - copper - magnesium - manganese alloy (solution treated, controlled stretched and aged at room temperature). It covers plate, including that which has been forged as an intermediate operation which is finished by hot or cold rolling.

Chemical Composition

The composition of the material is shown in table 2.4 where the specific limits of the alloying elements are given.

Table 2.4. : Chemical Composition Limits for 2L.97

Element	Percentage	
	Minimum	Maximum
Copper	3.8	4.9
Magnesium	1.2	1.8
Silicon	-	0.5
Iron	-	0.5
Manganese	0.3	0.9
Nickel	-	0.05
Zinc	-	0.2
Lead	-	0.05
Tin	-	0.05
Titanium plus Zirconium	-	0.2
Chromium	-	0.1
Aluminium	-	bal.

Condition

The material shall be supplied solution treated, controlled stretched to a permanent extension of not less than 1.5% nor more than 2.5% and aged at room temperature.

Heat Treatment

1. Solution treated by heating at a temperature of $495\pm5^{0}C$ and quenched in water at a temperature not exceeding $40^{0}C$.
2. Age at room temperature for no less than 48 hours.

Mechanical Properties

The mechanical properties obtained from test pieces selected and prepared in accordance with the relevant requirements of British Standard L.100 shall be no less than those seen in table 2.5.

Table 2.5. : Minimum Mechanical Property Requirements for 2L.97

Nominal Thickness (mm)		Direction	0.2% Proof Stress (N/mm2)	Tensile Strength (N/mm2)	Elongation on Gauge Length of	
Over	Up to and Including				50 mm %	5.65 $\sqrt{S_O}$ %
6	12.5	LT	280	430	10	–
12.5	25	LT	280	430	–	10
25	40	L	310	430	–	12
		LT	280	420	–	9
		ST	260	380	–	3.5
40	63	L	310	430	–	10
		LT	270	410	–	9
		ST	260	380	–	3.5
63	90	L	310	430	–	10
		LT	270	410	–	8
		ST	260	370	–	3.5
90	115	L	310	430	–	10
		LT	270	400	–	8
		ST	245	370	–	3.5
115	140	L	310	410	–	8
		LT	260	390	–	7
		ST	245	370	–	3.5

APPENDIX THREE

DETERMINATION OF GRAIN ASPECT RATIOS USING EXTREME VALUE STATISTICS

The grain aspect ratios for the 2014, 2024, 8090 and 2091 alloys were determined by the use of extreme value statistics. If all the grains in the material were the same size and shape then a metallographic section would display not a single grain size but an apparent distribution of sizes. This is due to the fact that only a small proportion of grains would be sectioned through the centre, revealing their true dimensions (grain length and width). The values of the length and width approximates to a normal distribution which gives a characteristic bell shaped curve and the true dimensions would be found at the upper tail end of the curve. The extreme value model has a cumulative distribution function given by:

$$F_{(I\,MAX)} = (X_e, ; \mu_e ; \sigma_e) = \exp [-\exp (- (X_e - \mu_e) / \sigma_e)]$$

Where X_e = an extreme value of grain size (length or width)

μ_e = location parameter

σ_e = scale parameter (standard deviation)

A plot of X_e against $-\ln(-\ln F_{(IMAX)})$ will give a straight line of gradient, $1/\sigma_e$ and intercept, μ_e/σ_e, where μ_e gives the most probable extreme value. $F_{(IMAX)}$ is the cumulative distribution function of the extreme values and is obtained by ranking the grain measurements in decreasing order and calculating R/(n+1) where R is the rank number and n is the total number of extreme values.

An example of the measured lengths and widths can be seen in table 3.1 which represents the grain sizes for the 2014 T/2 longitudinal section with the corresponding

$F_{(IMAX)}$ and $-\ln(-\ln F_{(IMAX)})$ values. Here 160 measurements were taken for each specimen, and the top 10% was taken for analysis. In this case the n+1 value is 17.

Table 3.1. : Top 10% of Measured Lengths and Widths for 2014 T/2 Longitudinal

Length (μm)	Width (μm)	Rank	$F_{(IMAX)}$	$-\ln(-\ln F_{(IMAX)})$
455	40	16	0.941	2.803
453	37	15	0.882	2.078
453	34	14	0.824	1.639
423	33	13	0.765	1.316
413	33	12	0.706	1.055
386	33	11	0.647	0.832
383	32	10	0.588	0.634
372	31	9	0.529	0.453
368	31	8	0.471	0.283
365	30	7	0.412	0.119
357	30	6	0.353	-0.041
356	29	5	0.294	-0.202
345	29	4	0.235	-0.369
338	29	3	0.176	-0.551
336	29	2	0.118	-0.761
333	29	1	0.059	-1.041

The graphs of X_e against $-\ln(-\ln F_{(IMAX)})$ for the length and width can be seen in figures 3.1 and 3.2 respectively. A computer program was used to calculate the line of best fit through the points which gave the gradient and intercept of the straight line. The results from the curve fitting can be seen in table 3.2. Included in these results are the errors for the slope and the Y intercept.

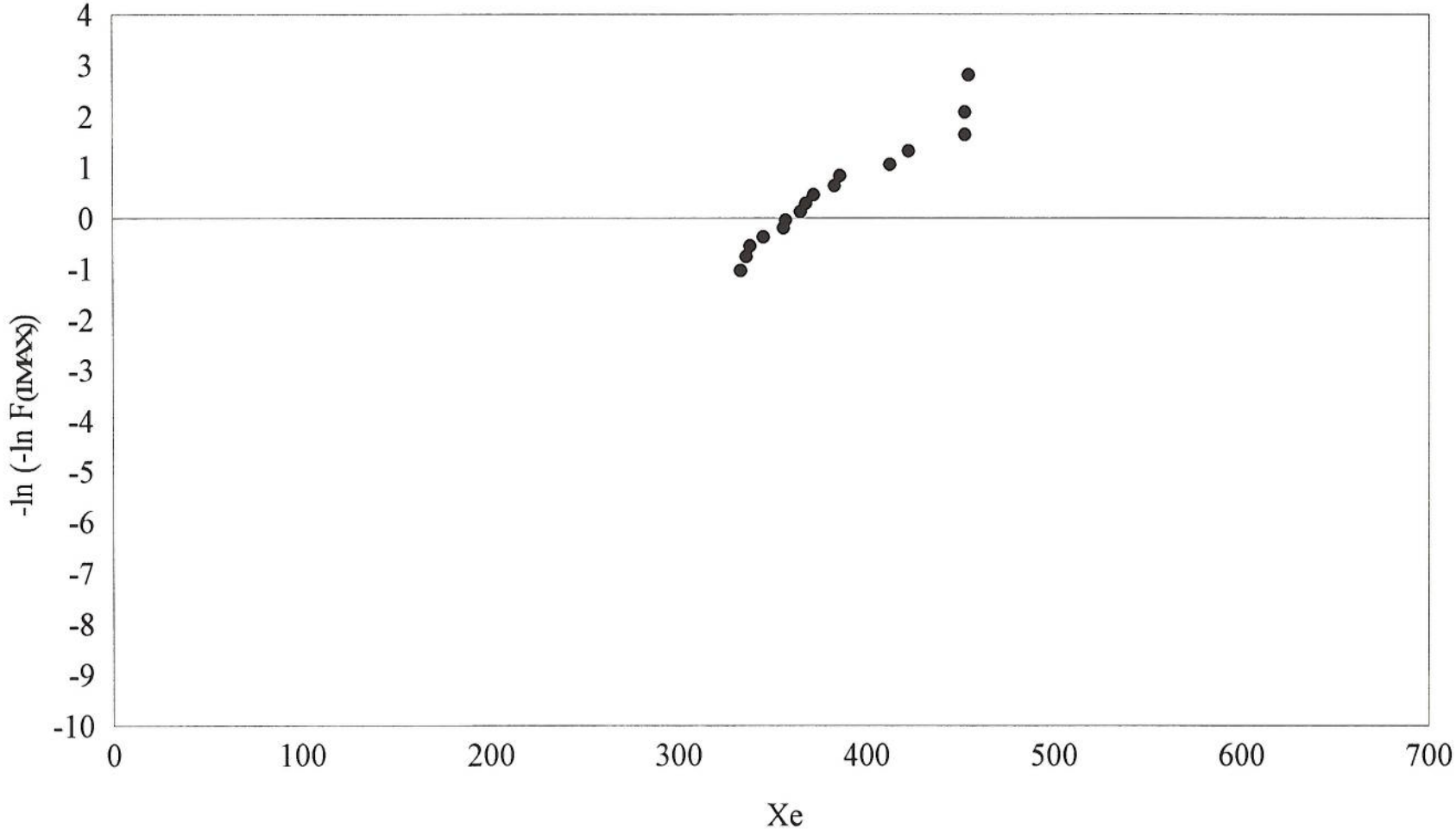

Figure 3.1. : Graph to determine the most probable grain length for 2014 T/2.

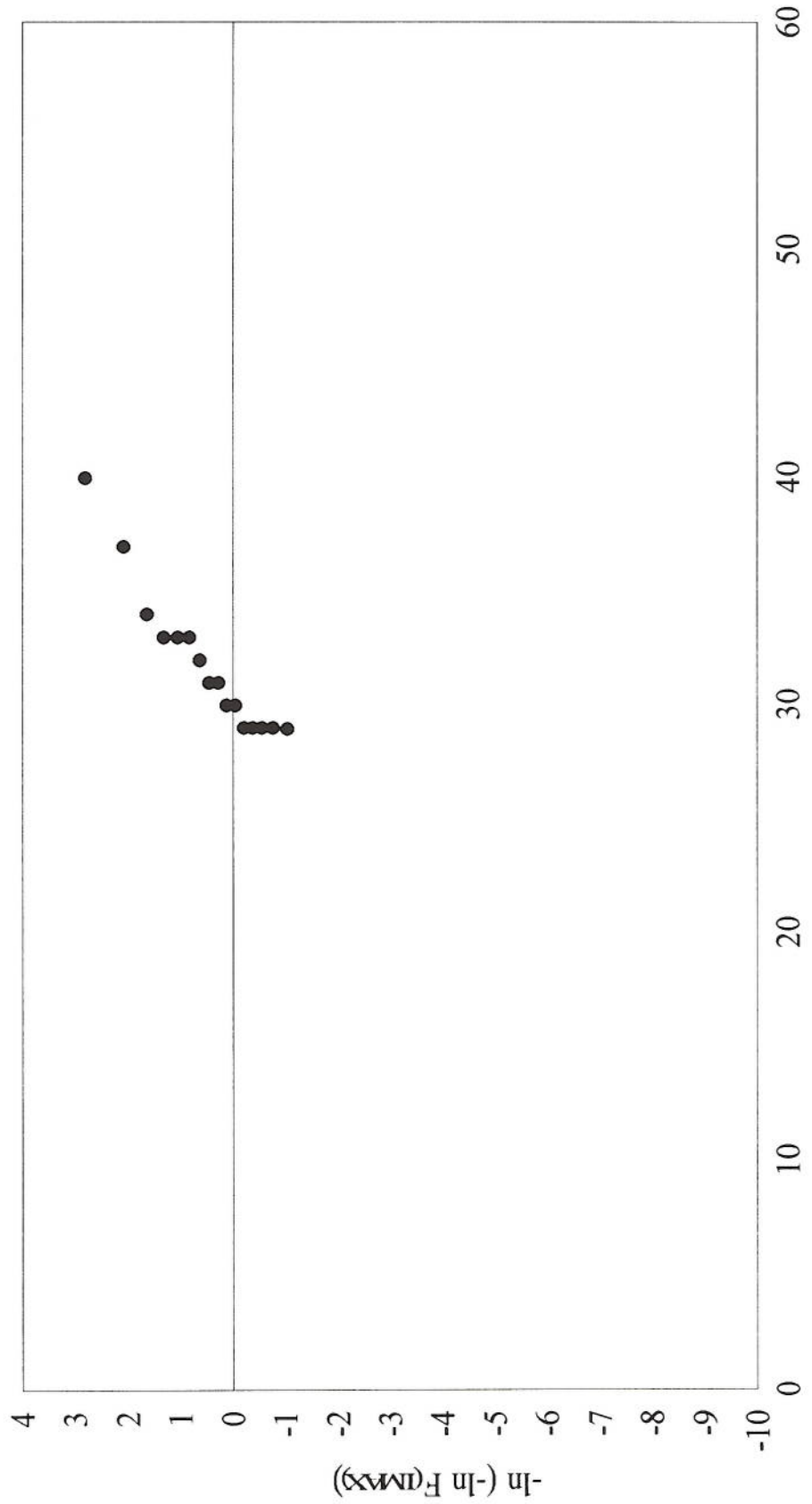

Figure 3.2. : Graph to determine the most probable grain width for 2014 T/2.

Table 3.2. : Extreme Value Statistics Results for 2014 T/2

	Grain Length	Grain Width
Slope	0.024	0.3237
Error in Slope	0.0016	0.024
Y Intercept	-8.694	-9.788
Error in Intercept	0.2657	0.2946
Correlation Coefficient	0.942	0.929

The most probable grain length and width can then be calculated using the errors with the following:

Grain dimension = Intercept / -gradient

Grain length = 362±50μm
Grain width = 30±9μm
Grain aspect ratio = 12.1±5.8.

This procedure was followed for all the specimens used.

APPENDIX FOUR

MASTMAASIS SALT SPRAY TEST

Apparatus

1. A commercial salt spray fog cabinet designed to comply with ASTM B 117-64 specification for salt spray testing and modified to permit automatic cycling. The test is operated at 49^0C.

2. The MASTMAASIS test normally consists of a 6 hour cycle as follows:

a) 45 minute spray

b) Two hour purge with air

c) Three hour, fifteen minute soak period at 40 - 95% relative humidity

Solution

5% NaCl solution using distilled water buffered to pH3 using acetic acid.

Test Procedure

1. Degrease the specimens.
2. Support or suspend the specimens at an angle of 45^0 from the vertical with the surface to be corroded facing upwards.
3. Clean the corroded specimens by immersing in concentrated nitric acid to remove the corrosion products formed on the surface of the specimen. Care must be taken so that no more flakes of exfoliated metal are dislodged.